Regulation of Intra-Organellar Calcium Homeostasis in the Golgi Apparatus of *Arabidopsis thaliana*

Dissertation

zur Erlangung des

Doktorgrades der Naturwissenschaften (Dr. rer. nat.)

der Naturwissenschaftlichen Fakultät III

der Martin-Luther-Universität

Halle-Wittenberg

vorgelegt

von Herrn M.Sc. Nico Rössner

geb. am 21.05.1995 in Hamburg-Harburg

verteidigt am 11.09.2023

Erstgutachter: Prof. Dr. Edgar Peiter

Zweitgutachter: Prof. Dr. Lorella Navazio

Table of Contents

Zusammenfassung

Calcium (Ca^{2+}) dient in Pflanzen als sekundärer Botenstoff. Die Konzentration von freiem Ca^{2+} wird im Zytosol aktiv gering gehalten, und zahlreiche biotische und abiotische Stressfaktoren lösen vorübergehende Erhöhungen aus und setzen somit verschiedene Ca^{2+}-abhängige Signalwege in Gang. Im Gegensatz zum Zytosol ist das Wissen über die Funktionen und die Homöostase von Ca^{2+} in den zellulären Kompartimenten des pflanzlichen Sekretionsweges immer noch gering. Dennoch gibt es Hinweise dafür, dass Ca^{2+} auch in diesen Organellen eine funktionelle Rolle hat. Neben Mn^{2+} dient Ca^{2+} dort als Kofaktor für Proteine, wie Glykosyltransferasen oder Calreticuline. In tierischen Zellen konnte außerdem gezeigt werden, dass Ca^{2+}, neben anderen Kationen und dem pH-Wert, den Vesikeltransport reguliert, und es gibt Hinweise darauf, dass Ca^{2+} in Pflanzen ähnliche Funktionen haben könnte

In dieser Studie wurde die Dynamik und Regulation von Ca^{2+} in diesen mobilen Organellen, insbesondere in den verschiedenen Golgi-Zisternen, untersucht. Die Ca^{2+}-Transportproteine BICAT3 und ECA3 wurden in *Arabidopsis thaliana* hinsichtlich subzellulärer Lokalisierung, Genexpression und Phänotypen von Knockoutmutanten charakterisiert. Ebenso wurden auf Aequorin basierende *cis*- und *trans*-Golgi-spezifische Ca^{2+}-Reporter erzeugt, mittels konfokaler Mikroskopie lokalisiert und transient in *Nicotiana benthamina* und stabil in *A. thaliana* exprimiert. Die Konzentrationen von freiem Ca^{2+} im Golgi ($[Ca^{2+}]_{Golgi}$) von Mesophyllprotoplasten wurden luminometrisch bestimmt. Sowohl *cis*- als auch *trans*-Zisternen reagierten auf NaCl mit einer transienten Erhöhung der $[Ca^{2+}]_{Golgi}$, letztere jedoch nur schwach. Es zeigte sich, dass ECA3 die NaCl-induzierte Erhöhung von $[Ca^{2+}]_{cisGolgi}$ stark beeinflusst, was mit einer erhöhten Salzstressempfindlichkeit der *eca3*-Mutante einher ging. BICAT3 trug nicht wesentlich zum $[Ca^{2+}]$-Anstieg im *cis*-Golgi bei, was mit seiner spezifischen Lokalisation im *trans*-Golgi korrespondierte. Dies deutet darauf hin, dass BICAT3 den Anstieg von $[Ca^{2+}]_{cisGolgi}$ durch NaCl nicht direkt bewirken kann. Im Gegensatz zu NaCl bewirkte H_2O_2 einen Anstieg der $[Ca^{2+}]$ in beiden Subkompartimenten in ähnlicher Weise. *Eca3* und *bicat3* zeigten eine veränderte Kinetik, jedoch kein reduziertes Peak-Maximum. Die Ergebnisse zeigen insgesamt, dass sich die freien Ca^{2+}-Konzentrationen im Golgi unter abiotischen Stressfaktoren wie NaCl und H_2O_2 ändern und dass ECA3 den vorübergehenden Ca^{2+}-Anstieg im *cis*-Golgi regulieren kann. Die gefundene Dynamik des freien Ca^{2+} deutet auf dessen

funktionelle Bedeutung in diesen Organellen hin. Dabei trat ein wesentlicher Unterschied zwischen frühen und späten Zisternen des Golgi zu Tage. Das in dieser Arbeit entwickelte Werkzeug zur Messung der freien Ca^{2+}-Konzentrationen in Subkompartimenten des Golgi ist eine Basis für weiterführende Untersuchungen zum Einfluss von Ca^{2+} in Organellen entlang des Sekretionswegs in Pflanzen.

Summary

Calcium (Ca^{2+}) serves as second messenger in plants. Concentrations of Ca^{2+} are actively kept low in the cytosol, and numerous biotic and abiotic stresses trigger transient elevations and thus initiate various Ca^{2+}-dependent signalling pathways. In contrast to the cytosol, the knowledge of the function and homeostasis of Ca^{2+} in the cellular compartments of the plant secretory pathway is still limited. Nevertheless, there is evidence that Ca^{2+} also has a functional role in these organelles. Ca^{2+} next to Mn^{2+} serves as cofactor for proteins such as glycosyltransferases or calreticulins in these organelles. In animal cells, Ca^{2+} has also been shown to regulate vesicle transport, along with other cations and pH, and there is evidence that Ca^{2+} may have similar functions in plants.

In this study, the dynamics and regulation of Ca^{2+} in these mobile organelles, particularly in the different Golgi cisternae, were investigated. The Ca^{2+} transport proteins BICAT3 and ECA3 were characterised in *Arabidopsis thaliana* with respect to subcellular localisation, gene expression, and knockout mutant phenotypes. Likewise, aequorin-based *cis*- and *trans*-Golgi-specific Ca^{2+} reporters were generated, localised by confocal microscopy and expressed transiently in *Nicotiana benthamina* and stably in *A. thaliana*. The concentrations of free Ca^{2+} in the Golgi ($[Ca^{2+}]_{Golgi}$) of mesophyll protoplasts were determined luminometrically. Both *cis*- and *trans*-cisternae responded to NaCl with a transient increase in $[Ca^{2+}]_{Golgi}$, but the latter only weakly. ECA3 strongly affected the NaCl-induced increase in $[Ca^{2+}]_{cisGolgi}$, which was accompanied by an increased salt sensitivity of the *eca3* mutant. BICAT3 did not contribute markedly to the $[Ca^{2+}]$ increase in the *cis*-Golgi, which corresponded with its specific localisation in the *trans*-Golgi. This suggests that BICAT3 cannot directly cause the increase of $[Ca^{2+}]_{cisGolgi}$ by NaCl. In contrast to NaCl, H_2O_2 caused an increase in $[Ca^{2+}]$ in both subcompartments in a similar manner. *eca3* and *bicat3* showed altered kinetics but no reduced peak maximum. Overall, the results show that free Ca^{2+} concentrations in the Golgi increase upon abiotic stresses such as NaCl and H_2O_2 and that ECA3 can regulate the transient Ca^{2+} increase in the *cis*-Golgi. The dynamics of free Ca^{2+} indicate a functional importance in these organelles, whereby a notable difference between early and late cisternae of the Golgi is apparent. The tool developed in this work to measure free Ca^{2+} concentrations in

subcompartments of the Golgi is a basis for further studies on the influence of Ca^{2+} in organelles along the secretory pathway in plants.

1 Introduction

1.1 Calcium as a Second Messenger

A permanent exposure to changing environmental conditions affect plant growth and require adaptations of the plant to complete its lifecycle. Calcium (Ca^{2+}) as a ubiquitous second messenger mediates one of the first plant responses to developmental and environmental cues. The occurrence of changes in the free cytosolic Ca^{2+} concentration ($[Ca^{2+}]_{cyt}$) was first observed in protoplasts of higher plants (Gilroy *et al.*, 1986), and the crucial role of Ca^{2+} began to raise interests since it was shown to regulate many cellular processes and thereby act as a messenger (Poovaiah & Reddy, 1987). This was followed by the generation of transgenic plants expressing the Ca^{2+} sensor *APOAEQUORIN* of the jellyfish *Aequoria victoria*, that enabled the visualisation of changes in $[Ca^{2+}]_{cyt}$ in response to touch and cold shock treatments *in planta* (Knight *et al.*, 1991). Subsequently, a multitude of studies reporting changes in $[Ca^{2+}]_{cyt}$ in response to abiotic and biotic stimuli, such as salinity, drought or oxidative stress, and biotic stresses followed (Price *et al.*, 1994, Knight *et al.*, 1997). Mainly, transient elevations of $[Ca^{2+}]_{cyt}$ occur in response to most stresses and stimuli; however, these transients differ in duration, shape, and time, making them unique for different stimuli. Ca^{2+} signals have therefore been hypothesised to encode information on the stimuli.

Proteins from a wide variety of families can bind and respond to Ca^{2+} and thereby decode the previously generated Ca^{2+} signal. These include Ca^{2+}-dependent protein kinases (CDPKs or CPKs), CDPK-related kinases (CRKs), calmodulins (CaMs), calmodulin-like proteins (CMLs), and calcineurin B-like proteins (CBLs) (Dodd *et al.*, 2010). These proteins were classified into sensor responders that directly modify a target, e.g. by phosphorylation upon Ca^{2+} binding, and sensor relays that in turn activate further components of the signalling cascade (Dodd *et al.*, 2010). CaMs and CMLs were described as sensor relays. CaMs are conserved in all eukaryotes, and the Arabidopsis genome harbours seven genes coding for four isoforms, whereas the abundance of CMLs with 50 isoforms is higher. Ca^{2+} binding leads to conformational changes of CaMs and CMLs which enables an interaction with other proteins (McCormack *et al.*, 2005). A large number of proteins is activated upon binding to CaMs or CMLs, such as kinases, phosphatases, ion transporters, metabolic enzymes, and transcription factors (Reddy *et al.*,

2011). CBLs might be seen as sensor relays, but can also be considered as bimolecular sensor responders together with CBL-interacting protein kinases (CIPKs). The genome of Arabidopsis contains 10 CBLs and 26 CIPKs (Kolukisaoglu *et al.*, 2004, Weinl & Kudla, 2009). Like in CaMs and CMLs, Ca^{2+} binding is enabled by helix-loop-helix EF hands (Lewit-Bentley & Réty, 2000), whereby CBLs contain four of these EF hand motifs. CIPKs contain a kinase domain and a NAF domain for CBL interaction (Albrecht *et al.*, 2001). Thus, Ca^{2+} binds to the EF hand of the respective CBL leading to an interaction of the CBL with a CIPK that in turn phosphorylates its target. In contrast, CDPKs are sensor responders that combine the function of CBLs and CIPKs. The genome of Arabidopsis contains 34 genes coding for CDPKs and eight for their relatives, CDPK-related kinases (CRKs) (Hrabak *et al.*, 2003). CDPKs contain a serine/threonine protein kinase domain, an autoinhibitory domain, and a CaM-like domain with four EF-hand motifs. Their kinase activity depends on a conformational change upon Ca^{2+} binding to these EF-hand motifs (Ludwig *et al.*, 2004). By contrast, the CRKs exhibit degenerated EF-hands unable to bind Ca^{2+}, while some CPKs appear to be regulated by CaMs (Harper *et al.*, 2004). Due to lipid modification by either myristoylation or S-acylation which provokes membrane attachment, CDPK/CPKs can be anchored in membranes, e.g. of the ER. For instance, CPK2 was shown to be localised in the ER, anchored in the membrane by myristoylation (Lu & Hrabak, 2002). Moreover, the Ca^{2+} pump ACA2, which is also resident in the ER, is negatively regulated by CPK1 via N-terminal phosphorylation. Thus a Ca^{2+} signal seems to further modulate Ca^{2+} transport processes by regulation of ACA2 (Hwang *et al.*, 2000). Intriguingly, it was shown that expressing the Ca^{2+} pump ACA2 in yeast, leads to a hypersensitivity to salt stress (Anil *et al.*, 2008).

Salt stress can play a critical role in plant development, and salt (NaCl) evokes an immediate elevation of $[Ca^{2+}]_{cyt}$ (Knight *et al.*, 1997). These $[Ca^{2+}]_{cyt}$ elevations upon NaCl were shown to be distinct in different root cell types with the pericycle showing the lowest increase in $[Ca^{2+}]_{cyt}$ followed by cells of the endodermis. The initial increases of $[Ca^{2+}]_{cyt}$ were followed by oscillation in both cell types (Kiegle *et al.*, 2000). To cope with salt stress, the salt overly sensitive (SOS) pathway was shown to be important for salt tolerance (reviewed by Ji *et al.* (2013) and Steinhorst and Kudla (2019)). Salt overly sensitive 1 (SOS1) is a H^+/Na^+ exchanger in the plasma membrane that confers tolerance upon salt stress by Na^+ export out of the plant cell (Quan-Sheng Qiu, 2002). This H^+/Na^+ exchanger is activated through phosphorylation by CIPK24 (SOS2) which binds to CBL4 (SOS3). The entire signalling cascade is activated by the

preceding increase of $[Ca^{2+}]_{cyt}$ upon NaCl sensing (Gong *et al.*, 2004). In addition, another CBL, CBL8, particularly contributes to salt tolerance under high-salt-stress conditions by also interacting with CIPK24 (Steinhorst *et al.*, 2022). Salt initiates that the ubiquitin carrier proteins (UBC) 1 and 2 promote *MYB42* expression which in turn binds to the *CIPK24* promoter leading to a rapid induction of its expression (Sun *et al.*, 2020). The generation of Ca^{2+} signals in response to salt was not fully understood until it was revealed that Na^+ binding to glycosyl inositol phosphorylceramide (GIPC) sphingolipids initiates the gating of Ca^{2+} influx channels. Hereby, monocation-induced $[Ca^{2+}]_i$ increases 1 (MOCA1) is a glucuronosyltransferase for GIPC sphingolipids in the plasma membrane, and the *moca1* mutant is affected under high-salt conditions (Jiang *et al.*, 2019). Next to the CBL4 and CBL8 interaction with CIPK24, it was shown that also CBL10 interacts with CIPK24 leading to (i) Na^+ detoxification by activating a vacuolar Na^+/H^+ antiporter (Kim *et al.*, 2007) and (ii) activating plasma membrane-localised Annexin4 to fine-tune salt-induced Ca^{2+}-signals (Ma *et al.*, 2019). Furthermore, an accumulation of H_2O_2 as form of reactive oxygen species in the apoplast is thought to be involved in acclimation responses of plants to salt stress, such as growth and cell wall formation (Hernandez *et al.*, 2001, Rodriguez *et al.*, 2004), and regulation of Na^+ and K^+ homeostasis (Zhang *et al.*, 2007, Sun *et al.*, 2010).

Reactive oxygen species (ROS) are highly reactive radicals derived from oxygen (O_2). Different forms of ROS are superoxide ($O_2^{\cdot-}$), peroxides (O_2^{2-}), hydroxyl radical (OH^-), alpha-oxygen, singlet oxygen, and hydrogen peroxide (H_2O_2), among others, causing oxidative damage to proteins, DNA, and lipids (Miller *et al.*, 2010). The synthesis of H_2O_2 occurs in many compartments within the plant cell, such as the mitochondria, chloroplasts, and peroxisomes, next to plasma membrane-associated synthesis in the apoplast. The distribution of H_2O_2 encompasses the entire plant cell, while its function in plant signalling is widespread (Smirnoff & Arnaud, 2019). For instance, plasma membrane-localised NADPH oxidases, called respiratory burst oxidase protein homologues (RBOH), convert O_2 into $O_2^{\cdot-}$ in the apoplast. The regulation of respiratory burst oxidase protein homologue D (RBOHD) and thus its ROS production, is mediated through C-terminal phosphorylation and ubiquitination (Lee *et al.*, 2020). In rapeseed, it was shown that phosphorylation of RBOHD is mediated by calcium-dependent protein kinase 6-like (CPK6L) possibly initiated by a previous Ca^{2+} signal (Pan *et al.*, 2019). It was shown that RBOHD mediates rapid systemic signalling in response to numerous stimuli, such as cold and salinity (Miller *et al.*, 2009), also in response to a previous Ca^{2+} signal

(Gilroy *et al.*, 2016). Apoplastic enzymes that catalyse the dismutation of $O_2^{\cdot-}$ into O_2 and H_2O_2 are superoxide dismutases (SODs). Thus, Ca^{2+} and ROS signalling influence each other and cannot be considered isolated (Steinhorst & Kudla, 2013). In tobacco cell cultures expressing *APOAEQUORIN*, it was shown that H_2O_2 leads to changes in $[Ca^{2+}]_{cyt}$ in a biphasic manner (Lecourieux *et al.*, 2002). Further studies with entire Arabidopsis seedlings expressing *APOAEQUORIN* revealed that a first increase of $[Ca^{2+}]_{cyt}$ appeared specifically in the cotyledons and a second one in the lower root (Rentel & Knight, 2004). A mechanism for the H_2O_2-triggered Ca^{2+} influx has been suggested. The H_2O_2 sensor hydrogen-peroxide-induced Ca^{2+} increases 1 (HPCA1) mediates H_2O_2-induced activation of plasma membrane-localised Ca^{2+} channels required for stomatal closure (Wu *et al.*, 2020).

Next to NaCl- and H_2O_2-induced $[Ca^{2+}]_{cyt}$ increases, other environmental cues like drought or nutrient imbalances, as well as biotic stresses, e.g. pathogen attack, trigger increases in $[Ca^{2+}]_{cyt}$ that lead to cellular responses (Kudla *et al.* (2018), Thor (2019), Tian *et al.* (2020)). Suitable calcium reporters enable the monitoring of changes in $[Ca^{2+}]$ and thus are powerful tools for Ca^{2+} signalling research.

1.1.1   Calcium Reporters

The challenge to elucidate the function of Ca^{2+} as a second messenger lies in the methods that enable the visualisation of changes in free Ca^{2+}. Thereby many factors play a role for the choice of the right reporter, such as resolution and sensitivity. The variety of Ca^{2+} reporters is large nowadays. There are two main types of Ca^{2+} indicators, chemical indicators and genetically encoded calcium indicators (GECI). Chemical indicators are small molecules, such as fura-2 or fluo-4 and its relatives, which contain a BAPTA-like Ca^{2+} chelator component covalently linked to a fluorogenic, fluorescein-like component that binds Ca^{2+}. For instance, fluo-4 is excited by light with a wavelength of 488 nm and its emission at approximately 506 nm increases upon Ca^{2+} binding (Gee *et al.*, 2000). They are loaded into the cytosol by means of covalently attached acetoxymethly esters and commonly used for measurements on cellular level in animal cells, but their loading into intact plants is problematic. In contrast, genetically encoded calcium indicators (GECIs) are powerful tools for imaging of free Ca^{2+} *in vivo* (Waadt *et al.*,

2017). The luminescent aequorin, discovered by Shimomura *et al.* (1962), is the longest-established and most prominent GECI. aequorin is a Ca^{2+}-binding photoprotein that is composed of APOAEQUORIN with an approximate molecular weight of 22 kDa and a prosthetic group, coelenterazine. The functional holoprotein aequorin reconstitutes in presence of oxygen. Aequorin exhibits three EF-hand Ca^{2+} domains, and upon Ca^{2+} binding, it changes its conformation and converts coelenterazine into excited coelenteramide while releasing carbon dioxide. The excited coelenteramide returns to the ground state and thereby emits blue light (λ = 469 nm) (Figure 1, Mithöfer & Mazars, 2002).
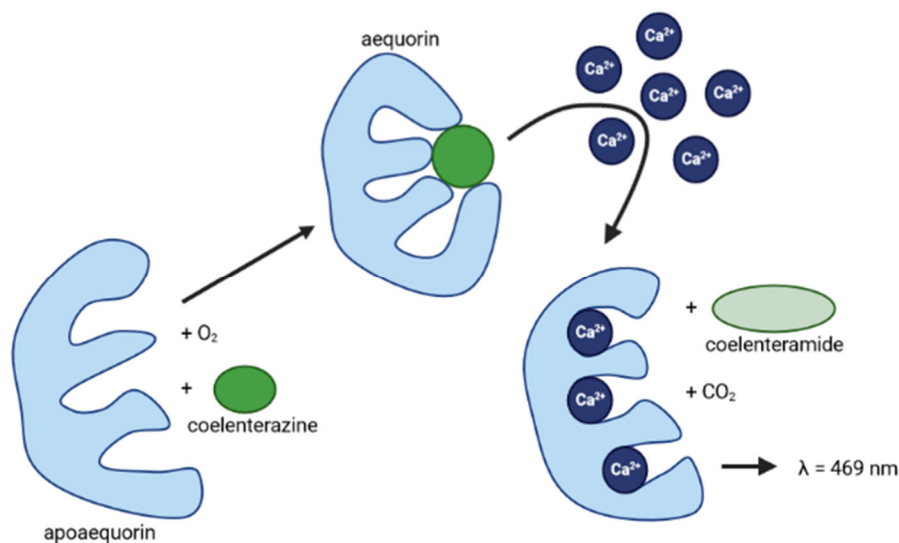
Figure 1: Mechanism of aequorin binding to Ca^{2+} and ensuing light emission at 469 nm (after Mithöfer & Mazars, 2002).

Moreover, modified aequorin variants with low Ca^{2+} affinity to measure Ca^{2+} signals in organelles with high Ca^{2+} levels, such as the ER, were developed (Montero *et al.*, 1995). Next to the luminescence-based aequorin, there are fluorescent Ca^{2+} reporters like the classical emission ratiometric GECI Yellow Cameleon (YC) variants. Their function is based on Förster resonance energy transfer (FRET) (Allen *et al.*, 1999, Miyawaki *et al.*, 1999). As YCs, most fluorescent GECIs exhibit a CaM domain and the CaM-binding 13 amino acids of the myosin light chain kinase (M13 peptide), enabling a conformational change upon Ca^{2+} binding (Waadt *et al.*, 2021). Several YCs have been employed in plants with YC3.6, consisting of a ECFP and a cpVenus fused by a CaM-M13 linker, being the most commonly used one (Nagai *et al.*, 2004). Commonly used intensiometric single fluorescent protein GECIs, e.g. GCaMP3, and genetically

encoded Ca^{2+} indicators for optical imaging (GECOs), e.g. R-GECO, have optimised fluorescence properties and a larger dynamic range (Tian *et al.*, 2009, Zhao *et al.*, 2011). GCaMPs consist of a circularly permutated FP (cpFP) (Baird *et al.*, 1999). The M13 peptide was fused to the N-terminus and CaM to the C-terminus (Nakai *et al.*, 2001). Upon Ca^{2+} binding the fluorescence intensity of the cpFP increases (Tian *et al.*, 2009, Zhao *et al.*, 2011). Recent variants, e.g. GCaMP6, show a higher saturated fluorescence intensity with similar basal fluorescence (Chen *et al.*, 2013). A low-affinity variant of GCaMP6 was developed by de Juan-Sanz *et al.* (2017), and Resentini *et al.* (2021) established this variant for Ca^{2+} measurements in the ER *in planta*. Nevertheless, fluorescence-based reporters have the disadvantage of sensitivity to low pH, while aequorin is pH-insensitive (Brini, 2008).

1.1.2 Calcium Transport across Membranes

The sophisticated function of Ca^{2+} as a second messenger is feasible due to the possibility of rapid changes in [Ca^{2+}]$_{cyt}$. To accomplish this, the steady-state concentration of free Ca^{2+} in the cytosol is kept very low, and Ca^{2+} is stored in specific cellular organelles or the apoplast. A rapid and transient change of [Ca^{2+}]$_{cyt}$ can be mediated by a variety of transport mechanisms of the plant cell. Channels, transporters, and pumps play an essential role in this process of Ca^{2+} transport during the emergence of the [Ca^{2+}] transient and the restoration of basal levels. In Arabidopsis, a variety of Ca^{2+}-permeable channels has been identified, such as ionotropic glutamate receptors (GLRs), cyclic nucleotide-gated channels (CNGCs), mitochondrial calcium uniporters (MCUs), the two-pore channel 1 (TPC1), PIEZO ion channel, and putative hyperosmolality-gated calcium-permeable channels (OSCAs) (Hamilton *et al.*, 2015, Demidchik *et al.*, 2018). The genome of Arabidopsis contains 20 genes encoding for GLRs which were divided in three phylogenetic clades. The plant GLRs are completely distinct from their animal counterparts. Until now, the selectivity or permeability for Ca^{2+} of many members is still not resolved. GLRs contain four transmembrane domains (TMDs) with an amino terminal domain (ATD) and a ligand-binding domain (LBD), both located at the N-terminus of the GLRs. GLRs are resident in different membranes within the plant cell, including the plasma membrane, the ER, and the vacuole (Demidchik *et al.*, 2018). GLRs were excellently reviewed

by Grenzi *et al.* (2022); organelle-localised GLRs will be described in the following chapters in more detail.

The characterized CNGCs are mostly resident at the plasma membrane (Gobert *et al.*, 2006, Jammes *et al.*, 2011). Apart from the CNGCs located in the plasma membrane, others were found to be localised in the nuclear envelope and contribute to nuclear Ca^{2+} signalling in legume roots (Charpentier *et al.*, 2016). The CNGC family in Arabidopsis is divided in five subfamily groups containing 20 members (Mäser *et al.*, 2001). CNGCs consist of six TMDs and a conserved cyclic nucleotide binding domain (CNBD) at the C-terminus. The opening of CNGCs occurs upon binding of cyclic nucleotide monophosphates, e.g. cyclic adenosine 5'monophosphate (cAMP), cyclic guanosine 5'monophosphate (cGMP) or guanosine 5' triphosphate (GTP) to the CNBD (Demidchik *et al.*, 2018). Furthermore, their activation is regulated by phosphorylation (Zhou *et al.*, 2014). The two pore channel 1 (TPC1) is the only member of two-pore channels (TPCs) in Arabidopsis. TPC1 is activated by depolarisation and an increase in cytosolic calcium concentration, and it was described to be regulated by phosphorylation (Kintzer & Stroud, 2016). TPC1 localises to the tonoplast and is assembled by two subunits with twelve TMDs each and two EF hand domains between TMD six and seven (Peiter *et al.*, 2005). Owing to their Ca^{2+}-binding capacity, the EF hands render the channel sensitive to cytosolic Ca^{2+}, so TPC1 may mediate Ca^{2+}-induced Ca^{2+} release in a positive feedback loop. The role of TPC1 in Ca^{2+} signalling will be further discussed in the following chapter. Another protein group that have a channel activity are OSCAs. Yuan *et al.* (2014) reported a hyperosmolarity-activated channel, called OSCA1.1, localised in the plasma membrane. Another member of this family, OSCA1.3, is regulated by phosphorylation by the Botrytis-induced kinase 1 (BIK1) upon the perception of pathogen-associated molecular patterns (PAMPs) that in turn leads to stomatal closure (Thor *et al.*, 2020).

To restore the basal level after $[Ca^{2+}]_{cyt}$ elevations, Ca^{2+} needs to be actively transported by transporters and pumps. Cation exchangers (CAXs) are Ca^{2+} transporters, and the genome of Arabidopsis contains six genes coding for CAXs which are divided in two types (1A and 1B) (Manohar *et al.*, 2011). They contain eleven TMDs with an autoinhibitory domain and a highly conserved cation binding region. The nine amino acid sequence between TMD one and two enables their transport specificity (Shigaki & Hirschi, 2006). The CAX family contains both, Ca^{2+}-specific transporters and those transporting Ca^{2+} and Mn^{2+}. They are energized by a pH

gradient generated by proton pumps, i.e. H^+-ATPase and H^+-pyrophosphatase. It was suggested that CAXs co-transport a single H^+ per Ca^{2+} ion (Kamiya & Maeshima, 2004, Waight *et al.*, 2013, Pittman & Hirschi, 2016, Demidchik *et al.*, 2018). The transport affinities of CAXs are lower compared to Ca^{2+} pumps (Demidchik *et al.*, 2018). In contrast to CAXs, the Ca^{2+} transport by CCXs is not clearly clarified. CCXs were classified beforehand as CAX (CAX7 to 11) and then reclassified, since phylogenetic analyses revealed that *CCX5* and, to a lesser extent *CCX3* and *CCX4*, showed a high homology to a mammalian K^+-dependent Na^+/Ca^{2+} exchanger (NCKX6) (Shigaki *et al.*, 2006, Emery *et al.*, 2012). The CCXs of Arabidopsis are also related to mammalian plasma membrane Na^+/Ca^{2+} exchangers (NCXs). NCX exchangers can operate in Ca^{2+} efflux or Ca^{2+} influx mode, which is mediated by the change in Na^+ gradients and the membrane potential (Cai & Lytton, 2004). Furthermore, they are currently described as Na^+/K^+ exchangers and thus might not transport Ca^{2+}. CCX3 was not able to complement a yeast mutant affected in Ca^{2+} transport (Morris *et al.*, 2008), but it is unclear whether CCXs might mediate Ca^{2+} transport *in planta*.

Bivalent Cation Transporters (BICATs) belong to a recently identified transporter family of which the Arabidopsis genome contains five members. They show a conserved 'E-x-GD-(KR)-(ST)' motif in their protein sequence and contain five TMDs (He *et al.*, 2022). Their founding member in yeast, GDT1, was initially described as Ca^{2+} transporter (Demaegd *et al.*, 2013) and subsequently shown to transport Mn^{2+} as well (Stribny *et al.*, 2020). Intriguingly, they were shown to transport both, Ca^{2+} and Mn^{2+} with a yet unresolved transport mechanism (Thines *et al.*, 2020). The yeast homologue GDT1 and the human homologue TMEM165 are crucial for Mn^{2+}-dependent glycosylation processes in the Golgi (Potelle *et al.*, 2016, Foulquier & Legrand, 2020). Members of this protein family will be described in more detail in the following chapters.

Next to transporters, P-type Ca^{2+}-ATPases also play a role in restoring basal Ca^{2+} levels. Based on their protein sequences, P-type Ca^{2+}-ATPases were classified into two subgroups (Axelsen & Palmgren, 1998), P_{2A}-type ATPases, also known as ER-type Ca^{2+}-ATPases (ECAs) which mostly occur in endomembranes, and P_{2B}-type ATPases, also known as autoinhibited Ca^{2+}-ATPases (ACAs) (Huda *et al.*, 2013). The genome of Arabidopsis contains four genes encoding for ECAs and 13 genes encoding for ACAs. Ca^{2+}-ATPases have ten TMDs, whereby TMDs one to six are responsible for the transport of Ca^{2+}, as shown schematically in Figure 2.

The main difference between both types is their N-terminal structure: ACAs contain an autoinhibitory domain overlapping with two CaM-binding domains, which are absent in ECAs (Baekgaard *et al.*, 2006). ACAs are activated by Ca^{2+} by means of the CaM-binding domain (Tidow *et al.*, 2012). Additionally, ACAs were shown to have a higher selectivity for Ca^{2+} compared to ECAs. Besides Ca^{2+}, ECAs are able to transport other bivalent cations like Mn^{2+}, cadmium (Cd^{2+}), and zinc (Zn^{2+}) (Huda *et al.*, 2013). In both types, P_{2A} and P_{2B}, the energy required for the active transport of these cations is provided by ATP binding to a phosphorylation domain (N-domain) shown in Figure 2, resulting in ATP hydrolysis (Palmgren & Harper, 1999).
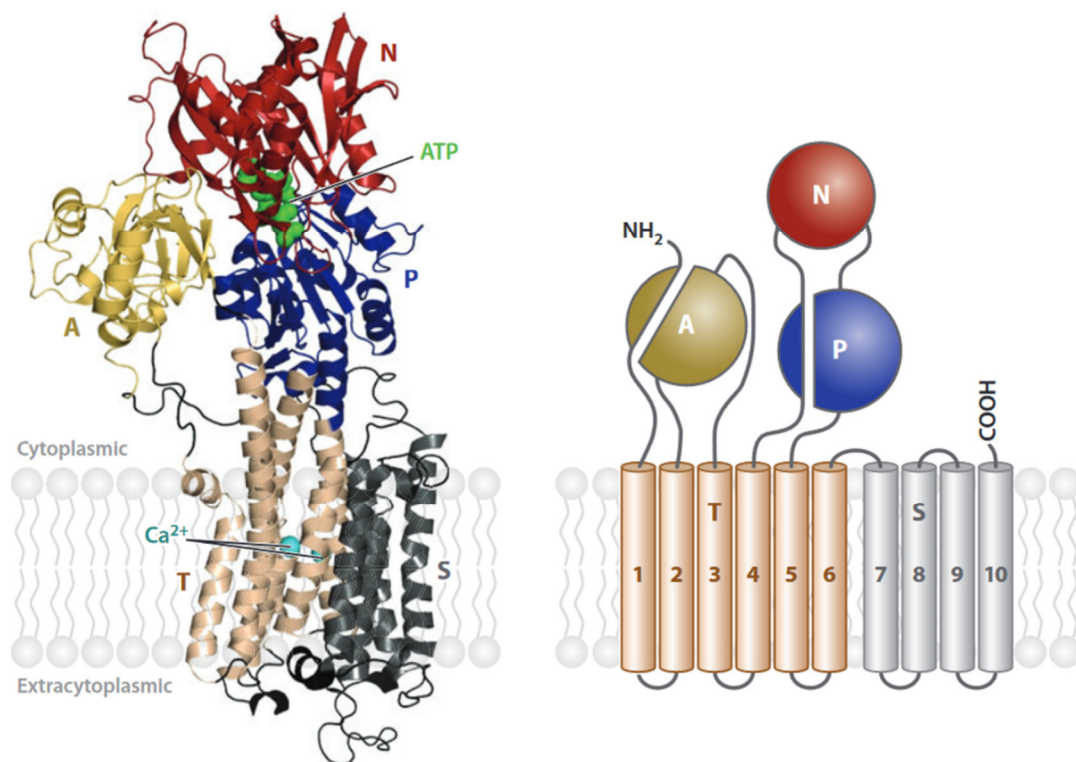
Figure 2: Schematic overview of the structure of P-type ATPases. Left: Ribbon model of the crystal structure of SERCA2a. The pump is organised into three cytoplasmic domains (A, P, and N) and two membrane-embedded domains (T and S). The N-domain binds ATP and phosphorylation occurs in the P-domain. The A-domain is an intrinsic protein phosphatase. The cation binds in the middle of the T-domain. Right: Topology of the respective Ca^{2+}-ATPase. Figure published in Palmgren and Nissen (2011).

Different ER- and Golgi-localised pumps will be described in the following chapters. The active transport by transporters and pumps is crucial for the efflux of Ca^{2+} to organelles or the apoplast after $[Ca^{2+}]_{cyt}$ elevations and further to maintain the low basal $[Ca^{2+}]_{cyt}$.

1.1.3   Functions of Calcium in Organelles

Organelles in the plant cell might contribute to the regulation of free $[Ca^{2+}]_{cyt}$, since Ca^{2+} is compartmentalised within the plant cell to ensure a low cytosolic concentration (Stael *et al.*, 2012, Nomura & Shiina, 2014). Ca^{2+} regulates the activities of enzymes resident within organelles, and organellar Ca^{2+} signalling is affected in various pathophysiological conditions in animal cell compartments (Suzuki *et al.*, 2016). This work primarily focuses on organelles of the secretory pathway and thus not all cell compartments and their transport proteins that transport Mn^{2+} and Ca^{2+} will be discussed in detail; they are shown in Figure 3. Further information on organelles not covered here can be found in recent reviews (Costa *et al.*, 2018, He *et al.*, 2021).
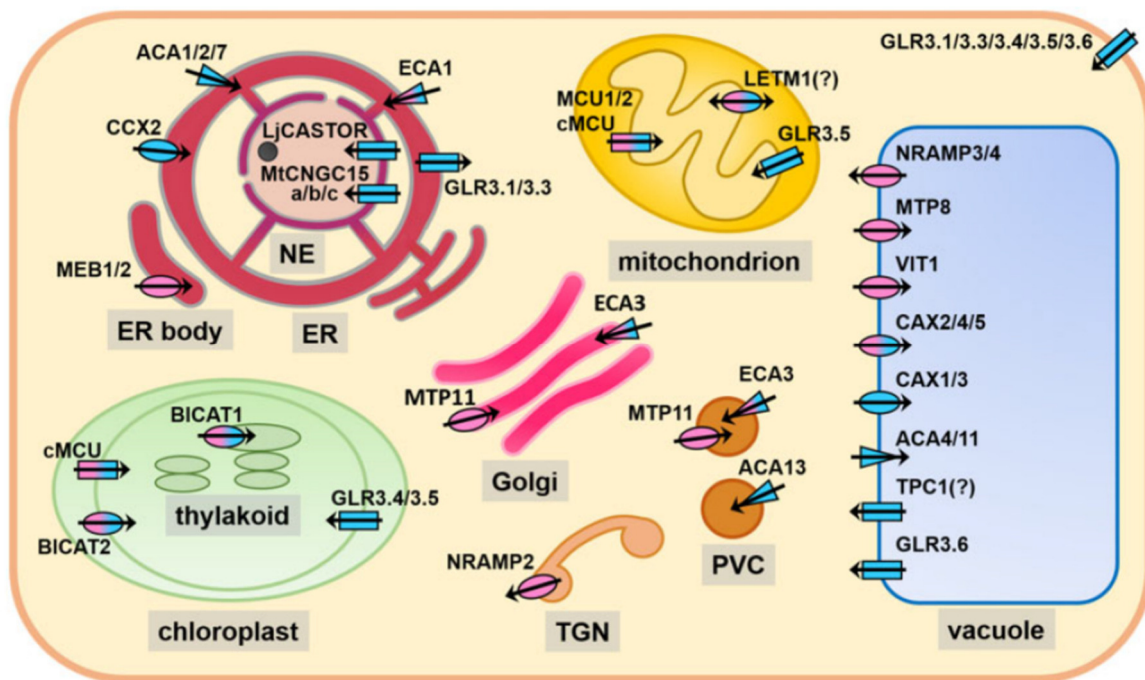
Figure 3: Transport proteins for Ca^{2+} and Mn^{2+}. Pumps (triangles), transporters (ellipses), and channels (rectangles) that were experimentally shown to permeate Ca^{2+} (blue), Mn^{2+} (magenta), or both (blue/magenta) are displayed in a hypothetical plant cell containing the organelles discussed in this review. Figure published in He *et al.* (2021).

In plants, chloroplasts are extensively studied organelles due to their involvement in photosynthesis, which is regulated by Ca^{2+} besides organelle division and protein import (Rocha & Vothknecht, 2012, Stael *et al.*, 2012, Hochmal *et al.*, 2015, Stael, 2019). The chloroplast comprises a double membrane with an intermembrane space, called chloroplast

envelope, surrounding the stroma and the thylakoids within. The free Ca^{2+} concentration in the stroma ($[Ca^{2+}]_{stroma}$) is only slightly higher than that of the cytosol, ranging from 100 nM to 200 nM, while the free Ca^{2+} concentration in the thylakoid lumen ($[Ca^{2+}]_{thylakoid}$) is around 500 nM (Costa *et al.*, 2018). Changes in $[Ca^{2+}]_{stroma}$ with different kinetics were shown to be induced by numerous biotic and abiotic stresses, such as flagellin 22 (flg22) and chitin treatment, salinity, drought, heat, and oxidative stress, as well as the adaption from light to darkness (Navazio *et al.*, 2020). Two Ca^{2+} transporters of the BICAT family in Arabidopsis, BICAT1 and BICAT2, localise to the envelope and the thylakoid membrane, respectively, and influence the $[Ca^{2+}]_{stroma}$ (Frank *et al.*, 2019). BICAT2 was shown to mediate Ca^{2+} transport across the envelope membrane and *bicat2* mutants showed a reduced dark-induced $[Ca^{2+}]_{stroma}$ increase. In contrast, the $[Ca^{2+}]_{stroma}$ transient was increased in *bicat1* mutants when transferred from light to dark. Thus, BICAT1 might transport Ca^{2+} into the thylakoid lumen.

Mitochondrial calcium uniporters (MCUs) were described to mediate Ca^{2+} influx across the inner membrane of animal mitochondria (Kirichok *et al.*, 2004). Intriguingly, plants have a MCU that next to the localisation in root mitochondria was shown to be chloroplast-localised und thus named cMCU (Teardo *et al.*, 2019). The Arabidopsis genome contains six genes encoding MCU homologs. MCU1 localises to the mitochondria and upon reconstitution in planar lipid bilayers, MCU1 shows Ca^{2+} channel activity (Teardo *et al.*, 2017). Mitochondrial Ca^{2+} uptake in roots is dependent on MCUs, and the lack of multiple MCUs lead to a lower Ca^{2+} increase (Ruberti *et al.*, 2022). Due to a poorly selective permeability, the outer mitochondrial membrane allows Ca^{2+} import (Wagner *et al.*, 2016). In plants, the free mitochondrial Ca^{2+} concentration ($[Ca^{2+}]_{mito}$) is about twice as high compared to the cytosol, and it was shown that there are also transient $[Ca^{2+}]_{mito}$ changes upon the perception of stimuli such as cold or oxidative stress (Logan & Knight, 2003). In animals, aerobic metabolic processes are regulated by the $[Ca^{2+}]_{mito}$ (Szabadkai & Duchen, 2008). For instance, $[Ca^{2+}]_{mito}$ triggers the activation of Ca^{2+}- dependent enzymes, e.g. the 2-oxoglutarate dehydrogenase (OGDH), in the tricarboxylic acid (TCA) cycle (McCormack *et al.*, 1990). Moreover, mitochondrial proteins that exhibit a Ca^{2+}-binding EF hand domain might also be activated by Ca^{2+}. An example of such a mechanism was found for the NAD(P)H-dependent glutamate dehydrogenase (GDH). GDH catalyses the reversible enzymatic reaction for the reductive amination of α-ketoglutarate to form glutamate under consumption of NAD(P)H (Turano *et al.*, 1997). The GDH holoenzyme is a

heterohexamer composed of different ratios of α- and β- subunits encoded by *GDH2* and *GDH1*, respectively. The *GDH2* gene product contains a putative EF hand loop, suggesting a role in Ca^{2+} binding and thus regulation of the holoenzyme by Ca^{2+} (Fontaine *et al.*, 2013).

Next to chloroplasts and mitochondria, vacuoles represent another Ca^{2+} store in plant tissues (Peiter, 2011). The free Ca^{2+} concentration in the vacuole $[Ca^{2+}]_{vacuole}$ was described to be in the micro- to millimolar range and thus much higher than that in the cytosol with concentrations in the nanomolar range, albeit this is not studied much (Peiter, 2011). As mentioned above, the two-pore channel TPC1 localises to the tonoplast (Peiter *et al.*, 2005) and is thought to contribute to systemic $[Ca^{2+}]_{cyt}$ elevations in response to NaCl and wounding (Choi *et al.*, 2014, Kiep *et al.*, 2015). In *tpc1-2* mutant plants, no systemic $[Ca^{2+}]_{cyt}$ elevations were detected upon wounding using the Ca^{2+} reporter aequorin (Kiep *et al.*, 2015). Another study suggested that TPC1 might not be involved in cytosolic Ca^{2+} signalling at all, but systemic Ca^{2+} signals were not studied (Ranf *et al.*, 2008). Recently, however, it was shown that TPC1 might not be involved in wounding-induced systemic $[Ca^{2+}]_{cyt}$ elevations, whereas GLRs were confirmed to contribute to this signal (Bellandi *et al.*, 2022). Still, the involvement of TPC1 in Ca^{2+} release in response to stresses or developmental stimuli is not clarified yet. A member of the GLRs, GLR3.6, was suggested to be resident in the tonoplast in xylem contact cells (Nguyen *et al.*, 2018). Ca^{2+} permeability of GLR3.6 has been shown (Shao *et al.*, 2020), although no influence of GLR3.6 on systemic Ca^{2+} signalling was shown in response to wounding, in contrast to GLR3.3 (Bellandi *et al.*, 2022), which will be discussed later. GLR3.6 additionally localises in the plasma membrane (Mou *et al.*, 2020), and its subcellular localisation ought to be further scrutinised.

The vacuole is connected via the prevacuolar compartment (PVC) with the secretory pathway, in which Ca^{2+} has important functions. The general secretory pathway functions, the influence of Ca^{2+}, and the Ca^{2+} transport proteins in these organelles will be described in the following chapters.

1.2 The Plant Secretory Pathway

The secretory pathway consists of a network of organelles that connects the Endoplasmic Reticulum (ER), the plasma membrane, and the vacuole. The ER is connected via COP vesicles with the Golgi, specifically the *cis*-Golgi cisternae, while the *trans*-Golgi cisternae face an independent compartment, the *trans*-Golgi network (TGN) (Viotti *et al.*, 2010). Thus, both compartments, the Golgi and the TGN, can be considered as the central hub for vesicle trafficking and secretion. In the TGN, clathrin-coated vesicles are budded towards the plasma membrane, or transport via the PVC to the vacuole occurs (Figure 4).
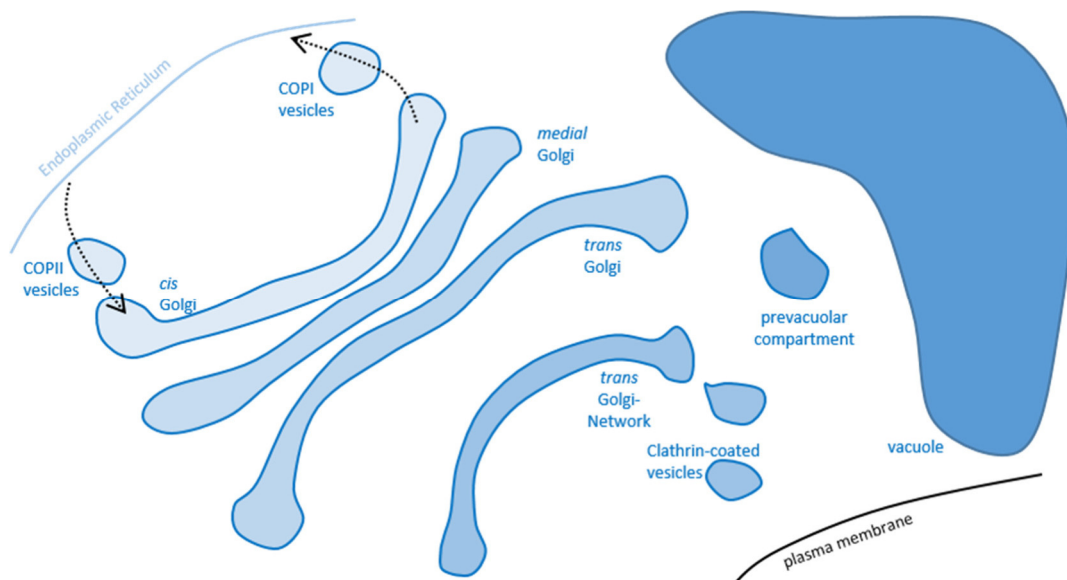
Figure 4: Compartments along the secretory pathway in plant cells. COPII and COPI vesicles connect the *cis*-Golgi and the Endoplasmic Reticulum. Golgi cisternae are shown simplified as single *cis-, medial-* and *trans-* Golgi cisternae. The *trans*-Golgi faces the *trans*-Golgi Network. Formation of prevacuolar compartment vesicles destined for the vacuole and clathrin-coated vesicles guided to the plasma membrane takes place at the bulbs of the *trans*-Golgi network.

Transport and secretion of proteins, lipids, and polysaccharides to the cell surface is mediated along the secretory pathway (Kanazawa & Ueda, 2017). The synthesis of many lipids occurs in the chloroplasts which can be exported to the ER (Wang & Benning, 2012). In plants, sphingolipids are synthesised in the ER and further transported to the Golgi (Sperling & Heinz, 2003). Sphingolipids were shown to promote a luminal Ca^{2+} increase that leads to vesicle formation for cargo transport in animal cells (Deng *et al.*, 2018). In plants, the lipid transport over the secretory pathway plays a crucial role in coping with abiotic stresses such as cold,

osmotic, and drought stress (Wang *et al.*, 2020). Cold stress or copper toxicity for instance were shown to lead to changes in the plasma membrane lipid composition (Uemura & Steponkus, 1999, Berglund *et al.*, 2000). Moreover, defective synthesis mechanisms lead to hypersensitivity to the respective stress. For example, *moca1* mutants contain lower levels of glycosyl inositol phosphorylceramide (GIPC) sphingolipids, but higher levels of inositol phosphorylceramides (IPCs) in the plasma membrane compared to the wild type. Binding of Na^+ to these GIPC sphingolipids triggers a $[Ca^{2+}]_{cyt}$ increase that initiates salt tolerance mechanisms (Jiang *et al.*, 2019), as mentioned before in this thesis.

Next to lipid synthesis and lipid transport, the secretory pathway is important for the vesicular transport of proteins. Proteins are transported via the secretory pathway towards the plasma membrane and apoplast, and to the vacuole (Hadlington & Denecke, 2000). In plants, the transport towards the vacuole is mediated by vacuolar sorting receptors (VSRs) via the PVC (Xiang *et al.*, 2013). This VSR-mediated protein transport was shown in barley for lectins or in tobacco for chintinases (Bednarek & Raikhel, 1991, Neuhaus *et al.*, 1991). Also, the cellulose synthase complex (CSC) is a motile transmembrane protein complex responsible for the synthesis of cellulose microfibrils and needs to be moved from the TGN to the plasma membrane (Wang *et al.*, 2020). A component of the CSC, the cellulose synthase (CESA) 6, was shown to be released to the plasma membrane via exocytosis (He *et al.*, 2018). Mutations in CESA6 lead to the accumulation of the protein in the ER and no further transport to neither the Golgi nor the plasma membrane takes place (Park *et al.*, 2019). Protein cargo can be transferred via the secretory pathway to other compartments such as the chloroplast (Radhamony & Theg, 2006). Moreover, next to the transport of proteins to their final destination, damaged proteins or non-required proteins at the plasma membrane need to undergo endocytosis for degradation (Fan *et al.*, 2015). For example, the iron-regulated transporter (IRT) 1 is localised in early endosomes and can be rapidly released to the plasma membrane for iron uptake, while IRT1 is internalised by clathrin-mediated endocytosis if no uptake is required (Barberon *et al.*, 2011, Barberon *et al.*, 2014).

Apart from protein trafficking, the secretory pathway also mediates detoxification via secretion. For instance, the secretory pathway-localised transport protein MTP11 plays a crucial role in detoxification of excessive Mn^{2+} (Peiter *et al.*, 2007, Delhaize *et al.*, 2007).

To mediate the transport of cargo along these compartments, the movement via vesicles occurs by various transport machineries (Rojo & Denecke, 2008) that will be described in the following. The ER represents an elaborate network consisting of internal membranes and with a connection to the outer membrane of the nuclear envelope (NE) by tubules, called perinuclear ER. The ER is further divided into two types, the rough and the smooth ER. As previously mentioned, the smooth ER functions in lipid synthesis alongside with the assembly of membranes, whereas the rough ER is covered with ribosomes which enable this compartment for translation. Additionally, the cortical ER and ER bodies represent two more ER types. The cortical ER forms tubules connecting the plasma membrane. Synaptotagmin 1 (SYT1) can promote this connectivity under ionic stress (Lee *et al.*, 2019). The ER bodies were exclusively found in Brassicaceae, like Arabidopsis, and are formed upon jasmonic acid (JA) treatment and thus, among others, in herbivory defence (Matsushima *et al.*, 2003, Stefanik *et al.*, 2020).

The secretion of secretory proteins starts with the rough ER, and therefore, the rough ER marks the first compartment of the secretory pathway. Further, the first steps of *N*-glycosylation (see 1.2.1) and protein folding take place in the rough ER. The ER is then linked via vesicles with the Golgi apparatus. The budding of vesicles that often occur along the secretory pathway is realised by coat proteins. The budding and transport from the ER to the Golgi is conveyed by coat protein II (COPII) vesicles, while the retrograde transport is assisted by coat protein I (COPI) vesicles. COPII vesicle formation requires the sequential recruitment of five components, the heterodimers SEC23/24 and SEC13/31 and the small GTPase SAR1 (Chung *et al.*, 2016). COPI consists of a complex (coatomer) composed of seven subunits ($\alpha/\beta/\beta'/\gamma/\delta/\epsilon/\zeta$). These subunits are divided into two sub complexes, the B- ($\alpha/\beta'/\epsilon$) and F-sub complex ($\beta/\delta/\gamma/\zeta$). The B-sub complex functions as outer layer, and the F-sub complex as inner layer of the COPI vesicles (Jackson, 2014). In Arabidopsis, two genes coding for the β-COP subunit have been identified and were shown to be required for plant growth, since mutants lacking β-COP showed an albino phenotype under salt stress (Sánchez-Simarro *et al.*, 2020). For COPI vesicles, there are two types, COPIa and COPIb, respectively. The vesicles that confer retrograde transport to the ER (COPIa) were shown to have a thicker coat mainly budded from early Golgi. In contrast, COPIb vesicles showed thinner coats and are formed only within the Golgi. Regarding this, it is thought that COP vesicles also mediate intra-Golgi trafficking (Donohoe *et al.*, 2007).

The Golgi apparatus directly connects to the ER and is built by membrane-engulfed stacks, which are called cisternae. The amount of those stacks varies in plant cells and depends on the plant tissue and species. The cisternae can be categorized in the *cis* cisternae which face the ER, the *medial* cisternae, and the *trans* cisternae which face an autonomous compartment, the TGN (Robinson, 2020). Since those stacks are not rigid, there are many machineries of trafficking. This includes, next to COP vesicles, small GTPases SAR1/Arf1/Rabs and their regulators, soluble *N*-ethylmaleimide-sensitive fusion attachment protein receptors (SNAREs), conserved oligomeric Golgi (COG) complexes, and golgins, that ensure the smooth transport and connection within the compartments of the secretory pathway (Pereira & Di Sansebastiano, 2021, Rui *et al.*, 2022). This interplay is very complex and intensively studied in animal cells, but not described for plant cells yet. In animal cells, transient inter-cisternal tubules are built to guarantee a rapid transfer of some cargo across the Golgi cisternae (San Pietro *et al.*, 2009, Yang *et al.*, 2011, Beznoussenko *et al.*, 2014, Park *et al.*, 2015), which has not been described for plant cells so far. In animal and plant cells, the budded vesicles and the Golgi stacks can move along actin filaments. Along with the microtubules and the intermediate filaments, they form the cytoskeleton, which enables the transport of these vesicular compartments within the cytosol. The organization of the cytoskeleton might be regulated by cytosolic Ca^{2+} that triggers for instance CDPK3 and confers plant immunity (Lu *et al.*, 2020).

A distinct characteristic of the plant cell is that the TGN is an independent compartment that also can be regarded as the early endosomes (EE) (Dettmer *et al.*, 2006, Lam *et al.*, 2007, Viotti *et al.*, 2010). The TGN can be considered as the central hub for cargo transport via vesicles. Here, the vesicle formation at the TGN depends on the pH, since the vacuolar H^+-ATPase (VHA-ATPase) activity in the TGN is required for exocytosis (Luo *et al.*, 2015). In BY-2 cells, the application of the specific VHA-ATPase inhibitor, Concanamycin A, leads to the loss of TGN/EE identity possibly due to an increase in the pH of the lumen. This resulted to a vacuolation of TGN/EE, while the Golgi cisternae were bending and got fragmented (Robinson *et al.*, 2004). Hence, the TGN integrity has an impact on the Golgi structure. Additionally, the tethering and the fusion of vesicles at the TGN might influence the Golgi structure maintenance. Syntaxin of plants (SYP) 41/42/43 and 61 are t-SNAREs that localise in the TGN and maintain its morphology. Intriguingly, a *syp42syp43* double mutant showed a curved *trans*-Golgi cisternae/TGN (Uemura *et al.*, 2012). Moreover, the putative tethering factor TNO1 interacts with SYP41 and is required for the correct localisation of SYP61. Their correct localisation and

operation is crucial for vesicle trafficking, e.g. under salt stress (Kim & Bassham, 2011). Vesicles from the TGN are released to their final destination either as clathrin-coated vesicles to the apoplast or via the prevacuolar compartment to the vacuole.

The entire secretory pathway can be further considered as an assembly line, which has different steps, and the cargos are passed on along the compartments. Along those steps, different processes take place and thus enzymes associated with these compartments have also a precise sub compartmental localisation, which is best shown by glycosyltransferases mediating glycosylation within the Golgi. Since glycosylation processes and glycan synthesis is a major task of secretory pathway function that is impacted by Ca^{2+}, it will be separately described in more detail in the following chapter.

1.2.1 Biosynthesis of Cell Wall Components and Glycosylation Processes in the Secretory Pathway

Glycosylation is a process that takes place in the compartments of the secretory pathway, starting mostly in the ER. The biosynthetic pathways of the required sugar monomers overlap with those used for cell wall polysaccharide precursors, including mannose, fucose, xylose, and galactose. Glycosylation describes the processes of posttranslational modifications of proteins, such like *O*-glycosylation and *N*-glycosylation among others (all shown in Figure 5). This process has been described in its complexity by Nagashima *et al.* (2018) for the *N*-glycosylation, Strasser *et al.* (2021), and He *et al.* (2021), whereby the latter includes the co-operation of the cations Ca^{2+} and Mn^{2+} for these modifications.
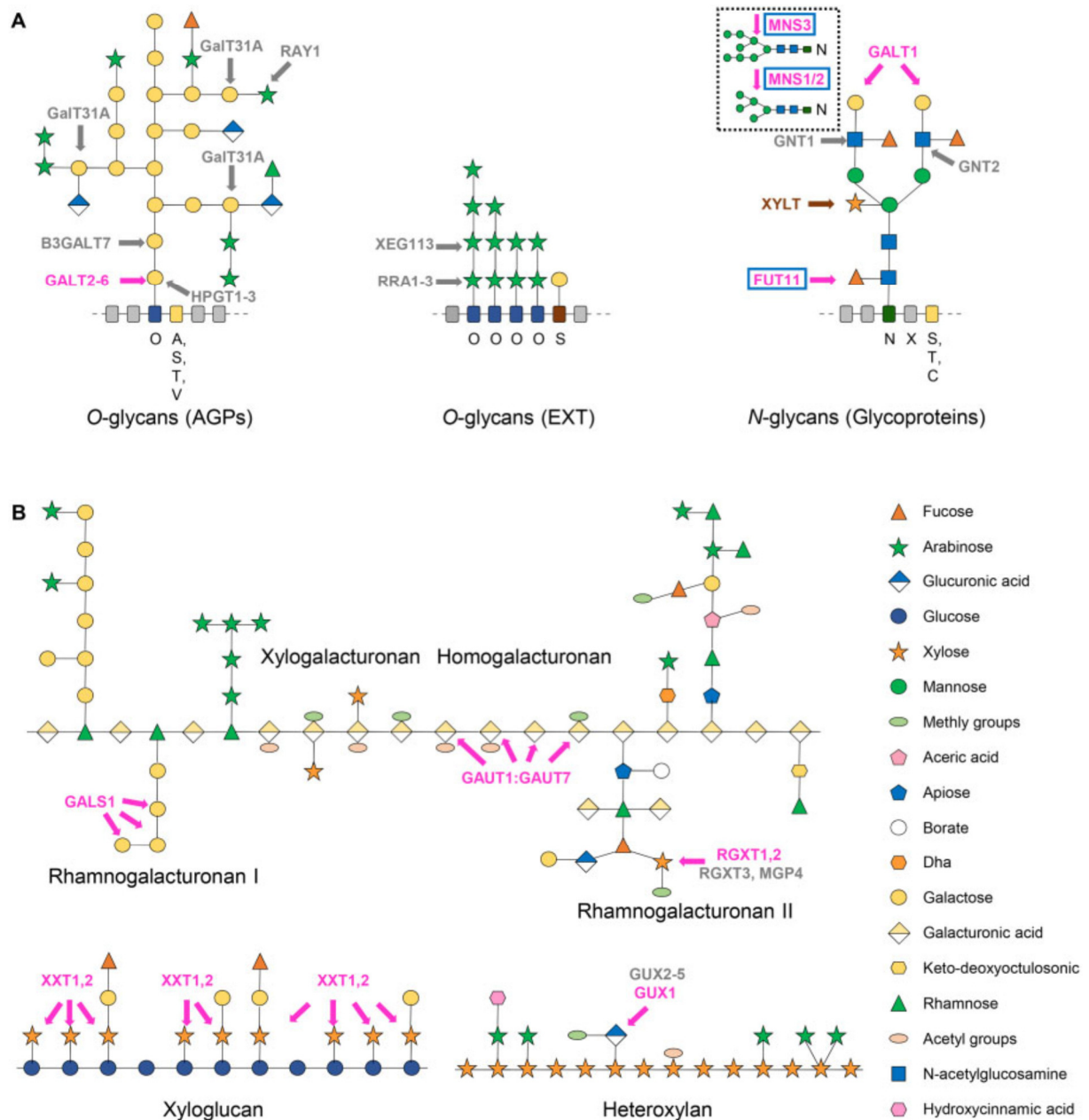
Figure 5: Glycosylation in the Golgi. Enzymes marked in magenta (experimentally shown) or in gray (predicted) to be Mn^{2+}-dependent. Enzymes that are also activated by Ca^{2+} are framed in blue and an enzyme that does not absolutely depend on Mn^{2+} is marked in brown. A, Schematic overview of enzymes that are involved synthesis of *O*-glycans (AGPs and EXTs), and enzymes involved in synthesis of *N*-glycans. B, Schematic overview of enzymes involved matrix sugar synthesis of the plant cell wall. Figure published in He *et al.* (2021).

The *O*-glycosylation is a form of protein glycosylation, and the *O*-glycans are attached to hydroxyproline (Hyp) in plant glycoproteins, occasionally attached to the hydroxyl group of serine (e.g. extensins (EXTs)). Arabinogalactan proteins (AGPs) and EXTs are the major *O*-glycosylated protein components next to the repetitive proline-rich proteins (PRPs). For instance, AtGALT2 to 6 are Golgi-localised Hyp-*O*-galactosyltransferases that transfer

galactose to the Hyp residues of AGPs; they require Mn^{2+} for their catalytic activity. EXTs include unbranched chains of up to five arabinose (Ara) units (Marzol *et al.*, 2018). Both, AGPs and EXTs occur in the plant cell wall, while AGPs are often anchored to the extracellular side of the plasma membrane and strongly glycosylated with arabinogalactan (AG) polysaccharides, but the molecular function of this glycosylation is still largely unknown. The AGs of the ß-glucuronyltransferase triple mutant *glcat14a/b/d* were shown to have lower Ca^{2+} binding capacities *in vitro* compared to those of the wild type, and GLCATs have an impact on cytosolic Ca^{2+} signalling (Lopez-Hernandez *et al.*, 2020).

The *N*-glycosylation (Figure 6) of proteins starts with the pre-assembled precursor, the *core*-oligosaccharide substrate glucose3mannose9glucoacetylglucosamine2 (Glc3Man9GlcNAc2) that is bound to dolichol phosphate, which is anchored in the ER membrane. The first step includes a transfer of this precursor to an asparagine (Asn) residue in the sequon "Asn-X-Ser/Thr" (NxS/T; x = any amino acid except proline) (Lowenthal *et al.*, 2016). This transfer is mediated by a conserved oligosaccharyltransferase (OT) complex in eukaryotes which is embedded in the ER membrane. Further, the OT complex was shown to be associated with ribosomes (Harada et al., 2009). The OT complex is nicely described in yeast, containing eight subunits which are encoded by nine genes, oligosaccharyltransferase (OST) 1, 2, 3, 4, 5, and 6, what germ agglutinin-binding (WBP) 1, suppressor of WB (SWP) 1, and saurosporine and temperature sensitive (STT) 3 (Knauer & Lehle, 1999). In Arabidopsis, the OT complex contains seven conserved subunits encoded by 12 genes, thereby two genes that encode *STT3* (*STT3a, STT3b*), the catalytically active subunits of the OT complex (Nagashima *et al.*, 2018). They bind the *core*-oligosaccharide substrate and thus mediate the transfer of the precursor (Ruiz-Canada *et al.*, 2009). Interestingly, it was shown that the depletion of STT3a causes lethality upon salt and osmotic stress in Arabidopsis (Koiwa *et al.*, 2003).
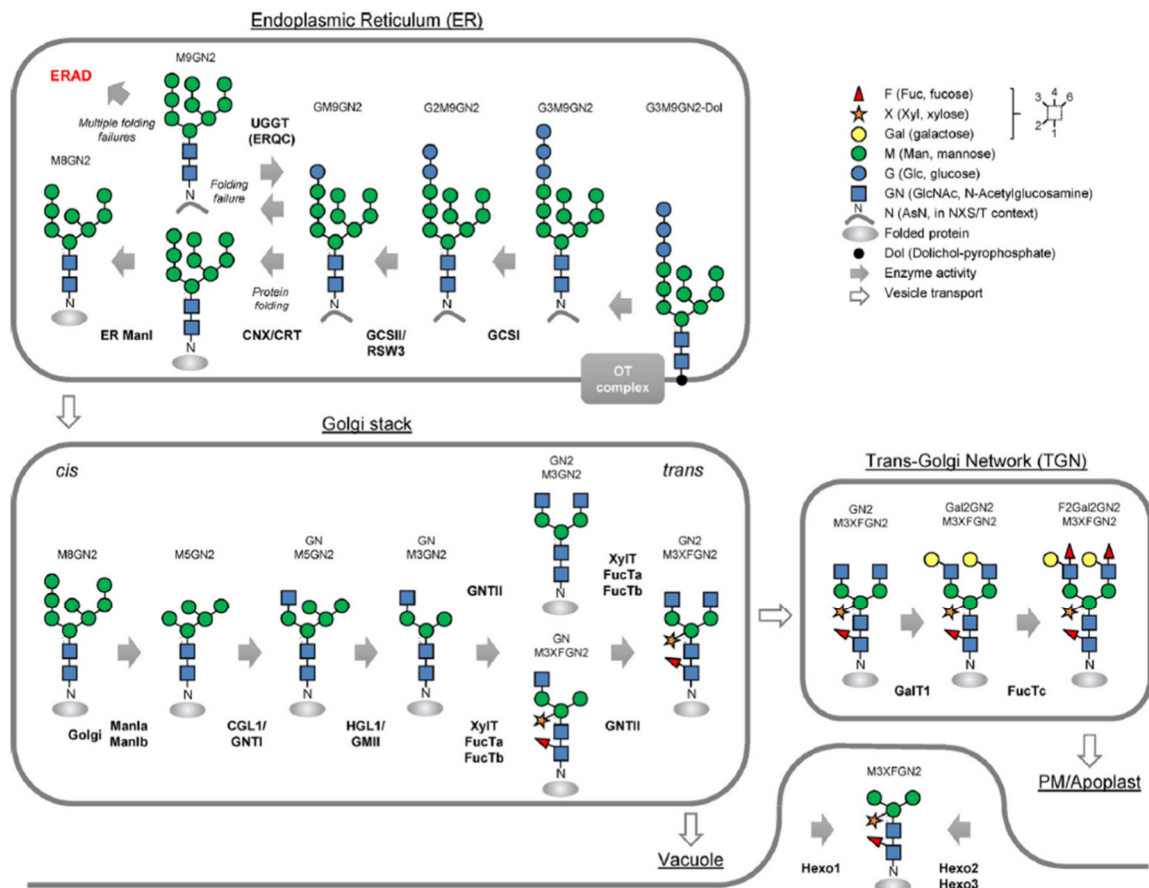
Figure 6: Process of *N*-glycosylation in the ER, the *cis*- to *trans*-Golgi, the *trans*-Golgi Network and the transport to their final destination. Figure published in Nagashima *et al.* (2018).

After the *core*-oligosaccharide is transmitted to the respective protein, glucosidase I (GCS1) removes a terminal glucose residue, followed by glucosidase II (GCS2) which removes another glucose residue. Afterwards, a further glucose residue is removed leading to a Man9GlcNAc2 structure. Subsequently, the proteins are folded by the lectin chaperones calnexin (CNX) and calreticulin, whereby the function of calreticulin is Ca^{2+}-dependent (1.2.2). If the proteins are not correctly folded, they are recognized by the UDP-glucose glycoprotein glucosyltransferase (UGGT). UGGT is a protein-folding sensor in the ER that can convey the wrongly folded protein to calreticulin and the lectin chaperon for refolding (Caramelo & Parodi, 2008). If this process fails, the proteins are going to be degraded by ER-associated degradation (ERAD) via ubiquitination. ERAD consists of an ubiquitin-activating enzyme (E1), an ubiquitin-conjugating enzyme (E2), an ubiquitin ligase (E3), and the 26S proteasome. Interestingly, a protein of the ERAD pathway, EMS-mutagenized bri1 suppressor 5 (EBS5), was shown to be crucial for salt

stress tolerance (Liu *et al.*, 2011). Further, ROS lead to ER stress that in turn promotes the accumulation of unfolded proteins due to lower chaperone activity (Ozgur *et al.*, 2015).

If proteins are not correctly folded and recognised by UGGT, a mannose residue is cleaved by the ER-resident α-mannosidase IV and V (MNS4, MNS5; ER ManI in Figure 6), and then proteins get degraded (Hüttner *et al.*, 2014). Properly folded proteins are transported by COPII vesicles to the *cis*-Golgi. α-1,2-Mannosidase I (MNS1) specifically localises to the *cis*- and *medial*-Golgi cisternae (Donohoe *et al.*, 2013), cleaves the terminal mannose residue (Kajiura *et al.*, 2010), and requires either Ca^{2+} or Mn^{2+} as cofactor (Liebminger *et al.*, 2009). The ß-1,2-*N*-acetylglucosaminyltransferase I, also called complex glycan-less (CGL1), adds an additional *N*-acetylglucosamine. Interestingly, *cgl1* mutants show a salt sensitivity. A lack of *N*-glycosylated proteins might play a role in cell wall formation (Kang *et al.*, 2008).

The glycosylation sequence then continues by the α-mannosidase II (MNS2), also called hybrid glycan I (HGL1) that removes another mannose residue, resulting in the *N*-linked glycosylic chain of GlcNAcMan3GlcNAc2. Liu *et al.* (2018) showed that a double mutant lacking *MNS1* and *MNS2* has a diminished growth when grown under salt stress. Hereafter, complex *N*-glycosylation takes place in the later Golgi by adding xylose by xylosyltransferase T (XylT) and fucose by fucosyltransferases such as FUT1, resident in the *trans*-Golgi (Parsons *et al.*, 2019). In animal cells, sialyltransferases further add sialic acid to the nascent oligosaccharide, which is absent in plants (Nagashima *et al.*, 2018). However, it was shown that the sialyltransferase of rats localises in the *trans*-Golgi of Arabidopsis (Wee *et al.*, 1998), which in accordance with its function in the final steps of *N*-glycosylation in animal cells.

The major carbohydrate fractions in the cell wall are cellulose, hemicellulose, and pectin, whereby the latter are linked with the secretory pathway, specifically with the Golgi (Zhang *et al.*, 2021). While cellulose synthesis occurs at the plasma membrane, the synthesis of hemicellulose and pectins occurs in the Golgi. The polysaccharides of the hemicelluloses consist of various monosaccharide residues, mostly pentoses like xylose and arabinose, but also hexoses such as glucose, mannose, and galactose (Figure 5). In contrast, pectins are complex acidic polysaccharides that are rich in galacturonic acid (GalA) and include homogalacturonan (HG), rhamnogalacturonan I (RG-I), and RG-II domains, as well as xylogalacturonan and apiogalacturonan in some plant species (Atmodjo *et al.*, 2013). HG

synthesis in the Golgi is catalysed by members of the galacturonosyltransferase (GAUT) family and has critical roles in pollen tube growth and male fertility in Arabidopsis (Lund *et al.*, 2020). In addition, pollen tube growth is also impaired in *alg11* mutants, and their pollen tubes burst during growth (Zupunski, 2020). In yeast, a homologue of *ALG11* codes for alpha-1,2-mannosyltransferase and is localised in the endoplasmic reticulum. Here, ALG11 plays a role in the synthesis of the *core*-oligosaccharide substrate for *N*-glycosylation (Cipollo *et al.*, 2001). Intriguingly, *alg11* mutants of Arabidopsis showed also a decreased germination rate under high salt conditions among other abiotic stimuli. Thus, ALG11 was shown to play a role in cell wall synthesis (Zhang *et al.*, 2009). Moreover, it is known that salt stress leads to the conversion of cell wall components, mainly pectin. FERONIA (FER), a receptor kinase from Arabidopsis, localises in the plasma membrane and recognizes these perturbations of cell wall components by binding to pectins, as shown *in vitro* (Feng *et al.*, 2018). FER was shown to be necessary for the restoration of root growth after high salt stress through Ca^{2+} signalling. Similar salt-induced phenotypes have also been observed for several mutants with defective enzymes of the *N*-glycosylation pathway resident in the ER and Golgi apparatus (Koiwa *et al.*, 2003, Kang *et al.*, 2008, Farid *et al.*, 2011, Liu *et al.*, 2018).

1.2.2   Functions of Calcium in the Endoplasmic Reticulum

Within the ER of eukaryotic cells, the Ca^{2+}-binding protein calreticulin is an important molecular chaperone with diverse functions (Jia *et al.*, 2009). Unlike its animal counterpart, plant calreticulin is glycosylated. As a molecular chaperone, it mediates folding of glycoproteins and determines growth, development, and stress responses. It has been shown in animals that calreticulin modulates Ca^{2+} homeostasis due to its high capacity for Ca^{2+}-binding. In animal cells, the ER indeed represents the main intracellular Ca^{2+} store for the

generation of cytosolic Ca^{2+} signals. Inverse changes of $[Ca^{2+}]_{cyt}$ and $[Ca^{2+}]_{ER}$ have been directly demonstrated by simultaneous imaging of reporters targeted to both compartments (Palmer *et al.*, 2004). Due to its reticulate structure, the ER is predestined to mediate localised Ca^{2+} fluxes, which are a prerequisite for spatio-temporally specific $[Ca^{2+}]_{cyt}$ signals. Polarization of Ca^{2+} fluxes across ER membranes allows some animal cell types to employ the ER as intracellular "Ca^{2+} tunnel" (Petersen *et al.*, 2017), a mechanism that has not been demonstrated in plants for Ca^{2+} yet, but, intriguingly, for Zn^{2+} (Sinclair *et al.*, 2018).

In plants, due to the overwhelming size of the vacuole, the role of the ER in Ca^{2+} signalling has been taken little into consideration in the past. However, this picture is currently changing. Using an ER-targeted Ca^{2+} reporter, distinct changes in $[Ca^{2+}]_{ER}$ upon stimulation have been revealed (Bonza *et al.*, 2013). Unlike in animals, $[Ca^{2+}]_{ER}$ in plants increased upon $[Ca^{2+}]_{cyt}$ transients, which implies a role of the ER as Ca^{2+} buffer rather than Ca^{2+} source (Bonza *et al.*, 2013). It has recently become apparent that $[Ca^{2+}]_{ER}$ homeostasis determines NaCl-induced $[Ca^{2+}]_{cyt}$ signals and plant sensitivity to salt stress (Corso *et al.*, 2018). Furthermore, the phloem ER has been identified as Ca^{2+} store mediating a long-distance $[Ca^{2+}]_{cyt}$ wave in response to H_2O potential gradients, hence determining the root growth toward H_2O (Shkolnik *et al.*, 2018). Specifically in some leguminous plants, Ca^{2+} release from the phloem ER plays a further role in the swelling of forisomes, proteins that expand upon Ca^{2+} binding and in turn block sieve tubes in response to disturbances (Furch *et al.*, 2009).

The ER is continuous with the nuclear envelope (NE), which engulfs the nucleus. The steady-state $[Ca^{2+}]$ in the nucleus is similar to that in the cytosol and increases transiently or repetitively upon perception of environmental and developmental stimuli (Mazars *et al.*, 2009), including pathogen-associated molecular patterns (PAMPs; Lecourieux *et al.*, 2005) or microbial-derived symbiotic molecules, such as Nod factors that initiate symbiosis with rhizobial bacteria (Sieberer *et al.*, 2009). The topic of nuclear Ca^{2+} signalling has recently been covered in an excellent review (Charpentier, 2018). Nuclear Ca^{2+} transients often follow cytosolic ones, but nuclei have also been demonstrated to be autonomous in the generation of Ca^{2+} signals, what requires Ca^{2+} release from the NE. Nuclear Ca^{2+} signals, whose kinetics differ with different stimuli, can be decoded by Ca^{2+}-regulated protein kinases, such as CCaMK in the initiation of symbioses (Singh & Parniske, 2012). Besides their central position in symbiotic signalling, nuclear Ca^{2+} signatures also regulate root development (Leitão *et al.*,

2019). As discussed, Ca^{2+}-permeable channels and transporters that generate those Ca^{2+} signals have been identified.

1.2.3 Evidence of Cellular Regulation by Calcium in the Golgi Apparatus, the *trans* Golgi Network and the Prevacuolar Compartment

This section has been published in: He J, Rössner N, Hoang MTT, Alejandro S, Peiter E (2021) Transport, functions, and interaction of calcium and manganese in plant organellar compartments. Plant Physiology, Vol 187, 1940–1972. DOI: 10.1093/plphys/kiab122. The section has been written by Nico Rössner.

The luminal homeostasis of ions, including Ca^{2+} and Mn^{2+}, next to the pH determines Golgi functions (Kellokumpu, 2019). However, our functional understanding of Ca^{2+} in the plant's Golgi apparatus and other vesicular compartments is still scant. In the Golgi, post-translational modifications like glycosylation often require bivalent cations as cofactors. Albeit this is mostly Mn^{2+}, some enzymes, such as ER-type α-mannosidase I (MNS3), employ Ca^{2+} or Mn^{2+} for their catalytic activity (Liebminger *et al.*, 2009). In tobacco (*Nicotiana tabacum*), Ca^{2+} serves as cofactor for a Golgi-localised calreticulin, likely required for correct protein folding similarly to ER-located calreticulin (Nardi *et al.*, 2006).

In animal cells, a $[Ca^{2+}]$ gradient exists along the compartments of the secretory pathway that is likely of functional relevance (Suzuki *et al.*, 2016). Whereas the basal free Ca^{2+} in the ER is around 700 mM, free Ca^{2+} in the Golgi is lower, decreasing from 150–300 µM in the *cis*-Golgi to 50–100 µM in the *trans*-Golgi (Aulestia *et al.*, 2015). Similarly, there is a pH gradient along the compartments of the animal secretory pathway (Kellokumpu, 2019). A gradient of decreasing pH is also observed along the plant secretory pathway (Shen *et al.*, 2013), whereby an increase from Golgi to pre-vacuolar compartment (PVC) and late PVC has been observed (Martinière *et al.*, 2013). In contrast, this has not been assessed for Ca^{2+} yet. Intriguingly, the single available report on $[Ca^{2+}]$ in the plant Golgi showed a concentration of merely 0.7 µM (Ordenes *et al.*, 2012). This indicates that $[Ca^{2+}]_{Golgi}$ homeostasis in plants may differ substantially from that in animals. However, determination of absolute $[Ca^{2+}]$ in the secretory

pathway is challenging. Albeit precise targeting to subcompartments is pursuable by genetically encoded Ca^{2+} indicators (GECIs), a formidable challenge lies in the pH dependence of most of those fluorescence-based reporters (Suzuki *et al.*, 2016). Because of this, the luminescent reporter aequorin is still a suitable tool to report Ca^{2+} in acid compartments due to its independence of pH (Brini, 2008).

Free Ca^{2+} in the plant Golgi is responsive to various stimuli. In response to cold shock, mechanical stimulation, or hyperosmotic stress, Ordenes *et al.* (2012) monitored an increase in $[Ca^{2+}]_{Golgi}$ that was delayed compared to the $[Ca^{2+}]_{cyt}$ rises. This led to the conclusion that Ca^{2+} is moved into the Golgi apparatus to restore the basal $[Ca^{2+}]_{cyt}$. Apart from that, an increase in $[Ca^{2+}]_{Golgi}$ induced by environmental stimuli may regulate vesicular trafficking, which is required to cope with stresses, for example, salt stress (Leshem *et al.*, 2006).

Secretory proteins, molecules, and lipids traverse through the secretory pathway including the Golgi apparatus, the *trans*-Golgi network (TGN), and the PVC. In plants, vacuolar sorting receptors (VSRs) are involved in cargo transport to the vacuole (Miao *et al.*, 2006). VSRs contain epidermal growth factor (EGF)-like repeats which play a role in Ca^{2+} interaction, and the binding of vacuolar sorting determinants (VSDs) to VSRs occurs in a Ca^{2+}-dependent manner (Suen *et al.*, 2010, Robinson & Pimpl, 2014). Consequently, Künzl *et al.* (2016) concluded that VSDs bind to VSRs in ER and Golgi at neutral pH and high $[Ca^{2+}]$, whereas VSRs release VSDs in the TGN or in PVCs under mildly acidic pH and low $[Ca^{2+}]$. In addition, in animals, the sorting of secretory proteins depends on the import of Ca^{2+} into the TGN by the secretory pathway Ca^{2+}- ATPase 1 (SPCA1) in a sphingomyelin-dependent manner (Deng *et al.*, 2018).

Besides the potential regulatory activity of Ca^{2+} within organelles of the secretory pathway, its release will cause local $[Ca^{2+}]_{cyt}$ elevations that may be sensed by secretory pathway-localised proteins. For instance, the auxin derivate 2,4-D induced a decrease in $[Ca^{2+}]_{Golgi}$ (Ordenes *et al.*, 2012). Several Ca^{2+}-sensing proteins associated with the secretory pathway have been identified. For instance, AGD12 and EHB1, located to the TGN, contain a cytosolic Ca^{2+}- binding C2 domain (Dümmer *et al.*, 2016). AGD12 is an activator of ARF GTPases that mediate vesicular transport and membrane docking (Nielsen *et al.*, 2008). Mutants lacking either of those proteins are affected in gravitropism, which is regulated by auxin (Dümmer *et al.*, 2016) and $[Ca^{2+}]_{cyt}$ -dependent (Monshausen *et al.*, 2011, Shih *et al.*, 2015). A decrease in $[Ca^{2+}]_{Golgi}$ might

thus lead to local $[Ca^{2+}]_{cyt}$ elevations around the Golgi that trigger AGD12 and EHB1. Interestingly, EHB1 has recently been described to inhibit the Fe^{2+} (and Mn^{2+}) uptake transporter IRT1 in a Ca^{2+}-dependent way, albeit in that study, EHB1 was localised to the plasma membrane (Khan *et al.*, 2019).

In Arabidopsis, two calmodulin-like proteins, CML4 and CML5, with yet unknown function are localised to organelles of the secretory pathway (Ruge *et al.*, 2016). Their CaM domain faces the cytosol and will thus sense $[Ca^{2+}]_{cyt}$ elevations around those compartments. Finally, synaptotagmins (SYTs), which contain two cytosolic C2 domains, are also predestined targets of such local $[Ca^{2+}]_{cyt}$ hotspots. In animals, SYTs regulate membrane trafficking and fusion in a Ca^{2+}-dependent manner (Südhof, 2013). Out of the five SYTs in Arabidopsis, SYT2 has been localised to the Golgi apparatus and suggested to be required for unconventional secretion (Zhang *et al.*, 2011) as well as for conventional exocytosis in pollen tubes, whereby it is additionally localised at the plasma membrane (Wang *et al.*, 2015).

1.2.4 Calcium and Manganese Transport within Compartments of the Secretory Pathway

The transport of Ca^{2+} cannot be regarded in isolation and coincides with that of other bivalent cations like Mn^{2+} (He *et al.*, 2021). Ca^{2+} homeostasis as well as Mn^{2+} homeostasis need to be guaranteed by passive and active transport mechanisms to ensure optimal concentrations of these elements. In animal cells, Ca^{2+} release from the ER is mediated by two types of ligand-gated channels, the Ryanodine receptors (RyRs) that are activated by cyclic adenosine diphosphate ribose (cADPR) and inositol trisphosphate receptors (IP3Rs) (Kellokumpu, 2019). There are no homologues of both transport proteins in plants (Nagata *et al.*, 2004). In plants, two channel proteins, GLR3.1 and GLR3.3, have been shown to localise in an ER-like structure in xylem contact cells and phloem sieve cell elements, respectively (Nguyen *et al.*, 2018), next to their previously shown localisation in the plasma membrane of other cell types (Meyerhoff *et al.*, 2005, Teardo *et al.*, 2011, Kong *et al.*, 2016, Mou *et al.*, 2020). These channels have an impact on systemic Ca^{2+} signals and electropotential waves induced by wounding upon an herbivory attack (Farmer *et al.*, 2020). When lacking the carboxy-terminal tail of GLR3.3, the

wound-induced electrical signal is damped (Wu *et al.*, 2022). A recent study of Bellandi *et al.* (2022) supported that GLR3.3 is a main player in systemic Ca^{2+} signalling upon wounding. Further studies ought to focus on the localisation of GLR3.3 and analyse the function of modified channels that are resident in the ER only.

In the Golgi of animal cells, Ca^{2+} release is also mediated by RyRs and IP3Rs, as in the ER (Kellokumpu, 2019). In contrast to the ER, there is no evidence of known channels that mediate the release of Ca^{2+} from the plant Golgi, yet. Since the free Ca^{2+} concentration in the Golgi is merely at around 0.7 µM (Ordenes *et al.*, 2012), it seems to be distinct to that in the animal Golgi, which is much higher, ranging from 0.5 to 1 mM (Suzuki *et al.*, 2016). The question how the lumenal Ca^{2+} concentration in plants is regulated to ensure a basal concentration optimal for Golgi Ca^{2+}-related processes needs to be addressed (He *et al.*, 2021).

In yeast, the Golgi-localised GDT1 protein (1.1.2) was suggested to operate as Ca^{2+}/Mn^{2+} antiporter (Dulary *et al.*, 2018) and thus might operate to release Ca^{2+} from the compartment. Initially, it was suggested that transporters of this family work as Ca^{2+}/H^+ antiporters (Demaegd *et al.*, 2013). The transport mechanism is not fully understood, yet, but there are hints that it is required for Mn^{2+} and Ca^{2+} supply of the Golgi and that it affects cellular pH. The closest homologue of yeast GDT1 and human TMEM165 in plants is BICAT3, which was shown to complement yeast mutants with impaired Ca^{2+} and Mn^{2+} homeostasis and thus might transport Mn^{2+} and Ca^{2+} (He *et al.*, 2022). BICAT3 was shown to localise to the Golgi (Yang *et al.*, 2021, He *et al.*, 2022). It was suggested that the role of BICAT3 in the Golgi was the supply of Mn^{2+} that is required for many glycosyltransferases. Indeed, the cell wall composition of *bicat3* changed under Mn^{2+} deficiency, and a decrease of fusose, galactose, xylose, and galacturonic acid was observed (He *et al.*, 2022). Furthermore, Yang *et al.* (2021) showed by Western blot analyses that there were less proteins with xylose and fucose modifications in *bicat3* mutants under Mn^{2+} deficiency. Next to the effects in Golgi-associated processes, photosynthetic performance under Mn^{2+} deficiency was increased in *bicat3*, although the mutant was diminished in growth (He *et al.*, 2022). It was concluded that, since the transport of Mn^{2+} into the Golgi was affected in *bicat3*, other compartments, e.g. chloroplasts received a larger quantity of this metal. Although the role for BICAT3 as Ca^{2+} transporter was indicated by yeast complementation assays, it is still unclear what impact it might have on Ca^{2+} homeostasis in the Golgi.

Two further proteins of the BICAT family that likely transport Ca^{2+} and Mn^{2+} localise to the secretory pathway, BICAT4 and BICAT5. Both of them were localised in the ER and they are expressed in distinct tissues, so that they might have partially redundant functions (Hoecker *et al.*, 2020). Their role has to be further investigated.

Next to BICATs that might load the Golgi and the ER with Ca^{2+} and Mn^{2+}, there are pumps that localised in compartments of the secretory pathway. Especially, P_{2A}-type ATPases are associated with secretory pathway compartments. In animal cells, the P_{2A}-type ATPases, sarcoendoplasmic reticulum Ca^{2+}-ATPase 2 (SERCA2) and secretory pathway Ca^{2+}-ATPase 1 and 2 (SPCA1 and 2), localise to the Golgi apparatus and the *trans*-Golgi Network (Kellokumpu, 2019). SPCA1 contains a N-terminal Ca^{2+}-binding EF hand motif that increases the relative turnover rate of Ca^{2+} (Chen *et al.*, 2019). This mechanism is similar to that of the yeast Ca^{2+}-transporting plasma membrane ATPase related 1 (PMR1) that is the only P_{2A}-type ATPase in *Saccharomyces cerevisiae*. PMR1 also mediates the sequestration of excess Mn^{2+} in yeast. In plants, there are four P_{2A}-type ATPases that are related to SERCAs of animal cells (Bossi *et al.*, 2019). The most extensively studied SERCA relative in Arabidopsis, endoplasmic reticulum-type Ca^{2+}-transporting ATPase 1 (ECA1) was shown to localise in the ER (Wu *et al.*, 2002). It has recently been shown that Mizu-Kussey 1 (MIZ1), a protein of unknown function associated with the ER membrane, interacts with and inhibits ECA1 to balance the Ca^{2+} influx and efflux required for systemic Ca^{2+} signals triggering root bending towards water (Shkolnik *et al.*, 2018). Furthermore, Arabidopsis *eca1* mutants showed a growth inhibition by high Mn^{2+}, indicating that ECA1 is important for tolerance to toxic levels of Mn^{2+} (Wu *et al.*, 2002). Two other ECA proteins, ECA2 and ECA4, might operate in the ER as well, since they have an ER retention motif and thus might localise in the ER (Bossi *et al.*, 2019). The absence of an impaired growth of *eca1* under standard growth conditions suggests the existence of other mechanisms responsible for Mn^{2+} and Ca^{2+} transport into the ER, with ECA2 and ECA4 being suitable candidates that might operate redundantly (He *et al.*, 2021). Intriguingly, ECA1 is insensitive to the SERCA inhibitor thapsigargin because it lacks the conserved binding site (Liang et al., 1998). However, an ECA1 protein from tomato showed a sensitivity to thapsigargin (Johnson *et al.*, 2009). ECA3 is the only protein of this family in Arabidopsis that does not localise in the ER, but in the Golgi (Mills *et al.*, 2008) and partially in the PVC (Li *et al.*, 2008a). ECA3 harbours the conserved binding site for thapsigargin (Li *et al.*, 2008a), although its sensitivity to thapsigargin has not been experimentally tested yet. However, Ca^{2+} pump

activity in the Golgi membranes of pea showed an inhibition by thapsigargin (Ordenes *et al.*, 2002). Taken together, inhibition by thapsigargin may only influence cation uptake by the Golgi, but not the ER. An Arabidopsis *eca3* mutant was shown to be sensitive to high Mn^{2+} supply, and thus ECA3 might pump excessive Mn^{2+} into the Golgi for detoxification by secretion like PMR1 does in yeast. In addition, *eca3* is sensitive to low-Ca^{2+} conditions, which suggests a role of ECA3 in Ca^{2+}-related processes within the Golgi (He et al., 2021).

While the mutant of the Golgi-localised transport protein BICAT3 showed a better photosynthesis (He *et al.*, 2022), photosynthesis was impaired in *eca3* (Mills *et al.*, 2008). Thus it was concluded that ECA3 and BICAT3 might have different tasks for metal supply in the Golgi (Wege, 2022). Next to ECAs, the P_{2B}-type Ca^{2+}-ATPases, ACA1, 2, and 7 are resident in the ER and contribute to growth and pollen fitness (Harper *et al.*, 1998, Rahmati Ishka *et al.*, 2021). ACA1, 2, and 7 might be functionally redundant since only the triple mutant showed affected pollen fitness (Rahmati Ishka *et al.*, 2021).

Besides those pumps, there are other transporters operating in compartments of the secretory pathway. CCX2 was shown to localise in the ER and appears to be directly involved in the control of Ca^{2+} fluxes between the ER and the cytosol, hence regulating Ca^{2+} dynamics within the ER. Its action strongly influences plant growth under salt and osmotic stress (Corso *et al.*, 2018). It remains unclear what function and localisation other CCXs might have and whether they might also impact Ca^{2+} concentrations in other compartments.

1.3 Objectives of this Thesis

This project aimed to achieve three main objectives: first, the characterisation of the two known Golgi-resident proteins involved in Ca^{2+} transport, BICAT3 and ECA3; second, the determination of free Ca^{2+} levels in the *cis-* and *trans-*Golgi ($[Ca^{2+}]_{cis\text{Golgi}}$, $[Ca^{2+}]_{trans\text{Golgi}}$); third, the elucidation of the impact of ECA3 and BICAT3 on $[Ca^{2+}]_{cis\text{Golgi}}$ and $[Ca^{2+}]_{trans\text{Golgi}}$.

The characterisation of two Ca^{2+} transport proteins, ECA3 and BICAT3, respectively, was pursued as first part of the project. Therefore, ECA3 needed to be localised anew since its localisation was still on debate and thus not clarified yet, and a precise sub compartmental localisation of BICAT3 should be implemented. Moreover, the expression patterns of *ECA3*

and *BICAT3* should be examined by fusing their promoters with a nuclear-targeted triple Venus (NLS3xVenus) and with ß-Glucuronidase. In addition, a co-expression analysis ought to be performed *in silico*. Based on the obtained data, the mutants lacking *BICAT3* and *ECA3* needed to be studied for impaired development under different environmental cues.

To analyse the free Ca^{2+} levels in the *cis*- and *trans*-Golgi ($[Ca^{2+}]_{Golgi}$), reporter protein fusions to specifically target these vesicular organelles were generated. Therefore, a TMD for targeting the fusion protein was fused to an EGFP to validate the correct localisation and to the Ca^{2+}-binding photoprotein aequorin. To discriminate between the measured $[Ca^{2+}]$ transients, the subcompartmental localisation ought to be confirmed. Stable transgenic *A. thaliana* lines expressing these fusion proteins should be generated. With the aid of these reporter lines the basal $[Ca^{2+}]$ levels of the *cis*- and *trans*-Golgi ought to be determined and compared to those of the cytosol. Moreover, these reporter lines should reveal insights in transient Ca^{2+} elevations in different compartments of the Golgi in response to environmental stresses.

To investigate the impact of ECA3 and BICAT3 on identified $[Ca^{2+}]_{Golgi}$ transients, *eca3* and *bicat3* single mutants and a double mutant expressing the aequorin reporter fusions should be generated. Changes in $[Ca^{2+}]_{Golgi}$ in those lines were to be compared to those in the wild type expressing these reporters.

2 Material & Methods

2.1 DNA Vectors and Constructs

All DNA vectors and constructs that were used or generated in this study are listed in the following Table 1. A short purpose of usage is mentioned as well as the source for possible inquires.

Table 1: DNA vectors that were used in this study and constructs that were generated for this research.

Name	Utilization	Resistence	Source
pART7-USER (Appendix Figure 33)	Empty pART7 for insertions by USER cloning	Amp^R	Gleave et al., 1992 modified by Tina Peiter-Volk
pART7-EGFP-USER (Appendix Figure 34)	Empty pART7-*EGFP* for insertions by USER cloning (N-terminal EGFP)	Amp^R	provided by Tina Peiter-Volk
pART7-USER-mCherry (Appendix Figure 35)	Empty pART7-*mCherry* for insertions by USER cloning (C-terminal mCherry)	Amp^R	provided by Tina Peiter-Volk
pBART	Empty pBART for insertion of NotI-digested pART7 insertion for further *A. thaliana* and *N. benthamiana* transformation	Spec^R BASTA^R	Gleave et al., 1992
pCambia3300-USER (Appendix Figure 36)	Empty pCambia3300 for further *A. thaliana* and *N. benthamiana* transformation	Kan^R BASTA^R	provided by Patrick Bienert
pART7-EGFP-ECA3 (Appendix Figure 37)	*EGFP* N-terminally fused to *ECA3* for subcellular localisation in *A. thaliana*	Amp^R	generated in this study
pART7-BICAT3-mCherry	*mCherry* C-terminally fused to *BICAT3* for subcellular localisation in *A. thaliana*	Amp^R	provided by Jie He
pBART-EGFP-ECA3	*EGFP* N-terminally fused to *ECA3* for subcellular localisation in *N. benthamiana*	Spec^R BASTA^R	generated in this study
pBART-BICAT3-mCherry	*mCherry* C-terminally fused to *BICAT3* for subcellular localisation in *N. benthamiana*	Spec^R BASTA^R	generated in this study
pART7-MNS1tmd-EGFP-AEQ (Appendix Figure 38)	Construct to specifically target an *EGFP-AEQ* fusion to the *cis*- and *medial*-Golgi cisternae	Amp^R	generated in this study

pART7-FUT1tmd-EGFP-AEQ (Appendix Figure 39)	Construct to specifically target an *EGFP-AEQ* fusion to the *trans*-Golgi cisternae	Amp[R]	generated in this study
pART7-EGFP-AEQ-BP-80(Y612A)	Construct to specifically target an *EGFP-AEQ* fusion to the *trans*-Golgi Network	Amp[R]	generated in this study
pART7-SYP41-EGFP-AEQ	Construct to specifically target an *EGFP-AEQ* fusion to the *trans*-Golgi Network	Amp[R]	generated in this study
pBART-MNS1tmd-EGFP-AEQ	Construct to specifically target an *EGFP-AEQ* fusion to the *cis*- and *medial*-Golgi cisternae for stable transformation of *A. thaliana*	Spec[R] BASTA[R]	generated in this study
pBART-FUT1tmd-EGFP-AEQ	Construct to specifically target an *EGFP-AEQ* fusion to the *trans*-Golgi cisternae for stable transformation of *A. thaliana*	Spec[R] BASTA[R]	generated in this study
pART7-SYP31-mCherry	*mCherry* C-terminally fused to a *cis*-Golgi marker SYP31 for subcellular co-localisation studies	Amp[R]	generated in this study
pART7-SYP41-mCherry	*mCherry* C-terminally fused to the *trans* Golgi Network marker SYP41 for subcellular co-localisation studies	Amp[R]	generated in this study
pART7-MNS1tmd-mGFP5	*mGFP5* C-terminally fused to the *cis*- and *medial*-Golgi marker *MNS1tmd* for subcellular co-localisation studies	Amp[R]	provided by Jie He
pART7-MNS1tmd-mCherry	*mCherry* C-terminally fused to the *cis*- and *medial*-Golgi marker *MNS1tmd* for subcellular co-localisation studies	Amp[R]	provided by Jie He
pART7-sialyltransferase-mGFP5	*mGFP5* C-terminally fused to the *trans*- Golgi marker *sialyltransferase* for subcellular co-localisation studies	Amp[R]	provided by Jie He
pART7-sialyltransferase-mCherry	*mCherry* C-terminally fused to the *trans*-Golgi marker *sialyltransferase* for subcellular co-localisation studies	Amp[R]	provided by Jie He
pBART-SYP31-mCherry	*mCherry* C-terminally fused to the *cis*-Golgi marker *SYP31* for subcellular co-localisation studies in *N. benthamiana*	Spec[R] BASTA[R]	generated in this study
pBART-MNS1tmd-mGFP5	*mGFP5* C-terminally fused to the *cis*- and *medial*-Golgi marker *MNS1tmd*	Spec[R] BASTA[R]	generated in this study

	for subcellular co-localisation studies in *N. benthamiana*		
pBART-MNS1tmd-mCherry	*mCherry* C-terminally fused to the *cis-* and *medial*-Golgi marker *MNS1tmd* for subcellular co-localisation studies in *N. benthamiana*	Kan^R BASTA^R	generated in this study
pBART-sialyltransferase-mGFP5	*mGFP5* C-terminally fused to the *trans-* Golgi marker *sialyltransferase* for subcellular co-localisation studies in *N. benthamiana*	Spec^R BASTA^R	generated in this study
pBART-sialyltransferase-mCherry	*mCherry* C-terminally fused to the *trans*-Golgi marker *sialyltransferase* for subcellular co-localisation studies in *N. benthamiana*	Spec^R BASTA^R	generated in this study
pCambia3300-pECA3-EGFP-GUS (Appendix Figure 40)	*EGFP-GUS* fusion under control of the promoter of *ECA3* for expression analysis	Kan^R BASTA^R	generated in this study
pCambia3300-pECA3-NLS3xVenus (Appendix Figure 41)	Triple *Venus* targeted to the nucleus under control of the promoter of *ECA3* for expression analysis	Kan^R BASTA^R	generated in this study
pCambia3300-pBICAT3-NLS3xVenus (Appendix Figure 42)	Triple *Venus* targeted to the nucleus under control of the promoter of *BICAT3* for expression analysis	Kan^R BASTA^R	generated in this study
pCambia3300-pECA3-EGFP-ECA3 (Appendix Figure 43)	*EGFP-ECA3* fusion under control of the promoter of *ECA3* for complementation of *eca3-2*	Kan^R BASTA^R	generated in this study

2.2 Oligonucleotides

The oligonucleotides that were used in this study are divided into two types which are listed in Table 2 and Table 3.

The melting temperature (T$_m$) was calculated by the following equation:

T$_M$ (°C) = 69.3 + [41 (n$_G$ + n$_C$) / s − (650 / s)]; n$_G$ = number of Guanin (G); n$_C$ = number of Cytosine (C); s = number of all nucleotides in the oligonucleotide sequence

T$_M$ was used for the calculation of annealing temperature (T$_A$) of two oligonucleotides in Polymerase Chain Reactions (PCR):

T_A (°C) = [($T_{M(1)}$ + $T_{M(2)}$) / 2] − 3; $T_{M(1)}$= T_M of the first oligonucleotide; $T_{M(2)}$= T_M of the second oligonucleotide

In Table 2, the oligonucleotides designed for amplification of fragments containing overhangs for USER cloning are listed. The specific Uracil (U)-containing sequence is underlined.

Table 2: USER oligonucleotides for amplification of USER fragments that were used in this study. Overhangs for USER cloning that were added to the oligonucleotides are underlined.

No	Name	Sequence (5´-> 3´)	Amplicon
1	U_MNS1tmd_for	GGCTTAAUATGGCGAGAGGGAGCAGATC	*MNS1tmd*
2	U_MNS1tmd_rev_linkerEGFP	ACCATGAGAGUTTGACGGTCCCAGA	*MNS1tmd*
3	U_EGFP_for_linkerMNS1tmd	ACTCTCATGGUGAGCAAGGGCGAGGA	*EGFP*
4	U_EGFP_rev_linkerAEQ	ATTCCTCCTCCCUGTACAGCTCGTCCATGCC	*EGFP*
5	U_AEQ_for_linkerEGFP	AGGGAGGAGGAAUGACCAGCGAACAATACTCA	*AEQ*
6	U_AEQ_rev	GGTTTAAUTTAGGGGACAGCTCCACCG	*AEQ*
7	U_FUT1tmd_for	GGCTTAAUATGGATCAGAATTCGTACAGGAG	*FUT1tmd*
8	U_FUT1tmd_rev_linkerEGFP	ACCATTCCGAAGCUAAGCTTATCAGAATTGATGT	*FUT1tmd*
9	U_EGFP_for_linkerFUT1tmd	AGCTTCGGAATGGUGAGCAAGGGCGAGGA	*EGFP*
10	U_promoterECA3_for	GGCTTAAUGTGTACAGTTGTATAGTTTACCAAC	promoter *ECA3*
11	U_promoterECA3_rev_linker	AGCCTCCTUAGCAGCTGCCTCTGCGTTGGAAAAGCCAAGGGTTTCTG	promoter *ECA3*
12	U_NLS3xVenusI_for_linker	AAGGAGGCUGCAGCTAAGGCTATGCCAAAGAAGAAGAGGAAGG	*NLSVenus*
13	U_NLS3xVenusI_rev_linker	AACCGGTTAUTCCTGCTCTTGTACAGCTCGTCC	*NLSVenus*
14	U_NLS3xVenusII_for_linker	ATAACCGGTUTGCAGGAATGGTGAGCAAGGGCGAGG	*Venus*
15	U_NLS3xVenusII_rev_linker	ACCGCTGCCGCUACCTGCCTTGTACAGCTCGTCC	*Venus*
16	U_NLS3xVenusIII_for_linker	AGCGGCAGCGGUAGCATGGTGAGCAAGGGCGAGG	*Venus*
17	U_NLS3xVenusIII_rev_linker	ATTTAGGUTCAGGAGCTGGTTTTTACTTGTACAGCTCGTCC	*Venus*
18	U_terminatorNOS_for_linker	ACCTAAAUGCACCTCCAATTCCCGATCGTTCAAAC	terminator *NOS*
19	U_terminatorNOS_rev	GGTTTAAUCCCCGATCTAGTAACATAGAT	terminator *NOS*
20	U_EGFP_for_linker	AAGGAGGCUGCAGCTAAGGCTATGGTGAGCAAGGGC	*EGFP*
21	U_EGFP_rev_linker	ACCGCTGCCGCUACCTGCCTTGTACAGCTCG	*EGFP*
22	U_AEQ_for_linker	AGCGGCAGCGGUAGCATGTTACGTCCTGTAGAAAC	*AEQ*
23	U_AEQ__rev_linker	ATTTAGGUTCAGGAGCTGGTTTTCATTGTTTGCCTCCCTGCTG	*AEQ*
24	U_promoterBICAT3_for	GGCTTAAUGCCCTGTTCGTTTGCCTGT	promoter *BICAT3*

No	Name	Sequence	Binding Site
25	U_promoterBICAT3_rev_linker	AGCCTCCTUAGCAGCTGCCTCTGCGAGTGATCTGAGAG TTTTGCAGAT	promoter *BICAT3*
26	U_ECA3_for	GGCTTAAUATGGAAGACGCCTACGCCAG	*ECA3*
27	U_ECA3_rev	GGTTTAAUCTACTTGTCACGCCGGTCC	*ECA3*
28	U_AEQ_for	GGCTTAAUATGACCAGCGAACAATACTCA	*AEQ*
29	U_AEQ_linker_rev	ATTTAGGUTCAGGAGCTGGTTTAATGGGGACAGCTCCA CCG	*AEQ*
30	U_BP-80(Y612A)_for_linker	ACCTAAAUGCACCTCCAGTAAAACTGCCAGTCAGGC	*BP-80(Y612A)*
31	U_BP-80(Y612A)_rev	GGTTTAAUTCAACCTCTTTGATGATTGACG	*BP-80(Y612A)*
32	U_SYP31_for	GGCTTAAUATGGGCTCGACGTTCAG	*SYP31*
33	U_SYP31_rev	GGTTTAAUAGCCACAAAGAAGAGGAAAAC	*SYP31*
34	U_SYP41_for	GGCTTAAUATGGCGACGAGGAATCGTA	*SYP41*
35	U_SYP41_rev	GGTTTAAUTTACAAGAATATTTCCTTGAGGAT	*SYP41*
36	U_ECA3_for_linker	AGCGGCAGCGGUAGCATGGAAGACGCCTACGCCAG	*ECA3*
37	U_ECA3_rev_linker	ATTTAGGUTCAGGAGCTGGTTTCTACTTGTCACGCCGG TCC	*ECA3*

Oligonucleotides that were used for colony polymerase chain reaction (C-PCR) and those that were used for sequencing are listed in Table 3.

Table 3: Oligonucleotides for C-PCR or sequencing that were used in this study.

No	Name	Sequence	Binding Site
1	M13_for	CGCCAGGGTTTTCCCAGTCAC	M13
2	M13_rev	CCAGGCTTTACACTTTATGCTTC	M13
3	ECA3_for	GTGCTCTTTGTGTCATGCA	*ECA3*
4	ECA3_for_II	CCTCCCTAAAAATCAGAAACCC	*ECA3*
5	ECA3_rev	TGCATGACACAAAGAGCAC	*ECA3*
6	ECA3_for_Mills_I	AAACCCTTGGCTTTTCCAAC	*ECA3*
7	ECA3_rev_Mills_I	GCTGTCAAAGACGGTACCTT	*ECA3*
8	ECA3_for_Mills_II	GTCGGTGTCTAAGATATGTG	*ECA3*
9	ECA3_rev_Mills_II	CGAAAAAGCCATCTCTTGCT	*ECA3*
10	BICAT3_for	TTGATATCGAGGAAGCACACC	*BICAT3*
11	BICAT3_rev_WT	CTCCTATGGCGTTCTTGTGAG	*BICAT3*
12	BICAT3_rev_t-DNA	ATATTGACCATCATACTCATTGC	*KO BICAT3*

13	ECA3_for_III	CAATATGATGCACGTTCATGC	*ECA3*
14	ECA3_rev_WT	AGTTCATGTGTGCACATGACC	*ECA3*
15	ECA3_rev_t-DNA	ATTTTGCCGATTTCGGAAC	Knock-out *ECA3*
16	Promoter_BICAT3_for_I	GTCAAGGCCAGCCATAGGTC	Promoter *BICAT3*
17	Promoter_BICAT3_rev_I	AACTTAGTCAGCGACCAGCG	Promoter *BICAT3*
18	Promoter_BICAT3_for_II	CGCTGTAATTGGTCGCTGAG	Promoter *BICAT3*
19	Promoter_BICAT3_rev_II	TGGTGGCGACGAGAATCAAA	Promoter *BICAT3*
20	Promoter_ECA3_for	GTCACACATACACACACG	Promoter *ECA3*
21	NLS3xVenus_for_I	GAGGCAGCTGCTAAGGAG	*NLS3xVenus*
22	NLS3xVenus_for_II	CAGGAATAACCGGTTTGC	*NLS3xVenus*
23	NLS3xVenus_for_III	CAGGTAGCGGCAGCGGTAG	*NLS3xVenus*
24	GUS_for	ATGTTACGTCCTGTAGAAACCCC	*GUS*
25	GUS_rev_I	TCATTGTTTGCCTCCCTGC	*GUS*
26	GUS_rev_II	ATCCAGACTGAATGCCCACAG	*GUS*
27	FUT1tmd_rev	ATCGGAGACGATCTTCT	*FUT1tmd*
28	AEQ_rev	TGGAGCTGTCCCCTAA	*AEQ*
29	EGFP_for	CAGCACGACTTCTTCAAGTCC	*EGFP*
30	ECA3_for_realtime	GCTATGACAGTACTTGTTGTTG	*ECA3*
31	ECA3_rev_realtime	GCCTGTATTTCTAGAGAGGA	*ECA3*
32	Actin_for_realtime	TCCCTCAGCACATTCCAGCAGAT	*ACT2*
33	Actin_rev_realtime	AACGATTCCTGGACCTGCCTCATC	*ACT2*

2.3 Organisms

2.3.1 *Escherichia coli* strain TOP10

Constructs were propagated and constructed by using *Escherichia coli* strain TOP10 (C4040-xx, Thermo Fisher Scientific, Waltham, United States). Bacteria were cultivated in liquid or solid LB medium (2.4.1) and incubated at 37 °C. If grown in liquid media, bacteria were shaken at 180 rpm (Certomat IS, Sartorius, Göttingen, Germany).

2.3.2 *Agrobacterium tumefaciens* strain GV3101

Agrobacterium tumefaciens were used for stable transformation of *Arabidopsis thaliana* by floral dip according to Clough and Bent (1998) or infiltrated for transient expression in *Nicotiana benthamiana*. The *A. tumefaciens* strain GV3101 is a cured strain that contains the disarmed octopine plasmid pPM6000 (Tinland *et al.*, 1994). Bacteria were cultivated in liquid or solid YEB medium (2.4.2) at 30 °C. If grown in liquid media, bacteria were shaken at 180 rpm (Certomat IS, Sartorius).

2.3.3 *Arabidopsis thaliana* lines and growth conditions

A. thaliana lines were grown under different conditions as required in the individual experiment (description below). All *A. thaliana* lines used and generated in this study are listed in Table 4. To generate seeds and propagate lines, plants were grown on a 2:1 mixture of potting soil (ED73, Einheitserde Werkverband e.V., Sinntal-Altengronau, Germany) and vermiculite (Gärtnereibedarf Kammlott GmbH, Erfurt, Germany) in the greenhouse until seeds were collected and stored.

Table 4: *A. thaliana* lines that were used in this study.

Name	Description	Resistence	Source
Col-0	*Arabidopsis thaliana* wild type (WT) ecotype Columbia-0	-	-
bicat3-1	GABI-Kat line: 027F07, T-DNA insertion in At5g36290	Sul[R]	Nottingham Arabidopsis Stock Centre (NASC)
eca3-2	SALK line: 070619, T-DNA insertion in At1g10130	Kan[R]	NASC
eca3-2bicat3-1	Cross of *bicat3-1* and *eca3-2*	Sul[R] Kan[R]	generated by Anja Janssen
p35S:AEQ WT Col-0 (cyt. AEQ)	Col-0 WT stably expressing cytosolic *Apoaequorin*	Kan[R]	Knight *et al.* (1991)
p35S:MNS1tmd:EGFP:AEQ WT Col-0 line 2 (short: M2)	Col-0 WT stably expressing an *EGFP-Apoaequorin* fusion targeted to the *cis-* and *medial*-Golgi by MNS1tmd (Table 1)	BASTA[R]	generated in this study

p35S:MNS1tmd:EGFP:AEQ WT Col-0 line 3 (short: M3)	Col-0 WT stably expressing an *EGFP-Apoaequorin* fusion targeted to the *cis-* and *medial*-Golgi by MNS1tmd (Table 1)	BASTA[R]	generated in this study
p35S:FUT1tmd:EGFP:AEQ WT Col-0 line 3 (short: F3)	Col-0 WT stably expressing an *EGFP-Apoaequorin* fusion targeted to the *trans*-Golgi by FUT1tmd (Table 1)	BASTA[R]	generated in this study
p35S:FUT1tmd:EGFP:AEQ WT Col-0 line 8 (short: F8)	Col-0 WT stably expressing an *EGFP-Apoaequorin* fusion targeted to the *trans*-Golgi by FUT1tmd (Table 1)	BASTA[R]	generated in this study
p35S:MNS1tmd:EGFP:AEQ *bicat3-1* line 3.1 (short: Mb3.1)	*bicat3-1* stably expressing an *EGFP-Apoaequorin* fusion targeted to the *cis-* and *medial*-Golgi by MNS1tmd (Table 1)	BASTA[R] Sul[R]	generated in this study
p35S:MNS1tmd:EGFP:AEQ *bicat3-1* line 7.1 (short: Mb7.1)	*bicat3-1* stably expressing an *EGFP-Apoaequorin* fusion targeted to the *cis-* and *medial*-Golgi by MNS1tmd (Table 1)	BASTA[R] Sul[R]	generated in this study
p35S:FUT1tmd:EGFP:AEQ *bicat3-1* line 13.1 (short: Fb13.1)	*bicat3-1* stably expressing an *EGFP-Apoaequorin* fusion targeted to the *trans*-Golgi by FUT1tmd (Table 1)	BASTA[R] Sul[R]	generated in this study
p35S:FUT1tmd:EGFP:AEQ *bicat3-1* line 7.4 (short: Fb7.4)	*bicat3-1* stably expressing an *EGFP-Apoaequorin* fusion targeted to the *trans*-Golgi by FUT1tmd (Table 1)	BASTA[R] Sul[R]	generated in this study
p35S:MNS1tmd:EGFP:AEQ *eca3-2* line 1.1 (short: Me1.1)	*eca3-2* stably expressing an *EGFP-Apoaequorin* fusion targeted to the *cis-* and *medial*-Golgi by MNS1tmd (Table 1)	BASTA[R] Kan[R]	generated in this study
p35S:MNS1tmd:EGFP:AEQ *eca3-2* line 5.2 (short: Me5.2)	*eca3-2* stably expressing an *EGFP-Apoaequorin* fusion targeted to the *cis-* and *medial*-Golgi by MNS1tmd (Table 1)	BASTA[R] Kan[R]	generated in this study
p35S:FUT1tmd:EGFP:AEQ *eca3-2* line 9.1 (short: Fe9.1)	*eca3-2* stably expressing an *EGFP-Apoaequorin* fusion targeted to the *trans*-Golgi by FUT1tmd (Table 1)	BASTA[R] Kan[R]	generated in this study
p35S:FUT1tmd:EGFP:AEQ *eca3-2* line 13.1 (short: Fe13.1)	*eca3-2* stably expressing an *EGFP-Apoaequorin* fusion targeted to the *trans*-Golgi by FUT1tmd (Table 1)	BASTA[R] Kan[R]	generated in this study
p35S:MNS1tmd:EGFP:AEQ *bicat3-1eca3-2* line 4.2 (short: Mbe4.2)	*bicat3-1eca3-2* stably expressing an *EGFP-Apoaequorin* fusion targeted to the *cis-* and *medial*-Golgi by MNS1tmd (Table 1)	BASTA[R] Sul[R] Kan[R]	generated in this study
p35S:MNS1tmd:EGFP:AEQ *bicat3-1eca3-2* line 7.3 (short: Mbe7.3)	*bicat3-1eca3-2* stably expressing an *EGFP-Apoaequorin* fusion targeted to the *cis-* and *medial*-Golgi by MNS1tmd (Table 1)	BASTA[R] Sul[R] Kan[R]	generated in this study
p35S:FUT1tmd:EGFP:AEQ *bicat3-1eca3-2* line 9.1 (short: Fbe8.2)	*bicat3-1eca3-2* stably expressing an *EGFP-Apoaequorin* fusion targeted to the *trans*-Golgi by FUT1tmd (Table 1)	BASTA[R] Sul[R] Kan[R]	generated in this study

p35S:FUT1tmd:EGFP:AEQ *bicat3-1eca3-2* line 9.4 (short: Fbe9.4)	*bicat3-1eca3-2* stably expressing an *EGFP-Apoaequorin* fusion targeted to the *trans*-Golgi by FUT1tmd (Table 1)	BASTA[R] Sul[R] Kan[R]	generated in this study
pECA3:NLS3xVenus WT Col-0 line 2 (short: pENV2)	Col-0 WT stably expressing a nuclear targeted triple *Venus* under the promoter of *ECA3* (pECA3) (Table 1)	BASTA[R]	generated in this study
pECA3:NLS3xVenus WT Col-0 line 3 (short: pENV3)	Col-0 WT stably expressing a nuclear targeted triple *Venus* under the promoter of *ECA3* (pECA3) (Table 1)	BASTA[R]	generated in this study
pECA3:EGFP:GUS WT Col-0 line 8 (short: pEEG8)	Col-0 WT stably expressing an an *EGFP-GUS* fusion under the promoter of *ECA3* (pECA3) (Table 1)	BASTA[R]	generated in this study
pECA3:EGFP:GUS WT Col-0 line 10 (short: pEEG10)	Col-0 WT stably expressing an *EGFP-GUS* fusion under the promoter of *ECA3* (pECA3) (Table 1)	BASTA[R]	generated in this study
pBICAT3:NLS3xVenus WT Col-0 line 5 (short: pBNV5)	Col-0 WT stably expressing a nuclear targeted triple *Venus* under the promoter of *BICAT3* (pBICAT3) (Table 1)	BASTA[R]	generated in this study
pBICAT3:NLS3xVenus WT Col-0 line 6 (short: pBNV6)	Col-0 WT stably expressing a nuclear targeted triple *Venus* under the promoter of *BICAT3* (pBICAT3) (Table 1)	BASTA[R]	generated in this study
pECA:EGFP:ECA3 *eca3-2* line 4-1	*eca3-2* stably expressing an *EGFP-ECA3* fusion under the promoter of *ECA3* (pECA3) (Table 1)	BASTA[R] Kan[R]	generated in this study
pECA:EGFP:ECA3 *eca3-2* line 5-3	*eca3-2* stably expressing an *EGFP-ECA3* fusion under the promoter of *ECA3* (pECA3) (Table 1)	BASTA[R] Kan[R]	generated in this study
pBICAT3:BICAT3:Venus *bicat3-1* line 23-4	*bicat3-1* stably expressing a *BICAT3-Venus* fusion under the promoter of *BICAT3* (pBICAT3)	BASTA[R] Sul[R]	He *et al.* (2022)

A. thaliana used for protoplast preparation (2.5.13) were grown on soil under long-day conditions [16 h light (150 µmol m^{-2} s^{-1}); 8 h darkness; 65 % rH] in a plant growth cabinet (AR75, Percival Scientific, Perry, United States).

To vertically grow *A. thaliana* on ½ MS agar plates, seeds were surface-sterilized in sterilisation solution (33 % bleach, 0.02 % Triton X-100) for five minutes. Prior to that, hydrophobicity of the seed coat was decreased by incubation of the seeds in 70 % ethanol for one minute. Sterile seeds were washed four times with ultra-pure H$_2$O and left in 400 µL ultra-pure H$_2$O until sowing. The seeds were sown on ½ MS plates (2.4.4). After stratification for two days at 4 °C in the dark, the seedlings were grown under long-day conditions as above.

2.3.4   Nicotiana bethamiana

N. benthamiana was used for Agroinfiltration and further localisation studies (2.5.20; 2.5.21). *N. benthamiana* seeds were sown on soil (2.3.3) and stratified for 2 days at 4 °C in the dark. The plants were cultivated in the greenhouse for up to five weeks and were used at the age of four weeks for Agroinfiltration (2.5.18).

2.4   Media

2.4.1   Lysogeny Broth (LB) Medium

For cultivation of *E. coli* strain TOP10 Lysogeny Broth (LB) medium (1 % tryptone, 0.5 % yeast extract, 86.5 mM NaCl) was prepared and sterilised for 20 minutes at 121 °C and a pressure of one bar. For solid medium 1.5 % agar (5210, Carl Roth, Karlsruhe, Germany) was added before autoclaving. Antibiotics were added after autoclaving. For the selection of transformed *E. coli* strain TOP10, 25 µg mL^{-1} kanamycin, 100 µg mL^{-1} ampicillin, or 50 µg mL^{-1} spectinomycin were added.

2.4.2   Yeast Extract Beef (YEB) Medium

For cultivation of *A. tumefaciens* strain GV3101 Yeast Extract Beef (YEB) medium (0.5 % meat extract, 0.1 % yeast extract, 0.5 % peptone, 0.5 % sucrose, 2 mM MgSO$_4$ x 7 H$_2$O) was prepared and sterilised for 20 minutes at 121 °C and a pressure of one bar. For solid medium 2 % agar (5210, Carl Roth) was added before autoclaving. Antibiotics were added after autoclaving. For selection, 25 µg mL^{-1} kanamycin, 25 µg mL^{-1} gentamycin, or 500 µg mL^{-1} spectinomycin were added.

2.4.3   Super Optimal Broth with Catabolite Repression (SOC) Medium

For recovery of bacteria after transformation (2.5.10; 2.5.16), Super Optimal broth with Catabolite repression (SOC) medium (2 % tryptone, 0.5 % yeast extract, 10 mM NaCl, 2.5 mM KCl, pH 7) was prepared and sterilised for 20 minutes at 121 °C and a pressure of one bar. After autoclaving 20 mM MgSO$_4$ x 7 H$_2$O and 20 mM glucose were added.

2.4.4   Murashige & Skoog (MS) Medium

For plant cultivation on plates (2.5.30, 2.5.31) half-strength Murashige & Skoog medium (½ MS) [(0.22 % MS powder including Gamborg's B5 vitamins (M0231, Duchefa, Haarlem, Netherlands)] with 0.8 % phytoagar (P1003, Duchefa) or 0.8 % agar (2266, Carl Roth) were used. The pH was adjusted to pH 5.8 with KOH. If not indicated otherwise, 0.5 % sucrose was added before medium was sterilised for 20 minutes at 121 °C and a pressure of one bar. For the selection of transformed *A. thaliana* seedlings, 25 µg mL^{-1} kanamycin or 10 µg mL^{-1} phosphinothricine (P0159, Duchefa) were added.

2.5   Methods

2.5.1   Rapid Isolation and Screening of Plant Genomic DNA by Polymerase Chain Reaction

For verification of *A. thaliana* mutant lines, genomic DNA was isolated and polymerase chain reaction (PCR) was performed. Leaf tips of the respective lines were collected in a 2 mL reaction tube, and 500 µL of extraction buffer (200 mM Tris, 250 mM NaCl, 25 mM EDTA, 0.5 % SDS, HCl to pH 7.5) was added. The tissue was mashed with a micropestle. Samples were centrifuged for 5 min at 13,400 rpm (MiniSpin, Eppendorf, Hamburg, Germany). 300 µL of the supernatant was transferred into a new 1.5 mL reaction tube before 300 µL of 100 %

isopropanol was added, briefly vortexed, and centrifuged at 13,400 rpm (MiniSpin, Eppendorf) for 10 min. The supernatant was discarded, and the pellet was washed with 70 % ethanol, followed by a centrifugation at 13,400 rpm (MiniSpin, Eppendorf) for 10 min. The ethanol was removed and the pellet was dried at 37 °C for 30 min. The DNA pellet was dissolved in 10 mM Tris-HCl (pH 8.5), and the DNA concentration was determined using a NanoDrop2000c spectrophotometer (Peqlab, Erlangen, Germany). The PCR was performed in a total volume of 20 µL [0.5 Units *taq* polymerase, 2 µL isolated genomic DNA, 0.2 mM dNTPs, 0.4 µM forward oligonucleotide, 0.4 µM reverse oligonucleotide, and 1 x *taq* buffer (50 mM KCl, 1.5 mM MgCl$_2$, 10 mM Tris-HCl pH 8.3)]. The PCR was carried out in a thermal cycler (Biometra, Jena, Germany) starting with an initial denaturation step (95 °C, 2 min), followed by 30 cycles of denaturation (95 °C, 45 s), annealing (oligonucleotide-dependent T$_A$, 30 s), and elongation (72 °C, 1 min per kb), respectively and a final elongation step (72 °C, 5 min). The resulting PCR products were separated and visualised by agarose gel electrophoresis (2.5.6).

2.5.2   Isolation of RNA and cDNA Synthesis

For RNA isolation plant material was harvested, shock-frozen in liquid nitrogen, and grinded (GenoGrinder 2010, SPEX SamplePrep, Metuchen, United States). The RNA was isolated using a Spectrum™ Plant Total RNA kit (Sigma-Aldrich, Saint Louis, United States). 500 µL lysis solution with 1 % ß-mercaptoethanol were added to 100 mg of the plant material. Samples were vortexed for approximately 30 sec, prior an incubation at 56 °C for five minutes. After centrifugation at 13,400 rpm (MiniSpin, Eppendorf), the supernatant was transferred to filtration columns and centrifuged at 13,400 rpm (MiniSpin, Eppendorf) for one minute. 500 µL of the binding solution were added to the flow-through and carefully mixed by pipetting. The mixed solution was transferred to binding columns followed by one minute of centrifugation at 13,400 rpm (MiniSpin, Eppendorf). The binding columns were washed with 300 µL of wash solution I before DNA digestion. For that, 75 µL of DNase I digestion buffer including RNase-free DNaseI (30 U) (Omega bio-tek, Norcross, USA) were added to the binding columns and incubated for 15 min at room temperature. Columns were washed with 500 µL wash solution I and two times with 500 µL wash solution II before columns were dried for one

minute by centrifugation at 13,400 rpm (MiniSpin, Eppendorf). The RNA was eluted in ultra-pure H_2O, and RNA concentrations were measured using a NanoDrop2000c (Peqlab).

The isolated RNA was reverse-transcribed into cDNA using two methods. To provide cDNA for gene amplification (2.5.4), 1 µg of RNA and 5 µM dTN_{37} oligonucleotide were incubated for 5 min at 65 °C before 1 x ProtoScript II buffer (B0368, New England Biolabs, Ipswich, United States), 100 mM dithreithiol (DTT), 200 Units ProtoScript II Reverse Transcriptase (M0368, New England Biolabs), and 8 Units of RNase inhibitor were added. The reaction was carried out for 5 min at 25 °C, followed by incubation at 42 °C for one hour, and inactivation of the enzyme at 65 °C for 20 min.

To provide cDNA for quantitative PCR (2.5.3), 5 µM of a 6 bp oligonucleotide mixture (random hexamers) were used instead of dTN_{37} oligonucleotides.

2.5.3   Real-Time Quantitative Polymerase Chain Reaction (qPCR)

Quantitative Polymerase Chain Reaction (qPCR) was conducted in a realplex[4] Mastercycler system (Eppendorf) using a half-concentrated POWER SYBR Green PCR mastermix (Applied Biosystems, Foster City, United States). The relative expression of the desired gene was quantified by employing a cDNA dilution series and normalised against actin2 (At3g18780) as indicated in the Results.

2.5.4   PhusionU Polymerase Chain Reaction (PhusionU PCR)

For amplification of DNA templates for cloning, PCR generating Uracil (U)-containing amplicons, was used. The PCR was performed in a reaction volume of 50 µL [1 Unit PhusionU Hot Start DNA Polymerase (F-555, Thermo Fisher Scientific), 20 ng DNA vector (Table 1), 0.2 mM dNTPs, 0.4 µM forward oligonucleotide, 0.4 µM reverse oligonucleotide, 1 x Phusion HF Buffer (F-518, Thermo Fisher Scientific)]. The PCR was carried out in a thermal cycler (Biometra) starting with an initial denaturation step (98 °C, 30 s), followed by 30 cycles of denaturation (98 °C, 10 s), annealing (oligonucleotide depend T_A, 20 s), and elongation (72 °C,

15 to 30 s per kb), and a final elongation step (72 °C, 5 min). The PCR products were separated and visualised by agarose gel electrophoresis (2.5.6) and purified (2.5.7).

2.5.5   USER Cloning of DNA Constructs

The restriction of USER-compatible vectors was performed in a total volume of 200 μL [70 Units PacI restriction endonuclease (R0547, New England Biolabs), 15 μg DNA vector, 1 x CutSmart Buffer (B7204, New England Biolabs)] and incubated for 6 h at 37 °C in an incubator (Memmert, Schwabach, Germany). Then, 20 Units of PacI restriction endonuclease (R3189, New England Biolabs) and 50 Units of nicking endonuclease Nt.BbvCI (R0632, New England Biolabs) were added and incubated overnight at 37 °C. The Uracil-Specific Exision Reagent (USER) cloning method (Nour-Eldin *et al.*, 2006) was used to insert multiple DNA fragments into the USER Cassette of pCambia3300-USER, pART7-EGFP-USER, or pART7-USER (Table 1). USER reactions were performed in a total reaction volume of 10 μL [0.75 Units USER enzyme (M5508, New England Biolabs), 10 ng per kb of purified DNA amplicons, 100 ng PacI- and Nt.BbvCI-digested DNA vector, and 1 x taq buffer (50 mM KCl, 1.5 mM $MgCl_2$, 10 mM Tris-HCl pH 8.3)]. The USER reaction was incubated for 30 min at 37 °C to cut USER-spacer-amplified DNA fragments and for 1 h at 25 °C to ligate DNA on the basis of spacer sequences. The USER cloning reaction was transformed into *E. coli* by heat shock without prior purification (2.5.10).

2.5.6   Agarose Gel Electrophoresis

For separation of the amplified DNA (2.5.4, 2.5.11, 2.5.1) or the digested DNA vectors (2.5.5), an agarose gel electrophoresis was performed. The separation was conducted in a 1 % agarose (840001, Biozym, Hessisch Oldendorf, Germany) gel in 1 x TAE buffer (40 mM Tris, 2 mM Na_2EDTA, 68.5 mM acetic acid, pH 8.2). Gels were supplemented with 0.05 ‰ SYBR® Safe DNA Gel Stain (S33102, Thermo Fisher Scientific). Samples were diluted with a 6 x loading dye (30 % glycerol, 50 mM Na_2EDTA, 0.3 % bromophenol blue, 0.3 % xylenecyanol, 10 mM Tris-HCl pH 7.5) and transferred to the agarose gel. The separations were carried out for 40 min at

80 V for Phusion amplicons (2.5.4) and for 30 min at 90 V for C-PCRs and screening PCRs (2.5.11; 2.5.1). For size determination, a commercial 2-log ladder (New England Biolabs) was used. Gels were documented in a gel documentation system with integrated UV excitation (Gel iX Imager, Intas, Göttingen, Germany). DNA was cut out with a scalpel and purified (2.5.7).

2.5.7   Purification of DNA from Agarose Gels

Purification of separated DNA was conducted by using a "Wizard® SV Gel and PCR Clean-Up System" (A9282, Promega, Madison, United States). The agarose cubes containing the target DNA were weighed, and an equal volume of dissolving buffer was added and incubated for 10 minutes at 65 °C. The mixture was transferred to a column and centrifuged for 60 s at 13,400 rpm (MiniSpin, Eppendorf). The column was washed two times with ethanol-containing washing buffer for 60 s at 13,400 rpm (MiniSpin, Eppendorf), and DNA was eluted in ultra-pure H_2O for 60 s at 13,400 rpm (MiniSpin, Eppendorf). The quantification of the yield of DNA was determined using a NanoDrop2000c spectrophotometer (Peqlab).

2.5.8   Subcloning of DNA Constructs

The restriction of pBART (Table 1) to insert pART7-derived expression cassettes was performed in a total volume of 50 µL [20 Units NotI restriction endonuclease (R0189, New England Biolabs), 5 µg DNA vector, 1 x CutSmart Buffer (B7204, New England Biolabs)]. The digest was incubated at 37 °C overnight. 5 Units of calf intestinal alkaline phosphatase (M0525, New England Biolabs) were added, and the reaction was further incubated for 1 h.

The digests were separated and visualised by agarose gel electrophoresis (2.5.6) and purified (2.5.7). Excised pART7-derived expression cassettes were cloned into pBART (2.5.6). The ligation was performed in a total reaction volume of 20 µL [400 Units T4 ligase (M0202, New England Biolabs), 100 ng NotI-digested pBART, 300 ng NotI-digested pART7 insert, 1 x Ligation Buffer (B0202, New England Biolabs)]. The ligation reaction was incubated overnight at 16 °C and then transformed into *E. coli* by electroporation (2.5.10).

2.5.9   Preparation of Chemically Competent *Escherichia coli*

E. coli strain TOP10 cells were plated on solid LB medium (2.4.1) and cultivated overnight at 37 °C. Then, bacteria were precultured in four mL LB medium overnight at 37 °C and 180 rpm in a shaking incubator (KS 4000 ic control, IKA, Staufen, Germany). Bacteria were propagated in 100 mL liquid LB medium after inoculation of the media with one mL of the preculture, and cells were incubated to an OD_{600} of 0.9 at 37 °C and 180 rpm in the same shaking incubator. Cells were stored in an ice bath for 30 min and harvested by centrifugation for 20 min at 2500 *g and 4 °C (5415R, Eppendorf). The resulting pellet was resuspended in 50 mL cold and sterile Transformation Solution A (TS-A) (50 mM $CaCl_2$, 10 mM Tris, pH 7.4) and centrifuged for 15 min at 2500 *g and 4 °C, followed by another resuspension step in 50 mL cold and sterile Transformation Solution B (TS-B) (50 mM $CaCl_2$ x 2 H_2O, 10 mM Tris, 10 % glycerol, pH 7.4). Afterwards, bacteria were incubated for 30 min at 4 °C, harvested by centrifugation for 20 min at 2500 *g and 4 °C, and resuspended in 2.5 mL cold and sterile TS-A. Aliquots of 100 µL were stored at -80 °C until required for transformation (2.5.10).

2.5.10 Transformation of *Escherichia coli* with DNA Vectors

Chemically competent cells (2.5.9) were incubated in an ice bath for five minutes prior to the addition of 100 ng DNA vector (Table 1), complete USER cloning reactions (2.5.5), or ligation reactions (2.5.8). The mixtures were incubated for another 20 min in an ice bath and heat-shocked for 60 s at 42 °C. Immediately, SOC Medium was added, and cells were allowed to recover for one hour at 37 °C and 180 rpm in a shaking incubator (KS 4000 ic control, IKA). The cells were plated on selective solid LB medium and incubated overnight at 37 °C in an incubator (Memmert).

2.5.11 Verification of Insertion by Colony Polymerase Chain Reaction (C-PCR)

Transformed colonies were picked and transferred onto a new plate containing selective solid LB medium and incubated for six hours at 37 °C. The respective colony was lysed for ten minutes at 95 °C in TE-t buffer (10 mM Tris, 1 mM EDTA, 0.1 % Triton X-100, pH 8) and centrifuged for five minutes at 5000 *g (Centrifuge 5415R, Eppendorf). The supernatant was used as DNA template for C-PCR. The C-PCR was performed in a total volume of 25 µL [0.5 Units taq polymerase, 2 µL DNA template, 0.2 mM dNTPs, 0.4 µM forward oligonucleotide, 0.4 µM reverse oligonucleotide, and 1 x taq buffer (50 mM KCl, 1.5 mM $MgCl_2$, 10 mM Tris-HCl pH 8.3)]. The C-PCR was carried out in a thermal cycler (Biometra) starting with an initial denaturation step (95 °C, 2 min), followed by 30 cycles of denaturation (95 °C, 45 s), annealing (oligonucleotide depend T_A, 30 s), and elongation (72 °C, 1 min per kb), and a final elongation step (72 °C, 5 min). The C-PCR was separated and visualised by agarose gel electrophoresis (2.5.6).

2.5.12 Isolation of DNA vectors and Sequencing

A single positive colony per transformation was transferred to four mL selective liquid LB medium and incubated overnight at 37 °C and 180 rpm in a shaking incubator (KS 4000 ic control, IKA). The isolation of DNA vectors was carried out by using a "Pure Yield^{TM} Plasmid Miniprep System" (Promega). The cells were harvested by centrifugation for two minutes at 13,400 rpm (MiniSpin, Eppendorf) and resuspended in Resuspend Buffer B1. After adding the Lysis Buffer B2, the tube contents were gently mixed and incubated for one minute at room temperature. Finally, Neutralisation Buffer B3 was added and mixed until a change in colour appeared. The lysate was centrifuged for five minutes at 13,400 rpm (MiniSpin, Eppendorf), and supernatant was transferred to a spin column. The column washing steps were performed by using Plasmid Wash Buffer 1 followed by using Plasmid Wash Buffer 2. The DNA was eluted with ultra-pure H_2O (prewarmed to ~ 60 °C) at 13,400 rpm (MiniSpin, Eppendorf), and DNA concentration was determined using a NanoDrop2000c (Peqlab)

spectrophotometer. The insertion was analysed by Sanger Sequencing (Micosynth, Balgach, Switzerland).

2.5.13 Isolation of *Arabidopsis thaliana* and *N. benthamiana* Mesophyll Protoplasts

Leaves of *A. thaliana* lines grown on soil for four weeks in a growth cabinet under long-day conditions (2.3.3) or infiltrated *N. benthamiana* (2.5.18) were cut into strips on a white paper using a razor blade and transferred to an enzyme solution [0.625 % Cellulase (C8003, Duchefa), 0.3 % Macerozyme (M8002, Duchefa), 400 mM mannitol, 20 mM KCl, 20 mM MES, 10 mM $CaCl_2$, 0.1 % BSA, pH 5.7]. The leaf strips were vacuum-infiltrated twice for 5 min and incubated without shaking for 3 h at 23 °C, followed by an incubation for 1 h with slow shaking. A 70 µm nylon mesh wetted with W5 buffer (125 mM $CaCl_2$, 154 mM NaCl, 2 mM MES, 5 mM KCl, pH 5.7). The suspension and leaf strips were washed with an equal amount of W5 buffer and filtered using the nylon mesh. The protoplasts were collected at 300 *g for 3 min (Centrifuge 5415R, Eppendorf), and the supernatant was discarded. Protoplasts were resuspended in W5 buffer to a concentration of approximately $2x10^6$ protoplasts mL^{-1} as determined by a Fuchs-Rosenthal chamber. The isolated protoplasts were used to measure free Ca^{2+} concentrations by luminometry (2.5.33) or for transient transformation (2.5.14).

2.5.14 Transformation of *Arabidopsis thaliana* Mesophyll Protoplasts

To transiently transform *A. thaliana* protoplasts according Peiter *et al.* (2007), isolated protoplasts (2.5.13) were incubated on ice for 30 min, centrifuged for one minute at 200 *g (Centrifuge 5415R, Eppendorf), and supernatant was removed. Then, protoplasts were resuspended in MaMg solution (400 mM mannitol, 15 mM $MgCl_2$ x 7 H_2O, 5 mM MES, pH 5.8) to a concentration of $2x10^5$ protoplasts mL^{-1}. $2x10^4$ protoplasts were added to 10-20 µg of the desired DNA vector and gently mixed. An equal amount of PEG-CMS solution [0.62 g mL^{-1} PEG4000, 308 mM mannitol, 154 mM $Ca(NO_3)_2$] was added, gently mixed, and incubated at 23 °C for 20 min. The protoplasts were diluted with 1.5 mL W5 buffer and centrifuged at 100 *g

for 2 min (Centrifuge 5415R, Eppendorf). The supernatant was removed, and 0.3 mL of protoplast culture medium [0.44 % MS powder including Gamborg's B5 vitamins (M0231, Duchefa), 350 mM mannitol, 50 mM glucose, 3 mM $CaCl_2$ x $2H_2O$, 0.01 % ampicillin, pH 5.8] were added. The protoplasts were stored overnight at 23 °C in the dark and placed in a ROC chamber (PeCon GmbH, Erbach, Germany) for confocal microscopy (2.5.20).

2.5.15 Preparation of Electrocompetent *Agrobacterium tumefaciens*

A. tumefaciens cells were plated on solid YEB medium (2.4.2) and cultivated overnight at 30 °C. Then, bacteria were precultured in four mL YEB medium overnight at 30 °C and 180 rpm in a shaking incubator (Certomat BS-1, Sartorius, Göttingen, Germany). Bacteria were propagated in 100 mL liquid YEB medium after inoculation with one mL of the preculture. Cells were allowed to incubate to an OD_{600} of 0.6 at 30 °C and 180 rpm in the same shaking incubator. Cells were stored on an ice bath for 30 min and harvested by centrifugation for 20 min at 2500 *g and 4 °C (Centrifuge 5415R, Eppendorf). The resulting pellet was resuspended in 50 mL cold sterile ultrapure H_2O, centrifuged for 15 min at 2500 *g and 4 °C, resuspended again in 50 mL cold sterile ultrapure H_2O, and incubated for another 30 min at 4 °C. Then, cells were collected by centrifugation for 20 min at 2500 *g and 4 °C and resuspended in 2 mL cold sterile ultrapure H_2O. Aliquots of 60 µL were stored at -80 °C until required for transformation (2.5.16).

2.5.16 Transformation of *Agrobacterium tumefaciens* Cells with DNA Vectors

Transformed *A. tumefaciens* were used for subsequent transformation of *A. thaliana* (2.5.17) and infiltration of *N. benthamiana* (2.5.18). The electrocompetent *A. tumefaciens* cells were incubated for two hours in an ice bath prior to the addition of 100 ng of desired DNA vector. The cells were electro-shocked with 2500 V (Electroporator 2510, Eppendorf), and SOC medium was added immediately after the shock. Cells were allowed to recover for 2.5 h at 30 °C and 180 rpm in a shaking incubator (Certomat BS-1, Sartorius) before they were plated

on selective solid YEB medium (2.4.2) and incubated for two days at 30 °C in the same incubator without shaking. For verification of transformation a C-PCR (2.5.11) was conducted.

2.5.17 Stable Transformation of *Arabidopsis thaliana* with DNA Vectors by Floral Dip

Stably transformed *A. thaliana* lines (Table 4) were generated by floral-dip method according to Clough and Bent (1998). To this end, *A. tumefaciens* GV3101 containing the DNA construct were plated on YEB medium with the respective antibiotics (2.4.2) and grown for two days at 30 °C. The entire cell lawn of one plate was collected, diluted in 30 mL of liquid YEB, and mixed with 120 mL of sucrose solution (5 % sucrose, 0.03 % Silwet L-77). Inflorescences of *A. thaliana* lines grown for six weeks in the greenhouse (2.3.3) were dipped in the mixture. The plants were covered and incubated for two days in the greenhouse. Seeds of the plants were collected and selected by 0.2 g L^{-1} glufosinate-ammonium (BASTA, Bayer Crop Science, Monheim, Germany) on soil or 10 mg L^{-1} DL-phosphinothricin on ½ MS plates (2.3.3).

2.5.18 Agrobacterium-Mediated Infiltration of *Nicotiana benthamiana* Leaves

A. tumefaciens GV3101 containing the desired constructs were transferred from cryostocks to fresh YEB plates containing gentamicin or spectinomycin (2.4.2). The Agrobacteria were grown for 2 days at 30 °C. A loop of bacteria was used to inoculate 4 mL liquid YEB medium containing antibiotics. Precultures were incubated at 30 °C and 160 rpm (Certomat IS, Sartorius) overnight and were used to inoculate 5 mL YEB media containing antibiotics to a starting OD_{600} of 0.1 till they were grown to OD_{600} of 0.6 at 28 °C and 160 rpm. The agrobacteria were collected by centrifugation for 5 min and 4,000 *g (Centrifuge 5415R, Eppendorf). The pellet was resupended in infiltration buffer [10 mM $MgCl_2$, 5 mM MES (pH 5.3), 150 µM acetosyringone)]. The desired combinations of transformed agrobacteria were mixed, and leaves of four-week-old *N. benthamiana* plants grown in the greenhouse (2.3.4) were infiltrated using a 1 mL syringe. The *N. benthamiana* plants were left in the greenhouse for 48

h before microscopic analyses. Infiltrated leaves were also used for protoplastation similar to *A. thaliana* mesophyll protoplasts (2.5.13).

2.5.19 Preparation of Infiltrated *Nicotiana benthamiana* Leaves for Microscopy

Leaf discs of infiltrated *N. benthamiana* leaves were water-soaked using a syringe. The leaf discs were placed on high precision coverslip (170 ± 5 µm, Marienfeld, Lauda-Königshofen, Germany) with water as mounting medium and covered with a second coverslip.

2.5.20 Confocal Microscopy of Infiltrated *Nicotiana benthamiana* Leaves and Transformed *Arabidopsis thaliana* Plants

The fluorescence of mCherry, propidium iodide, Venus, mGFP5 and EGFP was analysed by confocal laser scanning microscopy using a LSM 880 META containing a PMT detector and equipped with Plan-apochromatic lenses (40x/1.2 and 63x/1.4 Oil; Carl Zeiss, Jena, Germany). Pictures in channel mode were taken using the multitrack function. As excitation light source an argon multiline ion laser at 488 nm (for mGFP5, EGFP and Venus) and at 514 nm (for mCherry and propidium iodide) was used. Emission signals were filtered by using a 458 nm HFT and a 545 nm NFT beamsplitter. EGFP and autofluorescence were detected by using a band pass filter with 505-530 nm and a long pass filter with 615 nm, respectively. Images (512 x 512; 8 bit) were processed by using the ZEN blue light software (Carl Zeiss).

2.5.21 Superresolution Confocal Microscopy of *cis-* and *trans-*Golgi Markers in *Nicotiana benthamiana*

To distinguish between Golgi subcompartments a Stellaris 8 confocal laser scanning microscope (Leica, Wetzlar, Germany) equipped with a HC PL APO CS2 63x/1.30 glycerol

objective was used. The White Light Laser (WLL; 440-790 nm) was used as excitation light source. EGFP, mGFP5 and mCherry were excited using 489 nm and 587 nm, respectively. Emitted light was detected with the Hybrid-Detector (HyD) with the respective ranges of 494-572 nm and 592-649 nm. Images in super resolution were taken in lightning mode under the previous conditions and calculated by Leica lightning algorithm in the LAS X software (Leica). Images were edited using the LAS X software (Leica).

2.5.22 Electron Microscopy

For ultrastructural localisation of MNS1tmd-EGFP-AEQ, leaf disks of four-week-old *A. thaliana* plants were transferred into aluminium planchettes and high-pressure frozen with an HPM 10 instrument (BAL-TEC, Liechtenstein). Subsequently, the material was cryo-substituted in 0.25 % glutaraldehyde (Sigma-Aldrich) and 0.1 % uranyl acetate (Chemapol, Czech Republic) in acetone at -80 °C for 2 days by using the cryosubstitution equipment (FSU, BAL-TEC). This was followed by embedding the samples in HM20 (Polysciences Europe, Eppelheim, Germany) at -20 °C. Ultrathin sections were immunolabelled with a polyclonal GFP antibody (AB6556, Abcam, Cambridge, United Kingdom; diluted 1:300), which was detected by a rabbit anti goat secondary antibody conjugated with 10 nm gold particles (G5527, Sigma-Aldrich; diluted 1:100). The sections were post-stained with uranyl acetate and lead citrate using an EMSTAIN instrument (Leica) and observed with a Libra 120 transmission electron microscope (Carl Zeiss) operating at 120 kV. Images were taken by a dual-speed on-axis SSCCD camera (BM-2k-120; TRS, Moorenweis, Germany).

2.5.23 Protease Protection Assay

For verification of the luminal localisation of aequorin, a protease protection assay was performed. Therefore, protoplasts of stable lines expressing *MNS1tmd-EGFP-AEQ* and *FUT1tmd-EGFP-AEQ* were isolated (2.5.13) and after isolation incubated in W5 buffer at room temperature overnight. The protoplasts were collected by centrifugation at 100 *g for 2 min

(Centrifuge 5415R, Eppendorf), and the supernatant was removed carefully. The protoplasts were resuspended in 500 µL NaCl (250 mM) and mixed by pipetting several times. 1 mL of HEPES buffer (40 mM HEPES, 10 mM KCl, 1 mM EDTA, 400 mM Sucrose, pH 7.5) was added. The protoplasts were disrupted by forcing through a syringe with a needle for several times. The disrupted protoplasts were centrifuged at 600 *g for 3 min (Centrifuge 5415R, Eppendorf). The supernatant was used for ultra-centrifugation at 120,000 *g for 55 min and 4 °C (Optima MAX-E Ultracentrifuge, Beckman Coulter, Brea, United States). The supernatant was discarded and the pellet was resuspended in 80 µL of HEPES buffer mentioned above. The isolated membrane fraction was incubated with 20 ng proteinase K and 1 % Triton X-100 for 1 h on an ice bath. The reaction was stopped by adding 5 µM PMSF and analysed by SDS-PAGE (2.5.24).

2.5.24 Sodium Dodecyl Sulphate Polyacrylamide Gel Electrophoresis (SDS-PAGE)

For assessment of protein digests on a Western Blot, 20 µL of the membrane fraction sample (2.5.23) were mixed with 20 µL of 2 x SDS loading buffer [250 mM Tris, 20 % SDS, 20 % glycerol, 0,004 % bromophenol blue, 50 mM dithiothreitol (DTT), pH 6.8]. The sample-buffer mixture was heated at 95 °C for 10 min. The samples were transferred onto a 10 % SDS-PAGE gel [stacking gel: 500 mM Tris, 0.4 % SDS, 16.28 % acrylamide:bisacrylamide (37.5:1) (3029.1, Carl Roth), 0.042 % tetramethylenediamine (TEMED), 0.2 g ammonium persulfate, pH 6.8; separating gel: 1.5 M Tris, 0.4 % SDS, 0.33 % acrylamide:bisacrylamide (37.5:1), 0.0083 % TEMED, 0.083 g ammonium persulfate, pH 8.8] placed in a SDS-PAGE electrophoresis chamber filled with 1 x running buffer (192 mM glycine, 25 mM Tris, 0.1 % SDS). For size determination a pre-stained protein ladder (P7719, New England Biolabs) was used. The proteins were separated at 120-140 V for 1.5 h at 4 °C. The aperture was disassembled, and the SDS-PAGE gel was used for Western Blot analysis.

2.5.25 Immunodetection of Proteins by Western Blot

To determine intraorganellar targeting of protein fusions investigated by the protease protection assay (2.5.23), Western Blot analysis was performed. The SDS-PAGE gel (2.5.24), a nitrocellulose membrane (10600125, Amersham, Marlborough, United States), filter papers (CL73.1, Carl Roth), and fiber pads were wetted in tank blot buffer (25 mM Tris, 192 mM glycin, 20 % methanol, pH 8.3). The blotting set-up was assembled as a sandwich in the following order (from negative to positive pole): fiber pad, filter paper, SDS-PAGE gel, nitrocellulose membrane, filter paper, fiber pad. The assembled sandwich was set into the blotting tank, completely covered by tank blot buffer, and blotted for 800 min at 30 V and 4 °C. The blotting aperture was disassembled, and the nitrocellulose membrane was blocked with 5 % milk powder in TBS buffer (50 mM Tris, 150 mM NaCl, pH 7.2) for one hour, rinsed two times with TBS-T buffer [50 mM Tris, 150 mM NaCl, 0.1 % Tween 20 (9127.1, Carl Roth), pH 7.2], and then washed for five min in TBS-T buffer. The nitrocellulose membrane was incubated for another hour with a monoclonal antibody against GFP (MA5-15256, Invitrogen, Carlsbad, United States) diluted 1:1000 in TBS buffer containing 3 % milk powder. The nitrocellulose membrane was then rinsed two times with TBS-T buffer and washed four times for five min with TBS-T buffer. The second antibody conjugated to horseradish peroxidase (A9044, Sigma-Aldrich) was diluted 1:8000 in TBS buffer containing 1.5 % milk powder, and the nitrocellulose membrane was incubated in the solution for another hour. The nitrocellulose membrane was finally rinsed two times with TBS-T buffer and washed three times for five min with TBS-T buffer before a last washing step with TBS buffer. The blot was developed using Clarity Western ECL substrate (1705060, Bio-Rad, Hercules, United States), and images were taken using a ChemiDoc Imaging System (17001401, BioRad) in automatic mode.

2.5.26 Histochemical Analysis of Promoter Activity by ß-Glucuronidase

Tissue-specific expression was analysed by promoter-GUS studies. *A. thaliana* lines expressing *EGFP-GUS* under the native promoters of *ECA3* and *BICAT3* were grown on ½ MS plates (2.4.4) for 10 days under long-day conditions and incubated in staining solution [100 mM Na_2HPO_4,

10 mM EDTA, 3 mM $K_4[Fe_2(CN)_6]$, 0.1 % Triton X-100, 0.5 mM $K_3[Fe_2(CN)_6]$, 2 mM x-Gluc (dissolved in DMSO), pH 7]. The tissues were vacuum-infiltrated twice for five min and incubated for 2 h in dark at 37 °C. The staining solution was removed, and tissues were destained with 80 % ethanol until chlorophyll was completely removed. The staining was documented using an AxioCam 506 colour camera (Carl Zeiss) mounted on a stereo microscope (Stereo Discovery V.20, Carl Zeiss). The images were edited using the ZEN blue light software (Carl Zeiss).

2.5.27 Analysis of Promoter Activity by Nuclear-Targeted Triple Venus Reporter

Tissue-specific promoter activity was further visualised using lines expressing nuclear-targeted triple Venus under control of the promoter of *ECA3* and *BICAT3*. *A. thaliana* lines were grown on ½ MS plates (2.4.4) for 10 days under long-day conditions. Before monitoring expression in roots, the cell wall was stained with 1 µM propidium iodide. The root tissue was placed on a coverslip (170 ± 5 µm, Marienfeld), and images were taken with an LSM880 META confocal laser-scanning microscope equipped with a Plan-apochromatic lens (40x/1.2) (Carl Zeiss). As excitation light source an argon multiline ion laser was used at wavelength 488 nm and 514 for Venus and propidium iodide, respectively. For monitoring the shoot tissue, seedlings were analysed with an AxioZoom V16 microscope equipped with a PlanNeoFluar Z 1x lens (Carl Zeiss). As excitation light source a HXP 200 discharge lamp was used, and signals were acquired using Filter Set 38 (Ex BP470/40, Bs 495, Em BP525/50) (both Carl Zeiss) and an Orca Flash 4.0 V3 CMOS camera (Hamamatsu Photonics, Herrsching, Germany). The images were edited using the ZEN blue light software (Carl Zeiss).

2.5.28 *In silico* Co-Expression Analysis by GENEVESTIGATOR®

Genes that are co-expressed with *ECA3* were analysed by GENEVESTIGATOR® (Zimmermann *et al.*, 2004). *ECA3* (At1g10130) was searched in the database, and the co-expression tool was used and analysed by perturbations. The ten most correlated genes were displayed as

Person's correlation and a table. The graphic was exported by the export function and further modified.

2.5.29 Growth of *Arabidopsis thaliana* under Salt Stress on Agar Plates

A. thaliana were sown and cultivated on ½ MS plates (2.4.4) containing 1 % sucrose and additional 45 Mm $CaCl_2$ under long-day conditions [16 h light (150 µmol m^{-2} s^{-1}) and 20 °C; 8 h darkness and 18 °C; 65 % rH] in a plant growth cabinet (AR75, Percival Scientific). Growth of the seedlings was documented after 14 days by scanning (Perfection V750 PRO, EPSON, Suwa, Japan).

2.5.30 Growth of *Arabidopsis thaliana* under Salt Stress on Agar Plates

A. thaliana were sown and cultivated on ½ MS plates (2.4.4) containing 1 % sucrose and different concentrations of NaCl under long-day conditions [16 h light (150 µmol m^{-2} s^{-1}) and 20 °C; 8 h darkness and 18 °C; 65 % rH] in a plant growth cabinet (AR75, Percival Scientific). Growth of the seedlings was documented after 14 days by scanning (Perfection V750 PRO, EPSON, Suwa, Japan), and fresh weight of the seedlings was determined.

2.5.31 Growth of *Arabidopsis thaliana* under Calcium Toxicity in Liquid Culture Media

A. thaliana lines were sown on ½ MS medium containing 1 % sucrose (2.4.4), stratified for two days at 4 °C in the dark, and cultured for 12 days under short-day conditions [10 h light (150 µmol m^{-2} s^{-1}) and 20 °C; 14 h darkness and 18 °C; 65 % rH] in a plant growth cabinet (ATC26, Conviron, Winnipeg, Canada). Seedlings were inserted into a sliced polyethylene foam plug, placed in a decapitated 2 mL reaction tube, transferred to black 1 L boxes containing hydroponic solution [0.5 mM NH_4SO_4, 2 mM KNO_3, 2 mM $CaCl_2$ x 2 H_2O, 0.5 mM $MgSO_4$ x 7

H_2O, 0.3125 mM KH_2PO_4, 42.5 µM Fe-EDTA, 3.5 µM $MnSO_4$ x H_2O, 0.125 µM $CuSO_4$ x 5 H_2O, 0.25 µM $ZnSO_4$ x 7 H_2O, 17.5 µM H_3BO_3, 0.05 µM $NaMoO_4$, 0.0025 µM $CoCl_2$ x 6 H_2O, pH 5.8 (Arteca & Arteca, 2000)], and grown for nine days. Media was replaced twice a week before seedlings were transferred to black 4 L boxes and cultivated for another three weeks with a change of the media twice a week. For high-Ca^{2+} treatment, 45 mM $CaCl_2$ was added at day 24 of the experiment. Before harvesting, shoot growth was documented by a Pentax K20 equipped with a Pentax 18-55II objective (Pentax, Tokyo, Japan). Plants were separated into roots and shoots. The roots were washed with 1 mM MES-KOH pH 5.8 including 10 mM EDTA before root and shoot tissues were dried at 70 °C for seven days.

2.5.32 Analysis of Elemental Composition of *Arabidopsis thaliana* Plants

Dried root and shoot tissues were weighed into PFA vessels (CEM, Kamp-Lintfort, Germany) and digested in 65 % HNO_3 (X943.1, Carl Roth) ramped to 205 °C in 15 min and kept for 20 min in total in a MARS 5 Xpress (CEM) digestion system. Elements were analysed by microwave plasma - atomic emission spectrometry using a MP-AES 4210 instrument (Agilent Technologies, Santa Clara, United States). Ca^{2+} was analysed in a 1:10 dilution in ultra-pure H_2O.

2.5.33 Calcium Measurements using Aequorin

Free calcium in cytosol ($[Ca^{2+}]_{cyt}$) and Golgi ($[Ca^{2+}]_{Golgi}$) was determined using the luminescent calcium reporter aequorin. To this end, *N. benthamiana* protoplasts and *A. thaliana* lines expressing *Apoaequorin* (2.3.3) were used. Luminescence was determined in either four-days-old *A. thaliana* seedlings grown vertically on plates (2.4.4), in *A. thaliana* mesophyll protoplasts isolated (2.5.13) from plants grown for four weeks under long-day conditions in a growth cabinet (2.3.3), or in *N. benthamiana* protoplasts isolated 48 h post infiltration (2.5.18, 2.5.13). Seedlings in deion. H_2O or 2x 10^6 protoplasts mL^{-1} dissolved in W5 buffer were transferred to luminometer tubes (55.848, Sarstedt, Nümbrecht, Germany) and incubated in

reconstitution solution [deion. H_2O or W5 buffer containing 10 µM coelenterazine (4094.4, Carl Roth), total volume 200 µL]. Seedlings were incubated overnight, while protoplasts were incubated for two hours in the dark.

To determine total luminescence of seedlings, Relative Light Units (RLUs) were quantified in a tube luminometer (Sirius or FB-12, Berthold Detection Systems, Bad Wildbad, Germany) every 0.2 sec for 60 sec before applying an equal volume of discharge solution (2 M $CaCl_2$ x 2 H_2O, 20 % ethanol), and RLUs were determined for another 60 sec. The sum of the RLUs released within these 120 sec was considered as total RLU value.

To analyse stimulus responses of protoplasts, RLUs were determined in total for 10 to 12 min with an interval of 0.2 sec. After 180 sec, the sample was treated by manually injecting an equal volume of W5 buffer as control or two-fold concentrated treatment solutions in W5 buffer (2.5.15). After 5 to 7 min, aequorin was discharged using an equal amount of discharge solution.

Calculation of free Ca^{2+} concentrations from RLUs was based on the equation employed by Rentel and Knight (2004):

pCa = 0.332588 (-log k) + 5.5593

k = [RLU per sec] / [total RLU remaining]

2.5.34 Statistical Analysis

Diagrams were designed and statistical analyses performed using Sigma Plot 13.0 (Systat Software). Significance tests were used as indicated in the respective figure legends, and significance values are marked in the graphs by either asterisks or letters.

3   Results

3.1   Localisation of Calcium Transport Proteins in the Secretory Pathway

3.1.1   ECA3 and BICAT3 Co-localise in the Golgi Apparatus

The two Ca^{2+} transport proteins ECA3 and BICAT3 were previously shown to be localised in compartments of the secretory pathway (Mills *et al.*, 2008, Li *et al.*, 2008a, He *et al.*, 2022). To investigate a putative co-operation and see whether both of them might be localised in the Golgi, co-localisation of both proteins was analysed in *A. thaliana* mesophyll protoplasts (Figure 7, A - D). An EGFP-ECA3 fusion was transiently co-expressed with a BICAT3-mCherry construct, and fluorescence was imaged by confocal microscopy. Punctate structures were detected, and fluorescence of EGFP and mCherry overlapped, as apparent from a virtual line scan analysis (Figure 7, E). In addition, *N. benthamiana* leaves were infiltrated with *A. tumefaciens* containing the EGFP-ECA3 and BICAT3-mCherry fusions, and fluorescence was analysed using the same microscope (Figure 7, F - J). Localisation of both proteins also indicated a Golgi-like pattern, and co-localisation of both transport proteins. Subcompartmental localisation cannot be inferred from these experiments.
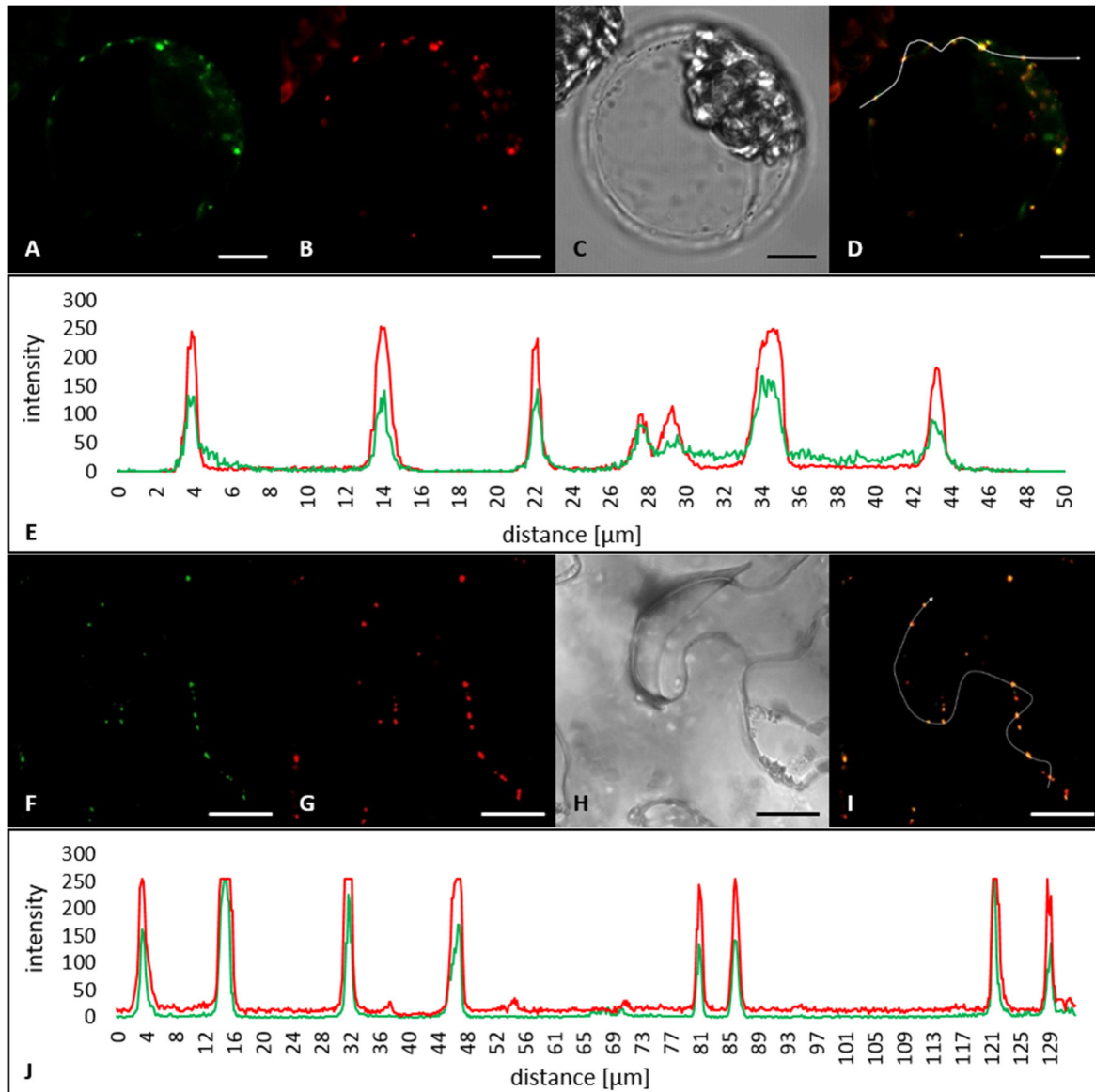
Figure 7: BICAT3 and ECA3 co-localisations. (A-E) Co-localisation of EGFP-ECA3 and BICAT3-mCherry transiently expressed in *Arabdopsis thaliana* mesophyll protoplasts of four-week-old Col0 plants. (A) EGFP, (B) mCherry, (C) PMT channel, (D) merged image, (E) virtual line scans showing the pixel intensity of EGFP (green line) and mCherry (red line) along the arrow shown in the merged image. (F-J) Co-localisation of EGFP-ECA3 with BICAT3-mCherry in leaf of five-week-old *N. benthamiana* plant 48 h post infiltration. (F) EGFP, (G) mCherry, (H) PMT channel, (I) merged image, (J) virtual line scan showing pixel intensity of EGFP (green line) and mCherry (red line) along the arrow shown in the merged image. Scale bars represent 10 µm (A-D) and 20 µm (F-I).

3.1.2 Subcompartmental Distinction of Golgi Cisternae

Since the distinction of cisternae within Golgi stacks is difficult due to their close proximity, confocal video imaging and superresolution microscopy were used to precisely analyse Golgi stacks on subcompartmental level. To this end, peptides localising to either early Golgi (*cis-*

and *medial*-Golgi) or late Golgi (*trans*-Golgi) were fused to a fluorescence protein. The TMD of mannosidase I (MNS1tmd) was fused to the fluorescent proteins mGFP5 or mCherry and used as *cis*-Golgi and *medial*-Golgi marker. The entire sequence of sialyltransferase (ST) of *Rattus norvegicus* was used as *trans*-Golgi marker and fused to mGFP5 or mCherry. Distinction by confocal video imaging (Figure 8, A - C) revealed a shift of both Golgi markers that was observed when the Golgi stacks were viewed from the side. Due to the movement of the Golgi, video imaging was required to capture side views. In addition, shifts were visible in front view if images were captured by superresolution microscopy (Figure 8, D - F). Based on the Leica lightning calculation-based deconvolution, the *trans*-Golgi marker showed a ring-like structure surrounding the *cis*- and *medial*-Golgi, resulting from the bulbs occurring in the *trans*-Golgi for vesicle formation.
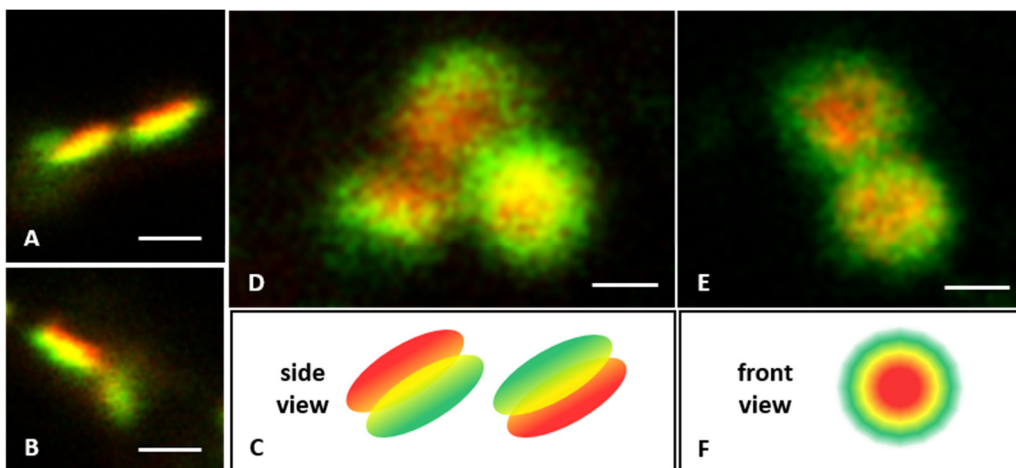
Figure 8: Distinction between *cis*- and *trans*-Golgi by confocal microscopy using a Leica Stellaris 8 microscope. (A, B) Captured frame of MNS1tmd-mCherry and sialyltransferase-mGFP5 in confocal mode during live video recording in side view of Golgi. (C) schematic representation. (D, E) Superresolution microscopy by further algorithmic calculation (Leica lightning) of MNS1tmd-mCherry and sialyltransferase-mGFP5 in front view of Golgi. (F) schematic representation. Scale bars represent 1 µm (A, B) and 0.5 µm (D, E).

3.1.3 Precise Localisation Reveals that BICAT3 is Predominantly Resident in the Late Golgi in *Nicotiana benthamiana*

The previously established method for subcompartmental distinction within the Golgi was applied to precisely localise BICAT3 by confocal video recording. The *cis*-Golgi marker

MNS1tmd fused to mGFP5 and mCherry, and the *trans*-Golgi marker ST fused to mGFP5 and mCherry, co-localised with themselves and showed no shift (Figure 9, A + B), while co-localisation of MNS1tmd and ST showed a shift when Golgi were captured in side view (Figure 9, C). This was additionally analysed by virtual line scans (Figure 9, F - H). The localisation of BICAT3 fused to mCherry showed a perfect overlap with the *trans*-Golgi marker ST (Figure 9, D + I), whereas a shift occurred with the *cis*-Golgi marker (MNS1tmd) (Figure 9, E + J). Hence, BICAT3 is localised predominantly or exclusively in the late Golgi and may be required for Ca^{2+} and Mn^{2+} homeostasis in this subcompartment.
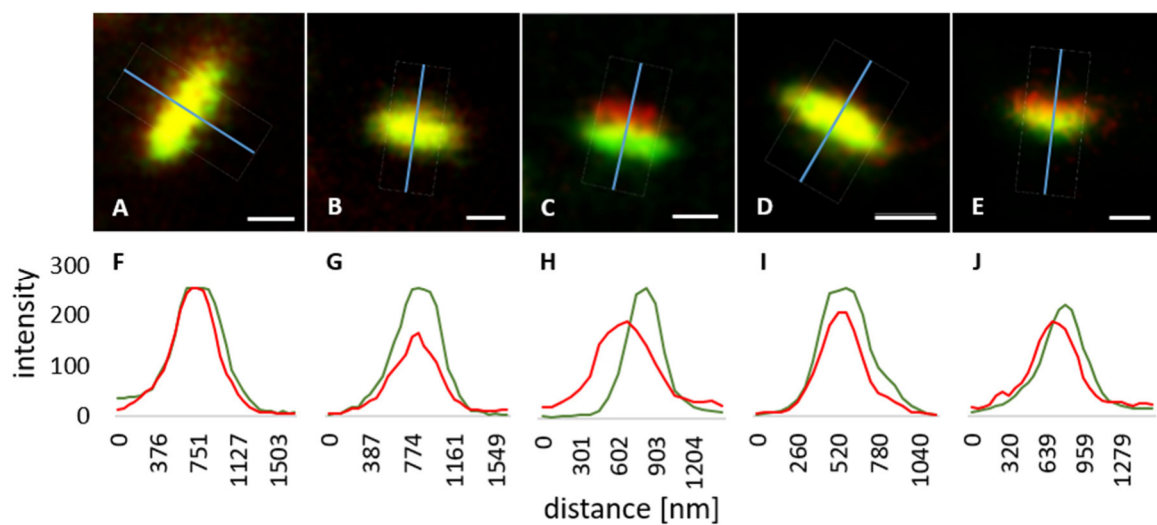
Figure 9: Precise localisation of BICAT3-mCherry to distinguish between *cis*- and *trans*-Golgi cisternae. (A-C, F-H) Co-localisation of *cis*- and *trans*-Golgi markers as controls. (A, F) Co-localisation and virtual line scan of MNS1tmd-mCherry and MNS1tmd-mGFP5. (B, G) Co-localisation and virtual line scan of ST-mCherry and ST-mGFP5. (C, H) Co-localisation and virtual line scan of MNS1tmd-mCherry and ST-mGFP5. Co-localisation and virtual line scan of BICAT3-mCherry with (D, I) sialyltransferase-mGFP5 and (E, J) MNS1tmd-mGFP5. Virtual line scans show the pixel intensity of the GFP (green line) and mCherry (red line) along the blue line in the respective image. Scale bars represent 0.5 µm (A- E).

3.2 Phenotyping of *bicat3-1, eca3-2*, and *bicat3-1eca3-2* Mutants

3.2.1 *bicat3-1*, *eca3-2*, and *bicat3-1eca3-2* mutants show no different growth under control conditions

The localisation of ECA3 and BICAT3 showed that these transport proteins operate in the Golgi, whereby BICAT3 specifically does so in the late Golgi. Moreover, since they were shown

to complement yeast mutant strains impaired in Ca^{2+} transport (Mills *et al.*, 2008, He *et al.*, 2022), an impact on Ca^{2+} concentrations in the Golgi might be concluded that may be relevant for development or stress responses. To assess growth under standard conditions, the knock-out mutants *bicat3-1* and *eca3-2*, and the *bicat3-1eca3-2* double mutant (Mills *et al.*, 2008, He *et al.*, 2022) were grown on soil under long-day conditions in a plant growth cabinet. Growth of the three mutants was comparable to that of the wild type (Figure 10, A). The T-DNA insertions were validated by PCR and insertion sites were determined by sequencing (Figure 10, B-C).
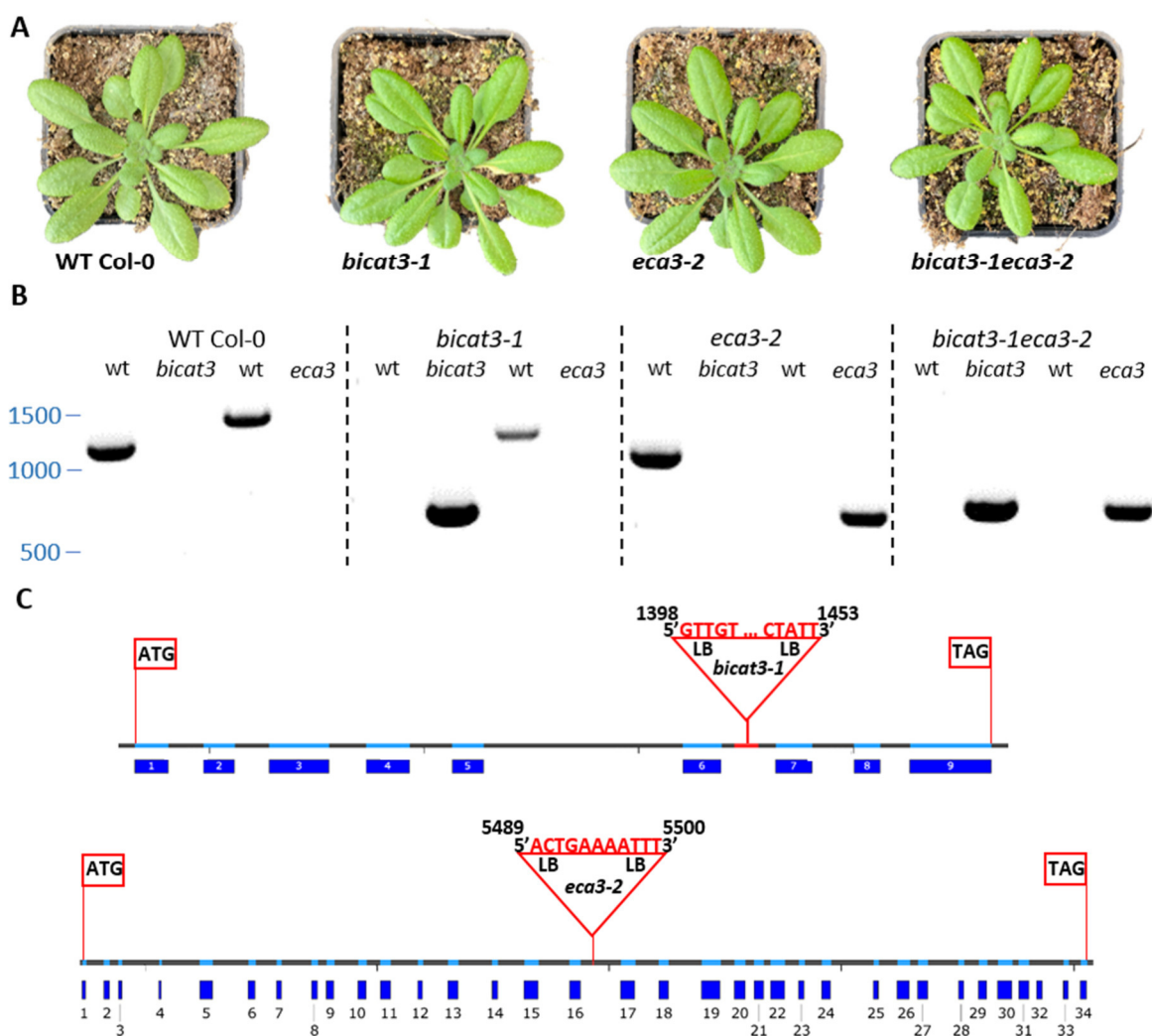
Figure 10: (A) WT Col-0, *bicat3-1*, *eca3-2*, and *bicat3-1eca3-2* grown for five weeks on soil under long-day conditions in a plant growth cabinet. (B) PCR screen to validate T-DNA insertions. (C) Mapping of T-DNA insertions in *bicat3-1* and *eca3-2*. Blue boxes indicate exons. Insertion sites are marked by a red triangle including the missing base pairs and the positions of the T-DNA left borders (LB).

3.2.2 *bicat3-1* and *eca3-2* Show a Severe Phenotype on High-Ca^{2+} Medium

Phenotypes of *eca3-2* and *bicat3-2* were already analysed in previous studies. Both mutations lead to a diminished growth under low-Mn^{2+} conditions (Mills *et al.*, 2008, He *et al.*, 2022). No growth defect was observed for *eca3-2* under low-Ca^{2+} conditions (Mills *et al.*, 2008). When grown on ½ MS plates supplemented with 45 mM CaCl$_2$ under long-day conditions, *eca3-2* and *bicat3-2* showed a growth defect (Figure 11). In the *bicat3-1eca-2* double mutant, this phenotype was already visible when plants were exposed to only 30 mM CaCl$_2$. Since Mn^{2+} and Ca^{2+} compete in transport (He *et al.*, 2021), high Ca^{2+} concentration might lead to an indirect Mn^{2+} deficiency, besides direct Ca^{2+} toxicity.
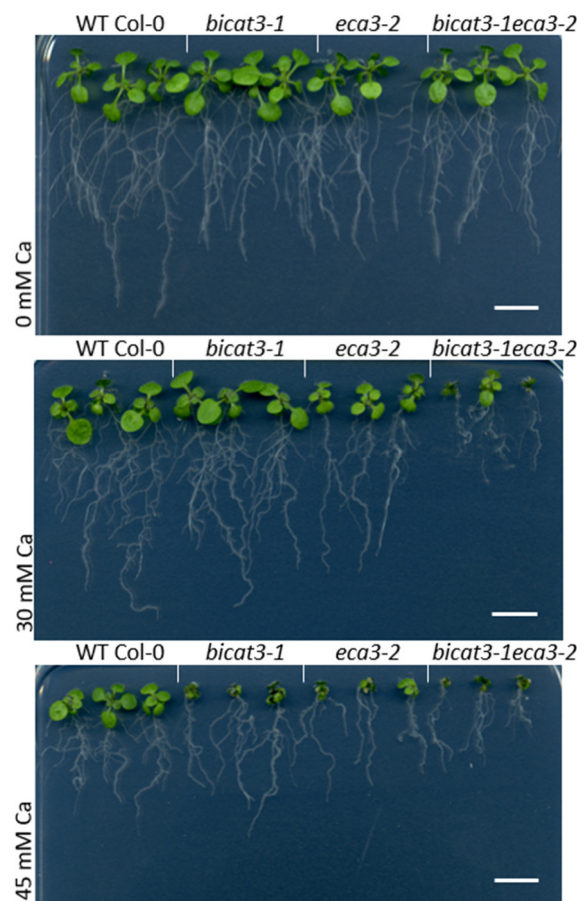
Figure 11: Calcium toxicity assay of *Arabidopsis thaliana* WT Col-0, *bicat3-1*, *eca3-2*, and *bicat3-1eca3-2* on ½ MS plates grown under long-day conditions in a plant growth cabinet. Images represent 14-day-old seedlings under control conditions (upper picture) and subjected to calcium toxicity induced by 30 mM CaCl$_2$ (middle picture) or 45 mM CaCl$_2$ (lower picture). Scale bars represent 10 mm.

A further Ca^{2+} toxicity experiment was conducted in hydroponic culture. Under control conditions, there was no obvious difference in shoot growth between wild type, *bicat3-1*, *eca3-2*, and *bicat3-1eca3-2* (Figure 10, A), whereas all mutants showed a diminished growth under Ca^{2+} toxicity induced by 45 mM CaCl$_2$ compared to the wild type (Figure 12, B).

Under control conditions, the mutants showed comparable shoot DW to the wild type; the root DW under control conditions was lower in *eca3-2* than in the other genotypes (Figure 12, C). The shoot DW was lower, but not significantly, in single and double mutants when grown under Ca^{2+} toxicity. There was no additional decrease when both BICAT3 and ECA3 were absent as compared to the single mutants. The root DW under Ca^{2+} toxicity was also lower in *bicat3-1*, *eca3-2*, and *bicat3-1eca3-2*.

Ca^{2+} and Mn^{2+} concentrations were determined by ICP-AES (Figure 12, C). Regarding the Ca^{2+} concentrations per DW, there were only minor increases in root Ca^{2+} concentrations when grown under Ca^{2+} toxicity. In shoots, Ca^{2+} concentrations of all genotypes were increased under Ca^{2+} toxicity with *eca3-2* showing the highest concentration, but without significance. Interestingly, the Mn^{2+} concentrations in shoots of all mutants were increased under Ca^{2+} toxicity compared to the wild type that showed a decrease of Mn^{2+} under the same condition. The Mn^{2+} concentrations in roots were tendentially increased in the mutants as well. A strong decrease of Mn^{2+} concentrations in wild type roots was observed under Ca^{2+} toxicity in comparison to the control conditions.
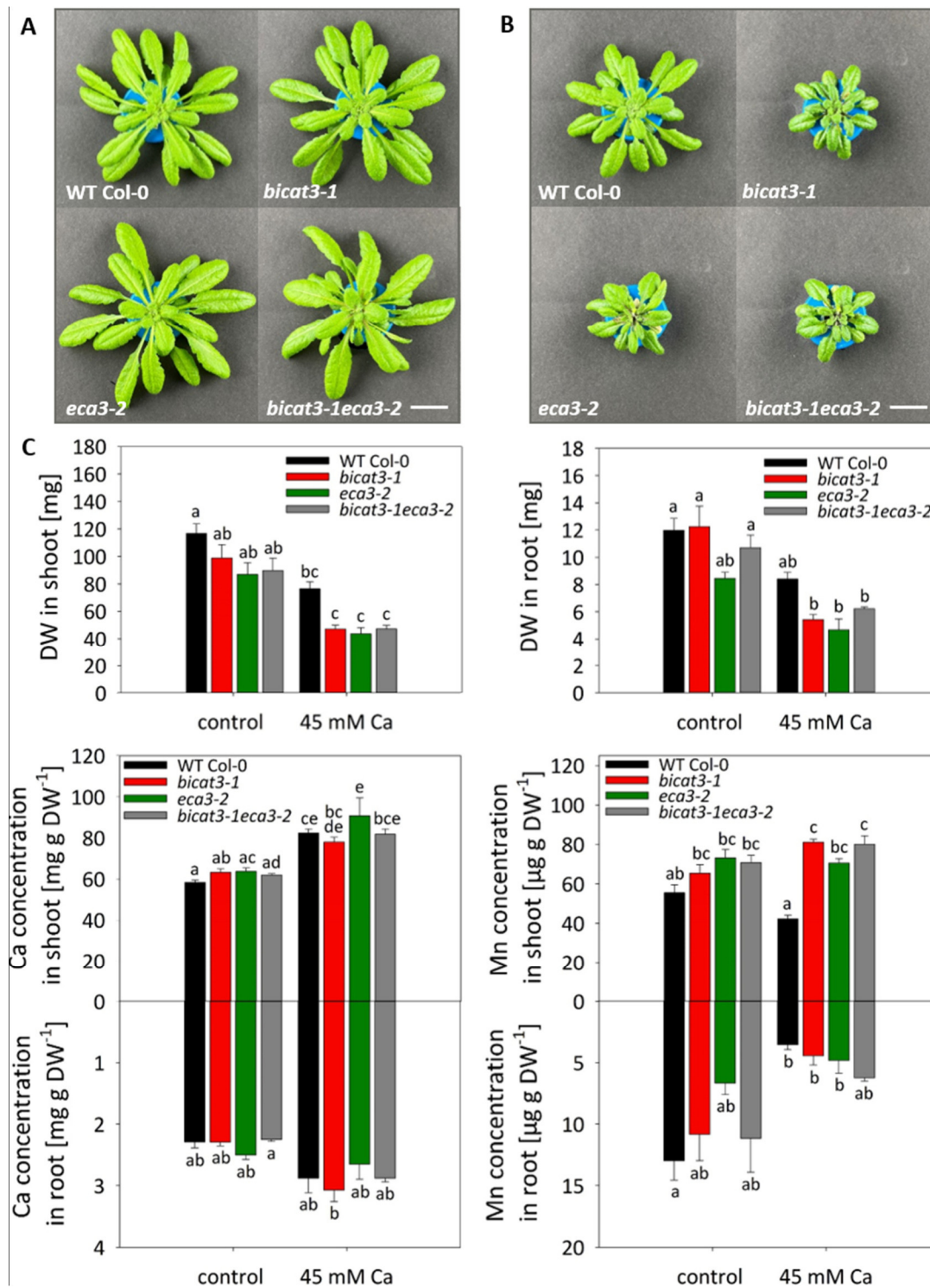
Figure 12: (A and B) Representative images of a WT Col-0, *bicat3-1*, *eca3-2*, and *bicat3-1eca3-2* under control (A) and calcium toxicity (45 mM CaCl₂) (B). (C) Dry weights of the shoots (left panel) and roots (right panel) of the plants shown in A and B. Calcium (left panel) and manganese (right panel) concentrations in roots and shoots of plants shown in A and B. Bars represent the means ± SE of four replicates. Statistical significance was tested by one-way ANOVA with Tukey post hoc test (different letters indicate significance with P<0.05). Scale bars represent 20 mm. Experiment was repeated twice with comparable results.

3.2.3 Expression of *ECA3* is Restored in *eca3-2* Expressing EGFP-ECA3 under the Native Promoter

To investigate whether the diminished growth of the mutants under Ca^{2+} toxicity resulted from lack of the transport proteins, the mutants were complemented by the coding sequence (CDS) fused to either EGFP or Venus under their native promoters. The complementation of *bicat3-1* with PrBICAT3-BICAT3-Venus was already investigated in He et al., 2022 and used in this study as well. *eca3-2* was complemented by *EGFP-ECA3* driven by its native promoter as described in Mills *et al.* (2008) (PrECA3-EGFP-ECA3).

Expression of *ECA3* in the complementation lines 4-1 and 5-3 relative to that in the wild type was analysed by quantitative RT-PCR (qRT-PCR) (Figure 13, A). In addition, the amplicons of an RT-PCR were analysed by gel electrophoresis to qualitatively show the expression (Figure 13, B). Both lines showed a slightly increased expression of *ECA3* compared to the wild type.
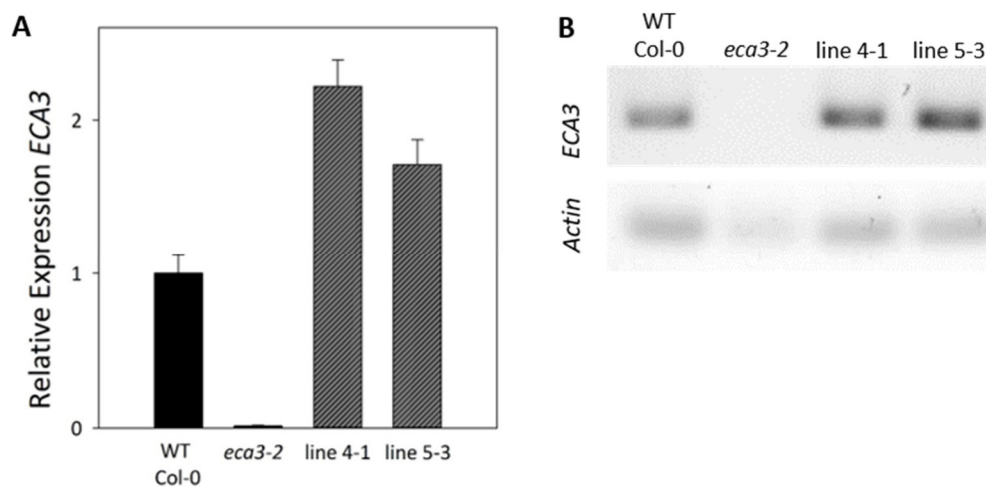
Figure 13: Complementation of *eca3-2* by *EGFP-ECA3* driven by the native promoter. (A) Relative expression as analysed by qRT-PCR. Expression was quantified using a cDNA dilution series and normalised against Actin2 (ACT2; At3g18780) (n=3). (B) RT-PCR of wild type Col-0 (WT Col-0), *eca3-2*, and *eca3-2 Pr-ECA3-EGFP-ECA3* complementation lines 4-1 and 5-3.

3.2.4 Growth Defects of *bicat3-1* and *eca3-2* under Ca^{2+} Toxicity are Partially Complemented by EGFP-ECA3 and BICAT3-Venus under their Native Promoters

Complementation lines of *eca3-2* by *EGFP-ECA3* and of *bicat3-1* by *BICAT3-Venus* (He *et al.*, 2022) were tested in a hydroponic culture with high Ca^{2+} supply. When grown under Ca^{2+} toxicity, *bicat3-1* and *eca3-2* showed the previously observed diminished growth (Figure 12, Figure 14, C + D), whereas the wild type was only slightly affected (Figure 14, B). Both complementation lines did not fully reverse the Ca^{2+} hypersensitivity of the mutants regarding the shoot size (Figure 14, C + D). This was supported by the fresh weight. Complementation lines of *bicat3-1* and *eca3-2* had a higher weight than the mutants, which was nevertheless lower than that of the wild type (Figure 14, A).
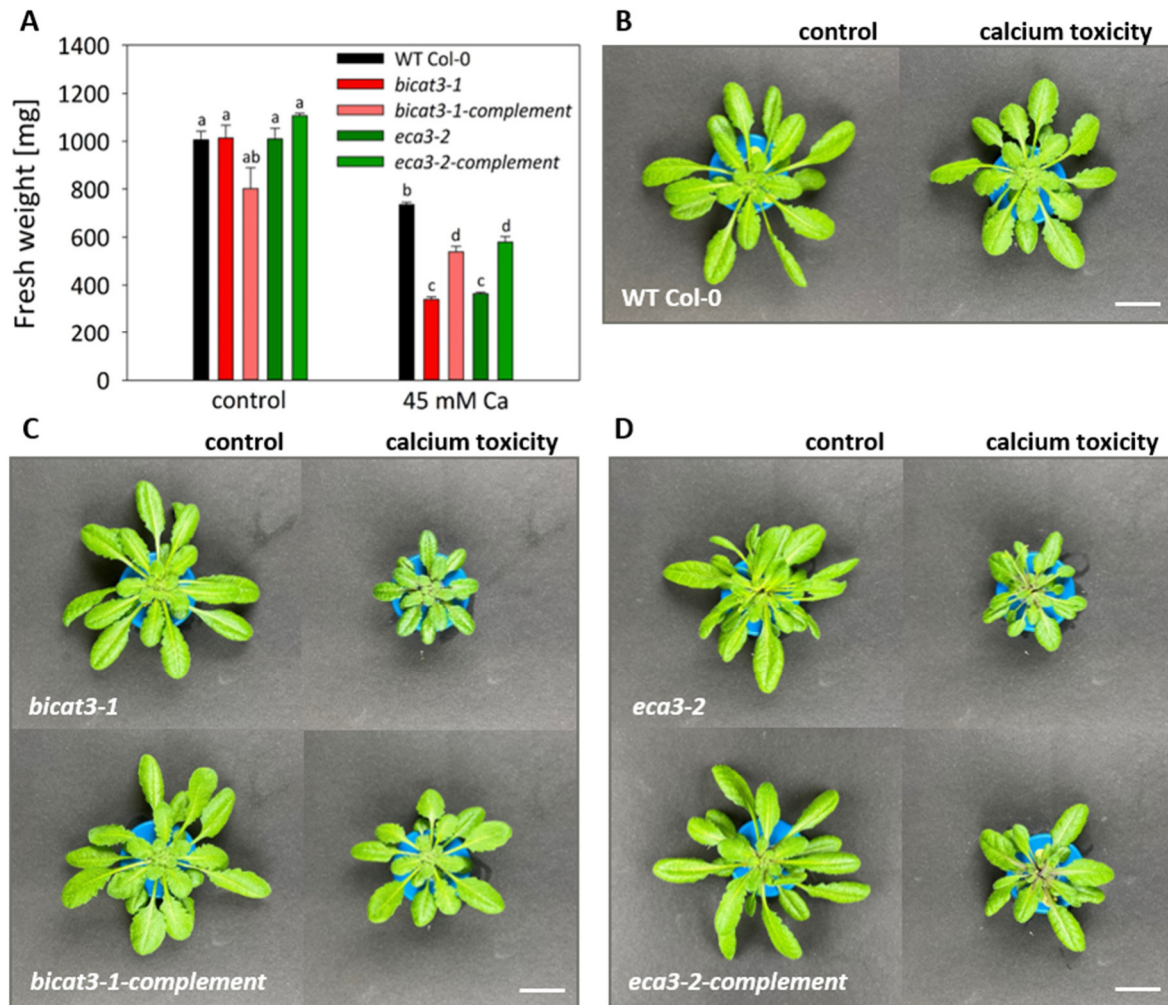
Figure 14: WT Col-0, *bicat3-1, eca3-2*, and the complementation lines of *bicat3-1* and *eca3-2* grown in liquid culture media under control conditions and calcium toxicity (45 mM CaCl$_2$). (A) Fresh weights of the shoots of the plants shown in B-D. (B-D) Representative images of a WT Col-0 (B), *bicat3-1* and *bicat3-1 BICAT3-Venus (bicat3-1-complement)* (C), and *eca3-2* and *eca3-2 EGFP-ECA3 (eca3-2-complement)* (D) under control conditions (left panels) and calcium toxicity (45 mM CaCl$_2$) (right panels). Bars represent the means ± SE of three replicates. Statistical significance was tested by one-way ANOVA with Tukey post hoc test (different letters indicate significance with P<0.05). Scale bars represent 20 mm.

3.2.5 *eca3-2* Shows a Growth Defect on Media Containing High Concentrations of Sodium Chloride

For further characterisation of *eca3* and *bicat3* mutants, a salt stress assay on half strength MS media was performed. Exposed to salt stress conditions (100mM NaCl), *eca3-2* and the double mutant *bicat3-1 eca3-2* showed a severe albino phenotype, while growth of all lines was comparable under control conditions (Figure 15, A). Growth was quantified by

determining the fresh weight of entire seedlings relative to control conditions. Seedlings grown under 75 mM NaCl showed no differences in growth. However, in presence of 100 mM NaCl, seedlings of *bicat3-1* showed only a slightly decreased relative fresh weight, while that of *eca3-2* and *bicat3-1eca3-2* was strongly reduced as compared to the wild type (Figure 15, B).

Figure 15: Salt stress assay of *Arabidopsis thaliana* WT Col-0, *bicat3-1*, *eca3-2*, and *bicat3-1eca3-2* grown for ten days on ½ MS plates under long-day conditions in a plant growth cabinet. (A) Representative images of two plates each of ten-days-old seedlings grown under control conditions (A, upper panel) or under salt stress (100 mM NaCl) (A, lower panel). (B) Fresh weight of the seedlings relative to control conditions (0 mM NaCl). Bars represent the means ± SE of ≥ three plates per treatment with four seedlings per line. Statistical significance was tested by one-way ANOVA with Tukey post hoc test for each treatment (n.s. = not significant; different letters indicate significance with P<0.05). Scale bars represent 10 mm. Experiment was repeated twice with comparable results.

After 14 days under control conditions, there were no observed differences in growth between genotypes, which is also reflected by the fresh weights. Exposed to 100 mM NaCl, *eca3-2* and *bicat3-1 eca3-2* showed a completely whitish phenotype and a decreased growth

and fresh weight (Figure 16), while *bicat3-1* showed a similar fresh weight like the wild type showing the plants compensated the subtle delay in growth reported after ten days (Figure 15).

Figure 16: Salt stress assay of *Arabidopsis thaliana* WT Col-0, *bicat3-1*, *eca3-2,* and *bicat3-1eca3-2* grown for 14 days on ½ MS plates under long-day conditions in a plant growth cabinet. (A) Representative images of 14-days-old seedlings grown under control conditions (upper panel) or under salt stress (100 mM NaCl, lower panel). (B) Fresh weight of the seedlings. Bars represent the means ± SE of ≥ three plates per treatment with four seedlings per line. Statistical significance was tested by one-way ANOVA with Tukey post hoc test for each treatment (n.s. = not significant; different letters indicate significance with P<0.05). Scale bars represent 10 mm. Experiment was repeated twice with comparable results.

To validate if the impaired growth of *eca3-2* under salt stress was a consequence of the missing *ECA3*, the assay was repeated with the complementation line 4-1 of *eca3-2* carrying an EGFP-ECA3 fusion under the native promoter. Under control conditions, all lines showed comparable growth and fresh weights (Figure 17). The severe whitish and diminished growth of *eca3-2* was restored in the complementation line.
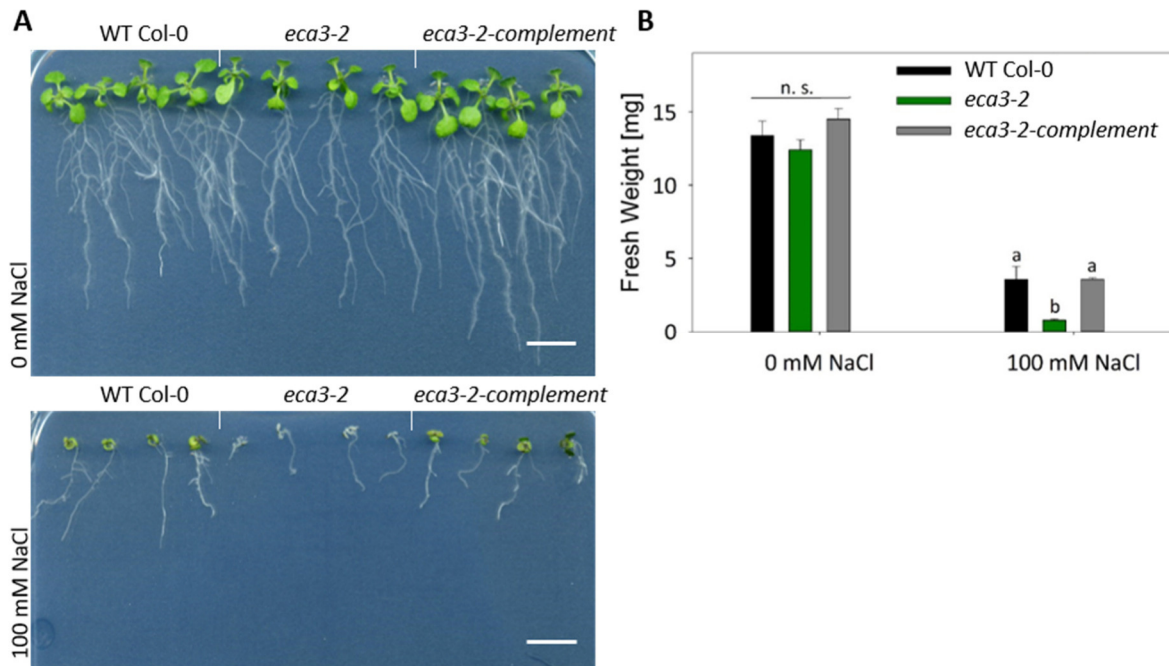
Figure 17: Salt stress assay of *Arabidopsis thaliana* WT Col-0, *eca3-2, and eca3-2 PrECA3-EGFP-ECA3* grown for 14 days on ½ MS plates under long-day conditions in a plant growth cabinet. (A) Representative images of 14-day-old seedlings grown under control conditions (upper panel) or under salt stress (100 mM NaCl, lower panel). (B) Fresh weight of the seedlings. Bars represent the means ± SE of ≥ three plates per treatment with four seedlings per line. Statistical significance was tested by one-way ANOVA with Tukey post hoc test for each treatment (n.s. = not significant; different letters indicate significance with P<0.05). Scale bars represent 10 mm.

When treated with 100 mM NaCl, WT Col-0, *bicat3-1*, and the complementation line 23-4, expressing *BICAT3-EGFP* under its native promoter, showed a similar growth and fresh weight (Figure 18). Interestingly, the complementation line of *bicat3-1* had a diminished growth under control condition compared to the wild type and *bicat3-1* (Figure 18, B) as observed tendencially before in hydroponics (Figure 14).
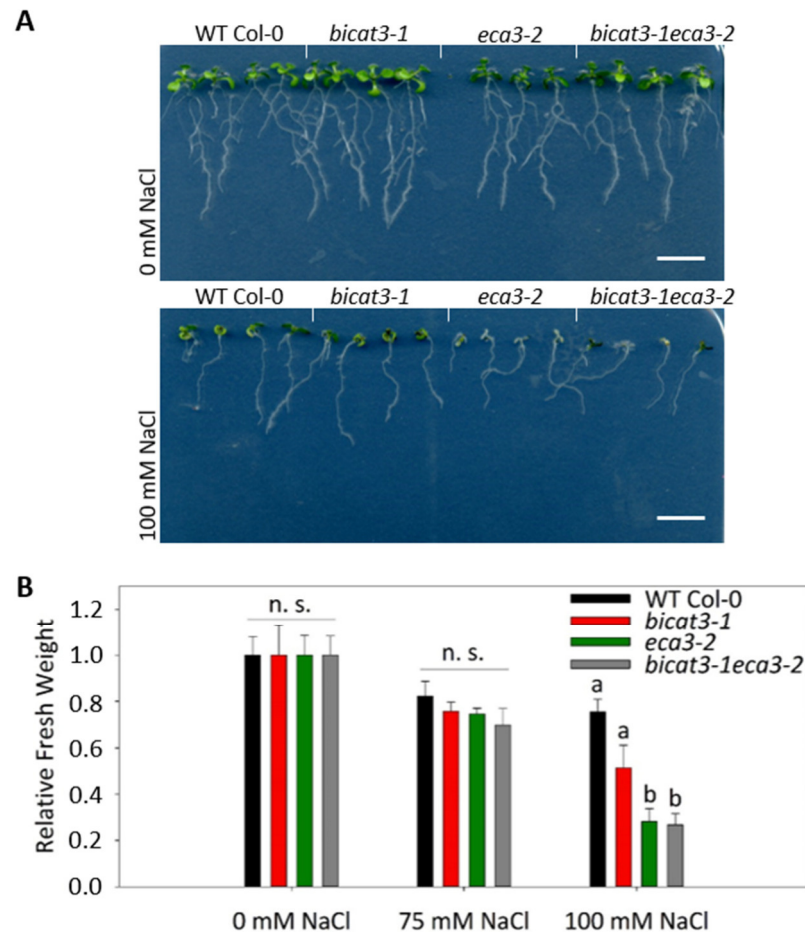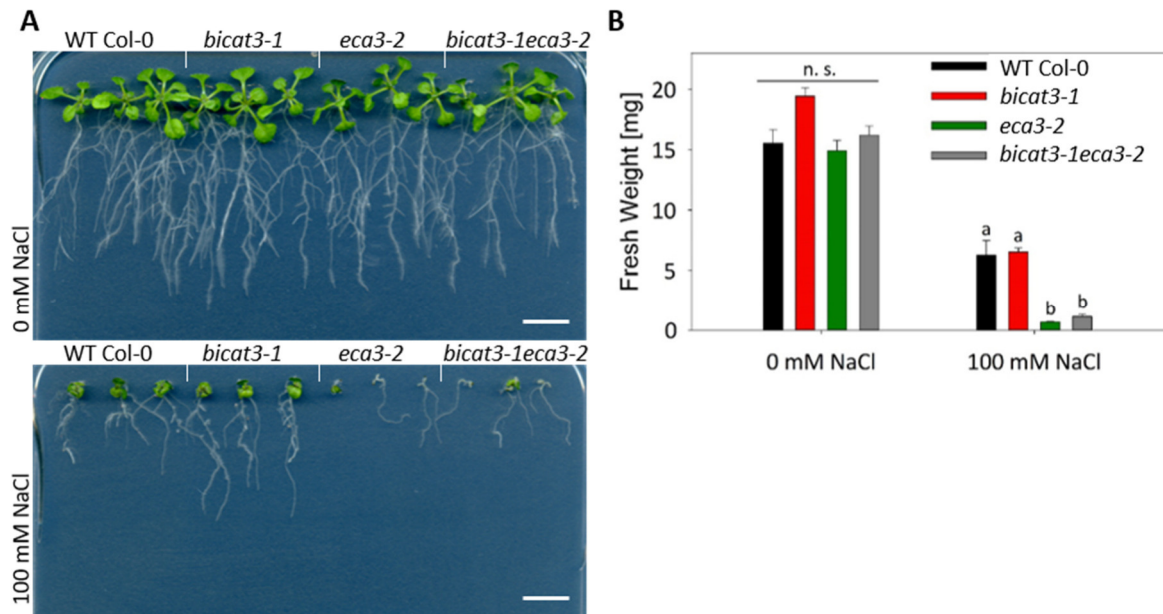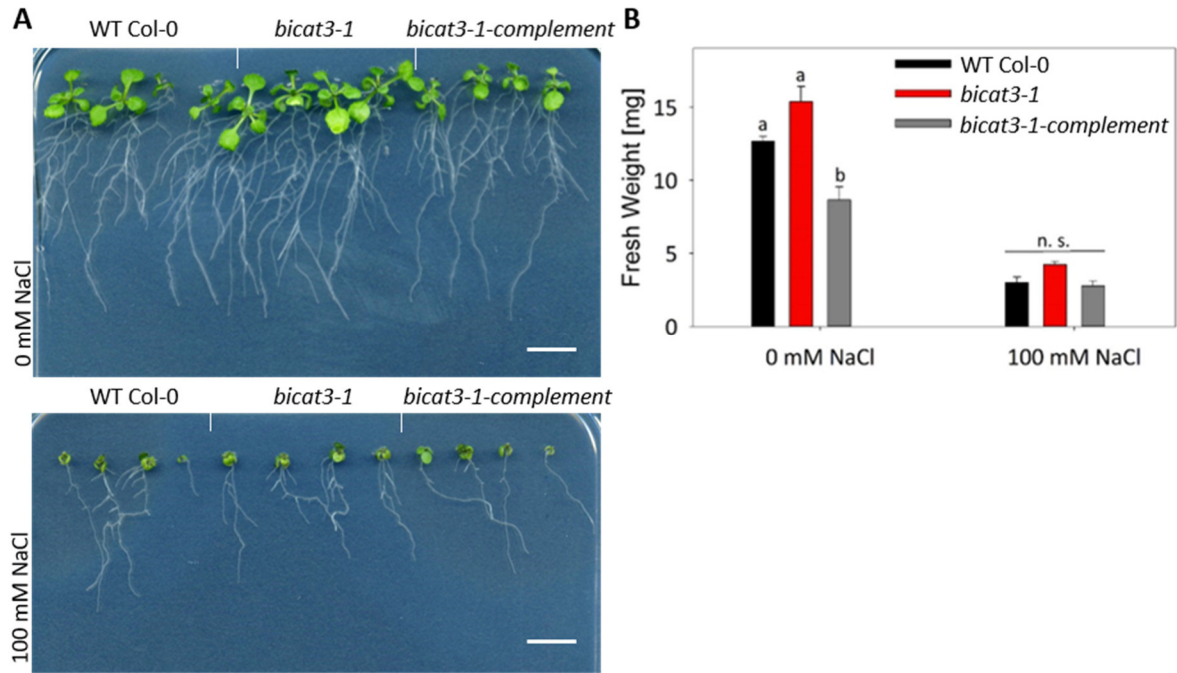
Figure 18: Salt stress assay of *Arabidopsis thaliana* WT Col-0, *bicat3-1*, and *bicat3-1-pBICAT3-BICAT3-Venus* grown for 14 days on ½ MS plates under long-day conditions in a plant growth cabinet. (A) Representative images of 14-day-old seedlings grown under control conditions (upper panel) or under salt stress (100 mM NaCl, lower panel). (B) Fresh weight of the seedlings. Bars represent the means ± SE of ≥ three plates per treatment with four individual seedlings per line. Statistical significance was tested by one-way ANOVA with Tukey post hoc test for each treatment (n.s. = not significant; different letters indicate significance with P<0.05). Scale bars represent 10 mm.

3.3 Expression Analysis of *ECA3* and *BICAT3*

3.3.1 *In silico* Analysis of Co-expression of the Ten Most Correlated Genes with *ECA3* by GENEVESTIGATOR

A co-expression analysis of *ECA3* may provide insights in its possible roles and in involvement in responses to environmental cues such as salt stress. Therefore, GENEVESTIGATOR (Zimmermann *et al.*, 2004) was used for *in silico* analyses, and ten genes that showed the highest correlation in expression with *ECA3* are shown. The dataset included 3240 perturbations from AT_AFFY_ATH1-0 data selection. Figure 19 shows the ten genes with the highest co-expression with *ECA3* (positive correlation above R^2=0.539) and visualises it in a Pearson's correlation plot. Thereby, four of them were not annotated so far, whereby *RPN2, OST48, UGGT, OST1B, STT3A,* and *STT3B* are coding for subunits of glycosyltransferases and ER-resident proteins involved in protein folding.
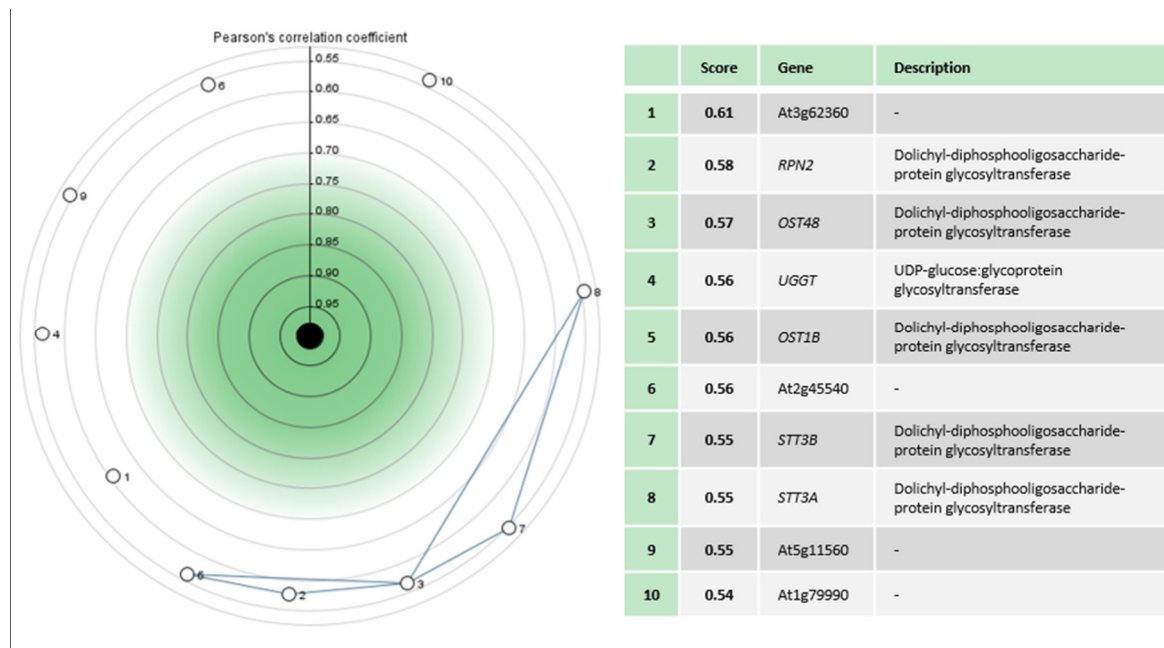
Figure 19: Co-expression of genes with *ECA3* analysed and created by GENEVESTIGATOR. Pearson's correlation coefficient shown in the scale of the plot (left) and mentioned as "Score" in the table (right) represents the linear correlation between the expression of two genes. Greater values indicate stronger correlation. Images exported by export function from GENEVESTIGATOR software.

3.3.2 Comparison of *ECA3* Promoter Activity by Nuclear-Targeted Triple Venus and ß-Glucuronidase Staining

To investigate the expression of *BICAT3* and *ECA3*, their native promoters were fused either to ß-Glucuronidase (GUS) for histochemical staining or to a nuclear-targeted triple Venus (NLS3xVenus). The expression pattern of *ECA3* analysed by both reporter proteins was comparable. The promoter of *ECA3* was predominantly active in the entire cotyledon, while the activity was slightly increased in the vasculature (Figure 20, A + H). In addition, cells of the hypocotyl showed a strong promoter activity (Figure 20, B + I). The promoter of *ECA3* was also active in epidermal and mesophyll cells (Figure 20, C + J) and guard cells (Figure 20, E + K), which suggests an impact on guard cell activity. In roots, the expression seemed to be limited to vascular tissues (Figure 20, D + F + M) and meristematic cells in the root tip (Figure 20, G + L).
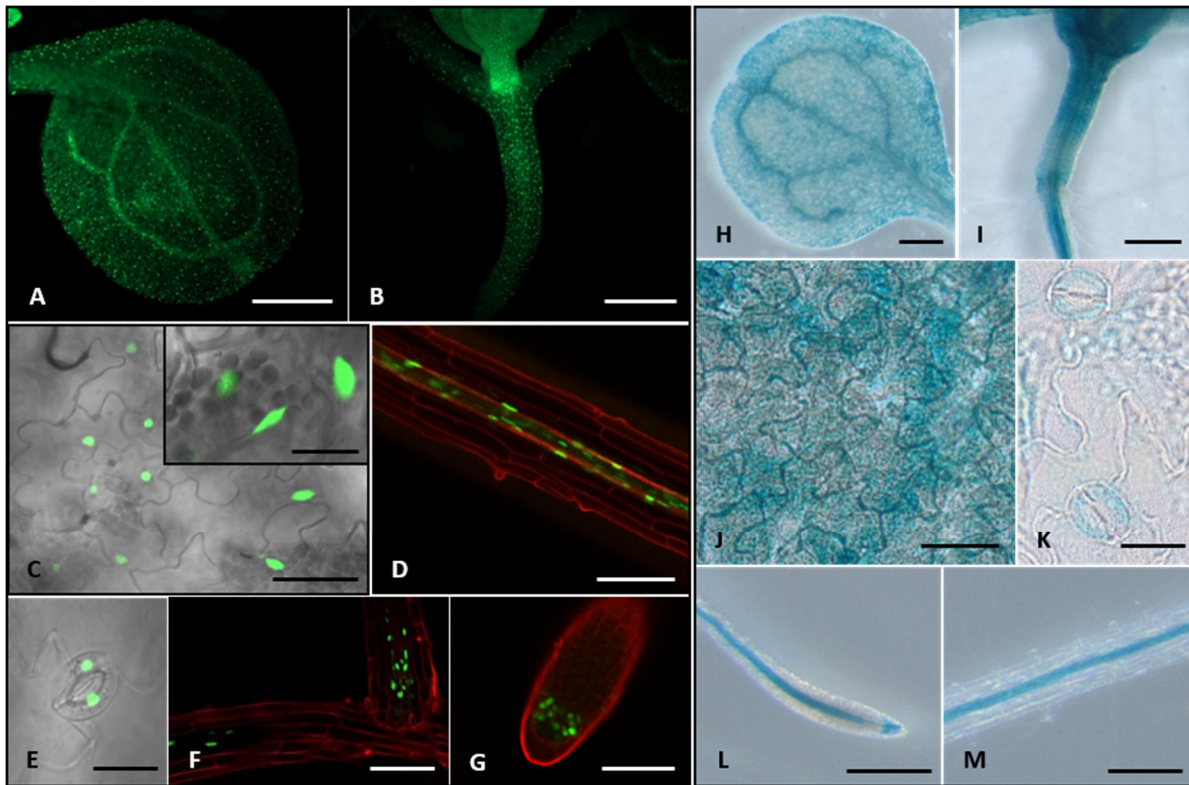
Figure 20: Promoter activity of *ECA3* shown by a fluorescence microscopy using a triple Venus targeted to the nucleus (NLS3xVenus; A-G) and by ß-Glucuronidase staining (GUS; H-K). Promoter activity in cotyledons (A: NLS3xVenus; H: GUS) and hypocotyls (B: NLS3xVenus; I: GUS) of ten-day-old *Arabidopsis thaliana* seedlings and in leaf epidermal cells (C: NLS3xVenus; J: GUS), leaf mesophyll (C, inset: NLS3xVenus) and guard cells (E: NLS3xVenus; K: GUS) of four-weeks-old *Arabidopsis thaliana* seedlings. Promoter activity in the vasculature of the main root and in lateral roots tips of ten-days-old *Arabidopsis thaliana* seedlings (D, F, G: NLS3xVenus; L, M: GUS). Images were taken by (A, B) a Hamamatsu ORCA flash 4.0 camera mounted on an AxioZoom.V16 (Zeiss), (C-G) confocal laser scanning microscopy using a LSM880 (Zeiss), (H, I, L, M) AxioCam 506 mounted on a Stereo Discovery.V20 (Zeiss) and (J, K) AxioCam HRc mounted on an Axioskop (Zeiss). (D, F, G) Red colour represents the cell wall staining by propidium iodide. Scale bars represent 200 µm (A, B, H, I), 100 µm (D, F, L, M), 50 µm (C, G), 20 µm (C (inset), E, J, K).

3.3.3 Visualisation of *BICAT3* Promoter Activity by Nuclear-Targeted Triple Venus Shows Expression Exclusively in Roots while quantitative RT-PCR Reveals Expression also in Shoots

In this study, the promoter activity of *ECA3* shown by nuclear-targeted triple Venus coincided with that determined by histochemical GUS staining. In contrast to this, He *et al.*, 2022 showed a promoter activity of *BICAT3* in the entire plant using GUS staining, while this was limited to root tissues using NLS3xVenus (Figure 21, A, c-f). No expression of NLS3xVenus was visible in shoots (Figure 21, A, a + b). To validate whether there was an expression of *NLS3xVenus* in

shoots, that was not visible using fluorescence microscopy, a quantitative RT-PCR was performed on ten-day-old seedlings. Intriguingly, despite of an absent fluorescence signal, there was a very strong expression of *NLS3xVenus* under control of *BICAT3* promoter in shoots (Figure 21, B). In roots, the expression of *NLS3xVenus* driven by the *ECA3* promoter was markedly lower than that driven by the *BICAT3* promoter.
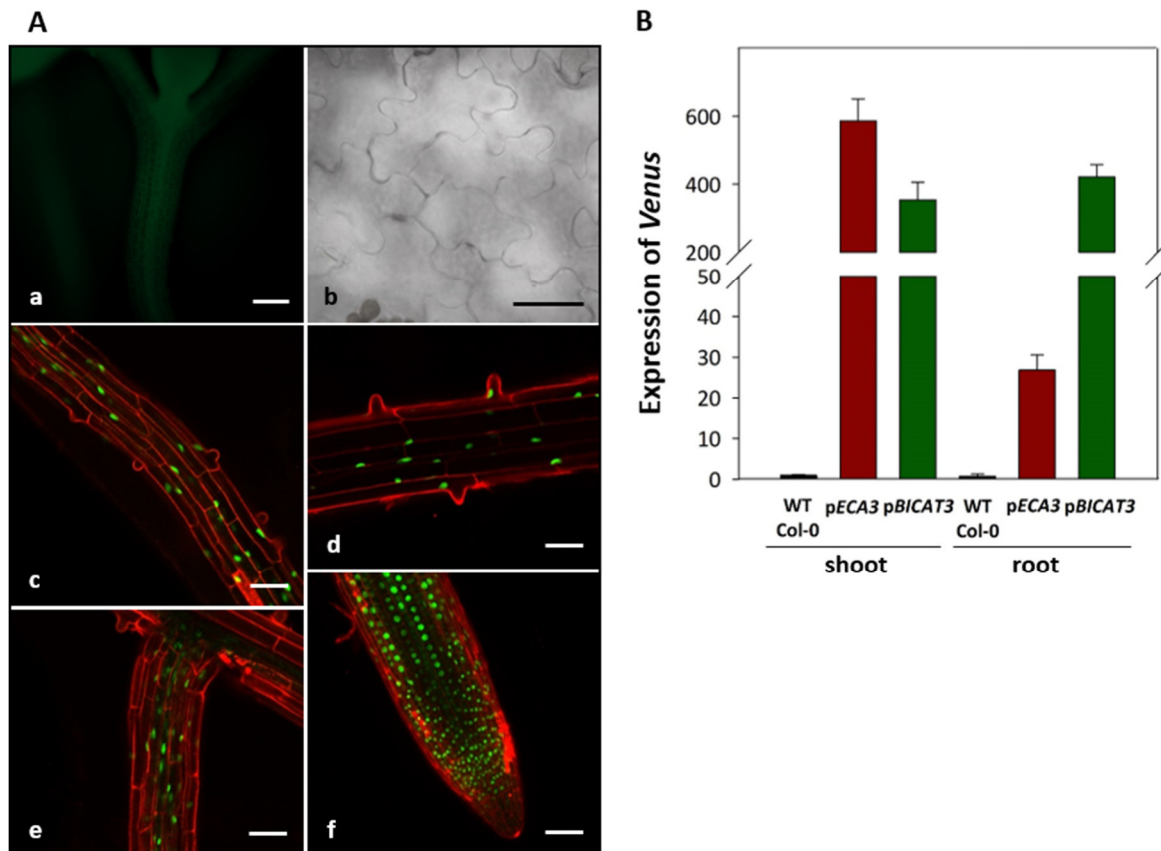
Figure 21: (A) Expression pattern of triple Venus targeted to the nucleus (NLS3xVenus) under control of the *BICAT3* promoter (p*BICAT3*). (a) Fluorescence of NLS3xVenus in the hypocotyl of ten-day-old *Arabidopsis thaliana* seedlings and (b) in the epidermal cells of four-week-old *Arabidopsis thaliana* leaves. (c-f) Fluorescence of NLS3xVenus in main roots, lateral roots, and main root tip of ten-day-old *Arabidopsis thaliana* seedlings. Images were acquired by laser-scanning microscopy as in Figure 19. Scale bars represent (a) 200 µm and (b-f) 50 µm. (B) Expression of *Venus* driven by the promoter of *ECA3* (p*ECA3*) and *BICAT3* (p*BICAT3*) determined by quantitative RT-PCR. Expression was quantified using a cDNA dilution series and normalised against Actin2 (ACT2; At3g18780) (n=3).

3.4 Intraorganellar Targeting of Golgi-specific EGFP-Aequorin Fusions

3.4.1 MNS1tmd-EGFP-AEQ Targets to the Golgi in *Arabidopsis thaliana* Mesophyll Protoplasts and Infiltrated *Nicotiana benthamiana* Leaves

BICAT3 and ECA3 are localised in the Golgi, and mutants display severe growth defects on media with high Ca^{2+} availability. To test the hypothesis that both proteins affect free Ca^{2+} concentration in the Golgi ($[Ca^{2+}]_{Golgi}$), a reporter system to determine $[Ca^{2+}]_{Golgi}$ was employed. Due to the acidic luminal pH of the Golgi, the pH-independent Ca^{2+} reporter aequorin appeared to be the most suitable tool. To target APOAEQUORIN to the *cis-* and *medial*-Golgi, the TMD of α-mannosidase I (MNS1tmd) was used because it was previously shown to be localised specifically in these Golgi cisternae by electron microscopy in *A. thaliana* roots (Donohoe *et al.*, 2013). To validate the correct targeting, an EGFP was fused N-terminally to APOAEQUORIN, and localisation studies were performed.

Targeting of MNS1tmd-EGFP-AEQ was examined first by transient co-expression with MNS1tmd-mCherry in *A. thaliana* mesophyll protoplasts (Figure 22, A - D), and co-localisation was analysed using a virtual line scan analysis (Figure 22, E). The localisation showed a punctate structure, and the MNS1tmd-EGFP-AEQ fusion overlapped with the MNS1tmd-mCherry marker. To further validate the targeting, MNS1tmd-EGFP-AEQ co-localised with the *cis*-Golgi SYP31-mCherry marker in infiltrated *N. benthamiana* leaves (Figure 22, F - I), which was also reflected by a virtual line scan (Figure 22, J).
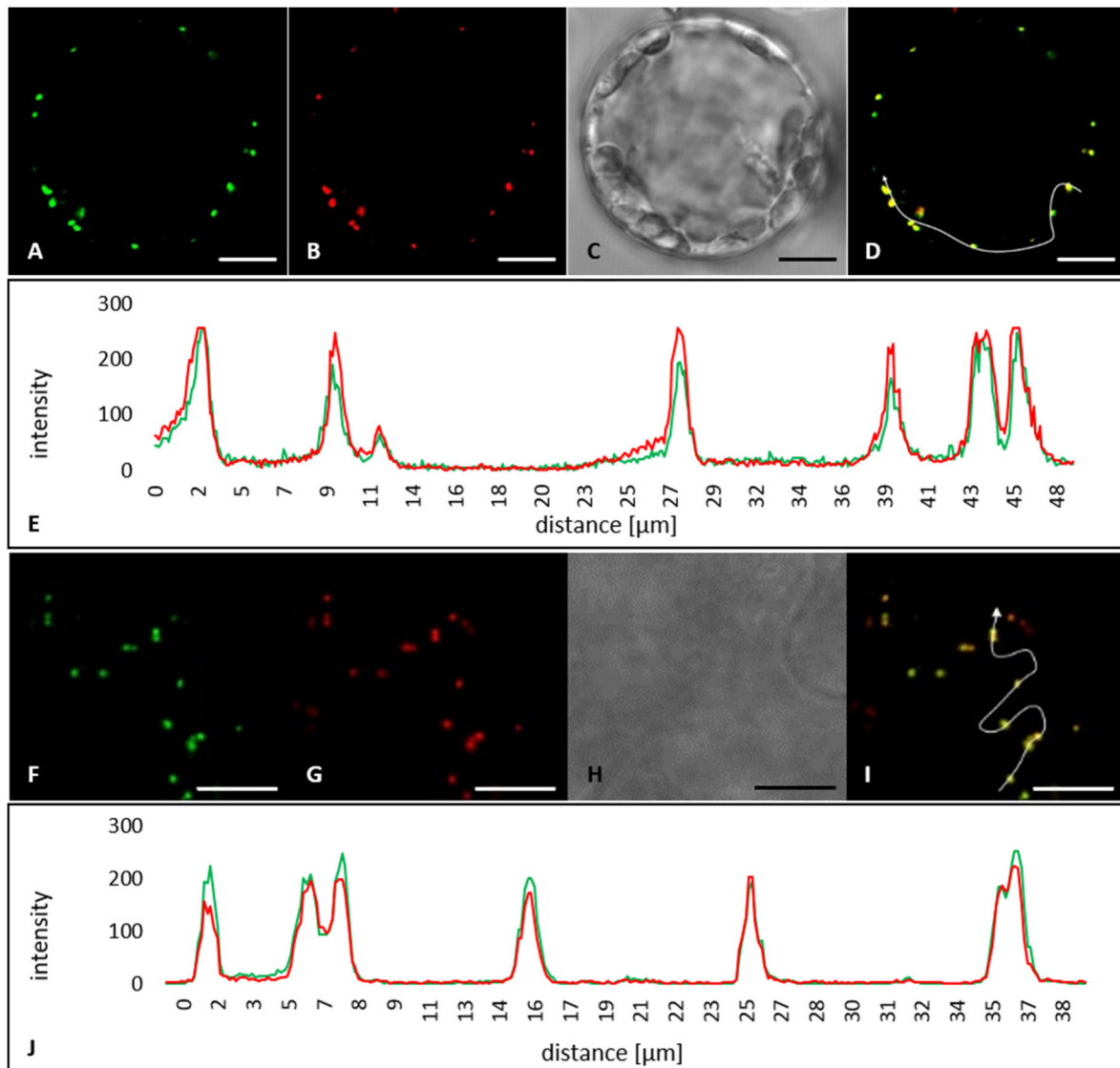
Figure 22: Co-localisation of MNS1tmd-EGFP-AEQ and MNS1tmd-mCherry in four-week-old *Arabidopsis thaliana* mesophyll protoplast. (A) EGFP, (B) mCherry, (C) PMT channel, (D) merged picture, and (E) virtual line scan showing the pixel intensity of EGFP (green line) and mCherry (red line) along the arrow in the merged image. Co-localisation of MNS1tmd-EGFP-AEQ and SYP31-mCherry in five-week-old infiltrated *N. benthamiana* leaf 48 h post infiltration. (F) EGFP, (G) mCherry, (H) PMT channel, (I) merged picture and (J) virtual line scan showing the pixel intensity of EGFP (green line) and mCherry (red line) along the arrow in the merged image. Scale bars represent 10 µm.

3.4.2 FUT1tmd-EGFP-AEQ Targets to the Golgi in *Arabidopsis thaliana* Mesophyll Protoplasts and Infiltrated *Nicotiana benthamiana* Leaves

To precisely analyse free Ca^{2+} concentrations in the *trans*-Golgi ($[Ca^{2+}]_{transGolgi}$), APOAEQUORIN was fused to the TMD of fucosyltransferase I (FUT1tmd) shown to be resident in the late Golgi

in immunogold electron microscopy studies (Parsons *et al.*, 2019). To validate the correct targeting, an EGFP was fused N-terminally to APOAEQUORIN, and localisation studies were performed. FUT1tmd-EGFP-AEQ was first co-expressed with the *trans*-Golgi marker sialyltransferase (ST)-mCherry in transiently transformed *A. thaliana* mesophyll protoplasts (Figure 23, A - D). A virtual line scan showed a co-localisation (Figure 23, E). Furthermore, FUT1tmd-EGFP-AEQ was co-infiltrated with ST-mCherry into *N. benthamiana* leaves (Figure 23, F - I). Virtual line scans again showed that the EGFP and the mCherry fluorescence were congruent (Figure 23, J).
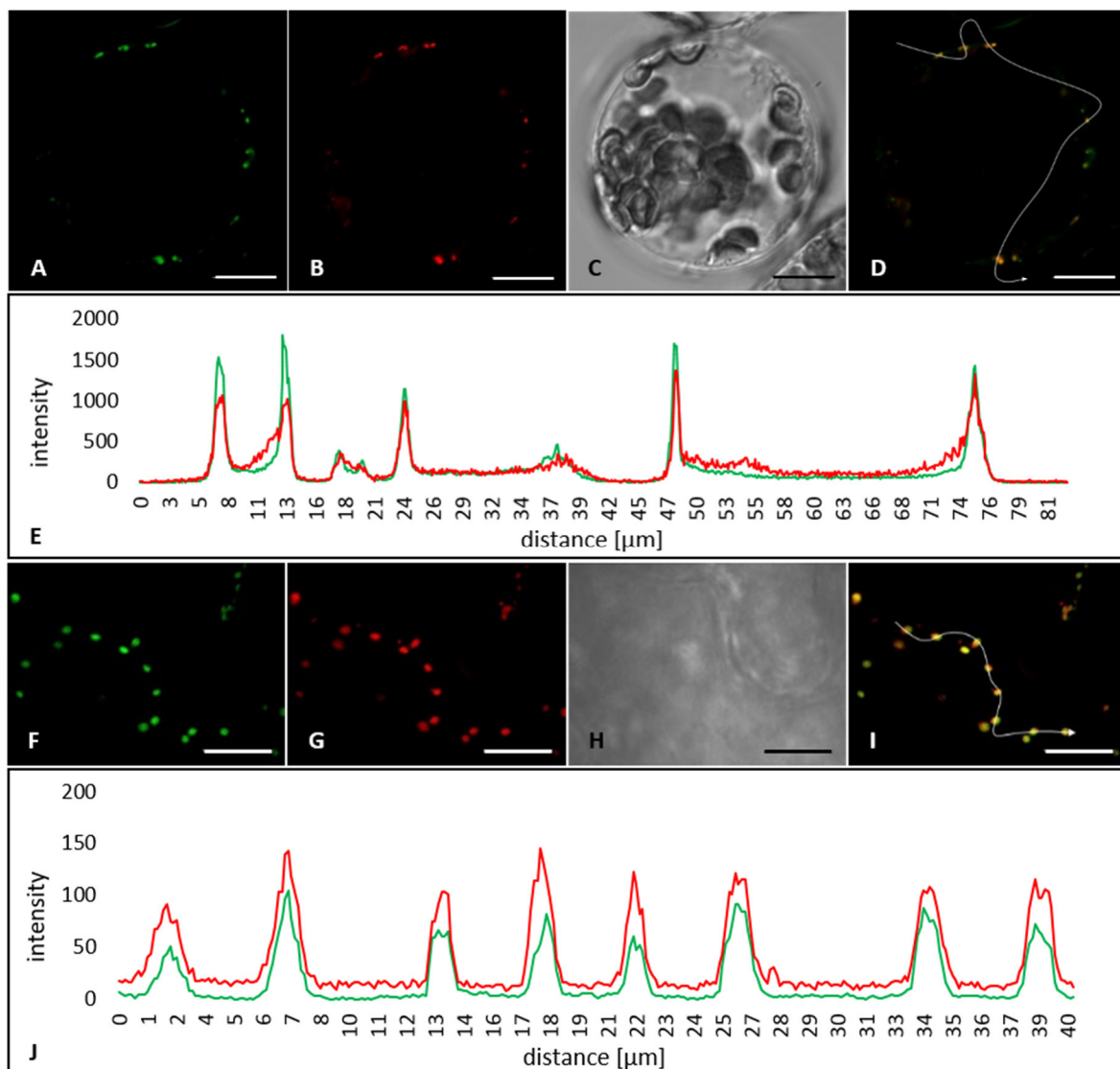
Figure 23: Co-localisation of FUT1tmd-EGFP-AEQ and sialyltransferase-mCherry in four-week-old *Arabidopsis thaliana* mesophyll protoplast. (A) EGFP, (B) mCherry, (C) PMT channel, (D) merged picture, and (E) virtual line scan showing the pixel intensity of EGFP (green line) and mCherry (red line) along the arrow in the merged image. Co-localisation of FUT1tmd-EGFP-AEQ and sialyltransferase-mCherry in five-week-old infiltrated *N. benthamiana* leaf 48 h post infiltration. (F) EGFP, (G) mCherry, (H) PMT channel, (I) merged picture, and (J) virtual line scan showing the pixel intensity of EGFP (green line) and mCherry (red line) along the arrow in the merged image. Scale bars represent 10 µm.

3.4.3 MNS1tmd-EGFP-AEQ Targets to Early Golgi Compartments and FUT1tmd-EGFP-AEQ to the Late Golgi in Infiltrated *Nicotiana benthamiana* Leaves

The localisation of MNS1tmd-EGFP-AEQ and FUT1tmd-EGFP-AEQ in *A. thaliana* mesophyll protoplasts and *N. benthamiana* leaves displayed the correct targeting to the Golgi by showing an overlap with the specific *cis-* and *trans*-Golgi markers, respectively. However, the small distance of the cisternae within the Golgi stack does not yet allow a conclusion of their sub-compartmental targeting. Therefore, the established method of confocal high-resolution video recording (2.5.21; Figure 8) to distinguish Golgi cisternae in side view was performed. Localisation of MNS1tmd-EGFP-AEQ in *N. benthamiana* leaves showed a clear correspondence with that of the *cis-* and *medial*-Golgi marker MNS1tmd-mCherry, while a shift occurred in the co-localisation with the *trans*-Golgi marker (Figure 24, A + B). This was also visualised by virtual line scan analysis which showed a shift in the peaks of intensity of EGFP and mCherry. The same experimental setup was used to verify FUT1tmd-EGFP-AEQ targeting to the *trans*-Golgi by co-infiltration of *N. benthamiana* leaves with MNS1tmd-mCherry and ST-mCherry. FUT1tmd-EGFP-AEQ showed a co-localisation with ST-mCherry, but not with MNS1tmd-mCherry. This clear shift was also visible in the virtual line scans (Figure 24, C + D).
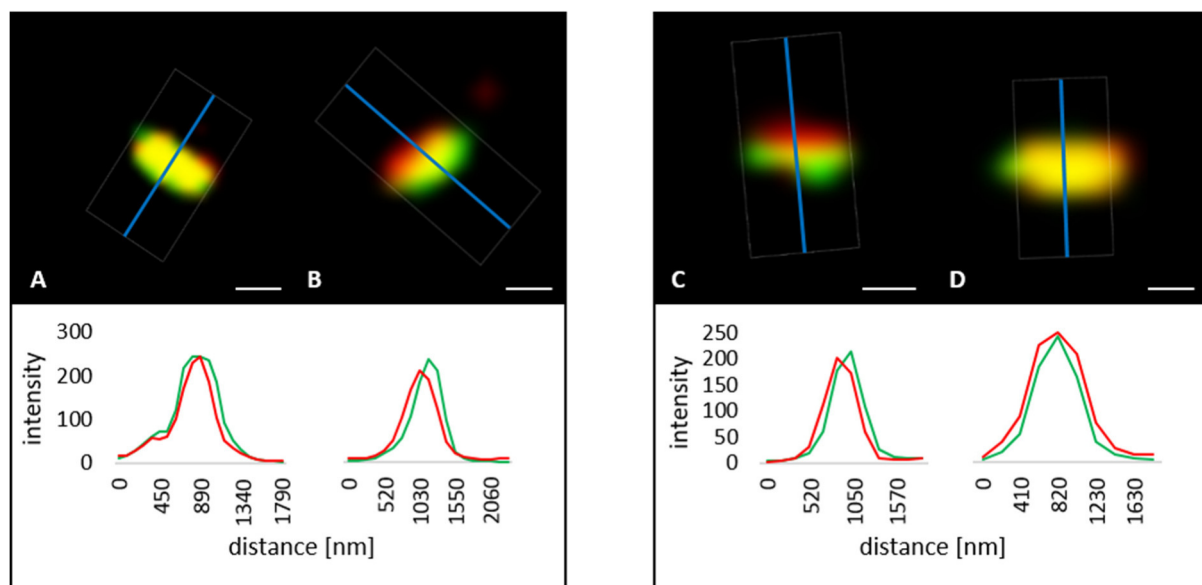
Figure 24: Precise localisation of MNS1tmd-EGFP-AEQ and FUT1tmd-EGFP-AEQ. Co-localisation of MNS1tmd-EGFP-AEQ and MNS1tmd-mCherry (A) or ST-mCherry (B). Co-localisation of FUT1tmd-EGFP-AEQ and MNS1tmd-mCherry (C) or ST-mCherry (D). Virtual line scans showing the pixel intensity of EGFP (green line) and mCherry (red line) along the lines shown in the pictures. Scale bars represent 0.5 μm.

3.4.4 Distinction of Golgi Cisternae by Immunogold Electron Microscopy in *Arabidopsis thaliana* mesophyll Cells Stably Expressing MNS1tmd-EGFP-AEQ

The constructed *cis*- and *trans*-Golgi-specific Ca^{2+} reporter fusions were used to generate stable lines. To further confirm the results of the targeting to distinct Golgi cisternae, immunostaining and electron microscopy was performed with plants stably expressing *MNS1tmd-EGFP-AEQ*. Therefore, a GFP antibody was used to detect the reporter fusion protein in a stably transformed *A. thaliana* line (M2; 2.3.3). The stacks of the Golgi were apparent, but the structures were not clearly visible. Labelling of MNS1tmd-EGFP-AEQ seemed to predominantly occur at one side of the Golgi stacks, suggesting that there is a subcompartmental preference (Figure 25, B). Unfortunately, the structures were not unequivocally distinguishable from each other, which prevents a conclusion of a localisation of MNS1tmd-EGFP-AEQ in early or late Golgi compartments by this technique. No labelling was detectable in the Col-0 wild type control (Figure 25, A).
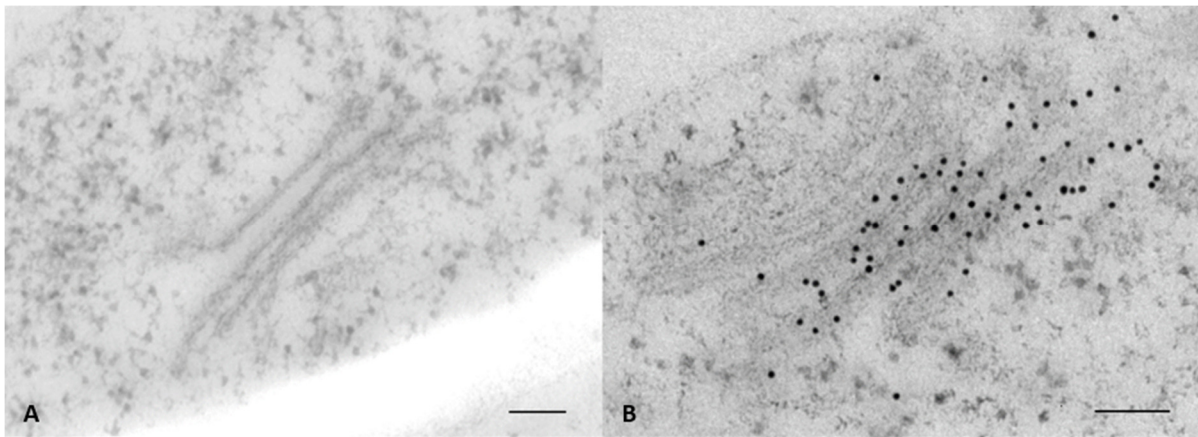
Figure 25: Localisation of MNS1tmd-EGFP-AEQ using electron microscopy. Immunolabelling with a GFP antibody performed in mesophyll cells of five-week-old wild type Col-0 (A) or stably transformed MNS1tmd-EGFP-AEQ plants (line M2) (B). Scale bars represent 100 nm.

3.4.5 Protease Protection Assay Shows Lumen-faced Orientation of Golgi-Targeted Aequorin

Since the two reporter fusions MNS1tmd-EGFP-AEQ and FUT1tmd-EGFP-AEQ were shown to have the correct localisation in the distinct Golgi subcompartments, the orientation of the reporter to the compartmental lumen needed to be validated. Thus, a protease protection assay was performed. *A. thaliana* mesophyll protoplasts of stable lines expressing *MNS1tmd-EGFP-AEQ* or *FUT1tmd-EGFP-AEQ* were prepared, and the membrane fractions were isolated by ultra-centrifugation. The membrane fractions were treated either by proteinase K to digest the protein fusion, Triton X-100 to disrupt the membrane, or both, proteinase K and Triton X-100. The protein samples were separated by SDS-PAGE for Western blot analysis using an EGFP antibody. The non-treated samples and samples treated with proteinase K only showed bands with the expected size of approximately 60 kDa [10.8 kDa (FUT1tmd) + 26.9 kDa (EGFP)+ 22.5 kDa (AEQ)] for FUT1tmd-EGFP-AEQ and 55 kDa [5.8 kDa (MNS1tmd) + 26.9 kDa (EGFP) + 22.5 kDa (AEQ)] for MNS1tmd-EGFP-AEQ. Due to dimerization of EGFP, a stronger band with a size of approx. 120 kDa (2 x 60 kDa) for FUT1tmd-EGFP-AEQ and 110 kDa (2 x 55 kDa) for MNS1tmd-EGFP-AEQ was detectable. A combined treatment with proteinase K and Triton X-100 showed bands with a size of approximately 34 kDa, while no bands in the expected size of intact reporter fusions were visible, indicating a digestion of these protein fusions (Figure 26). The protease protection assay showed that both, MNS1tmd-EGFP-AEQ and FUT1tmd-EGFP-AEQ, face the lumen of the respective Golgi compartment and are suitable to detect free Ca^{2+} concentrations in the *cis-* and *trans-*Golgi, respectively.
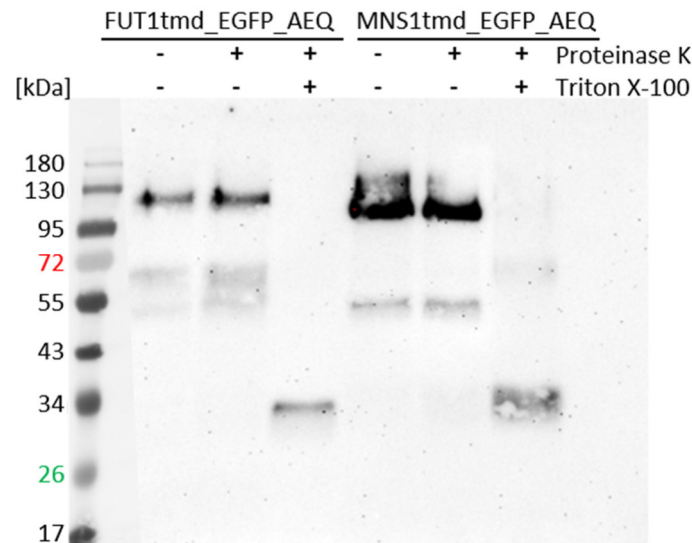
Figure 26: Protease Protection Assay. Membrane fractions of Arabidopsis mesophyll protoplasts expressing *FUT1tmd-EGFP-AEQ* or *MNS1tmd-EGFP-AEQ* were isolated, separated by SDS-PAGE, and blotted onto a nitrocellulose membrane for Western blot analysis using a GFP antibody. Proteins were either untreated, treated with proteinase K, or with proteinase K and Triton X-100.

3.5   Calcium Measurements

3.5.1   Analysis of Ca^{2+} Transients in Response to NaCl using *N. benthamiana* Protoplasts Transiently Expressing Golgi-Targeted Aequorin

Since the generation of Arabidopsis lines stably expressing the Golgi-targeted aequorin reporters requires a longer period, *MNS1tmd-EGFP-AEQ* and *FUT1tmd-EGFP-AEQ* were transiently expressed in *N. benthamiana* leaves, and protoplasts isolated from these leaves were used for initial [Ca^{2+}]$_{Golgi}$ measurements. Therefore, protoplasts were isolated 48 h post infiltration and reconstituted with coelenterazine, and [Ca^{2+}]$_{cisGolgi}$ and [Ca^{2+}]$_{transGolgi}$ were analysed using a tube luminometer. After recording the basal levels of [Ca^{2+}]$_{cisGolgi}$ and [Ca^{2+}]$_{transGolgi}$ for 180 sec, 200 mM NaCl was applied. [Ca^{2+}]$_{cisGolgi}$ immediately increased from approx. 0.2 µM up to approx. 0.7 µM and decreased after around 10 sec to a new basal level of 0.3 µM (Figure 27, A). In contrast to this, the [Ca^{2+}]$_{transGolgi}$ merely increased and not even reached 0.4 µM (Figure 27, B). Interestingly, the basal [Ca^{2+}]$_{transGolgi}$ ranged at 0.25 µM and thus was slightly higher than the basal [Ca^{2+}]$_{cisGolgi}$ (Figure 27).
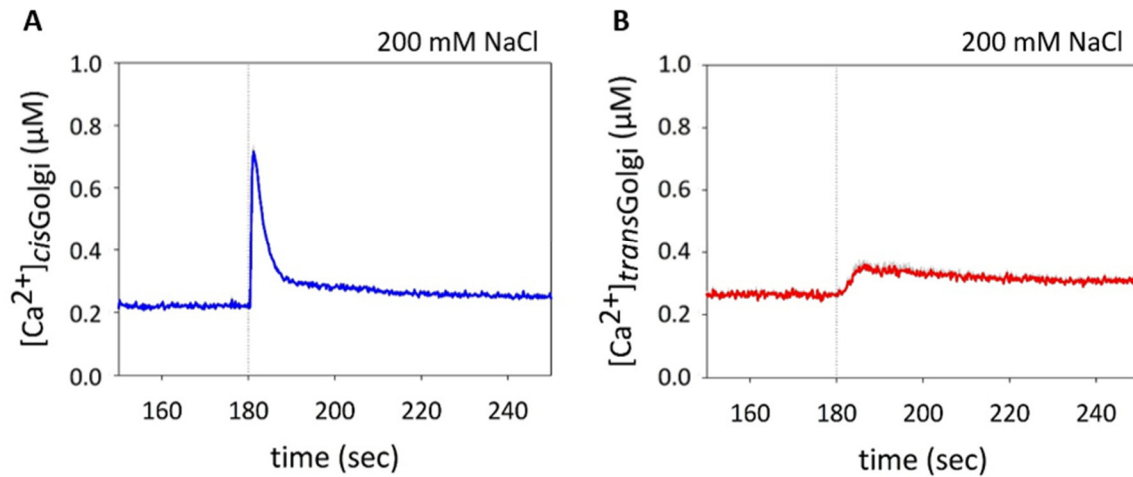
Figure 27: Changes in $[Ca^{2+}]_{cisGolgi}$ and $[Ca^{2+}]_{transGolgi}$ in response to 200 mM NaCl in *N. benthamiana* mesophyll protoplasts transiently expressing (A) *MNS1tmd-EGFP-AEQ* and (B) *FUT1tmd-EGFP-AEQ*. Dotted lines represent the time point of injection of the treatment. Lines represent means ± SE of n=3.

3.5.2   Luminescence of *Arabidopsis thaliana* Seedlings Stably Expressing Golgi-targeted Aequorin

As mentioned above, Arabidopsis lines expressing the *cis*- or *trans*-Golgi-specific Ca^{2+} reporter aequorin were generated. To select suitable lines, Relative Light Units (RLUs) upon a discharge by a 1 M $CaCl_2$ in 10 % ethanol solution were analysed in five-days-old seedlings and compared with those of seedlings expressing *APOAEQUORIN* localised in the cytosol (Knight *et al.*, 1991). Therefore, the aequorin was reconstituted with coelenterazine and discharged the next day. The emitted RLUs in response to the discharge of the Golgi-aequorin reporter lines were very low in comparison to the cytosolic aequorin line. Lines expressing *MNS1tmd-EGFP-AEQ* (*cis*-Golgi) showed higher RLUs of approx. 5-6 x 10^6 RLUs compared to those expressing *FUT1tmd-EGFP-AEQ* (*trans*-Golgi) with around 2 x 10^6 RLUs (Figure 28).
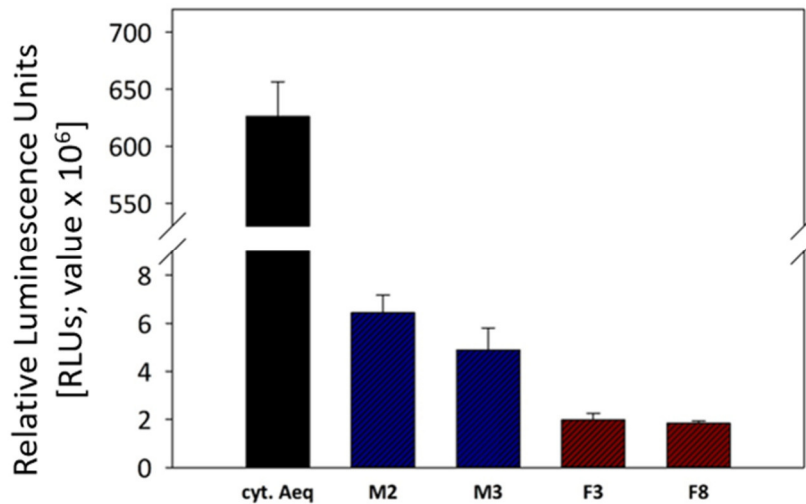
Figure 28: Cumulated Relative Light Units after discharge in five-days-old stably transformed *Arabidopsis thaliana* seedlings expressing cytosolic *APOAEQUORIN* (cyt. Aeq), *MNS1tmd-EGFP-AEQ* (M2, M3), and *FUT1tmd-EGFP-AEQ* (F3, F8). Bars represent means ± SE of n=3.

Since the Ca^{2+} measurements ought to be conducted with *A. thaliana* mesophyll protoplasts, the RLUs upon a discharge of these protoplasts were quantified. Here, the stable lines expressing the Golgi-targeted *APOAEQUORIN* in the *bicat3-1*, *eca3-2*, and *bicat3-1eca3-2* background were included. The number of protoplasts per sample was equilibrated to 2×10^6 cells per ml. The lines expressing *MNS1tmd-EGFP-AEQ* had higher RLUs of approx. $6\text{-}7 \times 10^6$ compared to those expressing *FUT1tmd-EGFP-AEQ* with approximately $4\text{-}5 \times 10^6$ RLUs (Figure 29). Protoplasts expressing *MNS1tmd-EGFP-AEQ* showed comparable discharge to seedlings expressing this construct, whereas protoplasts expressing *FUT1tmd-EGFP-AEQ* had almost double the RLU values than the respective seedlings (Figure 28, 29). Protoplasts of *bicat3-1, eca3-2*, and *bicat3-1eca3-2* expressing *MNS1tmd-EGFP-AEQ* (Mb7.1, Me5.2, Mbe4.2) showed higher total RLUs upon discharge than the lines expressing *MNS1tmd-EGFP-AEQ* in the WT Col-0 (M2, M3), reaching around $8\text{-}10 \times 10^6$ (Figure 29). *FUT1tmd-EGFP-AEQ*-expressing lines in the background of *bicat3-1, eca3-2*, and *bicat3-1eca3-2* (Fb13.1, Fe9.1, Fbe8.2) showed similar RLUs values in response to the discharge than the lines expressing *FUT1tmd-EGFP-AEQ* in the WT Col-0 (F3, F8) with approximately $4\text{-}5 \times 10^6$ RLUs (Figure 29).
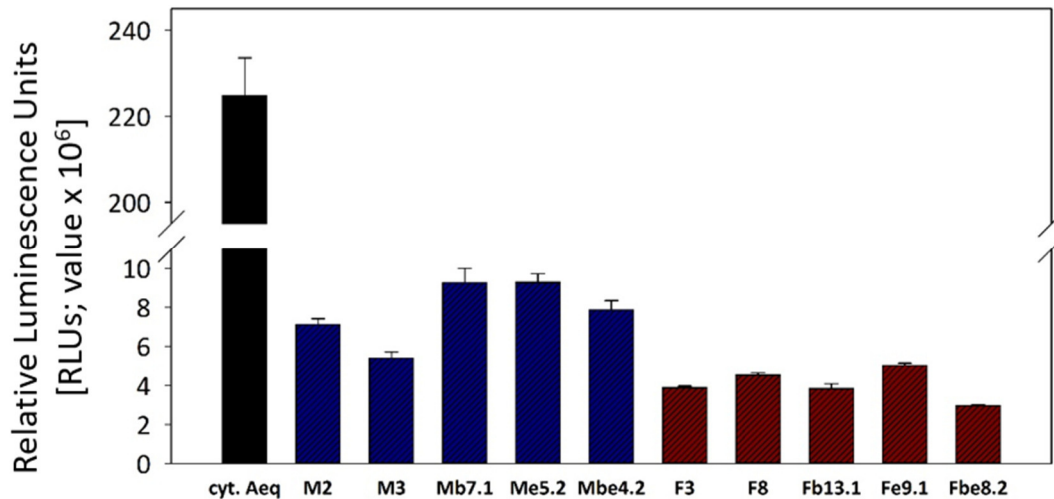
Figure 29: Cumulated Relative Light Units (RLUs) after discharge in *A. thaliana* mesophyll protoplasts in W5 Buffer. RLUs in protoplasts of five-week-old Arabidopsis plants expressing cytosolic *APOAEQUORIN* (cyt. Aeq) and *cis-* and *medial*-Golgi-targeted *APOAEQUORIN* (MNS1tmd-EGFP-AEQ) in WT Col-0 (M2, M3) and in mutant lines *bicat3-1* (Mb7.1), *eca3-2* (Me5.2), and *bicat3-1eca3-2* (Mbe4.2), as well as in protoplasts of plants expressing *trans*-Golgi-targeted *APOAEQUORIN* (FUT1tmd-EGFP-AEQ) in WT Col-0 (F3, F8) and in mutant lines *bicat3-1* (Fb13.1), *eca3-2* (Fe9.1), and *bicat3-1eca3-2* (Fbe8.2). Bars represent means ± SE of n=3.

3.5.3 *Arabidopsis thaliana* Mesophyll Protoplasts of Golgi-targeted Aequorin Lines Show no Response to Buffer Control

To further analyse $[Ca^{2+}]_{Golgi}$ from one specific cell type, *A. thaliana* mesophyll protoplasts were used. This excludes potential cell type-specific variability in the $[Ca^{2+}]$ response upon a stimulus. A mechanic stimulus was imposed by injecting the W5 buffer in which the protoplasts were suspended. This treatment led to an increase in the $[Ca^{2+}]_{cyt}$ to nearly 0.6 µM (Figure 30, C). After this increase in $[Ca^{2+}]_{cyt}$, the initial basal level was reached again after 10 sec. Intriguingly, the mechanical response was nearly absent in lines expressing *APOAEQUORIN* in the Golgi compartments. In some instances, a slight increase in $[Ca^{2+}]_{Golgi}$ was reported for WT Col-0, *bicat3-1, eca3-2, bicat3-1eca3-2* in both, *cis-* (Figure 30, A) and *trans*-Golgi (Figure 30, B). In general, the calculated basal $[Ca^{2+}]_{cisGolgi}$ can is presumed to be at around 0.3 µM, while the basal $[Ca^{2+}]_{transGolgi}$ was slightly higher with around 0.35 µM (Figure 30, A + B).
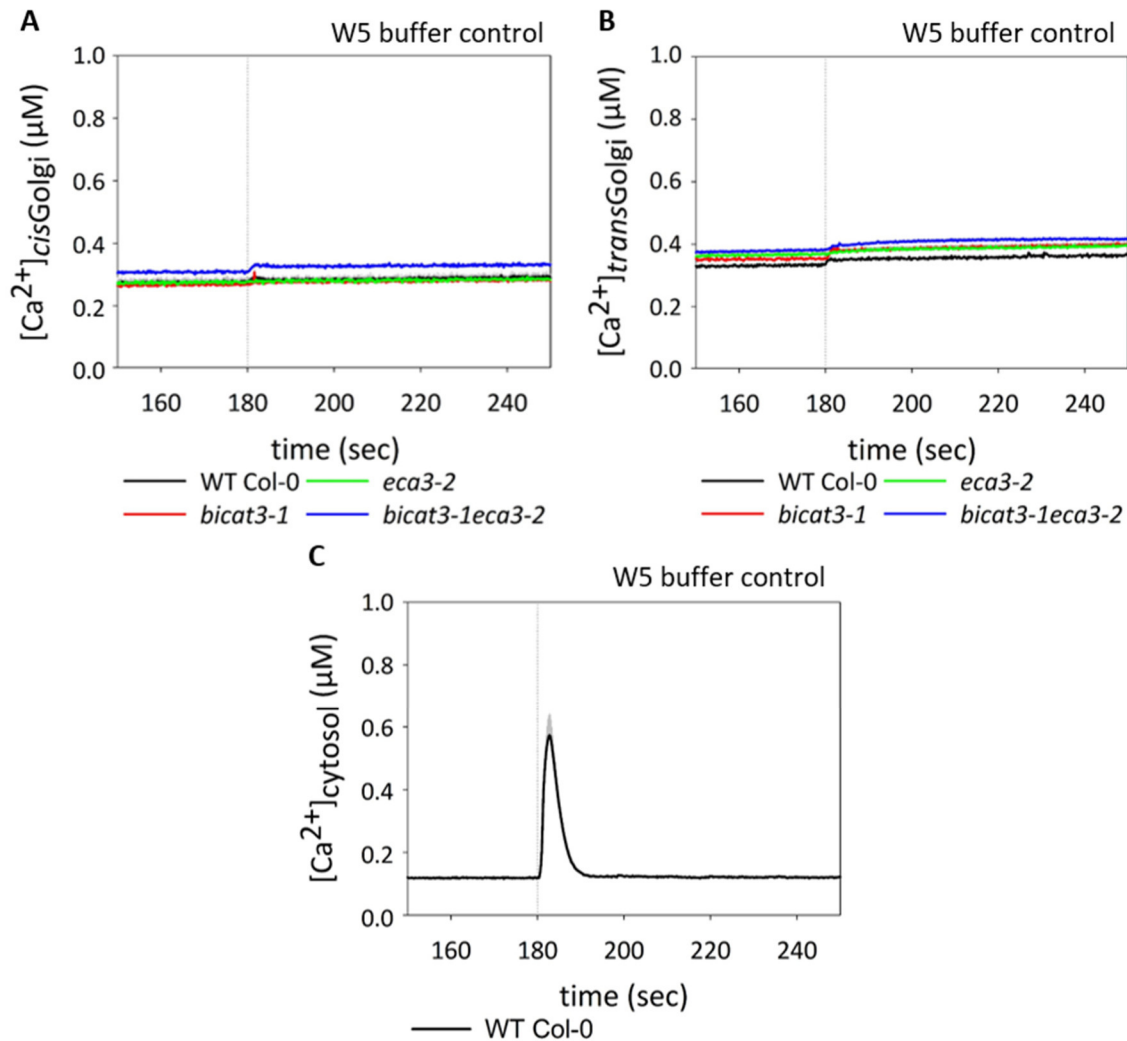
Figure 30: Changes in $[Ca^{2+}]_{cisGolgi}$ and $[Ca^{2+}]_{transGolgi}$ in response to injection of W5 buffer to suspension of *A. thaliana* mesophyll protoplasts of wild type (Col0) (black lines) and the mutant lines *eca3-2* (green lines), *bicat3-1* (red lines), and *bicat3-1eca3-2* (blue lines) expressing *MNS1tmd-EGFP-AEQ* (*cis-* and *medial-*Golgi targeted aequorin) (A) or *FUT1tmd-EGFP-AEQ* (*trans-*Golgi targeted aequorin) (B). As control, *A. thaliana* mesophyll protoplasts expressing cytosolic *APOAEQUORIN* (C) were used. Lines represent means ± SE of n=3. Dotted lines represent the time point of injection. Experiment was repeated twice with comparable results.

3.5.4 *Arabidopsis thaliana* Mesophyll Protoplasts of Golgi-targeted Aequorin Lines Show a Specific *ECA3*-Dependent Response in the Early Golgi to Sodium Chloride

As previously shown, mutation of *ECA3* led to an increased sensitivity to salt stress (Figure 15, Figure 16, and Figure 17). To analyse if this phenotype coincides with an altered Ca^{2+} signal in Golgi compartments, NaCl was applied as stimulus. Upon treatment with 200 mM NaCl, the $[Ca^{2+}]_{cyt}$ increase was more pronounced compared to the mechanically stimulated cells.

Furthermore, the time to reach the basal level again increased to 60 sec after NaCl application (Figure 31, C). The $[Ca^{2+}]_{cisGolgi}$ in the WT Col-0 also increased transiently after 200 mM NaCl application from the basal level of around 0.3 μM to 0.6 μM. A new basal $[Ca^{2+}]_{cisGolgi}$ was reached after 40 sec. In *bicat3-1*, the $[Ca^{2+}]_{cisGolgi}$ was slightly affected. In the mutant, the response was somewhat delayed, and the peak was tendentially diminished compared to the wild type, reaching less than 0.6 μM. Interestingly, *eca3-2* showed a strongly reduced increase in $[Ca^{2+}]_{cisGolgi}$ up to approximately 0.45 μM, while the basal concentration was comparable to the WT Col-0 and *bicat3-1*. The peak height of 0.45 μM was also recorded for the double mutant *bicat3-1eca3-2*. Both of them reached the basal $[Ca^{2+}]_{cisGolgi}$ again at around 15 sec after NaCl application. Likewise, the onset of the response of *eca3-2* was as fast as that of the WT Col-0, while *bicat3-1eca3-2* showed a slightly less steep rise like *bicat3-1* (Figure 31, A).

The changes in $[Ca^{2+}]_{transGolgi}$ in response to 200 mM NaCl differed from those in the *cis*-Golgi. In agreement with the previous experiments (Figure 30), the basal $[Ca^{2+}]_{transGolgi}$ was at around 0.35 μM and thus higher than $[Ca^{2+}]_{cisGolgi}$. Upon application of NaCl, the $[Ca^{2+}]_{transGolgi}$ increased to 0.45 μM only in the wild type. Unexpectedly, *eca3-2* showed an increase in $[Ca^{2+}]_{transGolgi}$ to 0.4 μM with a faster kinetic compared to all other lines (Figure 31, B). which was highly reproducible.
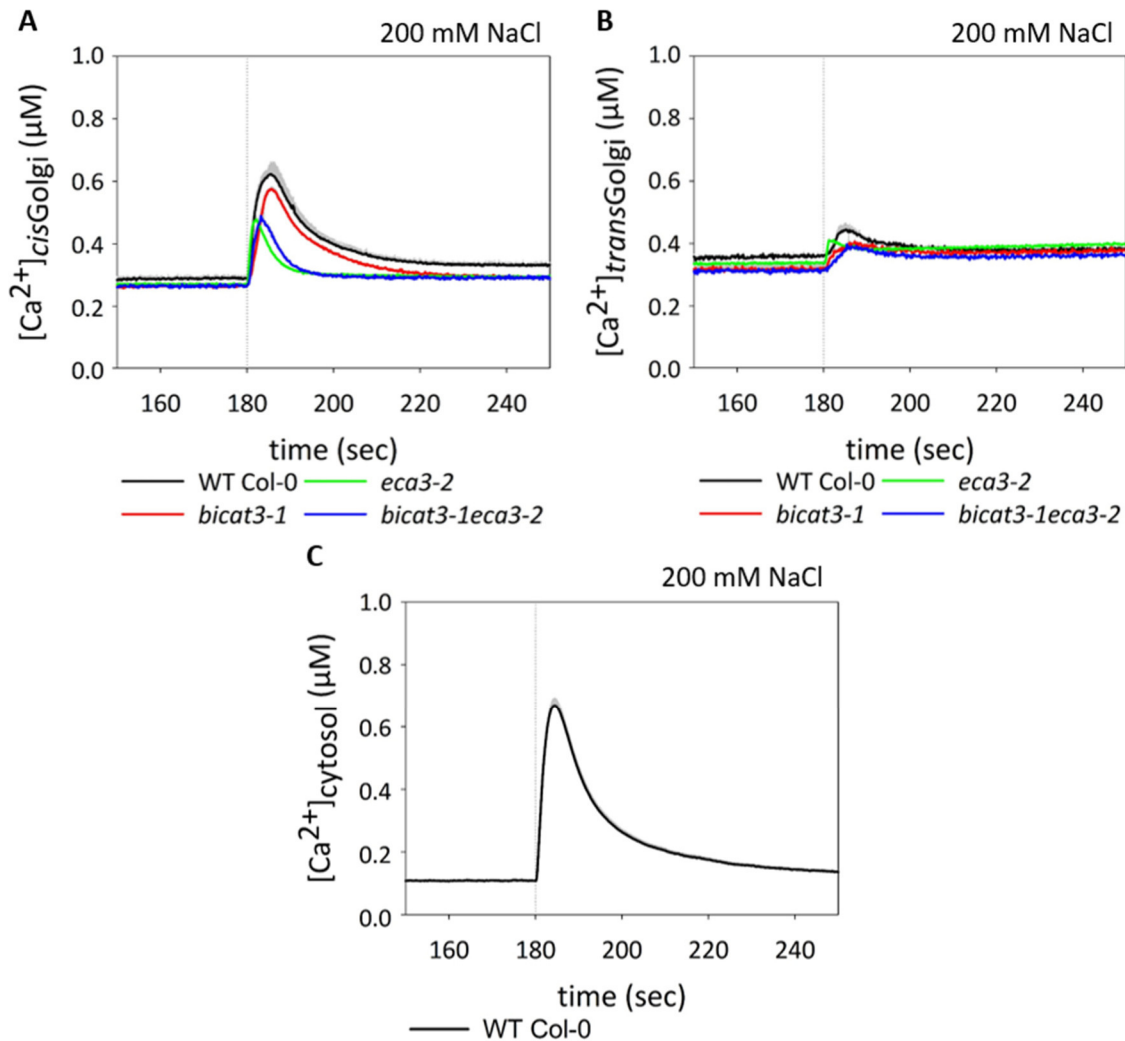
Figure 31: Changes in $[Ca^{2+}]_{cisGolgi}$ and $[Ca^{2+}]_{transGolgi}$ in response to 200 mM NaCl in *A. thaliana* mesophyll protoplasts of wild type (Col0) (black lines) and the mutant lines *eca3-2* (green lines), *bicat3-1* (red lines), and *bicat3-1eca3-2* (blue lines) expressing *MNS1tmd-EGFP-AEQ* (*cis-* and *medial-*Golgi targeted aequorin) (A) or *FUT1tmd-EGFP-AEQ* (*trans-*Golgi targeted aequorin). (B) As control *A. thaliana* mesophyll protoplasts expressing cytosolic *APOAEQUORIN* (C) were used. Lines represent means ± SE of n=3. Dotted lines represent the time point of injection of the treatment. Experiment was repeated twice with comparable results.

3.5.5 *Arabidopsis thaliana* Mesophyll Protoplasts of Mutant Lines Containing Golgi-targeted Aequorin Show Altered Kinetics and Higher Calcium Transients in Response to H_2O_2

Since H_2O_2-induced Ca^{2+} influx determines salt tolerance (Ma *et al.*, 2012), Ca^{2+} responses to H_2O_2 were tested. In both Golgi compartments, the H_2O_2-induced Ca^{2+} signals were distinct to that triggered by NaCl (Figure 31, Figure 32). Furthermore, the difference in the response of

cis- and *trans*-Golgi was opposite to that observed with NaCl. In the wild type, the $[Ca^{2+}]_{trans\text{Golgi}}$ transient showed a higher peak of around 0.6 µM when treated with 10 mM H_2O_2, while the $[Ca^{2+}]_{cis\text{Golgi}}$ peaked at approximately 0.5 µM (Figure 32, B). Inexplicably, the basal $[Ca^{2+}]_{cis\text{Golgi}}$ in the WT Col-0 here was at approximately 0.35 µM (Figure 32, A) and thus differed from the basal $[Ca^{2+}]_{cis\text{Golgi}}$ in previous experiments that was lower at approximately 0.25 µM (Figure 30, Figure 31). The basal $[Ca^{2+}]_{cis\text{Golgi}}$ in the background of *bicat3-1, eca3-2*, and *bicat3-1eca3-2* was comparable to the previously observed basal $[Ca^{2+}]_{cis\text{Golgi}}$. In stark contrast to the response to NaCl, the $[Ca^{2+}]_{cis\text{Golgi}}$ in these mutants reached 0.6 µM and was thus even higher compared to that of the wild type (Figure 32, A). A similar response was evident for $[Ca^{2+}]_{trans\text{Golgi}}$ in the background of *bicat3-1, eca3-2*, and *bicat3-1eca3-2* (Figure 32, B). In general, the mutants all responded with a kinetics distinct from the WT Col-0 in both, *cis-* and *trans*-Golgi. While $[Ca^{2+}]_{cis\text{Golgi}}$ and $[Ca^{2+}]_{trans\text{Golgi}}$ slowly decreased after having reached the maximum in mutant backgrounds, a second slight increase after the initial peak was detected in WT Col-0 . Similarly to the Golgi response, $[Ca^{2+}]_{cyt}$ also increased in response to 10 mM H_2O_2 with a peak of approximately 0.8 µM, and decreased to 0.2 µM before raising again to a new basal $[Ca^{2+}]_{cyt}$ level of 0.3 µM (Figure 32, C).
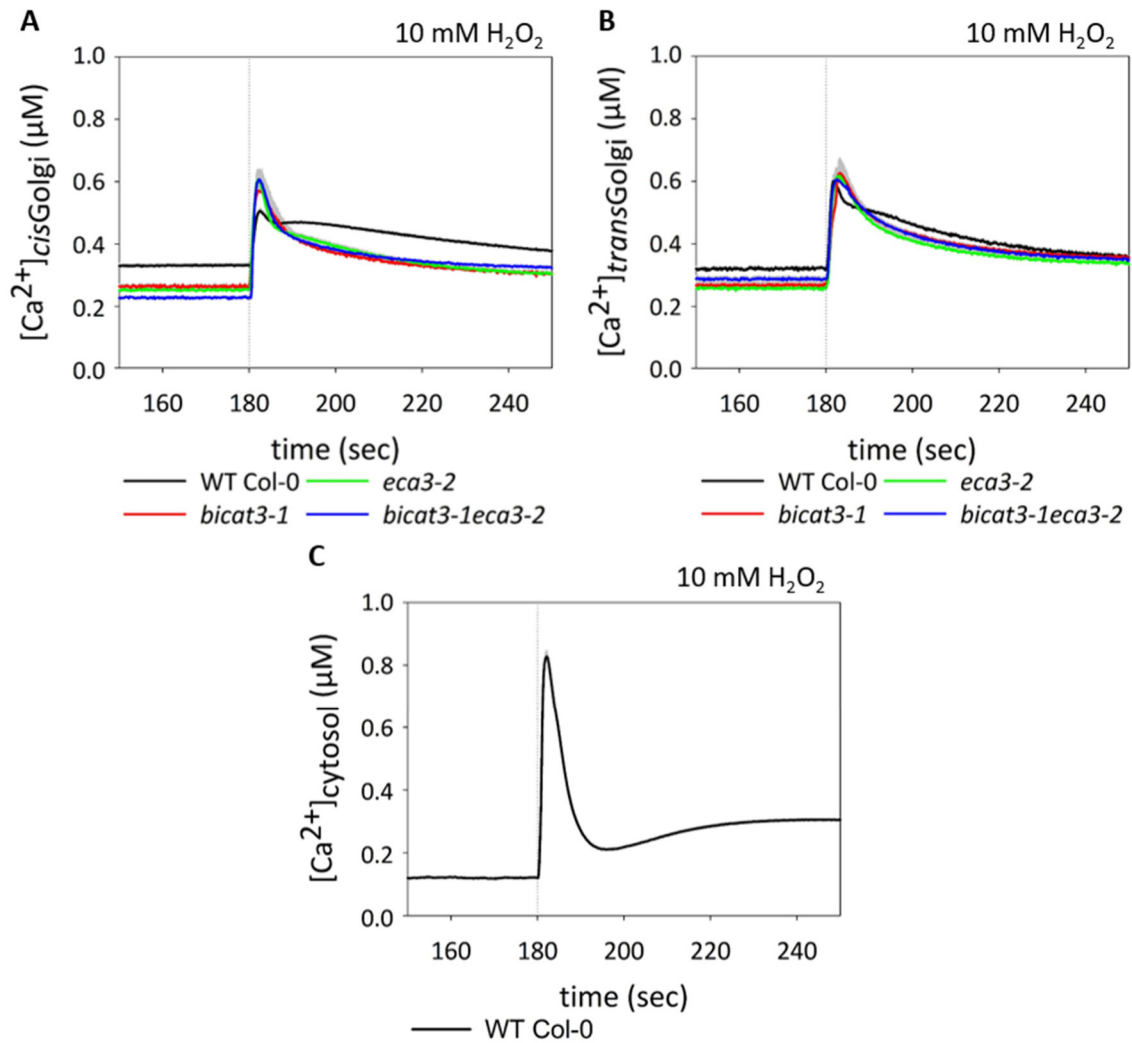
Figure 32: Changes in $[Ca^{2+}]_{cis}$Golgi and $[Ca^{2+}]_{trans}$Golgi in response to 10 mM H_2O_2 in *A. thaliana* mesophyll protoplasts of wild type (Col0) (black lines) and the mutant lines *eca3-2* (green lines), *bicat3-1* (red lines), and *bicat3-1eca3-2* (blue lines) expressing *MNS1tmd-EGFP-AEQ* (*cis-* and *medial*-Golgi targeted aequorin) (A) or *FUT1tmd-EGFP-AEQ* (*trans*-Golgi targeted aequorin) (B). As control *A. thaliana* mesophyll protoplasts expressing cytosolic *APOAEQUORIN* (C) were used. Lines represent means ± SE of n=3. Dotted lines represent the time point of injection of the treatment. Experiment was repeated twice with comparable results.

4 Discussion

This thesis mainly focused on, first, the analyses of functions and characteristics of the two known calcium transport proteins, BICAT3 (Yang *et al.*, 2021, He *et al.*, 2022) and ECA3 (Mills *et al.*, 2008, Li *et al.*, 2008a) in the Golgi, and second, the analyses of changes in [Ca^{2+}] concentrations in different subcompartments of the Golgi ([Ca^{2+}]$_{cis\text{Golgi}}$, [Ca^{2+}]$_{trans\text{Golgi}}$). The latter goal includes the importance of BICAT3 and ECA3 in shaping [Ca^{2+}]$_{cis\text{Golgi}}$ and [Ca^{2+}]$_{trans\text{Golgi}}$ and their impact on Ca^{2+} signals within the Golgi under stress conditions. To this end, it aimed to unravel the Ca^{2+} involvement in the function of this organelle and provide evidence for Ca^{2+} regulation required for processes such as trafficking, as described in animal cells (Kellokumpu, 2019).

4.1 Characterisation of BICAT3 and ECA3

4.1.1 BICAT3 and ECA3 Co-localise within the Golgi, and BICAT3 is Resident Primarily in the *trans*-Golgi Cisterna

In previous studies, BICAT3 and ECA3, were localised under different conditions. Mills *et al.* (2008) used an ECA3-YFP fusion to localise ECA3 in infiltrated *N. benthamiana* leaves. Here, ECA3 showed an overlap with the Golgi marker Golgi nucleotide sugar transporter (GONST) 1 thus suggesting a Golgi localisation. In contrast, Li *et al.* (2008a) revealed a partial co-localisation with the PVC marker Ras-related protein RABF2b (ARA7) in *A. thaliana* mesophyll protoplasts. The latter localisation is not quite clear, since there are non-punctual artefacts that have not been reported in other studies for the PVC (Lee *et al.*, 2004, Miao *et al.*, 2006), and the signals of both fluorescence proteins infrequently overlapped. The overlap might only appear due to a coincidence, and a partial PVC localisation can only be concluded by a three-dimensional localisation study. Apart from ECA3, BICAT3 is the only member of the BICAT protein family in Arabidopsis that co-localises with different Golgi markers (Hoecker *et al.*, 2020, Yang *et al.*, 2021, He *et al.*, 2022). To first validate the localisation of both proteins and assess whether there might be a co-operation of BICAT3 and ECA3 in supplying the Golgi with Ca^{2+} and Mn^{2+}, a co-localisation of EGFP-ECA3 and BICAT3-mCherry was performed. The EGFP

was fused to the N-terminus of ECA3 and should not affect the pump's function, since only ACAs have an autoinhibitory domain in the N-terminus (Baekgaard *et al.*, 2006). The localisation studies were performed in *A. thaliana* mesophyll protoplasts and infiltrated *N. benthamiana* leaves to assess a species or cell type effect on localisation. ECA3 and BICAT3-associated fluorescence showed a clear overlap in both, protoplasts (Figure 7, A - D) and *N. benthamina* epidermis (Figure 7, F - I). This was further confirmed by virtual line scans that show the pixel intensities of both signals (Figure 7, E + J). Thus, ECA3 and BICAT3 ought to be resident in the same compartment. Due to the previously observed Golgi localisations, it can be assumed that both localise in the Golgi. Nevertheless, the subcompartmental localisation cannot be concluded from these studies because of the close proximity and small size of the Golgi cisternae. A precise localisation of BICAT3 was already attempted by Yang *et al.* (2021). BICAT3, there denominated photosynthesis-affected mutant 71 like (PML) 3, co-localised with the *cis*- and *medial*-Golgi marker MNS1 (Donohoe *et al.*, 2013), while a shift to the *trans*-Golgi marker sialyltransferase (Wee *et al.*, 1998) was noted. The authors concluded that BICAT3 must be resident in the early Golgi. In contrast, the human BICAT3 homologue TMEM165 was shown to co-localise with the Mn^{2+}-dependent ß-1,4-galactosyltransferase 1 (B4GALT1) in the *trans*-Golgi (Foulquier *et al.*, 2012, Foulquier & Legrand, 2020). The precise localisation experiments performed in the present thesis unequivocally show a *trans*-Golgi localisation of BICAT3. To this end, a method to clearly distinguish between the *cis*- and *medial*-Golgi marker MNS1 and the *trans*-Golgi marker sialyltransferase and thus between the Golgi cisternae was employed. Two approaches to discriminate cisternae were employed. First, a side-view of the Golgi that transiently appeared in videos taken by confocal microscopy revealed a mismatch of the Golgi markers (Figure 8, A - C). Second, the lightning mode of the Leica Stellaris 8 microscope enabled superresolution microscopy via a mathematic algorithm. The latter localisation showed a punctual structure for the *cis*- and *medial*-Golgi and a ring-like structure for the *trans*-Golgi surrounding the *cis*- and *medial*-Golgi marker (Figure 8, D - F). A ring-like structure for the *trans*-Golgi marker sialyltransferase was also shown by Naramoto *et al.* (2014). This ring-like structure might occur due to the bulb formation in the *trans*-Golgi to pinch off vesicles. In conclusion, the advanced confocal fluorescence microscopy techniques allowed to faithfully distinguish early and late Golgi cisternae. The precise localisation of BICAT3 was performed by employing the first method and revealed a clear co-localisation with the *trans*-Golgi marker sialyltransferase (Figure 9). This localisation was reported in He *et al.*

(2022), where it was confirmed by immunogold staining and transmission electron microscopy. Hence, it can be concluded that BICAT3 is localised in the *trans*-Golgi.

BICAT3 was described as crucial for *N*-glycosylation and cell wall polysaccharide synthesis (Yang *et al.*, 2021, He *et al.*, 2022). Yang *et al.* (2021) showed a lower abundance of proteins that contain xylose and fucose residues and thus less complex *N*-glycosylation of proteins in *bicat3* under Mn^{2+} deficiency. Since complex *N*-glycosylation occurs in the late Golgi, this is in conflict with the early Golgi localisation of BICAT3 reported by Yang *et al.* (2021).

He and co-workers also showed a decrease of xylose, galactose, fucose, and galacturonic acid and an increase of glucose, rhamnose, and mannose in the cell wall of *bicat3* mutants under Mn^{2+} deficiency (He *et al.*, 2022). Xylan which is mainly composed of xylose, localises at the outer margin of the *trans*-Golgi cisterna, while its synthesis occurs in *medial*-Golgi (Meents *et al.*, 2019). A defective xylan synthesis might explain the lower abundance of xylose in the cell wall of *bicat3* under Mn^{2+} deficiency. Furthermore, two Mn^{2+}-dependent xyloglucan xylosyltransferases, XXT1 and XXT2, are Golgi-localised and involved in xyloglucan biosynthesis (Culbertson *et al.*, 2016, Culbertson *et al.*, 2018). The first appearance of xyloglucans occurs in the *trans*-Golgi (Zhang & Staehelin, 1992) which is in agreement with the localisation of BICAT3. Along with xyloglucans, galactan domains of rhamnogalacturonan I interact with cellulose microfibrils, thus maintaining cell wall structure (Zykwinska *et al.*, 2007). Since, the yeast Ca^{2+}/Mn^{2+}-ATPase PMR1 and the Ca^{2+}/Mn^{2+} transporter GDT1 are both required for protein glycosylation (Dürr *et al.*, 1998, Colinet *et al.*, 2016), it seems likely that ECA3 affects glycosylation as well, but there is no evidence for this, yet.

The precise localisation of ECA3 was not performed in this work due to time limitation. Due to its homology to animal SERCAs, ECA3 might localise, like SERCA2, to the *cis*-Golgi cisternae, while the secretory pathway Ca^{2+}-ATPase (SPCA) 1 and 2 that localise to the *trans*-Golgi and the *trans*-Golgi network, respectively, are absent in Arabidopsis (Kellokumpu, 2019). To address this question, more precise localisation studies, similar to that of BICAT3, should be performed. The co-localisation with the *cis*- and *medial*-Golgi marker MNS1 (Donohoe *et al.*, 2013), and the *trans*-Golgi marker sialyltransferase (Wee *et al.*, 1998) might reveal its exact subcompartmental localisation. Furthermore, the generated complementation lines of *eca3* expressing an *EGFP-ECA3* fusion (Figure 13) can be used for immunogold electron microscopy by means of a GFP antibody to confirm the subcompartmental ECA3 localisation.

4.1.2 Mutation of BICAT3 and ECA3 Leads to Growth Defects under high Calcium Supply

BICAT3 and ECA3 were shown to localise in the Golgi, and thus the question whether they operate in the supply of Ca^{2+} and/or Mn^{2+} to the Golgi needs to be addressed. Therefore, the growth of the knock-out mutants *bicat3-1*, *eca3-2*, and the double mutant *bicat3-1eca3-2* was analysed under different conditions in this work and previous studies. Intriguingly, on ½ MS plates the double knock-out mutant *bicat3-1eca3-2* showed a diminished growth when exposed to 30 mM $CaCl_2$, while the single mutants did not show severe symptoms (Figure 11). As previously described, the double knock-out mutant had also an exacerbation in growth reduction in comparison to the single mutants under Mn^{2+} deficiency (He *et al.*, 2022). Since Ca^{2+} toxicity may induce a physiological Mn^{2+} deficiency (He *et al.*, 2021), both phenotypes may be linked. When the stronger phenotype of the double mutant indicates a co-operation of BICAT3 and ECA3 in Ca^{2+}/Mn^{2+} homeostasis. However, this more severe phenotype of the double mutant under Ca^{2+} toxicity was not observed in older plants grown in a hydroponic set-up; all mutants were similarly affected in growth compared to the wild type when cultivated in liquid media with high Ca^{2+} supply (Figure 12). This discrepancy might indicate that the co-operational action of BICAT3 and ECA3 in the cation supply of the Golgi might be more crucial in seedlings than in older plants (Figure 11).

The absence of BICAT3 and ECA3 is likely to reduce loading of the Golgi with Ca^{2+} and Mn^{2+}. Unfortunately, total concentrations of these elements in the Golgi cannot be determined, and a reporter for free Mn^{2+} is not available yet. Interestingly, Ca^{2+} and Mn^{2+} concentrations in shoots and roots (Figure 12, C) were either unaffected or even elevated in the mutants, indicating alterations in Ca^{2+} and Mn^{2+} homeostasis with yet unknown mechanisms. He *et al.* (2022) showed a better photosynthesis in *bicat3* due to a higher Mn^{2+} supply of the chloroplast. Here, shoot Mn^{2+} concentrations under Ca^{2+} toxicity were higher in the mutants in comparison to the wild type. He *et al.* (2022) showed this effect for *bicat3-1* also under Mn^{2+} deficiency. Collectively, this may indicate that high Ca^{2+} indeed induces Mn^{2+} deficiency. These assays cannot provide information whether BICAT3 and ECA3 operate distinctly, but they show a possible co-operation of both proteins. Therefore, the different functional relevance for BICAT3 and ECA3 under salt stress was tested, since salt stress affected the glycosylation

and trafficking in the secretory pathway (Koiwa *et al.*, 2003, Kang *et al.*, 2008, Farid *et al.*, 2011, Liu *et al.*, 2018, Sánchez-Simarro *et al.*, 2020).

4.1.3 ECA3 is essential for Salt Tolerance Potentially by Facilitating *N*-glycosylation

The mutants *bicat3-1*, *eca3-2*, and the double mutant *bicat3-1eca3-2* were tested under high NaCl supply leading to osmotic and ionic stress. When grown for ten days with 75 mM NaCl, the mutants were barely affected in fresh weight (Figure 15). Exposed to 100 mM NaCl, *bicat3-1* was slightly affected, while *eca3-2* and *bicat3-1eca3-2* showed a diminished growth and fresh weight and loss of chlorophyll (Figure 15). After 14 days of salt stress, *eca3-2* and *bicat3-1eca3-2* showed an exacerbated phenotype, while *bicat3-1* still had a comparable growth to the wild type (Figure 16). The observed decrease in root growth was previously described to be a typical salt-related phenotype (Potters *et al.*, 2007, Bernstein *et al.*, 2013). The NaCl hypersensitivity indicates that ECA3 is more relevant for salt tolerance compared to BICAT3, since *bicat3-1* showed only mild growth defects under those conditions (Figure 15). To verify the importance of ECA3 in salt tolerance, the salt stress assays were repeated using a complementation line. The EGFP-ECA3 fusion complemented the phenotype of *eca3-2* (Figure 17), confirming that the dwarfish and albinous growth of *eca3-2* under high NaCl conditions is due to the lack of ECA3. This raises the question which role ECA3 has in coping with this stress. Many Golgi-resident enzymes require Mn^{2+}, especially those involved in the synthesis of polysaccharides and *N*-glycosylation (He *et al.*, 2021). ECA3 operates as Ca^{2+}/Mn^{2+} pump and supplies this organelle with these bivalent cations (Mills *et al.*, 2008). Since *N*-glycosylation appears to play an important role in coping with salt stress (Kang *et al.*, 2008, Liu *et al.*, 2018), ECA3 might thus be crucial for an adequate glycosylation. Intriguingly, yeast strains lacking the ECA3 homologue PMR1 show glycosylation defects (Dürr *et al.*, 1998). Mn^{2+} and Ca^{2+} act as cofactors for glycosyltransferases and glycosyl hydrolases, such as the Golgi-resident MNS1 and MNS2, which are required for removing mannose residues of unprocessed *N*-glycosylated proteins (Liebminger *et al.*, 2009). The *mns1mns2* double mutant exhibits a diminished growth when cultivated on ½ MS plates containing 160 mM NaCl (Liu *et al.*, 2018). By using GENEVESTIGATOR® (Zimmermann *et al.*, 2004), a co-expression of *ECA3* with multiple

members of the OT complex like *STT3a* was revealed (Figure 19). The OT complex marks the first step of *N*-glycosylation in the ER. It was shown that a lack of STT3a, required for the *N*-glycosylation *core*-oligosaccharide, leads to lethality under salt and osmotic stress (Koiwa *et al.*, 2003). Since *ECA3* and *STT3a*, besides other genes of the OT complex, are co-expressed, ECA3 might have an effect on early *N*-glycosylation in the ER.

Furthermore, the glycosyltransferase CGL1/GnT1 was also reported to be required for salt tolerance among other Arabidopsis *N*-glycan-processing enzymes, and the lack of *N*-glycosylated proteins was assumed to affect cell wall formation (Kang *et al.*, 2008). Whereas *bicat3* showed less glycans and alteration of the cell wall polysaccharides under Mn^{2+} deficiency, this has not been shown for *eca3*, yet (Yang *et al.*, 2021, He *et al.*, 2022). Also, the abundance of proteins modified by complex *N*-glycosylation was altered in *bicat3* under Mn^{2+} deficiency (Yang *et al.*, 2021), but the growth of this mutant was only slightly affected under NaCl after ten days (Figure 15), concluding that protein glycosylation might not be affected in *bicat3* under salt stress. The above-mentioned glycosyltransferase mutants that exhibit a salt phenotype were shown to localise in the ER and the *cis*-Golgi, while BICAT3 operates in the *trans*-Golgi [Figure 9, (He *et al.*, 2022)] and likely affect late steps of complex *N*-glycosylation (Yang *et al.*, 2021). Moreover, mutants lacking UDP-GlcNAc transporter 1 (UGNT1), leading to less complex *N*-glycans, does not show a salt related phenotype (Ebert *et al.*, 2018). This raises the questions which steps of *N*-glycosylation are crucial to cope with salt stress and how ECA3 is involved in this process. Therefore, *N*-glycosylation in both, *bicat3* and *eca3*, ought to be investigated under salt stress in future studies.

The first steps of *N*-glycosylation in the ER influence correct protein folding (Nagashima *et al.*, 2018). If proteins are not correctly folded, they get degraded in the ER-associated degradation (ERAD) leading to ER stress response and thus salt tolerance (Liu *et al.*, 2011). Intriguingly, the correct protein folding in the ER depends on the Ca^{2+}-binding calreticulin proteins (Jia *et al.*, 2009). In tobacco, a calreticulin was reported to be resident in the Golgi and likely required for correct protein folding (Nardi *et al.*, 2006). Interestingly, an Arabidopsis triple mutant lacking all of the three calreticulins localised in the ER was shown to be more sensitive to low Ca^{2+} conditions and to salt stress (Li *et al.*, 2008b). Since no Golgi-localised calreticulin has been reported in Arabidopsis, and ECA3 is localised in the Golgi, it is unlikely that ECA3 directly influences ERAD and ER-resident calreticulins, or the glycosyltransferases localised in the ER.

Furthermore, salt stress affects the COP vesicle transport that connects the Golgi with the ER (Sánchez-Simarro *et al.*, 2020). Deng *et al.* (2018) observed that luminal Ca^{2+} increases in the *trans*-Golgi by SPCA1 regulate vesicle formation in animal cells. ECA3-mediated $[Ca^{2+}]_{cisGolgi}$ increase might similarly promote the trafficking between the Golgi and the ER and thus have an effect on processes in the ER. It may therefore be interesting to investigate vesicle transport in *eca3.*

4.1.4 The ECA3 Promoter is Active in Specific Tissues that have been Associated with Salt Tolerance, while the BICAT3 Promoter shows a Ubiquitous Activity

The co-localisation of ECA3 and BICAT3 showed that both transport proteins are resident in the Golgi, while BICAT3 is specifically located in the *trans* cisternae. When plants lack both proteins, the stunted phenotype under high Ca^{2+} was exacerbated, suggesting a functional redundancy. However, the severe hypersensitivity to salt stress was only observed for *eca3-2* and the *bicat3-1eca3-2* double mutant. It seems that the proteins co-operate in supplying Ca^{2+} and/or Mn^{2+} to the Golgi under some conditions, but also operate distinctly under others, such as salt stress. A potential co-operation of BICAT3 and ECA3 depends on an overlapping expression pattern. To investigate the expression of *ECA3*, the promoter of *ECA3* (1507 bp, as used by Mills *et al.* (2008)) was cloned upstream of a nuclear-targeted triple Venus (*NLS3xVenus*) or ß-Glucuronidase (*GUS*). The *ECA3* promoter showed activity in the shoot, i.e. in cotyledons, vasculature, mesophyll, guard cells, and the hypocotyl. In roots, its activity was specific in the vasculature and root tips only. These observations were only partially confirmed by Li *et al.* (2008a), who showed that *ECA3* is not expressed in cotyledons, the shoot apex, and the hypocotyl of three-day-old seedlings. In contrast, Mills *et al.* (2008) showed a comparable expression pattern as reported in this study and extended their studies to specify the expression in the vasculature to cells of the pericycle and cells surrounding the xylem. The Ca^{2+} supply of the shoot requires Ca^{2+} transport across the root towards the xylem. Ca^{2+} must pass the Casparian strip to reach the xylem, making a symplastic transport through the cells of the endodermis mandatory. After reaching the cytosol of the endodermis cells, Ca^{2+} can be actively transported into the ER or the Golgi (Thor, 2019). Here, it might further travel via ER

tunnelling or vesicular trafficking and exocytosis. ECA3 might play a role in the latter mechanism, whereby Ca^{2+} may be transported into the Golgi and released via exocytosis into the stelar apoplast. A reliance of the plant on such a mechanism would implicate a reduced Ca^{2+} translocation to the shoot, which, however was not observed.

Since the lack of ECA3 causes a hypersensitivity to salt stress, it is likely to play a role in coping with salt in the cells surrounding the xylem. The plasma membrane localised Na^+/H^+ antiporter SOS1 was thought to be involved in regulating xylem loading of Na^+ (Shi *et al.*, 2002). Moreover, SOS1 is indirectly activated by a cytosolic Ca^{2+} signal, and this Ca^{2+} signal is initiated in the cells of the endodermis (Steinhorst *et al.*, 2022). The question whether the Golgi and thereby ECA3 plays a role here must be addressed, and the generated *ECA3* promoter reporter lines can be tested for changes in *ECA3* expression under salt stress. In plants, salinity also leads to a rapid increase of ABA levels in the xylem sap (Kefu *et al.*, 1991, Gómez-Cadenas *et al.*, 1998, Albacete *et al.*, 2008). Salt stress thereby induces the ABA biosynthesis, H_2O_2 accumulation, and reduced K^+ availability in the shoot. All these factors lead to stomata closure (Hedrich & Shabala, 2018), which involves an increase of free Ca^{2+} in the cytosol of the guard cells. Since the promoter of *ECA3* is active in guard cells (Figure 20), the question whether it has an impact on Ca^{2+} import into vesicular compartments in guard cells needs to be addressed. Guard cells undergo large and reversible changes in cell volume coinciding with alterations of the plasma membrane that require addition and removal of membrane material by exo- and endocytosis (Meckel *et al.*, 2005). Endocytic trafficking, among other TGN-mediated processes, are affected in mutants lacking the cation chloride cotransporter (CCC) 1, which is active in guard cells (McKay *et al.*, 2022). Thus, vesicular trafficking in guard cells is important for stomatal opening and closure. ECA3-mediated Ca^{2+} influx might promote vesicular trafficking mechanisms, which needs to be further addressed. Next to its expression in root stele and guard cells, *ECA3* is expressed in root tips. This may be relevant for salt tolerance because root meristem maintenance is affected by salt stress (Jiang *et al.*, 2016). These assumptions based on expression pattern need to be tested experimentally, and further studies to link the function of ECA3 and its impact on $[Ca^{2+}]_{Golgi}$ and salt tolerance should be performed.

The expression pattern of *ECA3* was compared with that of *BICAT3* to analyse a potential co-operation of both Golgi-localized transport proteins. He *et al.* (2022) showed a strong

ubiquitous expression of *BICAT3* in shoots and roots by GUS staining. To validate and extend these results, the *BICAT3* promoter used by He *et al.* (2022) was fused upstream of *NLS3xVenus* and stably transformed into Arabidopsis wild type plants. Using these reporter lines, no expression of *BICAT3* was found in shoots in seven independent lines, which is in contrast to the previous observations (Figure 21). This raises the question what lead to the different expression pattern of the NLS3xVenus and GUS reporters. Since the *BICAT3* promoter shows a strong expression, it seems possible that *NLS3xVenus* might be silenced in shoots. It was shown that high expression level of GFP can provoke its silencing (Hendrix *et al.*, 2021). To address this question, the expression of *NLS3xVenus* under control of the *BICAT3* promoter was quantified using quantitative RT-PCR and compared to the expression of *NLS3xVenus* under control of the *ECA3* promoter. In roots, the activity of the *BICAT3* promoter was stronger compared to that of *ECA3* (Figure 21). This is in accordance with the activity of the *BICAT3* promoter in the entire root (Figure 21, He *et al.*, 2022), as compared to the activity of the *ECA3* promoter only in the vasculature and root tips (Figure 20). Since the *ECA3* promoter showed a higher absolute expression compared to the *BICAT3* promoter in shoots and no silencing of *ECA3* expression occurred, the assumption of silencing due to a high expression seems to be unlikely. Alternatively, *BICAT3* might be expressed in deeper tissues, preventing detection of a strong fluorescence signal. Further work is required to clarify *BICAT3* expression in the shoot.

A ubiquitous expression does not allow assumptions on tissue-specific functions. Nevertheless, *BICAT3* and *ECA3* have a common expression in some tissues, such as the vasculature, and might affect the Golgi Ca^{2+} and Mn^{2+} homeostasis in co-operation. In order to reveal the impact of ECA3 and BICAT3 on $[Ca^{2+}]_{Golgi}$ it is necessary to investigate the $[Ca^{2+}]_{Golgi}$ in mutants and compare them with the wild type. For this, aequorin is a suitable tool owing to its pH-insensitivity. Since BICAT3 was shown to be exclusively localised in the *trans*-Golgi, changes in $[Ca^{2+}]_{trans Golgi}$ and $[Ca^{2+}]_{cis Golgi}$ were analysed separately and will be discussed in the next chapters.

4.2   Golgi Subcompartmental free Calcium and its Regulation by BICAT3 and ECA3

4.2.1   Generation of *cis*- and *trans*-Golgi-targeted Aequorin Reporter Lines

To address the determination of $[Ca^{2+}]_{Golgi}$ in different Golgi cisternae, a genetically encoded calcium indicator (GECI) ought to be employed. Since fluorescence-based reporters are affected by pH changes due to protonation and there is a pH gradient along the compartments of the secretory pathway (Shen *et al.*, 2013), aequorin (AEQ) appeared to be the most suitable candidate because of its pH independency (Costa *et al.*, 2018). In a previous study using Golgi-targeted aequorin, Ordenes *et al.* (2012) reported a $[Ca^{2+}]_{Golgi}$ at around 0.7 µM, so that an adapted version with low sensitivity for Ca^{2+}, similar to the ER-targeted aequorin employed by Cortese *et al.* (2022), was not necessary. The coding sequence of the *APOAEQUORIN* was fused to a compartment-specific TMD for targeting and to an *EGFP* to validate the correct localisation. To specifically target this fusion protein to the *cis-/medial-* and the *trans*-Golgi cisternae, the TMD of MNS1 (MNS1tmd; Donohoe *et al.* (2013) and the TMD of FUT1 (FUT1tmd) was used, respectively. FUT1 localises mainly in the *trans*-Golgi (Chevalier *et al.* (2010). Both MNS1 and FUT1 are glycosyltransferases and involved in *N*-glycosylation. MNS1 and FUT1 act in different steps of the *N*-glycosylation (Nagashima *et al.*, 2018). MNS1 is involved in the first step of removing mannose residues in the early Golgi, and FUT1 is involved in complex *N*-glycan synthesis in the late Golgi. To first validate the Golgi localisation, the fusion proteins were co-localised with Golgi markers in *A. thaliana* mesophyll protoplasts and infiltrated *N. benthamiana* leaves. MNS1tmd-EGFP-AEQ co-localised with MNS1-mCherry in Arabidopsis protoplasts and with SYP31-mCherry in *N. benthamiana* (Figure 22). FUT1tmd-EGFP-AEQ co-localised with sialyltransferase-mCherry in both expression systems (Figure 23). Since these localisation studies cannot distinguish individual cisternae in the Golgi stacks, precise localisation studies were performed with the system described before for the precise BICAT3 localisation (Figure 8, Figure 9). These precise localisation analyses in infiltrated *N. benthamiana* leaves showed that both AEQ constructs are correctly targeted (Figure 24) and were thus suitable for Ca^{2+} measurements in the different Golgi cisternae. In addition, the localisation of MNS1tmd-EGFP-AEQ was analysed by electron microscopy in mesophyll cells of stably transformed Arabidopsis plants (Figure 25). It revealed a preferential targeting to one side of the Golgi. Unfortunately, it is not clear from any of the obtained images, whether this

corresponds to the *cis-* or the *trans*-Golgi. Regarding that MNS1 was specifically described as *cis-* and *medial*-Golgi marker in many studies (Nebenführ *et al.*, 1999, Saint-Jore-Dupas *et al.*, 2006, Donohoe *et al.*, 2013, Schoberer *et al.*, 2019), a localisation in the *trans*-Golgi seems unlikely. In addition, the electron microscopy MNS1 localisation analysis by Donohoe *et al.* (2013) showed a *cis-* and *medial*-Golgi targeting, but was performed in root tissues. Nevertheless, the tissue type ought not to have an effect on the localisation, since the above-mentioned studies analysed different plant species and tissues, all resulting in an early Golgi localisation. Electron microscopy is an established tool to identify the subcompartmental localisation of the AEQ fusions, but to obtain conclusive information, these experiments need to be repeated with both, MNS1tmd-EGFP-AEQ and FUT1tmd-EGFP-AEQ constructs.

Since the AEQ fusions were targeted by TMDs, it might have been possible that AEQ did not face the Golgi lumen, but the cytosol instead. Measurements with such a wrongly oriented AEQ would reflect $[Ca^{2+}]_{cyt}$ around the Golgi, but not $[Ca^{2+}]_{Golgi}$. To exclude that and to confirm AEQ facing the Golgi lumen, a protease protection assay followed by Western blot analysis using a GFP-specific antibody was performed. This showed that both EGFP-AEQ fusions face the Golgi lumen, and thus the constructs were suitable to perform Ca^{2+} measurements in the Golgi. Nevertheless, in addition to the bands specific for EGFP, bands of double the expected size appeared on the membrane (Figure 26). EGFP forms dimers (Zimmer, 2002), which may have caused the observed dimerization of the EGFP-AEQ fusions. This is unlikely to affect the function of AEQ.

In conclusion, two AEQ-based Ca^{2+} reporter fusions, MNS1tmd-EGFP-AEQ and FUT1tmd-EGFP-AEQ were generated that are suitable to measure Ca^{2+} in the *cis-/medial-* and *trans*-Golgi, respectively.

4.2.2 NaCl triggers a Calcium Transient Primarily in the *Cis/Medial* Cisternae of the Golgi in *N. benthamiana* Protoplasts

To determine free Ca^{2+} in the early and late Golgi cisternae, the MNS1tmd-EGFP-AEQ and FUT1tmd-EGFP-AEQ constructs were used for *N. benthamiana* leaf infiltrations. Mesophyll protoplasts of the leaves were isolated 48 h post-infiltration and used for Ca^{2+} measurements.

As salt stress seemed to be a stress that affects $[Ca^{2+}]_{Golgi}$, the protoplasts were treated with 200 mM NaCl. Both, changes in $[Ca^{2+}]_{cisGolgi}$ and $[Ca^{2+}]_{transGolgi}$ were observed, albeit with notably different magnitude (Figure 27). Whereas the $[Ca^{2+}]_{transGolgi}$ increased only slightly, NaCl evoked a strong $[Ca^{2+}]_{cisGolgi}$ increase. This difference in $[Ca^{2+}]_{cisGolgi}$ and $[Ca^{2+}]_{transGolgi}$ responses confirms a distinct targeting of both AEQ fusions as shown by the precise localisations. If furthermore indicates that Ca^{2+} might play a role in salt tolerance specifically in the early Golgi. Here, steps of *N*-glycosylation that are required to cope with salt stress, such as removal of mannose residues by MNS1 and MNS2, occur (Liu *et al.*, 2018). It is conceivable that the $[Ca^{2+}]_{Golgi}$ increase might activate these glycosyltransferases, since they need Ca^{2+} as cofactor (Liebminger *et al.*, 2009). As mentioned above, salt stress also leads to vesicle formation (Leshem *et al.*, 2006), and COP vesicle transport was shown to be involved in coping with this stress (Sánchez-Simarro *et al.*, 2020).

The $[Ca^{2+}]_{cisGolgi}$-specific increase indicates that BICAT3 might not be involved in salt stress responses since BICAT3 is resident specifically in the *trans*-Golgi (Figure 9) and does not show a strong salt hypersensitive phenotype (Figure 15). Currently, ECA3 is the only known transport protein that might mediate the $[Ca^{2+}]_{cisGolgi}$ increase upon NaCl. One approach to address this question is the comparison of Ca^{2+} signals in the Golgi of wild type and *eca3* mutants that will be discussed in the following chapter.

4.2.3 Stable lines Harbouring Aequorin in the Golgi Reveal Transient Changes in $[Ca^{2+}]_{Golgi}$ in Response to Salt and Oxidative Stress with Different Kinetics and a Differential ECA3 Dependency

To answer the question if ECA3 and BICAT3 are involved in the generation of Ca^{2+} transients, stable *A. thaliana* lines of the wild type and mutants of *BICAT3* and *ECA3* expressing the specific subcompartmental-targeted *APOAEQUORIN* were generated. First, seedlings of the generated wild type (Col-0) lines were used to compare the emitted luminescence, quantified as Relative Light Units (RLUs), upon discharge with that of a cytosolic aequorin line (Knight *et al.*, 1991). The lines harbouring the Golgi-resident aequorin showed much lower RLU values upon discharge mediated by 1M $CaCl_2$ in 10 % of ethanol than the cytosolic aequorin line

(Figure 28). This is likely due to the small size of the Golgi compared to the cytosol and thus to a lower amount of aequorin per cell. The lines expressing *FUT1tmd-EGFP-AEQ* showed lower total RLUs than the lines expressing *MNS1tmd-EGFP-AEQ*. This difference is unlikely to affect the calculated $[Ca^{2+}]_{Golgi}$ upon stimulation, since this takes into account the total luminescence potential. However, it may affect the sensitivity in case of very weak signals. The amount of RLUs upon discharge were sufficient to allow calculations of the $[Ca^{2+}]_{Golgi}$ according to Rentel and Knight (2004).

It was shown before that $[Ca^{2+}]_{cyt}$ elevations are distinct in different root tissues (Steinhorst *et al.*, 2022). Furthermore, the growth of seedlings sometimes is not homogeneous and may lead to variability of Ca^{2+} responses that hamper the comparison between the lines. To avoid these sources of variation, measurements were performed on suspensions of mesophyll protoplasts isolated from of the lines stably expressing the respective Golgi markers. Both, *BICAT3* and *ECA3*, are expressed in the leaf mesophyll (Figure 20, He *et al.*, 2022). Therefore, *A. thaliana* mesophyll protoplasts appear to be a suitable tool to analyse $[Ca^{2+}]_{Golgi}$ in mutant backgrounds. The total RLUs upon discharge determined by using protoplasts showed a similar as the seedlings of the stable lines (Figure 28, Figure 29). RLUs released by lines expressing *MNS1tmd-EGFP-AEQ* were somewhat higher compared to those released by protoplasts expressing *FUT1tmd-EGFP-AEQ*. This trend was similar in the mutant background. Consequently, the total RLUs were sufficient for calculations of $[Ca^{2+}]_{cisGolgi}$ and $[Ca^{2+}]_{transGolgi}$ also under this experimental setup.

Ca^{2+} measurements in response to diverse stimuli were performed with a comparison of wild type, *bicat3-1, eca3-2*, and *bicat3-1eca3-2* to elucidate the role of the two known Ca^{2+} transport proteins, BICAT3 and ECA3, in shaping $[Ca^{2+}]_{cisGolgi}$ and $[Ca^{2+}]_{transGolgi}$ responses. Numerous studies have analysed cytosolic Ca^{2+} signals in response to various stresses. This parameter was therefore employed to assess the effectiveness of the applied stimuli. Upon injection of buffer, an increase in $[Ca^{2+}]_{cyt}$ was observed, that can be referred to as a response to touch stimulation (Figure 30). Touch stimulation was reported as one of the first stimuli that trigger $[Ca^{2+}]_{cyt}$ responses (Knight *et al.*, 1991). Interestingly, this response was largely absent in both the *cis*-Golgi and the *trans*-Golgi, not reflecting changes in $[Ca^{2+}]_{cyt}$ (Figure 30). Only marginal changes in $[Ca^{2+}]_{cisGolgi}$ and $[Ca^{2+}]_{transGolgi}$ occurred. This indicates that the Golgi might not be involved in touch adaptions at all. Further, these measurements support the

outcome of the protease protection assay (Figure 26) showing that the Golgi-targeted aequorin faces the luminal part of the Golgi and do not report on cytosolic $[Ca^{2+}]$. These measurements also demonstrate a difference in the basal $[Ca^{2+}]$ in early and late Golgi. The $[Ca^{2+}]_{transGolgi}$ seems to be higher with around 0.35 µM than the $[Ca^{2+}]_{cisGolgi}$ showing a basal level at approximately 0.25 µM. Interestingly, both concentrations are lower than the previously reported 0.7 µM, that was determined by a FUT1-targeted aequorin (Ordenes *et al.*, 2012). This discrepancy cannot be explained and may point to a dependence of $[Ca^{2+}]_{Golgi}$ steady state levels on cell type or experimental conditions. Nevertheless, both the present work and Ordenes *et al.* (2012) point to a generally lower $[Ca^{2+}]_{Golgi}$ in plant cells as compared to animal cells (Suzuki *et al.*, 2016, Kellokumpu, 2019). This might be related to a different physiological role of the plant Golgi, for example regarding its relevance in glycan synthesis required for the plant cell wall (Dupree & Sherrier, 1998). Since the $[Ca^{2+}]_{ER}$ is higher than the $[Ca^{2+}]_{Golgi}$, Künzl *et al.* (2016) speculated that the low $[Ca^{2+}]_{Golgi}$ might enable vacuolar sorting receptor-mediated cargo transport and sorting. In this respect, the Ca^{2+} concentration might increase in later compartments of the secretory pathway to release the cargo. The higher $[Ca^{2+}]_{transGolgi}$ in comparison to the $[Ca^{2+}]_{cisGolgi}$ might indicate such a mechanism. Nevertheless, to finally conclude that there is an increase in Ca^{2+} concentrations in the compartments along the secretory pathway, measurements with reporters that monitor the concentrations in the *trans*-Golgi network and the PVC need to be conducted in future studies. Unfortunately, the attempt to generate such reporters in this work was not successful.

Since *eca3-2* showed a severe and *bicat3-1* a mild phenotype under salt stress, NaCl-induced Ca^{2+} signals in the Golgi were analysed in the mutant backgrounds (Figure 31). As described in previous studies (e.g., Knight *et al.* (1997)) and confirmed in this work (Figure 31), NaCl leads to a transient $[Ca^{2+}]_{cyt}$ increase. As shown before in *N. benthamiana* protoplasts isolated from infiltrated leaves (Figure 27), changes in $[Ca^{2+}]_{cisGolgi}$ and $[Ca^{2+}]_{transGolgi}$ upon NaCl treatment were also produced by protoplasts of the stably transformed Arabidopsis lines (Figure 31). In the *bicat3-1* background, the $[Ca^{2+}]_{cisGolgi}$ increase was marginally lower compared to the wild type, with a reduced ascent rate. The lack of BICAT3 in the *trans*-Golgi thus influences the $[Ca^{2+}]_{cisGolgi}$, what might explain the slight growth defect of *bicat3-1* under salt stress (Figure 15). Furthermore, this delayed ascent was in accordance with that of the $[Ca^{2+}]_{cisGolgi}$ transient in the *bicat3-1eca3-2* double mutant, but here the peak maximum of the $[Ca^{2+}]_{cisGolgi}$ increase was also lower. A similar peak maximum of $[Ca^{2+}]_{cisGolgi}$ was determined in the *eca3-2* single

mutant. This clearly shows that ECA3 plays a substantial role in shaping the $[Ca^{2+}]_{cisGolgi}$ elevation upon NaCl. However, ECA3 is not the only mechanism in this respect, since the signal does disappear entirely. This points to other, not yet characterised Ca^{2+} transport proteins in the Golgi next to BICAT3 and ECA3, or to an impact of $[Ca^{2+}]_{ER}$ on $[Ca^{2+}]_{cisGolgi}$. As mentioned, it was shown that the $[Ca^{2+}]_{ER}$ increases upon a $[Ca^{2+}]_{cyt}$ transient, demonstrating the ER to play a role as Ca^{2+} buffer (Bonza *et al.*, 2013). Since the COP vesicles are required for salt tolerance (Sánchez-Simarro *et al.*, 2020), Ca^{2+} might be transported from the ER to the Golgi via those vesicles that then increases the $[Ca^{2+}]_{cisGolgi}$.

The NaCl-induced $[Ca^{2+}]_{cisGolgi}$ elevations indicate that the Golgi may act as a buffer sequestrating cytosolic Ca^{2+} after a $[Ca^{2+}]_{cyt}$ transient, in a similar way to the ER (Bonza *et al.*, 2013). ECA3 as only known Ca^{2+} pump in the Golgi (Bossi *et al.*, 2019) is likely to be crucial here. An increase of $[Ca^{2+}]_{Golgi}$ may promote the quick decrease of $[Ca^{2+}]_{cyt}$ after a peak. The subsequent fast return to the basal $[Ca^{2+}]_{cisGolgi}$ may be mediated for instance by exocytosis. In this case, a disturbed $[Ca^{2+}]_{cyt}$ can be assumed in *eca3* mutants because ECA3 would be required to pump Ca^{2+} into the Golgi lumen and thereby allow the quick $[Ca^{2+}]_{cyt}$ decrease. Therefore, $[Ca^{2+}]_{cyt}$ needs to be analysed in *eca3-2* in future studies.

Apart from Ca^{2+}, ECA3 is able to transport Mn^{2+} (Mills *et al.*, 2008) and thus may supply the Golgi also with this metal. Since there is no evidence for a selectivity of ECA3, the increase of $[Ca^{2+}]_{cisGolgi}$ might be associated with an increased transport of Mn^{2+} into the Golgi that may be required for salt stress adaptation by Mn^{2+}-dependent *N*-glycosylation (Kang *et al.*, 2008, Nagashima *et al.*, 2018, He *et al.*, 2021). Nevertheless, some glycosyltransferases are able to use Ca^{2+} as cofactor (Liebminger *et al.*, 2009). Therefore, also Ca^{2+} can mediate *N*-glycosylation required for salt tolerance. Regarding the clear overlap of Ca^{2+} and Mn^{2+} in physiological functions, further studies should aim to distinguish their roles and not view them in isolation. Taken together, a clear impact of ECA3 on $[Ca^{2+}]_{cisGolgi}$ upon salt stress can be concluded, but it remains elusive whether glycosylation or vesicular transport are impaired in the mutant.

Salt stress affects root meristem maintenance through changes in either redox potential or auxin transport (Jiang *et al.*, 2016). Moreover, it was shown that upon salt stress and other stresses, ROS such as H_2O_2 are produced in the apoplast (Choi *et al.*, 2017, Apel & Hirt, 2004). This leads to the question whether H_2O_2 itself can trigger changes in $[Ca^{2+}]_{cisGolgi}$ and $[Ca^{2+}]_{transGolgi}$ as previously described for $[Ca^{2+}]_{cyt}$ (Price *et al.*, 1994, Rentel & Knight, 2004).

Interestingly, applying H_2O_2 also changed $[Ca^{2+}]$ within the Golgi, but, in contrast to NaCl, a somewhat higher increase was observed in the *trans*-Golgi compared to the *cis*-Golgi (Figure 32). In animal cells, ROS promotes hypoxia and impairs ER and Golgi functions (Mennerich *et al.*, 2019). It was previously described that in animal cells correct protein folding in the ER depends on ROS spiking and low ROS levels (Erol, 2014). In plants, the knowledge on ROS effects on ER and Golgi functions is scant. The TGN-localised Mn^{2+} transporter NRAMP2 is required for the detoxification of ROS (Alejandro *et al.*, 2017), indicating that cation and ROS homeostasis are interconnected in plants. The $[Ca^{2+}]_{Golgi}$ alterations upon H_2O_2 stress were changed in *bicat3-1*, *eca3-2*, and *bicat3-1eca3-2* (Figure 32). However, intriguingly, the peak was rather exacerbated and declined faster in the mutants, which suggests that the involvement of BICAT3 and ECA3 in the $[Ca^{2+}]_{Golgi}$ increase is stimulus-specific. The lack of BICAT3 and/or ECA3 might result in defects of ROS signalling. This aspect ought to be investigated in future studies and might reveal a yet unknown interplay of Ca^{2+} and ROS signalling in the secretory pathway.

4.3   Conclusions

Our knowledge on Ca^{2+} signalling in plant cell compartments is still scant, and Ca^{2+} homeostasis has been little addressed in the Golgi. In animal cells, Ca^{2+} in interplay with ROS and pH regulates many processes in the Golgi, such as trafficking (Kellokumpu, 2019). In this study, $[Ca^{2+}]_{Golgi}$ was analysed upon NaCl and H_2O_2 treatment and related to the Golgi-localised Ca^{2+} transport proteins BICAT3 and ECA3. To be more precise, a distinction between the *cis/medium* and *trans* cisternae was made. Both subcompartments differ substantially in their response to NaCl, with the *cis*-Golgi being more responsive. The *trans*-Golgi localised BICAT3 only slightly impaired the $[Ca^{2+}]_{cisGolgi}$ rise upon NaCl stress, while ECA3 showed a greater effect in mediating this $[Ca^{2+}]_{cisGolgi}$ increase. Moreover, *eca3* showed a dwarfish and bleached phenotype under salt stress, which confirms this involvement. These results lead to the question of the function of the $[Ca^{2+}]_{cisGolgi}$ transient under salt stress, and which other mechanisms contribute to its generation, since it was not completely abolished in *eca3*. Other transport proteins that have not been described yet might be resident here. Likewise,

$[Ca^{2+}]_{cis\text{Golgi}}$ might also increase via vesicular transport deriving from the ER. Moreover, ROS signalling related to the Golgi needs to be further investigated, as also the question why the lack of both, BICAT3 and ECA3, lead to higher increases of $[Ca^{2+}]_{\text{Golgi}}$ needs to be addressed. The observed decrease in $[Ca^{2+}]_{\text{Golgi}}$ after a stress-induced rise implies that Ca^{2+} can be exported from the Golgi, either via Ca^{2+} channels, transporters, or vesicles.

All things considered, this study is a basis to futher our understanding of Ca^{2+} signalling in the plant secretory pathway and further demonstrates that organellar Ca^{2+} signalling is an emerging field that ought to be further explored.

5 References

Albacete A., Ghanem M. E., Martinez-Andujar C., Acosta M., Sanchez-Bravo J., Martinez V., Lutts S., Dodd I. C., Perez-Alfocea F. (2008). Hormonal changes in relation to biomass partitioning and shoot growth impairment in salinized tomato (*Solanum lycopersicum* L.) plants. *Journal of Experimental Botany* **59**: 4119-4131.

Albrecht V., Ritz O., Linder S., Harter K., Kudla J. (2001). The NAF domain defines a novel protein–protein interaction module conserved in Ca^{2+}-regulated kinases. *The EMBO journal* **20**: 1051-1063.

Alejandro S., Cailliatte R., Alcon C., Dirick L., Domergue F., Correia D., Castaings L., Briat J. F., Mari S., Curie C. (2017). Intracellular distribution of manganese by the *trans*-Golgi network transporter NRAMP2 is critical for photosynthesis and cellular redox homeostasis. *The Plant Cell* **29**: 3068-3084.

Allen G. J., Kwak J. M., Chu S. P., Llopis J., Tsien R. Y., Harper J. F., Schroeder J. I. (1999). Cameleon calcium indicator reports cytoplasmic calcium dynamics in Arabidopsis guard cells. *The Plant Journal* **19**: 735-747.

Anil V. S., Rajkumar P., Kumar P., Mathew M. K. (2008). A Plant Ca^{2+} Pump, ACA2, Relieves Salt Hypersensitivity in Yeast. Modulation of cytosolic calcium signature and activation of adaptive Na^{+} homeostasis. *The Journal of Biological Chemistry* **283**: 3497-3506.

Apel K., Hirt H. (2004). Reactive oxygen species: metabolism, oxidative stress, and signal transduction. *Annual Review in Plant Biology* **55**: 373-399.

Arteca R. N., Arteca J. M. (2000). A novel method for growing *Arabidopsis thaliana* plants hydroponically. *Physiologia Plantarum* **108**: 188-193.

Atmodjo M. A., Hao Z., Mohnen D. (2013). Evolving views of pectin biosynthesis. *Annual Review of Plant Biology* **64**: 747-779.

Aulestia F. J., Alonso M. T., Garcia-Sancho J. (2015). Differential calcium handling by the *cis* and *trans* regions of the Golgi apparatus. *Biochemical Journal* **466**: 455-465.

Axelsen K. B., Palmgren M. G. (1998). Evolution of substrate specificities in the P-type ATPase superfamily. *Journal of Molecular Evolution* **46**: 84-101.

Baekgaard L., Luoni L., De Michelis M. I., Palmgren M. G. (2006). The plant plasma membrane Ca^{2+} pump ACA8 contains overlapping as well as physically separated autoinhibitory and calmodulin-binding domains. *The Journal of Biological Chemistry* **281**: 1058-1065.

Baird G. S., Zacharias D. A., Tsien R. Y. (1999). Circular permutation and receptor insertion within green fluorescent proteins. *Proceedings of the National Academy of Sciences of the United States of America* **96**: 11241-11246.

Barberon M., Dubeaux G., Kolb C., Isono E., Zelazny E., Vert G. (2014). Polarization of iron-regulated transporter I (IRT1) to the plant-soil interface plays crucial role in metal homeostasis. *Proceedings of the National Academy of Sciences of the United States of America* **111**: 8293-8298.

Barberon M., Zelazny E., Robert S., Conéjéro G., Curie C., Friml J., Vert G. (2011). Monoubiquitin-dependent endocytosis of the iron-regulated transporter 1 (IRT1) transporter controls iron uptake in plants. *Proceedings of the National Academy of Sciences of the United States of America* **108**: 450-458.

Bednarek S. Y., Raikhel N. V. (1991). The barley lectin carboxyl-terminal propeptide is a vacuolar protein sorting determinant in plants. *The Plant Cell* **3**: 1195-1206.

Bellandi A., Papp D., Breakspear A., Joyce J., Johnston M. G., De Keijzer J., Raven E. C., Ohtsu M., Vincent T. R., Miller A. J. (2022). Diffusion and bulk flow of amino acids mediate calcium waves in plants. *Science Advances* **8**: eabo6693.

Berglund A., Quartacci M., Liljenberg C., 2000. Changes in plasma-membrane lipid composition: A strategy for acclimation to copper stress. In.: Portland Press 905-907.

Bernstein N., Eshel A., Beeckman T. (2013). Effects of salinity on root growth. *Plant roots: the hidden half* **10**.

Beznoussenko G. V., Parashuraman S., Rizzo R., Polishchuk R., Martella O., Di Giandomenico D., Fusella A., Spaar A., Sallese M., Capestrano M. G., Pavelka M., Vos M. R., Rikers Y. G., Helms V., Mironov A. A., Luini A. (2014). Transport of soluble proteins through the Golgi occurs by diffusion via continuities across cisternae. *eLife* **3**: 1-29

Bonza M. C., Loro G., Behera S., Wong A., Kudla J., Costa A. (2013). Analyses of Ca^{2+} accumulation and dynamics in the Endoplasmic Reticulum of Arabidopsis root cells using a genetically encoded Cameleon sensor. *Plant Physiology* **163**: 1230-1241.

Bossi J. G., Kumar K., Barberini M. L., Dominguez G. D., Rondon Guerrero Y. D. C., Marino-Buslje C., Obertello M., Muschietti J. P., Estevez J. M. (2019). The role of P-type IIA and P-type IIB Ca^{2+}-ATPases in plant development and growth. *The Journal of Experimental Botany* **71**: 1239-1248.

Brini M. (2008). Calcium-sensitive photoproteins. *Methods* **46**: 160-166.

Cai X., Lytton J. (2004). Molecular cloning of a sixth member of the K^+-dependent Na^+/Ca^{2+} exchanger gene family, NCKX6. *The Journal of Biological Chemistry* **279**: 5867-5876.

Caramelo J. J., Parodi A. J. (2008). Getting in and out from calnexin/calreticulin cycles. *The Journal of Biological Chemistry* **283**: 10221-10225.

Charpentier M. (2018). Calcium signals in the plant nucleus: Origin and function. *Journal of Experimental Botany* **69**: 4165–4173.

Charpentier M., Sun J., Martins T. V., Radhakrishnan G. V., Findlay K., Soumpourou E., Thouin J., Véry A.-A., Sanders D., Morris R. J. (2016). Nuclear-localized cyclic nucleotide–gated channels mediate symbiotic calcium oscillations. *Science* **352**: 1102-1105.

Chen J., Smaardijk S., Mattelaer C. A., Pamula F., Vandecaetsbeek I., Vanoevelen J., Wuytack F., Lescrinier E., Eggermont J., Vangheluwe P. (2019). An N-terminal Ca^{2+}-binding motif regulates the secretory pathway Ca^{2+}/Mn^{2+}-transport ATPase SPCA1. *The Journal of Biological Chemistry* **294**: 7878-7891.

Chen T.-W., Wardill T. J., Sun Y., Pulver S. R., Renninger S. L., Baohan A., Schreiter E. R., Kerr R. A., Orger M. B., Jayaraman V. (2013). Ultrasensitive fluorescent proteins for imaging neuronal activity. *Nature* **499**: 295-300.

Chevalier L., Bernard S., Ramdani Y., Lamour R., Bardor M., Lerouge P., Follet-Gueye M. L., Driouich A. (2010). Subcompartment localization of the side chain xyloglucan-synthesizing enzymes within Golgi stacks of tobacco suspension-cultured cells. *The Plant Journal* **64**: 977-989.

Choi W.-G., Toyota M., Kim S.-H., Hilleary R., Gilroy S. (2014). Salt stress-induced Ca^{2+} waves are associated with rapid, long-distance root-to-shoot signaling in plants. *Proceedings of the National Academy of Sciences* **111**: 6497-6502.

Choi W. G., Miller G., Wallace I., Harper J., Mittler R., Gilroy S. (2017). Orchestrating rapid long-distance signaling in plants with Ca^{2+}, ROS and electrical signals. *The Plant Journal* **90**: 698-707.

Chung K. P., Zeng Y., Jiang L. (2016). COPII paralogs in plants: Functional redundancy or diversity? *Trends in Plant Science* **21**: 758-769.

Cipollo J. F., Trimble R. B., Chi J. H., Yan Q., Dean N. (2001). The yeast *ALG11* gene specifies addition of the terminal α1,2-Man to the $Man_5GlcNAc_2$-PP-dolichol *N*-glycosylation intermediate formed on the cytosolic side of the Endoplasmic Reticulum. *The Journal of Biological Chemistry* **276**: 21828-21840.

Clough S. J., Bent A. F. (1998). Floral dip: A simplified method for Agrobacterium-mediated transformation of *Arabidopsis thaliana*. *The Plant Journal* **16**: 735-743.

Colinet A. S., Sengottaiyan P., Deschamps A., Colsoul M. L., Thines L., Demaegd D., Duchene M. C., Foulquier F., Hols P., Morsomme P. (2016). Yeast Gdt1 is a Golgi-localized calcium transporter required for stress-induced calcium signaling and protein glycosylation. *Scientific Reports* **6**: 1-11.

Corso M., Doccula F. G., De Melo J. R. F., Costa A., Verbruggen N. (2018). Endoplasmic reticulum-localized CCX2 is required for osmotolerance by regulating ER and cytosolic Ca^{2+} dynamics in Arabidopsis. *Proceedings of the National Academy of Sciences of the United States of America* **115**: 3966-3971.

Cortese E., Moscatiello R., Pettiti F., Carraretto L., Baldan B., Frigerio L., Vothknecht U. C., Szabo I., De Stefani D., Brini M., Navazio L. (2022). Monitoring calcium handling by the plant Endoplasmic Reticulum with a low-Ca^{2+}-affinity targeted aequorin reporter. *The Plant Journal* **109**: 1014-1027.

Costa A., Navazio L., Szabo I. (2018). The contribution of organelles to plant intracellular calcium signalling. *Journal of Experimental Botany* **69**: 4175-4193.

Culbertson A. T., Ehrlich J. J., Choe J.-Y., Honzatko R. B., Zabotina O. A. (2018). Structure of xyloglucan xylosyltransferase 1 reveals simple steric rules that define biological patterns of xyloglucan polymers. *Proceedings of the National Academy of Sciences of the United States of America* **115**: 6064-6069.

Culbertson A. T., Tietze A. A., Tietze D., Chou Y. H., Smith A. L., Young Z. T., Zabotina O. A. (2016). A homology model of xyloglucan xylosyltransferase 2 reveals critical amino acids involved in substrate binding. *Glycobiology* **26**: 961-972.

De Juan-Sanz J., Holt G. T., Schreiter E. R., De Juan F., Kim D. S., Ryan T. A. (2017). Axonal Endoplasmic Reticulum Ca^{2+} content controls release probability in CNS nerve terminals. *Neuron* **93**: 867-881.

Delhaize E., Gruber B. D., Pittman J. K., White R. G., Leung H., Miao Y., Jiang L., Ryan P. R., Richardson A. E. (2007). A role for the AtMTP11 gene of Arabidopsis in manganese transport and tolerance. *The Plant Journal* **51**: 198-210.

Demaegd D., Foulquier F., Colinet A.-S., Gremillon L., Legrand D., Mariot P., Peiter E., Van Schaftingen E., Matthijs G., Morsomme P. (2013). Newly characterized Golgi-localized family of proteins is involved in calcium and pH homeostasis in yeast and human cells. *Proceedings of the National Academy of Sciences of the United States of America* **110**: 6859-6864.

Demidchik V., Shabala S., Isayenkov S., Cuin T. A., Pottosin I. (2018). Calcium transport across plant membranes: Mechanisms and functions. *New Phytologist* **220**: 49-69.

Deng Y., Pakdel M., Blank B., Sundberg E. L., Burd C. G., Von Blume J. (2018). Activity of the SPCA1 calcium pump couples sphingomyelin synthesis to sorting of secretory proteins in the *trans*-Golgi network. *Developmental Cell* **47**: 464-478

Dettmer J., Hong-Hermesdorf A., Stierhof Y. D., Schumacher K. (2006). Vacuolar H^+-ATPase activity is required for endocytic and secretory trafficking in Arabidopsis. *The Plant Cell* **18**: 715-730.

Dodd A. N., Kudla J., Sanders D. (2010). The language of calcium signaling. *Annual Review of Plant Biology* **61**: 593-620.

Donohoe B. S., Kang B.-H., Staehelin L. A. (2007). Identification and characterization of COPIa-and COPIb-type vesicle classes associated with plant and algal Golgi. *Proceedings of the National Academy of Sciences of the United States of America* **104**: 163-168.

Donohoe B. S., Kang B. H., Gerl M. J., Gergely Z. R., Mcmichael C. M., Bednarek S. Y., Staehelin L. A. (2013). *Cis*-Golgi cisternal assembly and biosynthetic activation occur sequentially in plants and algae. *Traffic* **14**: 551-567.

Dulary E., Yu S. Y., Houdou M., De Bettignies G., Decool V., Potelle S., Duvet S., Krzewinski-Recchi M. A., Garat A., Matthijs G., Guerardel Y., Foulquier F. (2018). Investigating the function of Gdt1p in yeast Golgi glycosylation. *Biochimica et Biophysica Acta (BBA)-General Subjects* **1862**: 394-402.

Dümmer M., Michalski C., Essen L. O., Rath M., Galland P., Forreiter C. (2016). EHB1 and AGD12, two calcium-dependent proteins affect gravitropism antagonistically in *Arabidopsis thaliana*. *Journal of Plant Physiology* **206**: 114-124.

Dupree P., Sherrier D. J. (1998). The plant Golgi apparatus. *Biochimica et Biophysica Acta (BBA)-Molecular Cell Research* **1404**: 259-270.

Dürr G., Strayle J., Plemper R., Elbs S., Klee S. K., Catty P., Wolf D. H., Rudolph H. K. (1998). The *medial*-Golgi ion pump Pmr1 supplies the yeast secretory pathway with Ca^{2+} and Mn^{2+} required for

glycosylation, sorting, and Endoplasmic Reticulum-associated protein degradation. *Molecular Biology of the Cell* **9**: 1149-1162.

Ebert B., Rautengarten C., Mcfarlane H. E., Rupasinghe T., Zeng W., Ford K., Scheller H. V., Bacic A., Roessner U., Persson S., Heazlewood J. L. (2018). A Golgi UDP-GlcNAc transporter delivers substrates for *N*-linked glycans and sphingolipids. *Nature Plants* **4**: 792-801.

Emery L., Whelan S., Hirschi K. D., Pittman J. K. (2012). Protein phylogenetic analysis of Ca^{2+}/cation antiporters and insights into their evolution in plants. *Frontiers in Plant Science* **3**: 1-19.

Erol A. (2014). Type 2 diabetes and cancer as redox diseases? *The Lancet* **384**: 853-854.

Fan L., Li R., Pan J., Ding Z., Lin J. (2015). Endocytosis and its regulation in plants. *Trends in Plant Science* **20**: 388-397.

Farid A., Pabst M., Schoberer J., Altmann F., Glossl J., Strasser R. (2011). *Arabidopsis thaliana* alpha1,2-glucosyltransferase (ALG10) is required for efficient *N*-glycosylation and leaf growth. *The Plant Journal* **68**: 314-325.

Farmer E. E., Gao Y. Q., Lenzoni G., Wolfender J. L., Wu Q. (2020). Wound- and mechanostimulated electrical signals control hormone responses. *New Phytologist* **227**: 1037-1050.

Feng W., Kita D., Peaucelle A., Cartwright H. N., Doan V., Duan Q., Liu M. C., Maman J., Steinhorst L., Schmitz-Thom I., Yvon R., Kudla J., Wu H. M., Cheung A. Y., Dinneny J. R. (2018). The FERONIA receptor kinase maintains cell-wall integrity during salt stress through Ca^{2+} signaling. *Current Biology* **28**: 666-675

Fontaine J.-X., Tercé-Laforgue T., Bouton S., Pageau K., Lea P. J., Dubois F., Hirel B. (2013). Further insights into the isoenzyme composition and activity of glutamate dehydrogenase in *Arabidopsis thaliana*. *Plant Signaling & Behavior* **8**: e23329.

Foulquier F., Amyere M., Jaeken J., Zeevaert R., Schollen E., Race V., Bammens R., Morelle W., Rosnoblet C., Legrand D., Demaegd D., Buist N., Cheillan D., Guffon N., Morsomme P., Annaert W., Freeze H. H., Van Schaftingen E., Vikkula M., Matthijs G. (2012). TMEM165 deficiency causes a congenital disorder of glycosylation. *The American Journal of Human Genetics* **91**: 15-26.

Foulquier F., Legrand D. (2020). Biometals and glycosylation in humans: Congenital disorders of glycosylation shed lights into the crucial role of Golgi manganese homeostasis. *Biochimica et Biophysica Acta (BBA)-General Subjects* **1864**: 129674.

Frank J., Happeck R., Meier B., Hoang M. T. T., Stribny J., Hause G., Ding H., Morsomme P., Baginsky S., Peiter E. (2019). Chloroplast-localized BICAT proteins shape stromal calcium signals and are required for efficient photosynthesis. *New Phytologist* **221**: 866-880.

Furch A. C., Van Bel A. J., Fricker M. D., Felle H. H., Fuchs M., Hafke J. B. (2009). Sieve element Ca^{2+} channels as relay stations between remote stimuli and sieve tube occlusion in *Vicia faba*. *The Plant Cell* **21**: 2118-2132.

Gee K. R., Brown K. A., Chen W. N., Bishop-Stewart J., Gray D., Johnson I. (2000). Chemical and physiological characterization of fluo-4 Ca^{2+}-indicator dyes. *Cell Calcium* **27**: 97-106.

Gilroy S., Bialasek M., Suzuki N., Gorecka M., Devireddy A. R., Karpinski S., Mittler R. (2016). ROS, calcium, and electric signals: Key mediators of rapid systemic signaling in plants. *Plant Physiology* **171**: 1606-1615.

Gilroy S., Hughes W. A., Trewavas A. J. (1986). The measurement of intracellular calcium levels in protoplasts from higher plant cells. *FEBS Letters* **199**: 217-221.

Gobert A., Park G., Amtmann A., Sanders D., Maathuis F. J. (2006). *Arabidopsis thaliana* Cyclic Nucleotide Gated Channel 3 forms a non-selective ion transporter involved in germination and cation transport. *Journal of Experimental Botany* **57**: 791-800.

Gómez-Cadenas A., Tadeo F. R., Primo-Millo E., Talon M. (1998). Involvement of abscisic acid and ethylene in the responses of citrus seedlings to salt shock. *Physiologia Plantarum* **103**: 475-484.

Gong D., Guo Y., Schumaker K. S., Zhu J. K. (2004). The SOS3 family of calcium sensors and SOS2 family of protein kinases in Arabidopsis. *Plant Physiology* **134**: 919-926.

Grenzi M., Bonza M. C., Costa A. (2022). Signaling by plant glutamate receptor-like channels: What else! *Current Opinion in Plant Biology* **68**: 102253.

Hadlington J. L., Denecke J. (2000). Sorting of soluble proteins in the secretory pathway of plants. *Current Opinion in Plant Biology* **3**: 461-468.

Hamilton E. S., Schlegel A. M., Haswell E. S. (2015). United in diversity: Mechanosensitive ion channels in plants *Annual Review of Plant Biology* **66**: 113-137.

Harper J. F., Breton G., Harmon A. (2004). Decoding Ca^{2+} signals through plant protein kinases. *Annual Review of Plant Biology* **55**: 263.

Harper J. F., Hong B., Hwang I., Guo H. Q., Stoddard R., Huang J. F., Palmgren M. G., Sze H. (1998). A novel calmodulin-regulated Ca^{2+}-ATPase (ACA2) from Arabidopsis with an N-terminal autoinhibitory domain. *The Journal of Biological Chemistry* **273**: 1099-1106.

He J., Rössner N., Hoang M. T. T., Alejandro S., Peiter E. (2021). Transport, functions, and interaction of calcium and manganese in plant organellar compartments. *Plant Physiology* **187**: 1940-1972.

He J., Yang B., Hause G., Rössner N., Peiter-Volk T., Schattat M. H., Voiniciuc C., Peiter E. (2022). The *trans*-Golgi-localized protein BICAT3 regulates manganese allocation and matrix polysaccharide biosynthesis. *Plant Physiology* **190**: 2579-2600.

He M., Lan M., Zhang B., Zhou Y., Wang Y., Zhu L., Yuan M., Fu Y. (2018). Rab-H1b is essential for trafficking of cellulose synthase and for hypocotyl growth in *Arabidopsis thaliana*. *Journal of Integrative Plant Biology* **60**: 1051-1069.

Hedrich R., Shabala S. (2018). Stomata in a saline world. *Current Opinion in Plant Biology* **46**: 87-95.

Hendrix B., Hoffer P., Sanders R., Schwartz S., Zheng W., Eads B., Taylor D., Deikman J. (2021). Systemic *GFP* silencing is associated with high transgene expression in *Nicotiana benthamiana*. *PLoS One* **16**: 1-15.

Hernandez J. A., Ferrer M. A., Jimenez A., Barcelo A. R., Sevilla F. (2001). Antioxidant systems and $O^{2.-}$/H^2O^2 production in the apoplast of pea leaves. Its relation with salt-induced necrotic lesions in minor veins. *Plant Physiology* **127**: 817-831.

Hochmal A. K., Schulze S., Trompelt K., Hippler M. (2015). Calcium-dependent regulation of photosynthesis. *Biochimica et Biophysica Acta* **1847**: 993-1003.

Hoecker N., Honke A., Frey K., Leister D., Schneider A. (2020). Homologous Proteins of the Manganese Transporter PAM71 Are Localized in the Golgi Apparatus and Endoplasmic Reticulum. *Plants* **9**: 239.

Hrabak E. M., Chan C. W., Gribskov M., Harper J. F., Choi J. H., Halford N., Kudla J., Luan S., Nimmo H. G., Sussman M. R., Thomas M., Walker-Simmons K., Zhu J. K., Harmon A. C. (2003). The Arabidopsis CDPK-SnRK superfamily of protein kinases. *Plant Physiology* **132**: 666-680.

Huda K. M. K., Yadav S., Banu M. S. A., Trivedi D. K., Tuteja N. (2013). Genome-wide analysis of plant-type II Ca^{2+} ATPases gene family from rice and Arabidopsis: Potential role in abiotic stresses. *Plant Physiology and Biochemistry* **65**: 32-47.

Hüttner S., Veit C., Vavra U., Schoberer J., Liebminger E., Maresch D., Grass J., Altmann F., Mach L., Strasser R. (2014). Arabidopsis class I α-mannosidases MNS4 and MNS5 are involved in Endoplasmic Reticulum-associated degradation of misfolded glycoproteins. *The Plant Cell* **26**: 1712-1728.

Hwang I., Sze H., Harper J. F. (2000). A calcium-dependent protein kinase can inhibit a calmodulin-stimulated Ca^{2+} pump (ACA2) located in the Endoplasmic Reticulum of Arabidopsis. *Proceedings of the National Academy of Sciences of the United States of America* **97**: 6224-6229.

Jackson L. P. (2014). Structure and mechanism of COPI vesicle biogenesis. *Current Opinion in Cell Biology* **29**: 67-73.

Jammes F., Hu H. C., Villiers F., Bouten R., Kwak J. M. (2011). Calcium-permeable channels in plant cells. *The FEBS Journal* **278**: 4262-4276.

Ji H., Pardo J. M., Batelli G., Van Oosten M. J., Bressan R. A., Li X. (2013). The salt overly sensitive (SOS) pathway: Established and emerging roles. *Molecular Plant* **6**: 275-286.

Jia X.-Y., He L.-H., Jing R.-L., Li R.-Z. (2009). Calreticulin: Conserved protein and diverse functions in plants. *Physiologia Plantarum* **136**: 127-138.

Jiang K., Moe-Lange J., Hennet L., Feldman L. J. (2016). Salt stress affects the redox status of Arabidopsis root meristems. *Frontiers in Plant Science* **7**: 81.

Jiang Z., Zhou X., Tao M., Yuan F., Liu L., Wu F., Wu X., Xiang Y., Niu Y., Liu F., Li C., Ye R., Byeon B., Xue Y., Zhao H., Wang H. N., Crawford B. M., Johnson D. M., Hu C., Pei C., Zhou W., Swift G. B., Zhang H., Vo-Dinh T., Hu Z., Siedow J. N., Pei Z. M. (2019). Plant cell-surface GIPC sphingolipids sense salt to trigger Ca^{2+} influx. *Nature* **572**: 341-346.

Johnson N. A., Liu F., Weeks P. D., Hentzen A. E., Kruse H. P., Parker J. J., Laursen M., Nissen P., Costa C. J., Gatto C. (2009). A tomato ER-type Ca^{2+}-ATPase, LCA1, has a low thapsigargin-sensitivity and can transport manganese. *Archives of Biochemistry and Biophysics* **481**: 157-168.

Kajiura H., Koiwa H., Nakazawa Y., Okazawa A., Kobayashi A., Seki T., Fujiyama K. (2010). Two *Arabidopsis thaliana* Golgi α-mannosidase I enzymes are responsible for plant *N*-glycan maturation. *Glycobiology* **20**: 235-247.

Kamiya T., Maeshima M. (2004). Residues in internal repeats of the rice cation/H^+ exchanger are involved in the transport and selection of cations. *The Journal of Biological Chemistry* **279**: 812-819.

Kanazawa T., Ueda T. (2017). Exocytic trafficking pathways in plants: Why and how they are redirected. *New Phytologist* **215**: 952-957.

Kang J. S., Frank J., Kang C. H., Kajiura H., Vikram M., Ueda A., Kim S., Bahk J. D., Triplett B., Fujiyama K. (2008). Salt tolerance of *Arabidopsis thaliana* requires maturation of *N*-glycosylated proteins in the Golgi apparatus. *Proceedings of the National Academy of Sciences of the United States of America* **105**: 5933-5938.

Kefu Z., Munns R., King R. (1991). Abscisic acid levels in NaCl-treated barley, cotton and saltbush. *Functional Plant Biology* **18**: 17-24.

Kellokumpu S. (2019). Golgi pH, ion and redox homeostasis: How much do they really matter? *Frontiers in Cell and Developmental Biology* **7**: 93.

Khan I., Gratz R., Denezhkin P., Schott-Verdugo S. N., Angrand K., Genders L., Basgaran R. M., Fink-Straube C., Brumbarova T., Gohlke H., Bauer P., Ivanov R. (2019). Calcium-promoted interaction between the C2-domain protein EHB1 and metal transporter IRT1 inhibits Arabidopsis iron acquisition. *Plant Physiology* **180**: 1564-1581.

Kiegle E., Moore C. A., Haseloff J., Tester M. A., Knight M. R. (2000). Cell-type-specific calcium responses to drought, salt and cold in the Arabidopsis root. *The Plant Journal* **23**: 267-278.

Kiep V., Vadassery J., Lattke J., Maass J. P., Boland W., Peiter E., Mithofer A. (2015). Systemic cytosolic Ca^{2+} elevation is activated upon wounding and herbivory in Arabidopsis. *New Phytologist* **207**: 996-1004.

Kim B. G., Waadt R., Cheong Y. H., Pandey G. K., Dominguez-Solis J. R., Schultke S., Lee S. C., Kudla J., Luan S. (2007). The calcium sensor CBL10 mediates salt tolerance by regulating ion homeostasis in Arabidopsis. *The Plant Journal* **52**: 473-484.

Kim S. J., Bassham D. C. (2011). TNO1 is involved in salt tolerance and vacuolar trafficking in Arabidopsis. *Plant Physiology* **156**: 514-526.

Kintzer A. F., Stroud R. M. (2016). Structure, inhibition and regulation of two-pore channel TPC1 from *Arabidopsis thaliana*. *Nature* **531**: 258-262.

Kirichok Y., Krapivinsky G., Clapham D. E. (2004). The mitochondrial calcium uniporter is a highly selective ion channel. *Nature* **427**: 360-364.

Knauer R., Lehle L. (1999). The oligosaccharyltransferase complex from yeast. *Biochimica et Biophysica Acta (BBA)-General Subjects* **1426**: 259-273.

Knight H., Trewavas A. J., Knight M. R. (1997). Calcium signalling in *Arabidopsis thaliana* responding to drought and salinity. *The Plant Journal* **12**: 1067-1078.

Knight M. R., Campbell A. K., Smith S. M., Trewavas A. J. (1991). Transgenic plant aequorin reports the effects of touch and cold-shock and elicitors on cytoplasmic calcium. *Nature* **352**: 524-526.

Koiwa H., Li F., Mccully M. G., Mendoza I., Koizumi N., Manabe Y., Nakagawa Y., Zhu J., Rus A., Pardo J. M., Bressan R. A., Hasegawa P. M. (2003). The STT3a subunit isoform of the Arabidopsis oligosaccharyltransferase controls adaptive responses to salt/osmotic stress. *The Plant Cell* **15**: 2273-2284.

Kolukisaoglu U., Weinl S., Blazevic D., Batistic O., Kudla J. (2004). Calcium sensors and their interacting protein kinases: Genomics of the Arabidopsis and rice CBL-CIPK signaling networks. *Plant Physiology* **134**: 43-58.

Kong D., Hu H.-C., Okuma E., Lee Y., Lee H. S., Munemasa S., Cho D., Ju C., Pedoeim L., Rodriguez B. (2016). L-Met activates Arabidopsis GLR Ca^{2+} channels upstream of ROS production and regulates stomatal movement. *Cell Reports* **17**: 2553-2561.

Kudla J., Becker D., Grill E., Hedrich R., Hippler M., Kummer U., Parniske M., Romeis T., Schumacher K. (2018). Advances and current challenges in calcium signaling. *New Phytologist* **218**: 414-431.

Künzl F., Fruholz S., Fassler F., Li B., Pimpl P. (2016). Receptor-mediated sorting of soluble vacuolar proteins ends at the *trans*-Golgi network/early endosome. *Nature Plants* **2**: 16017.

Lam S. K., Siu C. L., Hillmer S., Jang S., An G., Robinson D. G., Jiang L. (2007). Rice SCAMP1 defines clathrin-coated, *trans*-Golgi-located tubular-vesicular structures as an early endosome in tobacco BY-2 cells. *The Plant Cell* **19**: 296-319.

Lecourieux D., Lamotte O., Bourque S., Wendehenne D., Mazars C., Ranjeva R., Pugin A. (2005). Proteinaceous and oligosaccharidic elicitors induce different calcium signatures in the nucleus of tobacco cells. *Cell Calcium* **38**: 527-538.

Lecourieux D., Mazars C., Pauly N., Ranjeva R., Pugin A. (2002). Analysis and effects of cytosolic free calcium increases in response to elicitors in *Nicotiana plumbaginifolia* cells. *The Plant Cell* **14**: 2627-2641.

Lee D., Lal N. K., Lin Z. D., Ma S., Liu J., Castro B., Toruno T., Dinesh-Kumar S. P., Coaker G. (2020). Regulation of reactive oxygen species during plant immunity through phosphorylation and ubiquitination of RBOHD. *Nature Communications* **11**: 1-16.

Lee E., Vanneste S., Perez-Sancho J., Benitez-Fuente F., Strelau M., Macho A. P., Botella M. A., Friml J., Rosado A. (2019). Ionic stress enhances ER-PM connectivity via phosphoinositide-associated SYT1 contact site expansion in Arabidopsis. *Proceedings of the National Academy of Sciences of the United States of America* **116**: 1420-1429.

Lee G.-J., Sohn E. J., Lee M. H., Hwang I. (2004). The Arabidopsis rab5 homologs rha1 and ara7 localize to the prevacuolar compartment. *Plant and Cell Physiology* **45**: 1211-1220.

Leitão N., Dangeville P., Carter R., Charpentier M. (2019). Nuclear calcium signatures are associated with root development. *Nature Communications* **10**: 1-9.

Leshem Y., Melamed-Book N., Cagnac O., Ronen G., Nishri Y., Solomon M., Cohen G., Levine A. (2006). Suppression of Arabidopsis vesicle-SNARE expression inhibited fusion of H_2O_2-containing vesicles with tonoplast and increased salt tolerance. *Proceedings of the National Academy of Sciences of the United States of America* **103**: 18008-18013.

Lewit-Bentley A., Réty S. (2000). EF-hand calcium-binding proteins. *Current Opinion in Structural Biology* **10**: 637-643.

Li X., Chanroj S., Wu Z., Romanowsky S. M., Harper J. F., Sze H. (2008a). A distinct endosomal Ca^{2+}/Mn^{2+} pump affects root growth through the secretory process. *Plant Physiology* **147**: 1675-1689.

Li Z., Cao Y., Zhang J., Chen S. (2008b). Characterization of Arabidopsis calreticulin mutants in response to calcium and salinity stresses. *Progress in Natural Science* **18**: 1219-1224.

Liebminger E., Huttner S., Vavra U., Fischl R., Schoberer J., Grass J., Blaukopf C., Seifert G. J., Altmann F., Mach L., Strasser R. (2009). Class I α-mannosidases are required for *N*-glycan processing and root development in *Arabidopsis thaliana*. *The Plant Cell* **21**: 3850-3867.

Liu C., Niu G., Zhang H., Sun Y., Sun S., Yu F., Lu S., Yang Y., Li J., Hong Z. (2018). Trimming of *N*-Glycans by the Golgi-localized α-1,2-Mannosidases, MNS1 and MNS2, is crucial for maintaining RSW2 protein abundance during salt stress in Arabidopsis. *Molecular Plant* **11**: 678-690.

Liu L., Cui F., Li Q., Yin B., Zhang H., Lin B., Wu Y., Xia R., Tang S., Xie Q. (2011). The Endoplasmic Reticulum-associated degradation is necessary for plant salt tolerance. *Cell Research* **21**: 957-969.

Logan D. C., Knight M. R. (2003). Mitochondrial and cytosolic calcium dynamics are differentially regulated in plants. *Plant Physiology* **133**: 21-24.

Lopez-Hernandez F., Tryfona T., Rizza A., Yu X. L., Harris M. O. B., Webb A. a. R., Kotake T., Dupree P. (2020). Calcium binding by arabinogalactan polysaccharides is important for normal plant development. *The Plant Cell* **32**: 3346-3369.

Lowenthal M. S., Davis K. S., Formolo T., Kilpatrick L. E., Phinney K. W. (2016). Identification of novel *N*-glycosylation sites at noncanonical protein consensus motifs. *Journal of Proteome Research* **15**: 2087-2101.

Lu S. X., Hrabak E. M. (2002). An Arabidopsis calcium-dependent protein kinase is associated with the Endoplasmic Reticulum. *Plant Physiology* **128**: 1008-1021.

Lu Y. J., Li P., Shimono M., Corrion A., Higaki T., He S. Y., Day B. (2020). Arabidopsis calcium-dependent protein kinase 3 regulates actin cytoskeleton organization and immunity. *Nature Communications* **11**: 6234.

Ludwig A. A., Romeis T., Jones J. D. (2004). CDPK-mediated signalling pathways: Specificity and cross-talk. *Journal of Experimental Botany* **55**: 181-188.

Lund C. H., Stenbaek A., Atmodjo M. A., Rasmussen R. E., Moller I. E., Erstad S. M., Biswal A. K., Mohnen D., Mravec J., Sakuragi Y. (2020). Pectin synthesis and pollen tube growth in Arabidopsis involves three GAUT1 Golgi-anchoring proteins: GAUT5, GAUT6, and GAUT7. *Frontiers in Plant Science* **11**: 585774.

Luo Y., Scholl S., Doering A., Zhang Y., Irani N. G., Rubbo S. D., Neumetzler L., Krishnamoorthy P., Van Houtte I., Mylle E., Bischoff V., Vernhettes S., Winne J., Friml J., Stierhof Y. D., Schumacher K., Persson S., Russinova E. (2015). V-ATPase activity in the TGN/EE is required for exocytosis and recycling in Arabidopsis. *Nature Plants* **1**: 15094.

Ma L., Ye J., Yang Y., Lin H., Yue L., Luo J., Long Y., Fu H., Liu X., Zhang Y., Wang Y., Chen L., Kudla J., Wang Y., Han S., Song C. P., Guo Y. (2019). The SOS2-SCaBP8 complex generates and fine-tunes an AtANN4-dependent calcium signature under salt stress. *Developmental Cell* **48**: 697-709

Ma L., Zhang H., Sun L., Jiao Y., Zhang G., Miao C., Hao F. (2012). NADPH oxidase AtrbohD and AtrbohF function in ROS-dependent regulation of Na^+/K^+ homeostasis in Arabidopsis under salt stress. *Journal of Experimental Botany* **63**: 305-317.

Manohar M., Shigaki T., Hirschi K. D. (2011). Plant cation/H^+ exchangers (CAXs): Biological functions and genetic manipulations. *Plant Biology* **13**: 561-569.

Martinière A., Bassil E., Jublanc E., Alcon C., Reguera M., Sentenac H., Blumwald E., Paris N. (2013). *In vivo* intracellular pH measurements in tobacco and Arabidopsis reveal an unexpected pH gradient in the endomembrane system. *The Plant Cell* **25**: 4028-4043.

Marzol E., Borassi C., Bringas M., Sede A., Rodriguez Garcia D. R., Capece L., Estevez J. M. (2018). Filling the gaps to solve the extensin puzzle. *Molecular Plant* **11**: 645-658.

Mäser P., Thomine S., Schroeder J. I., Ward J. M., Hirschi K., Sze H., Talke I. N., Amtmann A., Maathuis F. J., Sanders D. (2001). Phylogenetic relationships within cation transporter families of Arabidopsis. *Plant Physiology* **126**: 1646-1667.

Matsushima R., Kondo M., Nishimura M., Hara-Nishimura I. (2003). A novel ER-derived compartment, the ER body, selectively accumulates a ß-glucosidase with an ER-retention signal in Arabidopsis. *The Plant Journal* **33**: 493-502.

Mazars C., Bourque S., Mithofer A., Pugin A., Ranjeva R. (2009). Calcium homeostasis in plant cell nuclei. *New Phytologist* **181**: 261-274.

McCormack E., Tsai Y. C., Braam J. (2005). Handling calcium signaling: Arabidopsis CaMs and CMLs. *Trends in Plant Science* **10**: 383-389.

McCormack J. G., Halestrap A. P., Denton R. M. (1990). Role of calcium ions in regulation of mammalian intramitochondrial metabolism. *Physiological Reviews* **70**: 391-425.

McKay D. W., McFarlane H. E., Qu Y., Situmorang A., Gilliham M., Wege S. (2022). Plant *trans*-Golgi network/early endosome pH regulation requires cation chloride cotransporter (CCC1). *eLife* **11**: e70701.

Meckel T., Hurst A. C., Thiel G., Homann U. (2005). Guard cells undergo constitutive and pressure-driven membrane turnover. *Protoplasma* **226**: 23-29.

Meents M. J., Motani S., Mansfield S. D., Samuels A. L. (2019). Organization of xylan production in the Golgi during secondary cell wall biosynthesis. *Plant Physiology* **181**: 527-546.

Mennerich D., Kellokumpu S., Kietzmann T. (2019). Hypoxia and reactive oxygen species as modulators of Endoplasmic Reticulum and Golgi homeostasis. *Antioxidants & Redox Signaling* **30**: 113-137.

Meyerhoff O., Müller K., Roelfsema M. R. G., Latz A., Lacombe B., Hedrich R., Dietrich P., Becker D. (2005). AtGLR3. 4, a glutamate receptor channel-like gene is sensitive to touch and cold. *Planta* **222**: 418-427.

Miao Y., Yan P. K., Kim H., Hwang I., Jiang L. (2006). Localization of green fluorescent protein fusions with the seven Arabidopsis vacuolar sorting receptors to prevacuolar compartments in tobacco BY-2 cells. *Plant Physiology* **142**: 945-962.

Miller G., Schlauch K., Tam R., Cortes D., Torres M. A., Shulaev V., Dangl J. L., Mittler R. (2009). The plant NADPH oxidase RBOHD mediates rapid systemic signaling in response to diverse stimuli. *Science Signaling* **2**: ra45.

Miller G., Suzuki N., Ciftci-Yilmaz S., Mittler R. (2010). Reactive oxygen species homeostasis and signalling during drought and salinity stresses. *Plant, Cell & Environment* **33**: 453-467.

Mills R. F., Doherty M. L., Lopez-Marques R. L., Weimar T., Dupree P., Palmgren M. G., Pittman J. K., Williams L. E. (2008). ECA3, a Golgi-localized P_{2A}-type ATPase, plays a crucial role in manganese nutrition in Arabidopsis. *Plant Physiology* **146**: 116-128.

Mithöfer A., Mazars C. (2002). Aequorin-based measurements of intracellular Ca^{2+}-signatures in plant cells. *Biological Procedures Online* **4**: 105-118.

Miyawaki A., Griesbeck O., Heim R., Tsien R. Y. (1999). Dynamic and quantitative Ca^{2+} measurements using improved cameleons. *Proceedings of the National Academy of Sciences of the United States of America* **96**: 2135-2140.

Monshausen G. B., Miller N. D., Murphy A. S., Gilroy S. (2011). Dynamics of auxin-dependent Ca^{2+} and pH signaling in root growth revealed by integrating high-resolution imaging with automated computer vision-based analysis. *The Plant Journal* **65**: 309-318.

Montero M., Brini M., Marsault R., Alvarez J., Sitia R., Pozzan T., Rizzuto R. (1995). Monitoring dynamic changes in free Ca^{2+} concentration in the Endoplasmic Reticulum of intact cells. *The EMBO journal* **14**: 5467-5475.

Morris J., Tian H., Park S., Sreevidya C. S., Ward J. M., Hirschi K. D. (2008). AtCCX3 is an Arabidopsis endomembrane H^+-dependent K^+ transporter. *Plant Physiology* **148**: 1474-1486.

Mou W., Kao Y. T., Michard E., Simon A. A., Li D., Wudick M. M., Lizzio M. A., Feijo J. A., Chang C. (2020). Ethylene-independent signaling by the ethylene precursor ACC in Arabidopsis ovular pollen tube attraction. *Nature Communications* **11**: 4082.

Nagai T., Yamada S., Tominaga T., Ichikawa M., Miyawaki A. (2004). Expanded dynamic range of fluorescent indicators for Ca^{2+} by circularly permuted yellow fluorescent proteins. *Proceedings of the National Academy of Sciences of the United States of America* **101**: 10554-10559.

Nagashima Y., Von Schaewen A., Koiwa H. (2018). Function of *N*-glycosylation in plants. *Plant Science* **274**: 70-79.

Nagata T., Iizumi S., Satoh K., Ooka H., Kawai J., Carninci P., Hayashizaki Y., Otomo Y., Murakami K., Matsubara K., Kikuchi S. (2004). Comparative analysis of plant and animal calcium signal transduction element using plant full-length cDNA data. *Molecular Biology and Evolution* **21**: 1855-1870.

Nakai J., Ohkura M., Imoto K. (2001). A high signal-to-noise Ca^{2+} probe composed of a single green fluorescent protein. *Nature Biotechnology* **19**: 137-141.

Naramoto S., Otegui M. S., Kutsuna N., De Rycke R., Dainobu T., Karampelias M., Fujimoto M., Feraru E., Miki D., Fukuda H., Nakano A., Friml J. (2014). Insights into the localization and function of the membrane trafficking regulator GNOM ARF-GEF at the Golgi apparatus in Arabidopsis. *The Plant Cell* **26**: 3062-3076.

Nardi M. C., Feron R., Navazio L., Mariani P., Pierson E., Wolters-Arts M., Knuiman B., Mariani C., Derksen J. (2006). Expression and localization of calreticulin in tobacco anthers and pollen tubes. *Planta* **223**: 1263-1271.

Navazio L., Formentin E., Cendron L., Szabò I. (2020). Chloroplast calcium signaling in the spotlight. *Frontiers in Plant Science* **11**: 186.

Nebenführ A., Gallagher L. A., Dunahay T. G., Frohlick J. A., Mazurkiewicz A. M., Meehl J. B., Staehelin L. A. (1999). Stop-and-go movements of plant Golgi stacks are mediated by the acto-myosin system. *Plant Physiology* **121**: 1127-1141.

Neuhaus J.-M., Sticher L., Meins Jr F., Boller T. (1991). A short C-terminal sequence is necessary and sufficient for the targeting of chitinases to the plant vacuole. *Proceedings of the National Academy of Sciences of the United States of America* **88**: 10362-10366.

Nguyen C. T., Kurenda A., Stolz S., Chételat A., Farmer E. E. (2018). Identification of cell populations necessary for leaf-to-leaf electrical signaling in a wounded plant. *Proceedings of the National Academy of Sciences of the United States of America* **115**: 10178-10183.

Nielsen E., Cheung A. Y., Ueda T. (2008). The regulatory RAB and ARF GTPases for vesicular trafficking. *Plant Physiology* **147**: 1516-1526.

Nomura H., Shiina T. (2014). Calcium signaling in plant endosymbiotic organelles: Mechanism and role in physiology. *Molecular Plant* **7**: 1094-1104.

Nour-Eldin H. H., Hansen B. G., Norholm M. H., Jensen J. K., Halkier B. A. (2006). Advancing uracil-excision based cloning towards an ideal technique for cloning PCR fragments. *Nucleic Acids Research* **34**: 1-8.

Ordenes V. R., Moreno I., Maturana D., Norambuena L., Trewavas A. J., Orellana A. (2012). *In vivo* analysis of the calcium signature in the plant Golgi apparatus reveals unique dynamics. *Cell Calcium* **52**: 397-404.

Ordenes V. R., Reyes F. C., Wolff D., Orellana A. (2002). A thapsigargin-sensitive Ca^{2+} pump is present in the pea Golgi apparatus membrane. *Plant Physiology* **129**: 1820-1828.

Ozgur R., Uzilday B., Sekmen A. H., Turkan I. (2015). The effects of induced production of reactive oxygen species in organelles on Endoplasmic Reticulum stress and on the unfolded protein response in arabidopsis. *Annals of Botany* **116**: 541-553.

Palmer A. E., Jin C., Reed J. C., Tsien R. Y. (2004). Bcl-2-mediated alterations in Endoplasmic Reticulum Ca^{2+} analyzed with an improved genetically encoded fluorescent sensor. *Proceedings of the National Academy of Sciences of the United States of America* **101**: 17404-17409.

Palmgren M. G., Harper J. F. (1999). Pumping with plant P-type ATPases. *Journal of Experimental Botany* **50**: 883-893.

Palmgren M. G., Nissen P. (2011). P-type ATPases. *Annual Review of Biophysics* **40**: 243-266.

Pan G., Zhang H., Chen B., Gao S., Yang B., Jiang Y. Q. (2019). Rapeseed calcium-dependent protein kinase CPK6L modulates reactive oxygen species and cell death through interacting and phosphorylating RBOHD. *Biochemical and Biophysical Research Communications* **518**: 719-725.

Park S., Song B., Shen W., Ding S. Y. (2019). A mutation in the catalytic domain of cellulose synthase 6 halts its transport to the Golgi apparatus. *Journal of Experimental Botany* **70**: 6071-6083.

Park S. Y., Yang J. S., Schmider A. B., Soberman R. J., Hsu V. W. (2015). Coordinated regulation of bidirectional COPI transport at the Golgi by CDC42. *Nature* **521**: 529-532.

Parsons H. T., Stevens T. J., Mcfarlane H. E., Vidal-Melgosa S., Griss J., Lawrence N., Butler R., Sousa M. M. L., Salemi M., Willats W. G. T., Petzold C. J., Heazlewood J. L., Lilley K. S. (2019). Separating Golgi proteins from *cis* to *trans* reveals underlying properties of cisternal localization. *The Plant Cell* **31**: 2010-2034.

Peiter E. (2011). The plant vacuole: Emitter and receiver of calcium signals. *Cell Calcium* **50**: 120-128.

Peiter E., Maathuis F. J., Mills L. N., Knight H., Pelloux J., Hetherington A. M., Sanders D. (2005). The vacuolar Ca^{2+}-activated channel TPC1 regulates germination and stomatal movement. *Nature* **434**: 404-408.

Peiter E., Montanini B., Gobert A., Pedas P., Husted S., Maathuis F. J. M., Blaudez D., Chalot M., Sanders D. (2007). A secretory pathway-localized cation diffusion facilitator confers plant manganese tolerance. *Proceedings of the National Academy of Sciences of the United States of America* **104**: 8532-8537.

Pereira C., Di Sansebastiano G. P. (2021). Mechanisms of membrane traffic in plant cells. *Plant Physiology and Biochemistry* **169**: 102-111.

Petersen O. H., Courjaret R., Machaca K. (2017). Ca^{2+} tunnelling through the ER lumen as a mechanism for delivering Ca^{2+} entering via store-operated Ca^{2+} channels to specific target sites. *The Journal of Physiology* **595**: 2999-3014.

Pittman J. K., Hirschi K. D. (2016). CAX-ing a wide net: $Cation/H^+$ transporters in metal remediation and abiotic stress signalling. *Plant Biology* **18**: 741-749.

Poovaiah B. W., Reddy A. S. (1987). Calcium messenger system in plants. *Critical Reviews in Plant Sciences* **6**: 47-103.

Potelle S., Morelle W., Dulary E., Duvet S., Vicogne D., Spriet C., Krzewinski-Recchi M. A., Morsomme P., Jaeken J., Matthijs G., De Bettignies G., Foulquier F. (2016). Glycosylation abnormalities in Gdt1p/TMEM165 deficient cells result from a defect in Golgi manganese homeostasis. *Human Molecular Genetics* **25**: 1489-1500.

Potters G., Pasternak T. P., Guisez Y., Palme K. J., Jansen M. A. (2007). Stress-induced morphogenic responses: Growing out of trouble? *Trends in Plant Science* **12**: 98-105.

Price A. H., Taylor A., Ripley S. J., Griffiths A., Trewavas A. J., Knight M. R. (1994). Oxidative signals in tobacco increase cytosolic calcium. *The Plant Cell* **6**: 1301-1310.

Quan-Sheng Qiu Y. G., Margaret A. Dietrich, Karen S. Schumaker, Jian-Kang Zhu (2002). Regulation of SOS1, a plasma membrane Na^+/H^+ exchanger in *Arabidopsis thaliana*, by SOS2 and SOS3. *Proceedings of the National Academy of Sciences of the United States of America* **99**: 8436 - 8441.

Radhamony R. N., Theg S. M. (2006). Evidence for an ER to Golgi to chloroplast protein transport pathway. *Trends in Cell Biology* **16**: 385-387.

Rahmati Ishka M., Brown E., Rosenberg A., Romanowsky S., Davis J. A., Choi W. G., Harper J. F. (2021). Arabidopsis Ca^{2+}-ATPases 1, 2, and 7 in the Endoplasmic Reticulum contribute to growth and pollen fitness. *Plant Physiology* **185**: 1966-1985.

Ranf S., Wunnenberg P., Lee J., Becker D., Dunkel M., Hedrich R., Scheel D., Dietrich P. (2008). Loss of the vacuolar cation channel, AtTPC1, does not impair Ca^{2+} signals induced by abiotic and biotic stresses. *The Plant Journal* **53**: 287-299.

Reddy A. S., Ali G. S., Celesnik H., Day I. S. (2011). Coping with stresses: Roles of calcium- and calcium/calmodulin-regulated gene expression. *The Plant Cell* **23**: 2010-2032.

Rentel M. C., Knight M. R. (2004). Oxidative stress-induced calcium signaling in Arabidopsis. *Plant Physiology* **135**: 1471-1479.

Resentini F., Grenzi M., Ancora D., Cademartori M., Luoni L., Franco M., Bassi A., Bonza M. C., Costa A. (2021). Simultaneous imaging of ER and cytosolic Ca^{2+} dynamics reveals long-distance ER Ca^{2+} waves in plants. *Plant Physiology* **187**: 603-617.

Robinson D. G. (2020). Plant Golgi ultrastructure. *Journal of Microscopy* **280**: 111-121.

Robinson D. G., Albrecht S., Moriysu Y. (2004). The V-ATPase inhibitors concanamycin A and bafilomycin A lead to Golgi swelling in tobacco BY-2 cells. *Protoplasma* **224**: 255-260.

Robinson D. G., Pimpl P. (2014). Receptor-mediated transport of vacuolar proteins: A critical analysis and a new model. *Protoplasma* **251**: 247-264.

Rocha A. G., Vothknecht U. C. (2012). The role of calcium in chloroplasts-an intriguing and unresolved puzzle. *Protoplasma* **249**: 957-966.

Rodriguez A. A., Cordoba A. R., Ortega L., Taleisnik E. (2004). Decreased reactive oxygen species concentration in the elongation zone contributes to the reduction in maize leaf growth under salinity. *Journal of Experimental Botany* **55**: 1383-1390.

Rojo E., Denecke J. (2008). What is moving in the secretory pathway of plants? *Plant Physiology* **147**: 1493-1503.

Ruberti C., Feitosa-Araujo E., Xu Z., Wagner S., Grenzi M., Darwish E., Lichtenauer S., Fuchs P., Parmagnani A. S., Balcerowicz D., Schoenaers S., De La Torre C., Mekkaoui K., Nunes-Nesi A., Wirtz M., Vissenberg K., Van Aken O., Hause B., Costa A., Schwarzländer M. (2022). MCU proteins dominate *in vivo* mitochondrial Ca^{2+} uptake in Arabidopsis roots. *The Plant Cell* **34**: 4428-4452.

Ruge H., Flosdorff S., Ebersberger I., Chigri F., Vothknecht U. C. (2016). The calmodulin-like proteins AtCML4 and AtCML5 are single-pass membrane proteins targeted to the endomembrane system by an N-terminal signal anchor sequence. *Journal of Experimental Botany* **67**: 3985-3996.

Rui Q., Tan X., Liu F., Bao Y. (2022). An Update on the Key Factors Required for Plant Golgi Structure Maintenance. *Frontiers in Plant Science* **13**: 1-13.

Ruiz-Canada C., Kelleher D. J., Gilmore R. (2009). Cotranslational and posttranslational *N*-glycosylation of polypeptides by distinct mammalian OST isoforms. *Cell* **136**: 272-283.

Saint-Jore-Dupas C., Nebenfuhr A., Boulaflous A., Follet-Gueye M. L., Plasson C., Hawes C., Driouich A., Faye L., Gomord V. (2006). Plant *N*-glycan processing enzymes employ different targeting mechanisms for their spatial arrangement along the secretory pathway. *The Plant Cell* **18**: 3182-3200.

San Pietro E., Capestrano M., Polishchuk E. V., Dipentima A., Trucco A., Zizza P., Mariggiò S., Pulvirenti T., Sallese M., Tete S., Mironov A. A., Leslie C. C., Corda D., Luini A., Polishchuk R. S. (2009). Group IV phospholipase A$_2$a controls the formation of inter-cisternal continuities involved in intra-Golgi transport. *PLoS Biology* **7**: 1-21.

Sánchez-Simarro J., Bernat-Silvestre C., Gimeno-Ferrer F., Selvi-Martínez P., Montero-Pau J., Aniento F., Marcote M. J. (2020). Loss of Arabidopsis ß-COP Function Affects Golgi Structure, Plant Growth and Tolerance to Salt Stress. *Frontiers in Plant Science* **11**: 1-14.

Schoberer J., Konig J., Veit C., Vavra U., Liebminger E., Botchway S. W., Altmann F., Kriechbaumer V., Hawes C., Strasser R. (2019). A signal motif retains Arabidopsis ER-α-mannosidase I in the *cis*-Golgi and prevents enhanced glycoprotein ERAD. *Nature Communications* **10**: 1-15.

Shao Q., Gao Q., Lhamo D., Zhang H., Luan S. (2020). Two glutamate- and pH-regulated Ca^{2+} channels are required for systemic wound signaling in Arabidopsis. *Science Signaling* **13**: eaba1453.

Shen J., Zeng Y., Zhuang X., Sun L., Yao X., Pimpl P., Jiang L. (2013). Organelle pH in the Arabidopsis endomembrane system. *Molecular Plant* **6**: 1419-1437.

Shi H., Quintero F. J., Pardo J. M., Zhu J. K. (2002). The putative plasma membrane Na^+/H^+ antiporter SOS1 controls long-distance Na^+ transport in plants. *The Plant Cell* **14**: 465-477.

Shigaki T., Hirschi K. D. (2006). Diverse functions and molecular properties emerging for CAX cation/H^+ exchangers in plants. *Plant Biology* **8**: 419-429.

Shigaki T., Rees I., Nakhleh L., Hirschi K. D. (2006). Identification of three distinct phylogenetic groups of CAX cation/proton antiporters. *Journal of Molecular Evolution* **63**: 815-825.

Shih H. W., Depew C. L., Miller N. D., Monshausen G. B. (2015). The cyclic nucleotide-gated channel CNGC14 regulates root gravitropism in *Arabidopsis thaliana*. *Current Biology* **25**: 3119-3125.

Shimomura O., Johnson F. H., Saiga Y. (1962). Extraction, purification and properties of aequorin, a bioluminescent protein from the luminous hydromedusan, Aequorea. *Journal of cellular and comparative physiology* **59**: 223-239.

Shkolnik D., Nuriel R., Bonza M. C., Costa A., Fromm H. (2018). MIZ1 regulates ECA1 to generate a slow, long-distance phloem-transmitted Ca^{2+} signal essential for root water tracking in Arabidopsis. *Proceedings of the National Academy of Sciences of the United States of America* **115**: 8031-8036.

Sieberer B. J., Chabaud M., Timmers A. C., Monin A., Fournier J., Barker D. G. (2009). A nuclear-targeted cameleon demonstrates intranuclear Ca^{2+} spiking in *Medicago truncatula* root hairs in response to rhizobial nodulation factors. *Plant Physiology* **151**: 1197-1206.

Sinclair S. A., Senger T., Talke I. N., Cobbett C. S., Haydon M. J., Kramer U. (2018). Systemic Upregulation of MTP2- and HMA2-Mediated Zn Partitioning to the Shoot Supplements Local Zn Deficiency Responses. *The Plant Cell* **30**: 2463-2479.

Singh S., Parniske M. (2012). Activation of calcium- and calmodulin-dependent protein kinase (CCaMK), the central regulator of plant root endosymbiosis. *Current Opinion in Plant Biology* **15**: 444-453.

Smirnoff N., Arnaud D. (2019). Hydrogen peroxide metabolism and functions in plants. *New Phytologist* **221**: 1197-1214.

Sperling P., Heinz E. (2003). Plant sphingolipids: Structural diversity, biosynthesis, first genes and functions. *Biochimica et Biophysica Acta* **1632**: 1-15.

Stael S. (2019). Chloroplast calcium signalling quenches a thirst. *Nature Plants* **5**: 559-560.

Stael S., Wurzinger B., Mair A., Mehlmer N., Vothknecht U. C., Teige M. (2012). Plant organellar calcium signalling: An emerging field. *Journal of Experimental Botany* **63**: 1525-1542.

Stefanik N., Bizan J., Wilkens A., Tarnawska-Glatt K., Goto-Yamada S., Strzalka K., Nishimura M., Hara-Nishimura I., Yamada K. (2020). NAI2 and TSA1 drive differentiation of constitutive and Inducible ER body formation in Brassicaceae. *Plant and Cell Physiology* **61**: 722-734.

Steinhorst L., He G., Moore L. K., Schültke S., Schmitz-Thom I., Cao Y., Hashimoto K., Andrés Z., Piepenburg K., Ragel P., Behera S., Almutairi B. O., Batistič O., Wyganowski T., Köster P., Edel K. H., Zhang C., Krebs M., Jiang C., Guo Y., Quintero F. J., Bock R., Kudla J. (2022). A Ca^{2+}-sensor switch for tolerance to elevated salt stress in Arabidopsis. *Developmental Cell* **57**: 2081-2094.

Steinhorst L., Kudla J. (2013). Calcium and reactive oxygen species rule the waves of signaling. *Plant Physiology* **163**: 471-485.

Steinhorst L., Kudla J., 2019. How plants perceive salt. In.: Nature Publishing Group.

Strasser R., Seifert G., Doblin M. S., Johnson K. L., Ruprecht C., Pfrengle F., Bacic A., Estevez J. M. (2021). Cracking the "sugar code": A snapshot of *N-* and *O*-glycosylation pathways and functions in plants cells. *Frontiers in Plant Science* **12**: 1-19.

Stribny J., Thines L., Deschamps A., Goffin P., Morsomme P. (2020). The human Golgi protein TMEM165 transports calcium and manganese in yeast and bacterial cells. *The Journal of Biological Chemistry* **295**: 3865-3874.

Südhof T. C. (2013). Neurotransmitter release: the last millisecond in the life of a synaptic vesicle. *Neuron* **80**: 675-690.

Suen P. K., Shen J., Sun S. S. M., Jiang L. (2010). Expression and characterization of two functional vacuolar sorting receptor (VSR) proteins, BP-80 and AtVSR4 from culture media of transgenic tobacco BY-2 cells. *Plant Science* **179**: 68-76.

Sun J., Wang M. J., Ding M. Q., Deng S. R., Liu M. Q., Lu C. F., Zhou X. Y., Shen X., Zheng X. J., Zhang Z. K., Song J., Hu Z. M., Xu Y., Chen S. L. (2010). H_2O_2 and cytosolic Ca^{2+} signals triggered by the PM H^+-coupled transport system mediate K^+/Na^+ homeostasis in NaCl-stressed *Populus euphratica* cells. *Plant, Cell & Environment* **33**: 943-958.

Sun Y., Zhao J., Li X., Li Y. (2020). E2 conjugases UBC1 and UBC2 regulate MYB42-mediated SOS pathway in response to salt stress in Arabidopsis. *New Phytologist* **227**: 455-472.

Suzuki J., Kanemaru K., Iino M. (2016). Genetically encoded fluorescent indicators for organellar calcium imaging. *Biophysical Journal* **111**: 1119-1131.

Szabadkai G., Duchen M. R. (2008). Mitochondria: The hub of cellular Ca^{2+} signaling. *Physiology* **23**: 84-94.

Teardo E., Carraretto L., Moscatiello R., Cortese E., Vicario M., Festa M., Maso L., De Bortoli S., Calì T., Vothknecht U. C., Formentin E., Cendron L., Navazio L., Szabo I. (2019). A chloroplast-localized mitochondrial calcium uniporter transduces osmotic stress in Arabidopsis. *Nature Plants* **5**: 581-588.

Teardo E., Carraretto L., Wagner S., Formentin E., Behera S., De Bortoli S., Larosa V., Fuchs P., Lo Schiavo F., Raffaello A., Rizzuto R., Costa A., Schwarzländer M., Szabò I. (2017). Physiological

characterization of a plant mitochondrial calcium uniporter *in vitro* and *in vivo*. *Plant Physiology* **173**: 1355-1370.

Teardo E., Formentin E., Segalla A., Giacometti G. M., Marin O., Zanetti M., Schiavo F. L., Zoratti M., Szabò I. (2011). Dual localization of plant glutamate receptor AtGLR3. 4 to plastids and plasmamembrane. *Biochimica et Biophysica Acta (BBA)-Bioenergetics* **1807**: 359-367.

Thines L., Stribny J., Morsomme P. (2020). From the uncharacterized protein family 0016 to the GDT1 family: Molecular insights into a newly-characterized family of cation secondary transporters. *Microbial Cell* **7**: 202-214.

Thor K. (2019). Calcium-Nutrient and Messenger. *Frontiers in Plant Science* **10**: 1-7.

Thor K., Jiang S., Michard E., George J., Scherzer S., Huang S., Dindas J., Derbyshire P., Leitão N., Defalco T. A., Köster P., Hunter K., Kimura S., Gronnier J., Stransfeld L., Kadota Y., Bücherl C. A., Charpentier M., Wrzaczek M., Maclean D., Oldroyd G. E. D., Menke F. L. H., Roelfsema M. R. G., Hedrich R., Feijó J., Zipfel C. (2020). The calcium-permeable channel OSCA1.3 regulates plant stomatal immunity. *Nature* **585**: 569-573.

Tian L., Hires S. A., Mao T., Huber D., Chiappe M. E., Chalasani S. H., Petreanu L., Akerboom J., Mckinney S. A., Schreiter E. R., Bargmann C. I., Jayaraman V., Svoboda K., Looger L. L. (2009). Imaging neural activity in worms, flies and mice with improved GCaMP calcium indicators. *Nature Methods* **6**: 875-881.

Tian W., Wang C., Gao Q., Li L., Luan S. (2020). Calcium spikes, waves and oscillations in plant development and biotic interactions. *Nature Plants* **6**: 750-759.

Tidow H., Poulsen L. R., Andreeva A., Knudsen M., Hein K. L., Wiuf C., Palmgren M. G., Nissen P. (2012). A bimodular mechanism of calcium control in eukaryotes. *Nature* **491**: 468-472.

Tinland B., Hohn B., Puchta H. (1994). *Agrobacterium tumefaciens* transfers single-stranded transferred DNA (T-DNA) into the plant cell nucleus. *Proceedings of the National Academy of Sciences of the United States of America* **91**: 8000-8004.

Turano F. J., Thakkar S. S., Fang T., Weisemann J. M. (1997). Characterization and expression of NAD(H)-dependent glutamate dehydrogenase genes in Arabidopsis. *Plant Physiology* **113**: 1329-1341.

Uemura M., Steponkus P. L. (1999). Cold acclimation in plants: Relationship between the lipid composition and the cryostability of the plasma membrane. *Journal of Plant Research* **112**: 245.

Uemura T., Kim H., Saito C., Ebine K., Ueda T., Schulze-Lefert P., Nakano A. (2012). Qa-SNAREs localized to the *trans*-Golgi network regulate multiple transport pathways and extracellular disease resistance in plants. *Proceedings of the National Academy of Sciences of the United States of America* **109**: 1784-1789.

Viotti C., Bubeck J., Stierhof Y. D., Krebs M., Langhans M., Van Den Berg W., Van Dongen W., Richter S., Geldner N., Takano J., Jürgens G., De Vries S. C., Robinson D. G., Schumacher K. (2010). Endocytic and secretory traffic in Arabidopsis merge in the *trans*-Golgi network/early endosome, an independent and highly dynamic organelle. *The Plant Cell* **22**: 1344-1357.

Waadt R., Krebs M., Kudla J., Schumacher K. (2017). Multiparameter imaging of calcium and abscisic acid and high-resolution quantitative calcium measurements using R-GECO1-mTurquoise in Arabidopsis. *New Phytologist* **216**: 303-320.

Waadt R., Kudla J., Kollist H. (2021). Multiparameter *in vivo* imaging in plants using genetically encoded fluorescent indicator multiplexing. *Plant Physiology* **187**: 537-549.

Wagner S., De Bortoli S., Schwarzländer M., Szabò I. (2016). Regulation of mitochondrial calcium in plants versus animals. *Journal of Experimental Botany* **67**: 3809-3829.

Waight A. B., Pedersen B. P., Schlessinger A., Bonomi M., Chau B. H., Roe-Zurz Z., Risenmay A. J., Sali A., Stroud R. M. (2013). Structural basis for alternating access of a eukaryotic calcium/proton exchanger. *Nature* **499**: 107-110.

Wang H., Han S., Siao W., Song C., Xiang Y., Wu X., Cheng P., Li H., Jásik J., Mičieta K., Turna J., Voigt B., Baluska F., Liu J., Wang Y., Zhao H. (2015). Arabidopsis synaptotagmin 2 participates in pollen germination and tube growth and is delivered to plasma membrane via conventional secretion. *Molecular Plant* **8**: 1737-1750.

Wang X., Xu M., Gao C., Zeng Y., Cui Y., Shen W., Jiang L. (2020). The roles of endomembrane trafficking in plant abiotic stress responses. *Journal of Integrative Plant Biology* **62**: 55-69.

Wang Z., Benning C. (2012). Chloroplast lipid synthesis and lipid trafficking through ER-plastid membrane contact sites. *Biochemical Society Transactions* **40**: 457-463.

Wee E. G.-T., Sherrier D. J., Prime T. A., Dupree P. (1998). Targeting of active sialyltransferase to the plant Golgi apparatus. *The Plant Cell* **10**: 1759-1768.

Wege S. (2022). Manganese management in plants: Golgi transporter determines manganese allocation and cell wall composition. *Plant Physiology* **190**: 2077-2079.

Weinl S., Kudla J. (2009). The CBL-CIPK Ca^{2+}-decoding signaling network: Function and perspectives. *New Phytologist* **184**: 517-528.

Wu F., Chi Y., Jiang Z., Xu Y., Xie L., Huang F., Wan D., Ni J., Yuan F., Wu X., Zhang Y., Wang L., Ye R., Byeon B., Wang W., Zhang S., Sima M., Chen S., Zhu M., Pei J., Johnson D. M., Zhu S., Cao X., Pei C., Zai Z., Liu Y., Liu T., Swift G. B., Zhang W., Yu M., Hu Z., Siedow J. N., Chen X., Pei Z. M. (2020). Hydrogen peroxide sensor HPCA1 is an LRR receptor kinase in Arabidopsis. *Nature* **578**: 577-581.

Wu Q., Stolz S., Kumari A., Farmer E. E. (2022). The carboxy-terminal tail of GLR3.3 is essential for wound-response electrical signaling. *New Phytologist* **236**: 2189-2201.

Wu Z., Liang F., Hong B., Young J. C., Sussman M. R., Harper J. F., Sze H. (2002). An Endoplasmic Reticulum-bound Ca^{2+}/Mn^{2+} pump, ECA1, supports plant growth and confers tolerance to Mn^{2+} stress. *Plant Physiology* **130**: 128-137.

Xiang L., Etxeberria E., Van Den Ende W. (2013). Vacuolar protein sorting mechanisms in plants. *The FEBS Journal* **280**: 979-993.

Yang C. H., Wang C., Singh S., Fan N., Liu S., Zhao L., Cao H., Xie W., Yang C., Huang C. F. (2021). Golgi-localised manganese transporter PML3 regulates Arabidopsis growth through modulating Golgi glycosylation and cell wall biosynthesis. *New Phytologist* **231**: 2200-2214.

Yang J. S., Valente C., Polishchuk R. S., Turacchio G., Layre E., Moody D. B., Leslie C. C., Gelb M. H., Brown W. J., Corda D., Luini A., Hsu V. W. (2011). COPI acts in both vesicular and tubular transport. *Nature Cell Biology* **13**: 996-1003.

Yuan F., Yang H., Xue Y., Kong D., Ye R., Li C., Zhang J., Theprungsirikul L., Shrift T., Krichilsky B., Johnson D. M., Swift G. B., He Y., Siedow J. N., Pei Z. M. (2014). OSCA1 mediates osmotic-stress-evoked Ca^{2+} increases vital for osmosensing in Arabidopsis. *Nature* **514**: 367-371.

Zhang B., Gao Y., Zhang L., Zhou Y. (2021). The plant cell wall: Biosynthesis, construction, and functions. *Journal of Integrative Plant Biology* **63**: 251-272.

Zhang F., Wang Y., Yang Y., Wu H., Wang D., Liu J. (2007). Involvement of hydrogen peroxide and nitric oxide in salt resistance in the calluses from Populus euphratica. *Plant, Cell & Environment* **30**: 775-785.

Zhang G. F., Staehelin L. A. (1992). Functional compartmentation of the Golgi apparatus of plant cells: Immunocytochemical analysis of high-pressure frozen-and freeze-substituted sycamore maple suspension culture cells. *Plant Physiology* **99**: 1070-1083.

Zhang H., Zhang L., Gao B., Fan H., Jin J., Botella M. A., Jiang L., Lin J. (2011). Golgi apparatus-localized synaptotagmin 2 is required for unconventional secretion in Arabidopsis. *PLoS One* **6**: 1-14.

Zhang M., Henquet M., Chen Z., Zhang H., Zhang Y., Ren X., Van Der Krol S., Gonneau M., Bosch D., Gong Z. (2009). *LEW3*, encoding a putative α-1,2-mannosyltransferase (ALG11) in *N*-linked glycoprotein, plays vital roles in cell-wall biosynthesis and the abiotic stress response in *Arabidopsis thaliana*. *The Plant Journal* **60**: 983-999.

Zhao Y., Araki S., Wu J., Teramoto T., Chang Y. F., Nakano M., Abdelfattah A. S., Fujiwara M., Ishihara T., Nagai T., Campbell R. E. (2011). An expanded palette of genetically encoded Ca^{2+} indicators. *Science* **333**: 1888-1891.

Zhou L., Lan W., Jiang Y., Fang W., Luan S. (2014). A calcium-dependent protein kinase interacts with and activates a calcium channel to regulate pollen tube growth. *Molecular Plant* **7**: 369-376.

Zimmer M. (2002). Green fluorescent protein (GFP): Applications, structure, and related photophysical behavior. *Chemical reviews* **102**: 759-782.

Zimmermann P., Hirsch-Hoffmann M., Hennig L., Gruissem W. (2004). GENEVESTIGATOR. Arabidopsis microarray database and analysis toolbox. *Plant Physiology* **136**: 2621-2632.

Zupunski A., 2020. *Role of Protein N-glycosylation during the Pollen Tube Reception in Arabidopsis thaliana*: University of Zurich.

Zykwinska A., Thibault J.-F., Ralet M.-C. (2007). Organization of pectic arabinan and galactan side chains in association with cellulose microfibrils in primary cell walls and related models envisaged. *Journal of Experimental Botany* **58**: 1795-1802.

6 Tables and Figures

Tables

Figures

7   Abbreviations

µg	Microgramme
µm	Micrometer
µM	Micromolar
µmol	Micromole
½ MS	Half-strength Murashige & Skoog medium
AGPs	Arabinogalactan proteins
Amp	Ampicillin
Arabidopsis	*Arabidopsis thaliana* L.
ATD	Amino terminal domain
ATP	Adenosine triphosphate
A. thaliana	*Arabidopsis thaliana* L.
A. tumefaciens	*Agrobacterium tumefaciens*
Asp	Asparagine
BASTA	Glufosinate-ammonium (Bayer Crop Science, Germany)
BICAT	Bivalent Cation Transporter
bp	Base pair
BSA	Bovine serum albumin
B4GALT1	β-1,4-galactosyltransferase 1
Ca^{2+}	Calcium
$[Ca^{2+}]_{cisGolgi}$	*cis*-Golgi free Calcium
$[Ca^{2+}]_{cyt}$	Cytosolic free Calcium
$[Ca^{2+}]_{ER}$	Endoplasmic Reticulum free Calcium
$[Ca^{2+}]_{Golgi}$	Golgi free Calcium
$[Ca^{2+}]_{Mito}$	Mitochondrial free Calcium
$[Ca^{2+}]_{transGolgi}$	*trans*-Golgi free Calcium
CaM	Calmodulins
CAX	Calcium/anion exchanger
CBL	calcineurin B-like proteins
CCX	Cation/calcium exchanger

cDNA	Complementary desoxyribonucleic acid
CDPK/CPK	Ca^{2+}-dependent protein kinases
CDS	Coding sequence
cMCU	Chloroplast-localised mitochondrial calcium uniporter
CML	Calmodulin-like proteins
CNGC	Cyclic nucleotide-gated channels
Co	Cobalt
CO2	Carbon dioxide
ConA	Concanavalin A
CPK6L	Calcium-dependent protein kinase 6-like
CRK	CDPK-related kinases
CT	Cytoplasmic tail
Cu	Copper
d	Day
DMSO	Dimethyl sulfoxide
DNA	Desoxyribonucleic acid
DW	Dry weight
DTT	Dithiothreitol
DxD	Asp-[any amino acid]-Asp
ECA	Endoplasmic reticulum-type calcium ATPase
E. coli	*Escherichia coli*
EDTA	Ethylene diamine tetraacetic acid
EGFP	Enhanced green fluorecent protein
EGTA	Ethylenglycol diamine tetraacetic acid
ER	Endoplasmic reticulum
EXT	Extensin
YFP	Yellow fluorescent protein
Fe	Iron
FER	Feronia
FUT1	α-1,2-fucosyltransferase
FW	Fresh weight

g	Gram
G	Glycine
GalA	Galacturonic acid
GALT1	β-1,3-galactosyltransferase
GALT2-6	Hyp-O-galactosyltransferases
GAUT	Galacturonosyltransferase
GDH	Glutamate dehydrogenase
gDNA	Genomic desoxyribonucleic acid
GDT1	Gcr1-dependent translation factor 1
GECI	Genetically encoded calcium indicators
GECO	Ca^{2+} indicators for optical imaging
Glc	Glucose
GlcA	Glucuronic acid
GLR	Glutamate receptors
GNT1	N-acetylglucosaminyltransferase I
GNT2	N-acetylglucosaminyltransferase II
GT	Glycosyltransferase
GUS	β-glucoronidase (activity)
h	Hour
H^+	Proton
HG	Homogalacturonan
H_2O_2	Hydrogen peroxide
HPAT	Hydroxyproline O-arabinosyltransferase
HPCA1	hydrogen-peroxide-induced Ca^{2+} increases 1
HPGT	Hydroxyproline O-galactosyltransferase
HRGP	Hydroxyproline-rich glycoprotein
IAA	Indole-3-acetic acid
ICP-MS	Inductively coupled plasma-mass spectrometry
IPUT1	Inositol phosphoryl-ceramide glucuronosyl transferase 1
IRX9	β-1,4-xylosyltransferase in xylan biosynthesis
JA	Jasmonate

K$^+$	Potassium
Kan	Kanamycin
KanR	Kanamycin resistence
LBD	Ligand-binding domain
LRXs	Leucine-rich repeat extensins
M	Molar
MCU	Mitochondrial calcium uniporter
MES	2-(N-morpholino) ethanesulfonic acid
Mg^{2+}	Magnesium
mg	Milligram
MICU1	Mitochondrial calcium uptake 1
min	Minute
mM	Milimolar
Mn^{2+}	Manganese
MnSOD	Manganese superoxide dismutase
MNS	α-mannosidase
mRNA	Messenger ribonucleic acid
MTP	Metal tolerance protein
NLS	Nuclear localisation signal
N-terminus	Amino terminus of a protein
NBT	Nitro tetrazolium blue
ng	Nanogram
nM	Nanomolar
NRAMP	Natural resistance associated macrophage protein
O$_2$	Oxygen
O$_2^{\cdot-}$	superoxide
O$_2^{2-}$	peroxides
OH$^-$	hydroxyl radical
H$_2$O$_2$	hydrogen peroxide
OSCA	Hyperosmolality-gated calcium-permeable channels
PAM71	Photosynthesis affected mutant 71

PML	Photosynthesis affected mutant-like
PCR	Polymerase chain reaction
PGSIPs	Plant glycogenin-like starch initiation proteins
pH	Negative decadic logarithm of proton activity
PM	Plasma membrane
PMR1	Plasma membrane ATPase related 1
PS	Photosynthesis
PSII	Photosystem II
PVC	Prevacuolar compartment
qRT-PCR	Quantitative reverse transription polymerase chain reaction
RBOHD	Respiratory burst oxidase protein homologue D
RG	Rhamnogalacturonan
rH	Relative humidity
RLU	Relative Light Unit
RNA	Ribonucleic acid
ROS	Reactive oxygen species
sec	Second
S. cerevisiae	*Saccharomyces cerevisiae*
SERCA	Sarco/endoplasmic reticulum calcium ATPase
SOD	Superoxide dismutase
SPCA	Secretory pathway calcium ATPase
TCA	Citric acid cycle
T-DNA	Transfer desoxyribonucleic acid
TGN	*trans*-Golgi network
TMD	Transmembrane domain
TMEM165	Transmembrane protein 165
TPC	Two-pore channel
UPF0016	Uncharacterized protein family 16
UTR	Untranslated region
WT	Wild type
x-Gluc	5-Bromo-4-chloro-3-indolyl-β-D-glucuronic acid

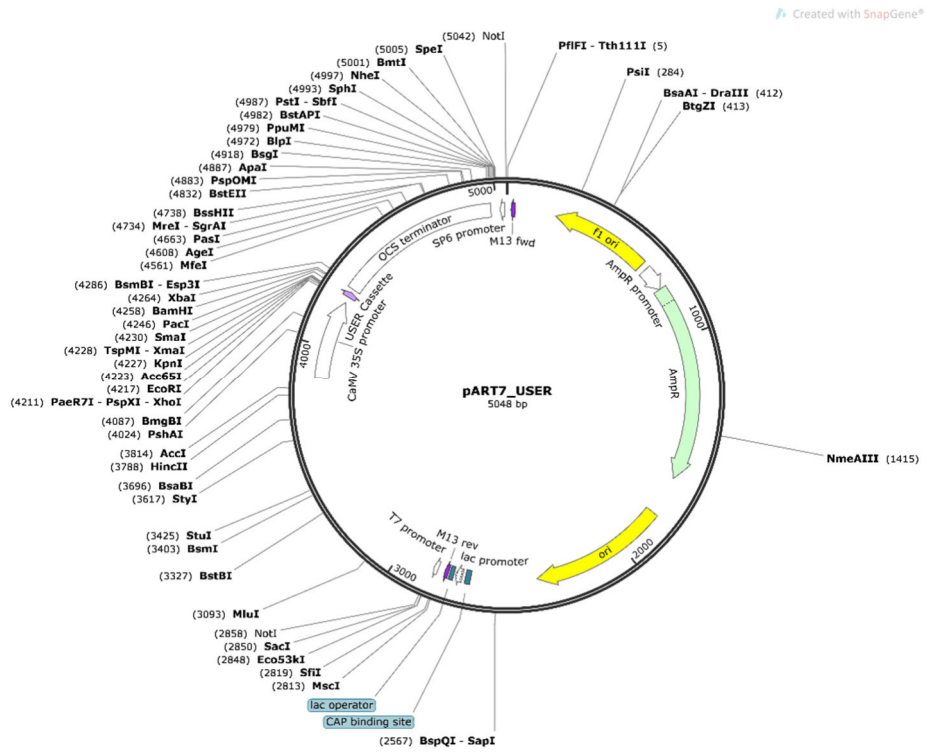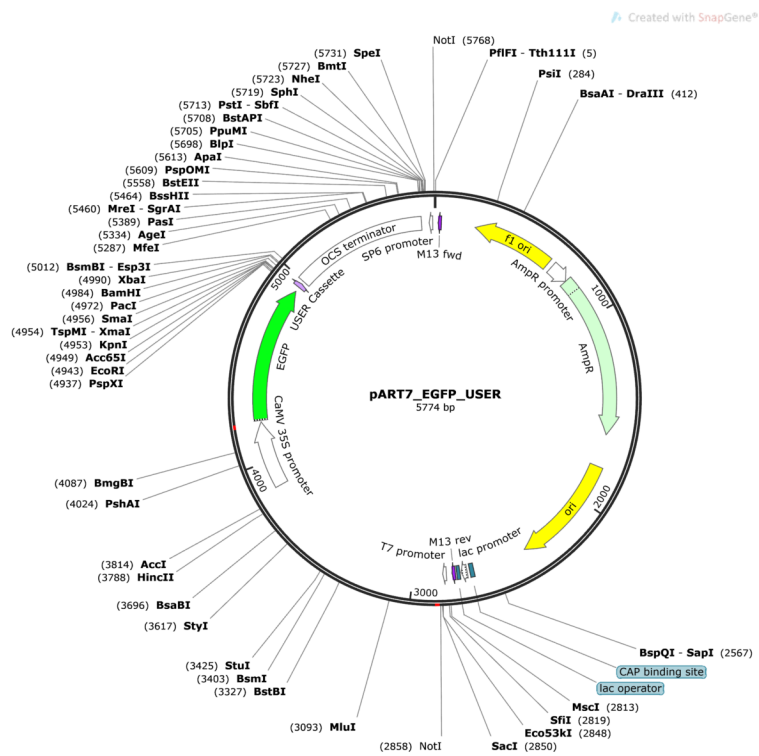| XXT | Xyloglucan xylosyltransferases |
Xyl	Xylose
XYLT	β-1,2-xylosyltransferase
Zn^{2+}	Zinc

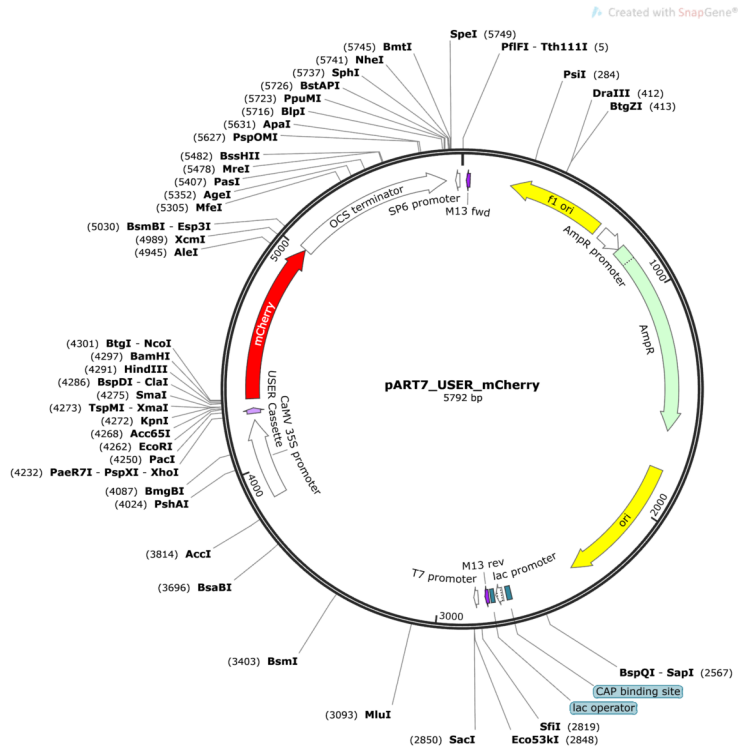# 8 Appendix

Figure 33: pART7-USER

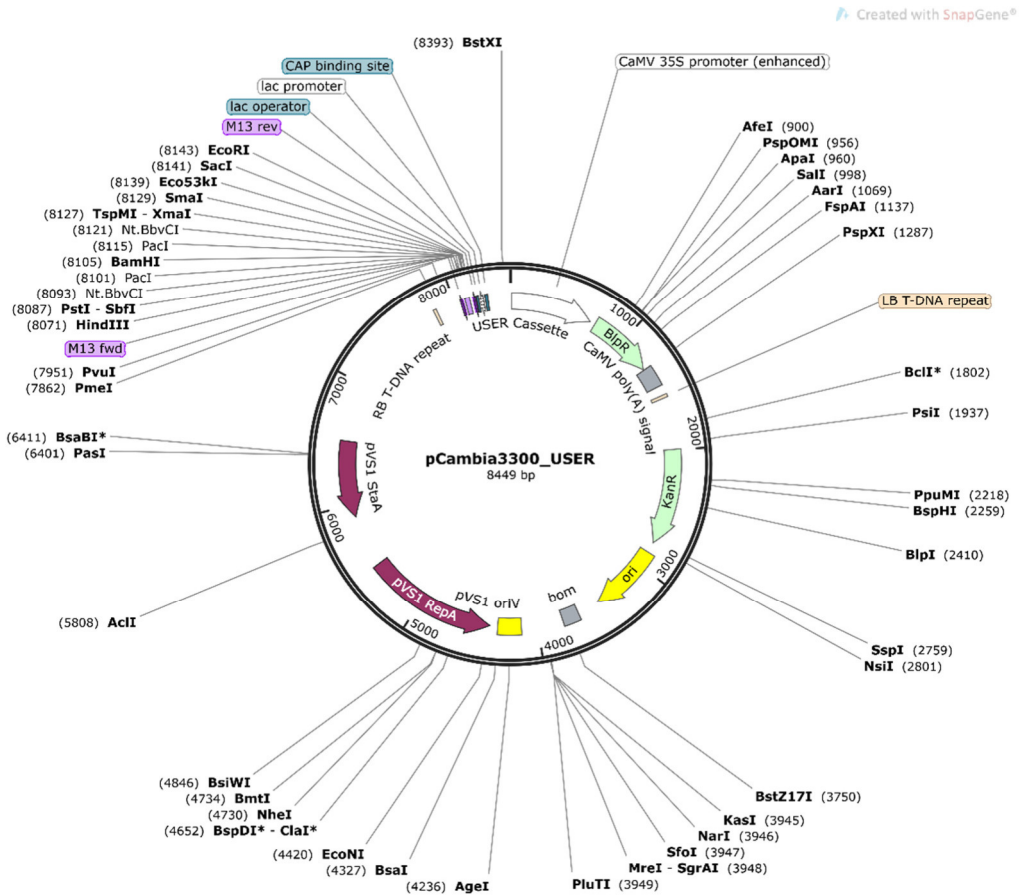Figure 34: pART7-EGFP-USER

Figure 35: pART7-USER-mCherry

Figure 36: pCambia3300-USER

Figure 37: pART7-EGFP-ECA3
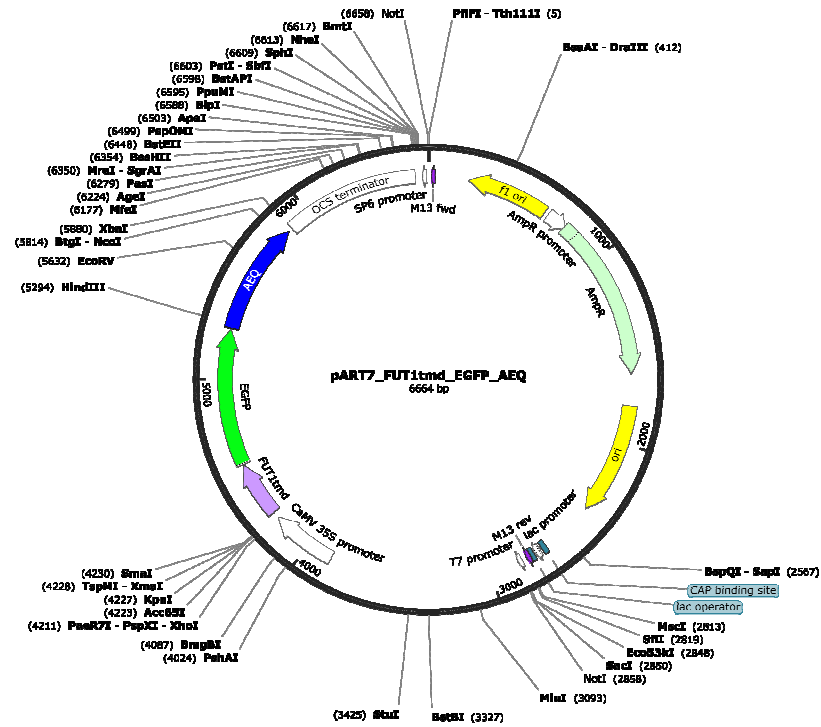

Figure 38: pART7-MNS1tmd-EGFP-AEQ

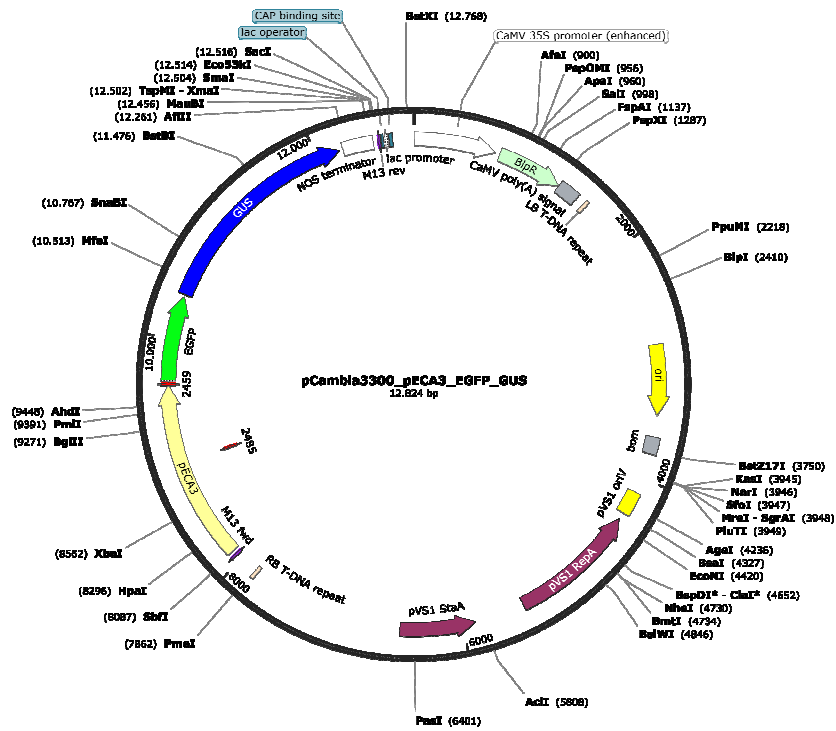Figure 39: pART7-FUT1tmd-EGFP-AEQ

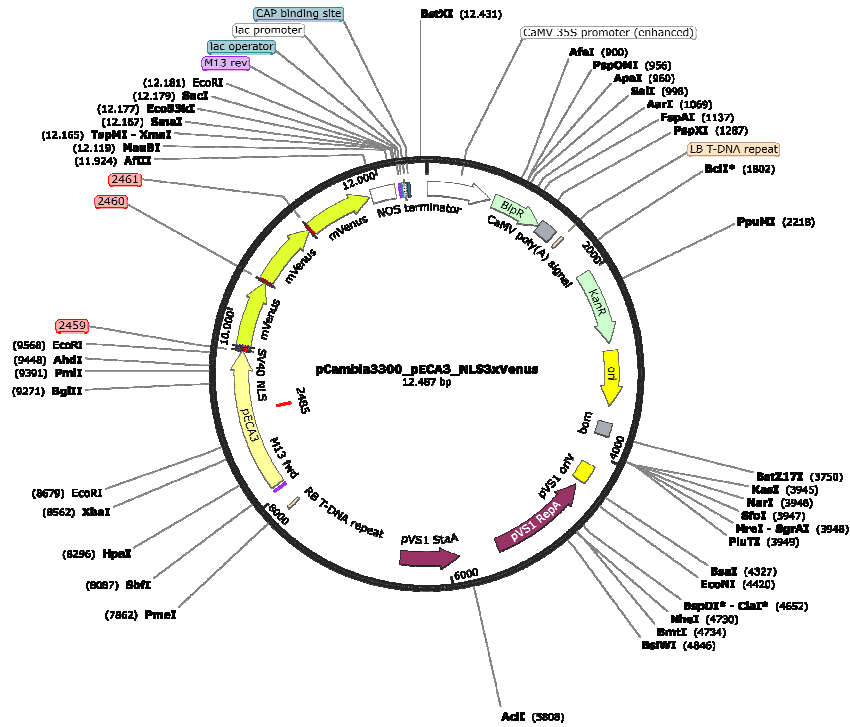Figure 40: pCambia3300-pECA3-EGFP-GUS
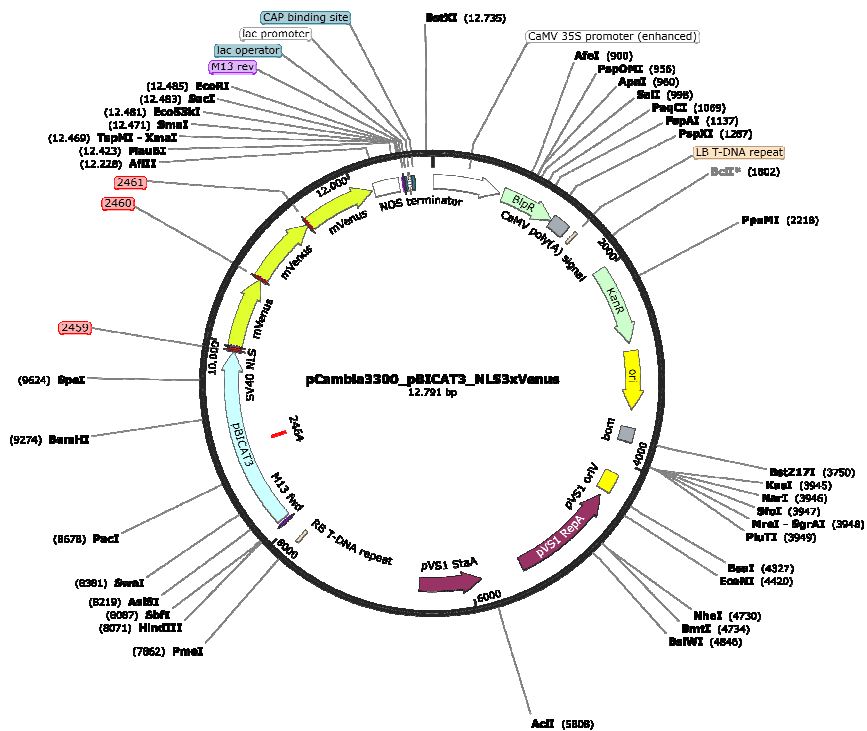
Figure 41: pCambia3300-pECA3-NLS3xVenus

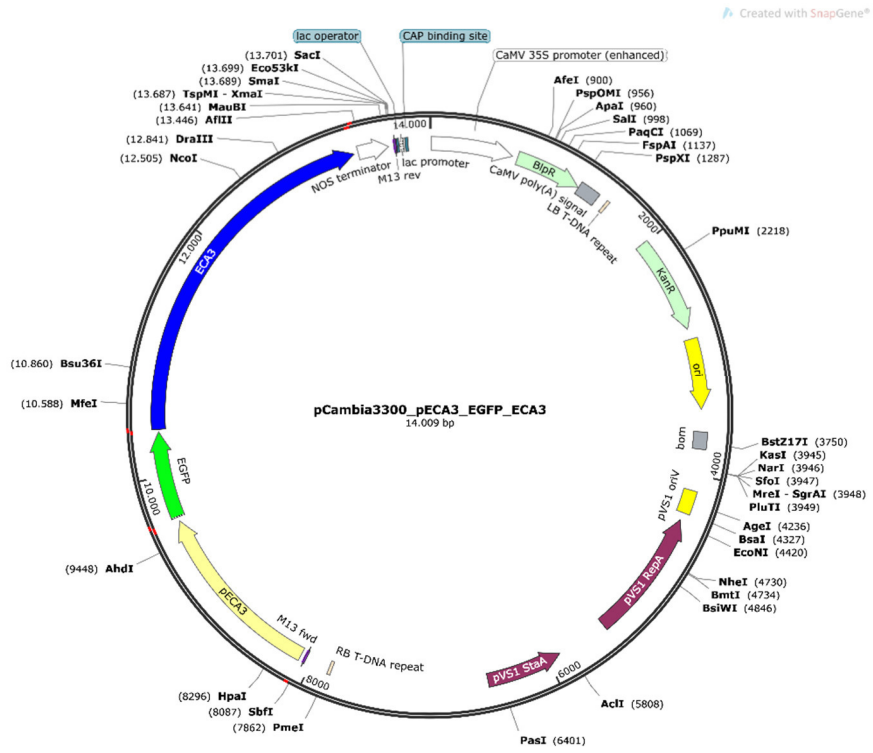Figure 42: pCambia3300-pBICAT3-NLS3xVenus

Figure 43: pCambia3300-pECA3-EGFP-ECA3

9 Danksagung / Acknowledgement

Ich habe beschlossen die Danksagung dieser Arbeit speziell auf deutsch zu verfassen.

Zunächst möchte ich mich bei der Deutschen Forschungs Gemeinschaft (DFG) für die Finanzierung meines Projekts im Rahmen des Graduiertenkollegs (GRK2498) bedanken. Mithilfe dieser üppigen finanziellen Mittel konnte ich meine Dissertation bestreiten. Ein sehr großer Dank geht somit auch an alle Beteiligten und Initiatioren des Graduiertenkollegs, darunter besonders Professor Dr. Ingo Heilmann und Dr. Julia Grimmer.

Ein außerordentlicher Dank geht aber an meinen Doktorvater Professor Dr. Edgar Peiter ohne den ich es wahrscheinlich niemals so weit geschafft hätte. Ich war wirklich immer beeindruckt bei seinem umfassenden Wissen sowie seiner Begeisterung für die Wissenschaft. Ohne sein großes Wissen und Ideenreichtum wäre mein Projekt nicht so beeinflusst worden. Dank seiner großartigen Unterschützung konnte mein Projekt reibungslos verlaufen. Ich danke ihm dafür, dass er mir in der Wissenschaft somit den richtigen Einstieg ermöglicht hat. Ich hoffe, dass bei ihm für mich immer seine offene Tür bleibt und dass wir weiterhin in engen Kontakt bleiben.

Die Arbeitsgruppe und ihre Mitglieder waren für mich wie eine zweite Familie. Ich bin jedem so unendlich dankbar. Besonders hervorheben möchte ich gerne Dr. Bastian Meier. Ich habe in ihm nicht nur einen Arbeitskollegen, sondern auch einen sehr guten Freund gefunden. Ein Mensch, der immer versucht zu helfen und mich nie fallen gelassen hat. Ich kann meinen Dank für ihn gar nicht in Worte fassen, aber meine Dankbarkeit währt ein lebenlang. Auch bei Dr. Stefanie Höller möchte ich mich bedanken für ihre immer guten Ratschläge, ihren seelischen sowie labortechnischen Beistand. Die großartige Laborfertigkeit von Tina Peiter-Volk, Anja Janssen und Liane Freitag werde ich niemals vergessen. Danke für jede Hilfe und dass ihr immer für mich da wart. Danke Tina für jede warme Dusche, danke Anja für jede Minute deines dann verzögerten Feierabend und danke Liane für deine unglaublich liebenswerte Art. Ebenso danke ich allen anderen Mitgliedern der Pflanzenernährung. Darunter auch meine ehemalige Kollegin und Freundin Dr. Jie He. Ebenso auch meine lieben Kollegen aus dem Büro, Oriana Mariani und Srijana Raj.

Insgesamt möchte ich auch bei allen Mitgliedern des DFG Graduiertenkollegs 2498 bedanken. Ich danke hier besonders Dr. Mareike Heilmann und Professor Dr. Steffen Abel, die in meinen Thesis Committee waren. Ich kann leider nicht alle Mitglieder namentlich nennen, dennoch

möchte ich allen hier so unendlich danken für diese schöne Zeit. Ich danke Dr. Dr. Gerd Hause für die Elektronenmikroskopie. Ich danke Dr. Martin Schattat für die tollen Stunden am Mikroskop.

Und nun würde ich gerne auch noch Menschen aus meinem persönlichen Umfeld danken. Ich danke meinen Freunden, die ich hier in Halle gewonnen habe. Die Zeit in Halle war für mich eine besonders schöne Zeit und ich möchte sie nie in meinem Leben vermissen. Ich danke auch meinen Freunden in Hamburg oder wo überall sie mittlerweile auch sind. Eine besonders gute Freundin, muss namentlich genannt werden. Danke Bianca Kubiak für jeden Anruf, den ich tätigen konnte, wenn ich abends noch lange im Büro oder Labor war und für jede Ablenkung, wenn ich sie wirklich nötig hatte.

Ich möchte zum Schluss meinen Eltern Gabriele und Franz danken. Danke für alles. Wir wissen alle, dass wir nicht einfach sind, aber ihr bedeutet mir sehr viel. Ebenso auch mein Bruder Nils. Ich danke jedem nicht namentlich genannten, der mich unterstützt hat.

Danke.

10 Publications

10.1 Peer-reviewed publications

He J., Yang B., Hause G., <u>Rössner N.</u>, Peiter-Volk T., Schattat M. H., Voiniciuc C., Peiter E. (2022). The *trans*-Golgi-localized protein BICAT3 regulates manganese allocation and matrix polysaccharide biosynthesis. *Plant Physiology* 190: 2579-2600.

He J., <u>Rössner N.</u>, Hoang M. T. T., Alejandro S., Peiter E. (2021). Transport, functions, and interaction of calcium and manganese in plant organellar compartments. *Plant Physiology* 187: 1940-1972.

10.2 Poster presentations

Mariani O., He J., <u>Rössner N.</u>, Frank J., Jacob T., Hoang M. T. T., Schattat M., Meier B., Baginsky S., Peiter E. (2023). Distribution of calcium and manganese to plant cell compartments by BICAT proteins. *Presented at:* 36th Conference on Molecular Biology of Plants, 06-09 February 2023, Hennef, Germany.

<u>Rössner N.</u>, Mariani O., Meier B., Peiter E. (2022). Calcium as a regulator of organellar function in the compartments along the secretory pathway. *Presented at:* Plant Nutrition 2022: From Molecules to Traits - how Plants Feed the Future, 04 - 05 October 2022, Raitenhaslach, Germany.

<u>Rössner N.</u>, Würsig H., Meier B., Peiter E. (2022). Calcium as a regulator of organellar function in the compartments along the secretory pathway. *Presented at:* Plant Calcium Signalling Conference 2022, 11-13 July 2022, Milan, Italy; Botanik-Tagung 2022: Plant Sciences for a Sustainable Future, 28 August - 01 September 2022, Bonn, Germany.

Rössner N., He J., Meier B., Peiter E. (2021). Ca^{2+} as a regulator of organellar function in the compartments along the secretory pathway. *Presented at:* 3rd FEBS workshop Plant Organellar Signalling, 19-23 September 2021, Primošten, Croatia.

Meier B., Zimmermann L., Rössner N., Steudtel T., Peiter E. (2019). The involvement of calcium in mechanisms of ammonium uptake and assimilation. *Presented at:* Plant Nutrition meets social expectations of sustainable plant production: International Conference of the German Society of Plant Nutrition, 25 - 27 September 2019, Berlin, Germany.

11 Curriculum Vitae

Personal data

Name	Nico Rössner
Birthday	21st May 1995
Place of Birth	Hamburg-Harburg
Nationality	German

Work Experience

Since October 2019	Employed as Researcher at the Martin Luther University (MLU) Halle-Wittenberg in the Plant Nutrition Group of Prof. Dr. Edgar Peiter DFG Research Training Group 2498

Education

October 2017	- September 2019	M.Sc. in Crop Science at the MLU Halle-Wittenberg
October 2014	- September 2017	B.Sc. in Biology at the University of Hamburg
August 2005	- June 2013	General University entrance qualification *Allgemeine Hochschulreife,* Gymnasium Neu Wulmstorf

Voluntary Social Year

July 2013	- July 2014	Lebenshilfe Buxtehude e.V.

Awards

October 2019		Best graduation in M.Sc. Crop Science, MLU Halle-Wittenberg
October 2018	- September 2019	Scholarship "Deutschlandstipendium", MLU Halle-Wittenberg

12 Eidesstattliche Erklärung / *Declaration under Oath*

Ich erkläre an Eides statt, dass ich die Arbeit selbstständig und ohne fremde Hilfe verfasst, keine anderen als die von mir angegebenen Quellen und Hilfsmittel benutzt und die den benutzten Werken wörtlich oder inhaltlich entnommenen Stellen als solche kenntlich gemacht habe.

I declare under penalty of perjury that this thesis is my own work entirely and has been written without any help from other people. I used only the sources mentioned and included all the citations correctly both in word or content.

_____   _____

Datum / *Date*   Unterschrift des Antragstellers / *Signature of the applicant*